LEVEL II

RELATION BETWEEN THE SURFACE FRICTION OF PLATES AND THEIR STATISTICAL MICROGEOMETRY

BY

M.J. KING

(Thesis submitted to Teesside Polytechnic for the degree of Master of Philosophy)

January 1980

SECURITY CLASSIFICATION OF THIS PAGE (When Data Entered)

REPORT DOCUMENTATION PAGE		READ INSTRUCTIONS BEFORE COMPLETING FORM
1. REPORT NUMBER	2. GOVT ACCESSION NO.	3. RECIPIENT'S CATALOG NUMBER
4. TITLE (and Subtitle) Relation between the surface friction of plates and their statistical microgeometry.		5. TYPE OF REPORT & PERIOD COVERED Interim April 1979 - January 1980 6. PERFORMING ORG. REPORT NUMBER
7. AUTHOR(s) M.J. King		8. CONTRACT OR GRANT NUMBER(s) N00014-78-G-0059
9. PERFORMING ORGANIZATION NAME AND ADDRESS Department of Mechanical Engineering, Teesside Polytechnic, Middlesbrough, Cleveland. TS1 3BA. U.K.		10. PROGRAM ELEMENT, PROJECT, TASK AREA & WORK UNIT NUMBERS NR 062-629
11. CONTROLLING OFFICE NAME AND ADDRESS ONR Washington D.C.		12. REPORT DATE January 1980 13. NUMBER OF PAGES
14. MONITORING AGENCY NAME & ADDRESS(if different from Controlling Office)		15. SECURITY CLASS. (of this report) Unclassified 15a. DECLASSIFICATION/DOWNGRADING SCHEDULE

16. DISTRIBUTION STATEMENT (of this Report)

APPROVED FOR PUBLIC RELEASE; DISTRIBUTION UNLIMITED

17. DISTRIBUTION STATEMENT (of the abstract entered in Block 20, if different from Report)

18. SUPPLEMENTARY NOTES

Dissertation

19. KEY WORDS (Continue on reverse side if necessary and identify by block number)

surface friction; boundary layer; flow channel; roughness; replication; friction plane; surface topography.

20. ABSTRACT (Continue on reverse side if necessary and identify by block number)

Microgeometry of rough surfaces is related to their resistance to fluid flow. Flow measurements were carried out in an open flume 20m long x 30cm wide at free stream velocities between 35 and 85 cm/s. Velocity profiles and hence friction factors were measured by hot-film anemometry. Surface profiles were recorded digitally and their statistical characterizations related to friction factors.

DD FORM 1 JAN 73 1473 EDITION OF 1 NOV 65 IS OBSOLETE
S/N 0102-LF-014-6601

SECURITY CLASSIFICATION OF THIS PAGE (When Data Entered)

(6) RELATION BETWEEN THE SURFACE FRICTION OF PLATES AND THEIR STATISTICAL MICROGEOMETRY.

BY

(10) M.J KING

(9) Interim rept. Apr 79-Jan 80

(21) Master's thesis

(Thesis submitted to Teesside Polytechnic for the degree of Master of Philosophy)

(15) N00014-79-G-0159

(12) 284

(11) January 1980

ABSTRACT

An attempt is made to relate the geometry of nominally flat surfaces to their resistance to fluid flow. The experimental work was carried out in an open-flume, 20 metres in length, 30 cm wide, and 30 cm deep. The flow measurements were carried out over a range of free stream velocities from 35 cm/sec to 85 cm/sec. Hot film anemometry using a single sensor was used to measure the boundary layer velocity profile development along a 2.4 metre section of the channel floor which provides the base for the test surfaces. The velocity profiles are analysed to determine the surface friction coefficient using the simplified momentum integral equation as well as the logarithmic inner law approach.

The test surfaces, including a 4.8 metre long replica of a ship hull surface, were examined using a number of surface measurement instruments capable of recording surface wavelengths from microns to metres. Surface profiles were recorded and digitised and the data statistically analysed to give an overall characterisation of the surfaces under investigation using both amplitude and spatial parameters.

PREFACE

This investigation was carried out in the Mechanical Engineering Department, Teesside Polytechnic. The work was under the internal supervision of Dr T R Thomas and Mr S T Olszowski to whom I give my sincere thanks for encouragement, advice and helpful suggestions. The work was also under the external supervision of Dr D Clarke, BSRA, to whom I also give my thanks for helpful suggestions.

I wish to thank BSRA for the loan of a roto-dynamic pump which was installed into the flow system and for the use of a BSRA Wall Gauge, and also for supplying a marine paint for coating the test surfaces. I also wish to thank Shell Research Ltd for supplying a 4.8 metre long replica of part of a ship hull surface and Smiths Dock, Middlesborough, for supplying 3 lengths of shot-blasted steel plate which made up the initial work surface in the flow channel. I also wish to thank Dr D J Cockerall of the University of Leicester for supplying a program to compute local coefficients of surface friction using the inner law.

The work embodied in this thesis is the result of the author's own research except where stated otherwise.

Finally I wish to thank Rolls Royce Limited and Rank Precision Industries Limited for their help and cooperation and Jane Waterfield for so carefully typing this thesis.

CONTENTS

CONTENTS (continued) PAGE NO.

CONTENTS (continued) PAGE NO.

CONTENTS (continued)

CONTENTS (continued) PAGE NO.

NOMENCLATURE

ENGLISH SYMBOLS

a,A	Area
A_1,A_2	Cross-sectional areas for the Dall Flow Tube (Chapter 3.3)
a,b	Empirical constants (Chapter 4.0)
A,B	Empirical constants (Chapter 3.1)
b	Width (Chapter 2.4)
B,C	Law-of-the-wall constants (Chapter 2.4)
C_1,C_2	Empirical constants determined from the roughness function (Chapter 2.4)
$C(\tau)$	Autocovariance function, ACVF (Chapter 5.0)
e_j	Unit vector (Chapter 2.4)
e	Exponential
f_D	Doppler shift in frequency (Chapter 2.4)
F	Force
f,F	Frictional resistance (Appendix 2)
g	Roughness function (Chapter 4.0)
g	Gravitational acceleration
G	Ratio of moments (Appendix 2)
G(w)	Power spectral density function (Chapter 5.0)
h	Height
H	Shape factor, δ_1/θ (Chapter 2.4)
H	Differential Head (Chapter 3.3)
I	Electric current
k	Surface height parameter

ENGLISH SYMBOLS (continued)

K	Empirical constant (Chapter 3.1 and Appendix 1)
K_u	Kurtosis of the surface height distribution (Chapters 4 and 5)
L	Length
m	Area ratio, A_2/A_1 (Chapter 3.3)
$\dot{m}$	Mass flow (Chapter 4.0)
M	Torque or moment (Chapter 2.4)
M	Empirical constant (Appendix 1)
M	Linear momentum (Appendix 2)
MAA	Mean apparent amplitude, surface parameter (Chapter 5.0)
n	Refractive index (Chapter 2.4)
n	Revolutions per second (Chapter 3.1)
$P(\zeta)$	Probability or distribution function (Chapter 5.0)
P(z)	Probability density function (Chapter 5.0)
Q	Heat loss rate (Chapter 3.1)
Q	Flow rate (Chapter 3.2)
r,R	Radius (Chapter 2.4)
r,R	Fluid resistance (Appendix 1)
R	Electrical resistance (Chapter 3.1)
R_a	Centre line average, CLA, roughness amplitude parameter (Chapter 5.0)
R_q	Root mean square, RMS, roughness amplitude parameter (Chapter 5.0)
$R(\tau)$	Autocorrelation function, ACF (Chapter 5.0)

ENGLISH SYMBOLS (continued)

$\tilde{R}$	Surface geometry (Chapter 2.4)
S_p	Average slope (Chapter 4.0)
$S(\tau)$	Structure function (Chapter 5.0)
S_{abs}	Absolute mean value of surface slope (Appendix 1)
S_k	Skewness of the surface height distribution (Chapters 4 and 5)
t	Time
T	Temperature (Chapter 3.1)
u,v	Cartesian velocity components
u_i	Fluid velocity vector
u_τ	Friction velocity, $(\tau_\omega/\rho_\omega)^{\frac{1}{2}}$
U	Free stream velocity component
V	Voltage
V	Three-dimensional velocity vector (Appendix 2)
w	Angular velocity (Chapter 2.4)
W	Wake function, $W(z/\delta)$ (Chapter 2.4)
W	Weight (Chapter 4.0)
x,y,z	Cartesian coordinates
x_c	Convergence point for side-wall boundary layers (Chapter 2.4)
x_δ	Half-width value, a measure of the mutual top distance between roughness elements in the flow direction (Appendix 1)

GREEK SYMBOLS

α	Taper sectioning angle (Chapter 5.2)
β_1	Throat to pipe diamter ratio, Dall flow tube (Chapter 3.3)
β	Correlation length, autocorrelation function (Chapter 5.0)
γ	Specific gravity (Appendix 1)
δ	Velocity boundary layer thickness
δ_1	Displacement thickness, $\int_0^\infty (1 - \frac{\overline{u}}{U_e})\, dz$
δ_3	Dissipation thickness, $\int_0^\infty \frac{\overline{u}}{U_e}(1 - \frac{\overline{u^2}}{U_e^2})\, dz$
Δ	Defect thickness, $\int_0^\infty \frac{U_e - \overline{u}}{u_\tau}\, dz$
ΔB	Profile-shift parameter (Chapter 2.4)
Δ_1	Empirical constant, water current meter (Chapter 3.1)
ε	Height measured from crests of roughness elements (Chapter 4.0)
ε_1	Eddy viscosity (Appendix 2)
ζ	Measured height (Chapter 5.0)
η	Similarity variable (Appendix 2)
θ	Momentum thickness, $\int_0^\infty \frac{\overline{u}}{U_e}(1 - \frac{\overline{u}}{U_e})\, dz$
κ	Karman constant, ≈ 0.4
λ	Wavelength
λ_0	Vacuum wavelength (Chapter 2.4)
μ	Viscosity

GREEK SYMBOLS (continued)

ν	Kinematic viscosity, μ/ρ
π	3.14159....
Π	Coles' wake parameter (Chapter 2.4)
ρ	Density
σ	Standard deviation of surface heights, $\left[\frac{1}{L_y}\int_0^{L_y} z^2\ dy\right]^{\frac{1}{2}}$
τ_{ij}	Stress tensor
τ_ω	Wall shear stress
τ	Spatial distance (Chapter 5.0)
χ	Roughness function (Chapter 2.4)
ω	Radial frequency, $2\pi/\lambda$

DIMENSIONLESS GROUPS

C_{bv}	Bulk viscosity
C_d	Discharge coefficient
C_D	Dissipation coefficient
C_f	Local coefficient of surface friction
$C_{f(1)}$	C_f calculated from the momentum equation
$C_{f(2)}$	C_f calculated from the inner law
$C_{f(3)}$	C_f calculated from the inner law plus wake function
$C_{f_{L-T}}$	C_f calculated from the Ludwieg & Tillman formula
C_F	Moment coefficient
R_c	Channel Reynolds number, $U_e x/\nu$
R_e	Reynolds number
R_k	Roughness Reynolds number, ku_τ/ν
R_s	Ship Reynolds number, $U_s L_s/\nu$
∇	Gradient operator

SUBSCRIPTS

∞	Far field
e	Edge
w	Wall
0	Initial value
C	Critical
sc	Scattered beam
in	Incident beam
t	Turbulent
p	Probe
s	Sensor
L	Electrical leads
eff	Effective
x	x-component
cv	Control volume
cs	Control surface
1,0	Smooth walls

SUPERSCRIPTS

$\bar{}$	Time mean
'	Turbulent fluctuation
$\dot{}$	Time derivative
+	Law-of-the-wall variable

1. INTRODUCTION

The frictional resistance of a surface and its correlation to the surface geometry is of interest to workers in a wide range of disciplines. Manufacturers of extruded materials, for example, are interested in the flow of the material through the extrusion nozzle. The shape and surface geometry of the nozzle will affect the subsequent mechanical properties of the extruded product.

The flow around the relatively complex shape of a ship's hull is dependent on both the form of the hull and on its surface finish. Ideally, if surfaces could be made hydro- or aero-dynamically smooth then the naval architect's job of designing a ship form with minimum pressure drag and minimum shear drag would provide the optimum solution in terms of power required to propel the vessel at set conditions.

The process of transforming the architect's idealised ship form to the manufactured product superimposes a surface finish onto the ship form. This practical surface finish, even when the ship is brand-new, fails to satisfy the requirement of hydrodynamically smooth condition.

The study of the relationship between the surface finish and the overall performance of the ship hull (see Appendix 1) has shown there to be potentially very rewarding reductions in power consumption with the introduction of quality control on surface finish.

This investigation sets out to correlate specific parameters of surface finish to significant increases in the frictional drag for the case of open-channel flow over nominally flat surfaces. The work is

specifically related to the problem of the frictional drag of ship hull surfaces and the surfaces investigated include a 4.8 metre long replica surface of part of a ship hull.

In an investigation of the viscous shear and pressure forces resisting the motion of a ship hull it is important to know what the enveloping fluid 'sees' of the hull surface. On a typical in-service ship hull the external surface is made up of:

1. The roughness of the component sections of the hull surface - painted steel plates whose surface is made up of wavelengths from microns to metres. The short wavelengths are made up from: (a) the substrate surface finish; (b) the method of paint application; (c) the physical properties of the paint; and (d) the paint composition. The longer wavelengths are the waviness and errors of form of the hull plates.

2. A spectrum of surface wavelengths produced from the fabrication techniques used in constructing the hull surface. The short wavelengths are made up of joints, bulges and dents. The longer surface wavelengths, of up to hundreds of metres, make up the overall shape or curvature of the hull and the errors of form of the hull shape.

3. The smaller scale roughness, wavelengths from microns to several metres, can be substantially altered by: (a) chemical and mechanical damage; (b) the attachment of rigid marine growths such as barnacles; (c) the attachment of compliant growths of slimes and weeds.

Thus, the surface of a typical ship hull comprises a large number of surface features. Each of the surface features on the hull is bound to effect both a viscous shear component and a pressure (form) component to the frictional resistance of the surface.

The positioning of a surface feature on the hull will determine its contribution to the total resistance of the hull surface, since the outline shape of the hull will produce a variety of flow regimes around the hull. Hence for a full analysis of the frictional resistance of a ship hull surface a large selection of surface textures and flow regimes must be examined and the interaction between the different flow regimes and surfaces investigated.

The momentum balance of the flow provides the fundamental equations for the determination of the flow parameters whilst a statistical analysis of the surface geometry is used to characterise the surface. The existence of a logarithmic relationship for a region of the flow near to a solid boundary can be used as an alternative means of determining the flow parameters. Whilst the logarithmic 'law' (see Appendix 2), in its simplest form, is valid for two dimensional flow over hydrodynamically smooth surfaces, leading researchers have modified it to include surface roughness effects. Hence a number of empirical equations have been formed with various roughness function terms in an attempt to correlate surface frictional resistance with specific roughness parameters such as mean apparent amplitude and root-mean-square roughness. Although the basic logarithmic relationship has been shown to exist using the principles of dynamical similarity and other criteria the various off-shoot correlations have no real theoretical basis and therefore their use in this investigation is

merely as a means of obtaining the surface friction coefficient by an alternative method.

2. TECHNIQUES FOR THE EVALUATION OF THE FRICTIONAL DRAG OF SURFACES

2.1 The choice of flow system

An appropriate method of investigating the relation between the surface frictional resistance of a ship hull surface and its geometry would be to take flow measurements around the hull of a ship whilst she is in service and then correlate the resulting flow characteristics with the corresponding surface parameters measured whilst the vessel is in dry dock.

The practicalities of obtaining surface friction values around a ship hull present economic and instrumentation problems.

A number of workers have carried out ship trials from which the contribution the hull roughness makes to the hull's total drag has been determined from an analysis of the ship's propulsion power requirements. There is the inherent difficulty of separating the form (pressure-based) drag from the roughness (viscous-based) drag. This stems from the absence of flow measurements on hydrodynamically smooth hulls (Granville 1956).

More economically viable drag measurements on scaled-down models of ships suffer from the difficulties of the subsequent scaling-up of the ship model results to full-size. This involves checking the ship-model correlation using full-scale ship trials (see Appendix 1).

Apart from the methods of evaluating surface frictional resistance

from measurements of the energy required to propel the ship through the viscous fluid, the frictional resistance can also be determined from measurements of the velocity distribution in the shear layer around the moving ship. This can be done using rakes of probes set parallel to the flow stream lines around the submerged hull. Again there are a number of practical and economic difficulties to be overcome, and the derived values of the local coefficient of surface friction need to be treated with caution.

Thus, the difficulties encountered in measuring the surface frictional resistance of relatively complex ship hull forms, led to attention being directed towards the measurements of surface frictional resistance on simpler forms such as on plates (Schoenherr 1932) and in pipes (Nikuradse 1933). Relations were proposed for the correlation between pipes and plate friction measurements by Prandtl and Von Karman and between plate and ship frictional resistance values.
These correlations made it possible to study the effect of roughness found on ship hulls in a controlled laboratory environment. Thus neglecting the effect the shape of the ship hull has on the frictional resistance, ship hull surfaces can be reproduced on plates and on the inside of pipes and the frictional resistance determined. Thus the problem of measuring the frictional resistance of ship hull surfaces has been reduced to one of measuring the frictional resitance of pipes or of plates.

The removal of the long surface wavelengths when going from the curved body of a ship to the parallel flow situation on a flat plate or in a pipe assumes that these relatively long surface wavelengths, or features, make no contribution to the frictional resistance of the

surface. We are therefore faced with the problem of deciding when a surface wavelength is such that it no longer contributes to the frictional resistance of the surface.

As yet there is no theory to call upon to distinguish this limiting value of surface wavelength and therefore it would be presumptious to neglect surface features above or below any arbitrary value. Also, in attempting to make a comparison between hull frictional resistance and plate/pipes frictional resistance we are dealing with three fundamentally different flow patterns each of which will be affected differently by the surfaces under investigation.

In the pipe, the flow is constrained on all sides and therefore the shear layer is confined to the diameter of the pipe, in comparison to flow around a ship where there are no constraining boundaries and the boundary layer is free to develop around the greater part of the submerged hull.

In plate flow if we assume the plate to be infinitely wide, the flow will bear a closer resemblance to the flow around a ship, but the flow will be affected by the water-air interface. If the plate comprises the floor of a channel, then there will be three-dimensional effects due to the channel sides. Therefore, in order to reduce the number of differences in the comparison of the ship and laboratory flow regimes to a minimum, a flow channel is required which is as wide and as deep as possible and even then account must be taken of the inherent modifications to the flow (Grass 1971).

Using laboratory tests in pipes and on plates it is only possible

to measure the frictional resistance of a specimen piece of the hull surface and not the total contribution of all the different types of roughness in all the different flow regimes present on a hull surface.

2.2 The flow system

The flow system used in the present investigation consists of a parallel glass-sided, variable slope water channel. The channel sides are glass panels, 1.5 metres long, carefully butted together and the joints filled. The channel's variable slope facility along with an adjustable outlet weir enable a wide variation in the flow configuration within the open top channel. The flow conditions were, in fact, restricted to sub-critical (i.e. tranquil) mode to obviate the phenomena of shock waves forming at the sensing probes and oblique shocks generated from the imperfections of the channel sides. The channel is approximately 20 m long and 30.5 cm wide and can accommodate a plate or replica of a ship hull 30.5 cm wide up to 20 m long. A deturbulating tank with a streamlined converging section is bolted to the channel at inlet and is used to produce reasonably uniform flow at inlet, free of swirl and flow stratification - ideally one-dimensional potential flow.

The floor of the channel provides the base for the working surface, and is made up of box sections 30.5 cm wide by 3.05 m long which are securely bolted together and supported at three points, - on rollers at two jacking points and at one hinge point. A schematic diagram of the flow system is shown in Figure 2-1.

Preliminary tests were made in the flow configuration to be used,

to determine its suitability as applied to a study of the frictional resistance of ship hull surfaces. It is realised that the flow around the hull of a ship is very different to the confined flow of a water channel, and a comparison is only valid if account is taken of these differences and any results from the flow measurements adjusted accordingly.

2.3 Components of the flow system

Two pumps are available to provide the fluid motion through the open channel. The first of these, pump A, is capable of producing channel Reynolds numbers, Rc of up to a maximum of 3×10^6, where $Rc = U_e\chi/\nu$. Comparing this Reynolds number with typical ships Reynolds number, a modern sea-going vessel such as a 400 metre long tanker cruising at 15 knots (7.7 m/sec) develops a Reynolds number of 3×10^9. The ships Reynolds number is given by $R_S = U_S L_S/\nu$ where U_S = speed of the ship and L_S = the length of the ship.

A second, larger capacity pump B, loaned by BSRA has been installed into the flow system and this has been used to develop Reynolds numbers of up to 10^7.

The maximum usable value of R_c from pump B is somewhat less than this, in the region of 7×10^6. This is because at the higher Reynolds numbers the channel flow becomes supercritical which is undesirable for the present flow instrumentation. Apart from the limiting value of Reynolds numbers due to the onset of critical flow there is also a limiting depth of flow below which the flow effects due to the water-air interface become significant. The limiting depth

of flow in the channel was found to be in the region of 6 inches (15 cm).

The two pumps are operated separately, the inactive pump is isolated from the flow system using valves I and II (Figure 2-1). Pump B, the main pump, is a roto-dynamic pump of the radial flow type with a 36 cm (internal diameter) inlet and an 18 cm (internal diameter) outlet. In the present system the pump outlet is connected into the 15 cm (internal diameter) supply line to the flow channel. A Dall flow tube is positioned in the supply line with its pressure tappings connected to a mercury underwater manometer. From the supply line the water enters the flow channel via the deturbulating tank and a series of honeycombs.

Pump B operates under conditions of a negative static suction head, drawing water from a below ground level pit, 2 metres deep with a water capacity of 7.5 m^3 (1.7 thousand gallons). The pump when commissioned could deliver 4.0 m^3/min. at 960 rpm, but the pump has subsequently been derated by reducing the size of the impeller, to approximately 3.5 m^3/min. at 960 rev/min.

The smaller capacity pump A is an axial flow extraction pump with the pump head submerged in the water pit. The pump is capable of delivering 1.2 m^3/min. at 2900 rev/min.

For both pumps it was found necessary to introduce two honeycomb sheets into the deturbulating tank in order to remove large scale eddies and swirl which was otherwise entering the channel and producing non-uniform flow at the channel inlet. The swirl probably originates from two ninety degree bends in the pipe line preceding the

deturbulating tank. One of the honeycomb flow straighteners is positioned horizontally over the deturbulating tank inlet, and the other vertically across the channel inlet. Such an arrangement produced the desirable flow conditions at the inlet to the channel.

A continuous cycle filtration unit is incorporated in the system in order to keep the water at a high level of purity required to operate the flow instrumentation. For this, a portable extraction pump draws water from the sump. The water is then allowed to cascade by gravity through a series of different mesh size filter gauzes back into the sump. The gauzes are periodically removed and cleaned.

2.4 Techniques for measuring Cf

There are several techniques available for the measurement of the local coefficient of friction of a surface. Only a few of these are suitable for the particular experimental set-up used. These can be divided into four main types:

1. Pressure measurements.
2. Force measurements.
3. Heat transfer measurements.
4. Optical methods.

2.4.1 Pressure measurements

Devices such as Preston or Stanton tubes can be used to measure the surface friction directly. These are probably the most widely used of the manometric methods. Both are based or the universality of the velocity profile in the inner wall region. Preston's (1954)

method of determining C_f was to use a calibrated pitot tube placed in contact with the wall. The dynamical pressure p exerted on the tip of the tube depends on ρ, ν, τ_ω, the outer radius r and the inner radius r_i of the tube. The pressure measured by the total-head tube in conjunction with the surface static pressure measured at the same station along the plate was calibrated by Preston in terms of the local surface-shear stress.

There are several other types of pressure devices which can be used directly or indirectly to determine the surface friction. Devices such as the Preston tube can only be used on relatively smooth flat surfaces and provide an obstruction to the flow with subsequent alterations in the flow pattern around the area of measurement. Pitot-static tubes can be used to measure mean velocity profiles in the boundary layer which can then be used in the computation of C_f. The velocity measurements are absolute but they cannot be made near to the work surface since the resulting gap between the tube and the surface will act as a constriction to the flow, producing secondary flow effects which may be measured by the tube itself.

In a fully developed turbulent pipe flow the friction loss or pressure drop, simply related to the wall shear stress τ_ω, can be functionally related to the average velocity U of the pipe flow, pipe diameter D, fluid properties of density ρ and kinematic viscosity ν, and a geometrical description of the rough wall k, k_1, k_2,..... Musker et al (1976) used measurements from pipe flow to predict local surface friction coefficients for a ship hull surface, assumed equivalent to a plane surface. The pipe flow average velocity is chosen so that dynamic similarity between the flow in the inner regions of the

pipe flow and that on the ship hull can be assumed. The law of the wall combined with the law of the wake (Coles 1956) can be used to represent both the boundary layer flow on a flat plate without pressure gradient and the fully developed turbulent pipe flow for smooth surfaces. The effect of surface roughness on the mean velocity distribution is assumed to be given by

$$\frac{u}{u_\tau} = \frac{1}{\kappa} \log_e \frac{zu_\tau}{\nu} + C\left[\frac{ku_\tau}{\nu}\right] + \frac{\Pi}{\kappa}\omega\left(\frac{z}{\delta}\right)$$

where C is the law of the wall constant which depends on ku_τ/ν, k is the 'typical' roughness height.

Alternatively, the mean velocity distribution can be written as

$$\frac{u}{u_\tau} = \frac{1}{\kappa} \log_e \frac{z}{k} + \chi\left[\frac{ku_\tau}{\nu}\right] + \frac{\Pi}{\kappa}\omega\left(\frac{z}{\delta}\right)$$

where χ is a roughness function primarily dependent on the roughness Reynolds number ku_τ/ν.

From measurements of the static pressure drop and the mean velocity profiles in the pipe flow the roughness function χ, given by

$$\chi = \frac{1}{\kappa} \log_e \left[\frac{R_k e^{B\kappa}}{e^{-C_1 R_k} + C_2 R_k}\right] \qquad \text{(Musker et al 1976)}$$

where B = law of the wall constant, $R_k = ku_\tau/\nu$, and C_1 and C_2 are empirical constants determined from the roughness function, is calculated for a given surface. The working section of the pipe is lined with twelve identical 61 cm long cylindrical replicas of the surface under investigation.

Thus, by using dynamical similarity which requires that the roughness Reynolds numbers for the pipe and flat plate are identical, the full scale flat plate surface friction coefficients can be calculated knowing the roughness function for a given surface geometry.

2.4.2 Force measurements

The local surface friction can be measured directly on a specimen surface mounted movably in a sector of the principal surface. The arrangement is given the name floating-element sur ce friction balance (Smith & Walker 1957, Reda 1974, Driftmyer 1975 and Karlsson 1978).

The floating element is used by Karlsson (1978) to measure local surface friction values in a flat plate turbulent boundary layer. The measurements are part of an investigation into the effect of irregular ship hull roughness on the frictional resistance of full scale ships.

The floating element is located on the centre line of a wind tunnel wall covered with a positive replica of a rough ship hull surface. the floating surface is located flush with the surrounding surface using a dial gauge. Pressure tappings are located on the upstream and downstream edges of the element to allow the measurement of the pressure in the gaps ($\sim$ 0.3 mm wide).

The flow exerts a force F on the element surface and the element is displaced in the flow direction. F is given by

$$F = \tau_{\omega} . A$$

where A is the area of the floating surface.

A micrometer screw is used to restore the element to its unloaded position, which is indicated by a differential transformer. If there is no pressure difference around the edge of the element, the restoring force F_R will equal the force exerted by the flow. Pressure differences in the gap around the element will produce an additional force F_P given by

$$F_P = \Delta p b h$$

where b is the width of the floating element, h is the height of the floating element edge. Thus, resolving the forces in the direction of the fluid motion, gives

$$F = F_R + F_P \quad \text{(Figure 2-2)}$$

The local surface friction coefficient is obtained from the equation

$$C_f = \frac{2F}{\rho U_e^2 A}$$

The reference velocity U_e was recorded for all the measurements using a pitot-static tube of Prandtl's design and an accurate single-limb micromanometer (Preston 1954). Thus, readings taken from the floating element together with the velocity U_e and appropriate values of atmospheric pressure, wind tunnel temperature etc., were used to calculate the local surface friction coefficient as a function of unit Reynolds number U_o/ν

Roughness functions (Hama 1954) were also determined for each of

the replicated surfaces investigated.

Although the boundary-layer flow on a rotating disc is three-dimensional in constrast to the two-dimensional flow on a flat plate or axi-symmetric through a pipe, the rotating disc provides a convenient means of measuring surface friction effects particularly at high speeds. The torque or moment M of one side of a rotating disc in an unbounded fluid medium can be assumed to depend upon the angular velocity ω, the radius R, fluid properties of density ρ and kinematic viscosity ν, and the geometry of the disc's surface k, k_1, k_2 .....

By dimensional analysis the moment coefficient C_m is a function of two dimensionless groups, a Reynolds number R_e and a relative roughness R/k for a particular surface geometry $\tilde{R}$. Hence

$$C_m = f\left|R_e, \frac{R}{k}, \tilde{R}\right|$$

where $C_m = \dfrac{4M}{\rho R^5 \omega^2}$ and $R_e = \dfrac{\omega R^2}{\nu}$

Application of the similarity laws results in a logarithmic formula (Granville 1973) for rough surfaces

$$\frac{1}{\sqrt{C_m}} = A\sqrt{\frac{5}{8\pi}}\log_e R_e\sqrt{C_m} + \sqrt{\frac{5}{8\pi}}\left[B_{1,0} + (\Delta B)_e\right] - \frac{A}{\sqrt{10\pi}}$$

$$- A\sqrt{\frac{5}{8\pi}}\log_e \frac{55}{18}\sqrt{4\pi}A^2 - \frac{(\Delta B)_e'}{\sqrt{40\pi}}$$

where ΔB is the similarity-law roughness characterisation, $(\Delta B)_e$ and $(\Delta B)_e'$ are the values of ΔB and $(\Delta B)'$ at the edge of the disc. $B_{1,0}$ is the value of the inner law constant for smooth walls, and $(\Delta B)' = \dfrac{d\Delta B}{d \log_e R_k}$. R_k is a roughness Reynolds number, $u_\tau k/\nu$.

For a smooth surface $\Delta B = 0$ and $(\Delta B)' = 0$.

Hence,

$$\frac{1}{\sqrt{C_m}} = A\sqrt{\frac{5}{8\pi}}\log_e R_e\sqrt{C_m} + \sqrt{\frac{5}{8\pi}}B_{1,0} - \frac{A}{\sqrt{10}} - A\sqrt{\frac{5}{8\pi}}\log_e\frac{55}{18}\sqrt{4\pi}\ A^2$$

Thus, correlating plots of $1/\sqrt{C_m}$ against $\log R_e\sqrt{C_m}$ for smooth and rough surfaces, the local friction at the edge of the disc is given by

$$\left(\frac{u_r}{\omega R}\right)_e = \sqrt{\frac{5}{8\pi}}\sqrt{C_m}\left\{1 - \left[2A + (\Delta B)_e'\sqrt{\frac{1}{40\pi}}\sqrt{C_m}\right]\right\}$$

A similar analysis can be used to relate the torque or a rotating drum in an unbounded fluid to its surface geometry. This technique is presently used by workers at Newcastle University to investigate the frictional properties of ship hull surfaces.

2.4.3 Heat transfer measurements

Instruments based on a heat transfer principle such as the hot-wire anemometer have a small size of the sensing element producing negligible disturbances to the flow, good response to high-frequency fluctuations and suitability for electronic instrumentation. The instrument can be used within a few thousandths of an inch of a solid surface. The detecting element consisting of a very fine short metal wire or film, only a few microns in diameter. The element is heated by ar electrical current and when placed in a flowing fluid is cooled by the fluid, causing the temperature to drop and, consequently, the electrical resistance of the wire to diminish. Hence the anemometer

can be used to record fluctuating velocities of very high frequency and in the case of evaluating C_f can be used to measure the mean velocity distribution down to very near to the solid surface. The main disadvantage of the anemometer is that it is comparative rather than absolute and thus its accuracy depends on the method of calibration. Ideally the detecting element should be calibrated in the same flow situation as that in which it is to be used so as to reduce the number of variables affecting the calibration. The heat-transfer characteristics of the sensing element can change if it becomes contaminated with dirt or if in the case of water flow, bubbles form on it. Hence the instrument can only be operated in a 'clean' environment. When the sensor is placed in close proximity to a solid boundary having a different thermal conductivity than the surrounding fluid, the heat loss from the sensing element will vary (Wills 1962).

The standard anemometer unit has one sensing element which can measure velocity fluctuations in two dimensions, but measuring probes with two sensing elements perpendicular to one another are available for measurement of the turbulence intensity in three dimensions. This measurement is essential for the correct computation of the flow parameters. For an approximate analysis of the flow the turbulence term is generally assumed to be negligible but for cases such as flow over 'rough' surfaces the turbulence term becomes increasingly significant in any subsequent analysis.

2.4.4 Optical methods

Included in this section is the measurement of fluid velocities using the Doppler shift of a scattered laser beam, first used and

suggested by Yeh and Cummins (1967). Light scattered by a moving particle causes a Doppler shift f_D in frequency, giving the following approximate relation, when the velocity is very small compared with the velocity of light

$$f_D = (n/\lambda_0)\ U_i \left| (ej)_{sc} - (ej)_{in} \right|$$

where n is the refraction index of the fluid, U_i is the fluid velocity vector, λ_0 the vacuum wavelength and $(ej)_{sc}$ and $(ej)_{in}$ are the unit vectors in the direction of the scattered beam and of the incident beam respectively.

The experimental set up is shown in Figure 2-3. The light from the incident beam scattered by the fluid particles, in the direction of the photomultiplier, combines with the non-scattered reference beam. The photomultiplier acts as an amplifier and as a heterodyne receiver. Such a receiver mixes two signals of different frequencies and produces an output signal with a frequency equal to the difference in the frequencies of the input signals. Hence the receiver generates a current whose AC component is equal to the difference, Doppler, frequency. When U is the velocity of the fluid at the point of intersection of the two beams, the difference frequency is

$$f_D = (2n/\lambda_0)\ U\ \mathrm{Sin}(\theta_i/2)$$

where angle θ_i is measured in the fluid.

The advantage that optical methods have over all the other techniques available is that they do not physically interfere with the

flow and also they are absolute. The instrument is ideally suited to measuring high-frequency velocity fluctuations. Information about the turbulence can be obtained by utilising a spectrum analyser whose output is scanned and integrated.

2.4.5 The measurement of C_f in this investigation

It can be seen from the preceding notes that the two most versatile and appropriate techniques for the measurement of the coefficient of frictional resistance, or for that matter any other flow parameter, are the Hot-wire/film anemometer and the Laser Doppler-Shift instrument. The Laser Doppler-Shift method is more attractive than the Hot-wire/film anemometer in that it requires no calibration and does not interfere with the flow. In fact, the Laser method would be ideally suited to the task of calibrating the anemometer sensing elements in the working fluid. However, such an instrument was not available for the present investigation. Hence the hot-film anemometer with a single cylindrical sensor is used to record the velocity distributions across the boundary layer adjacent to the work surface. The anemometer was calibrated, in 'fully' developed smooth turbulent flow, on the axis of a horizontal glass flow tube connected to a constant-head water tank (Chapter 3).

The resulting boundary layer velocities are analysed using the streamwise momentum integral, given by

$$\frac{d\theta}{dx} + (H + 2)\frac{\theta}{U_e}\frac{dU_e}{dx} = \frac{C_f}{2} + \frac{\theta}{x_c - x} + \frac{1}{U_e^2}\frac{d}{dx}\int_0^{\delta} (\overline{U^2} - \overline{V^2})\, dx$$

[Flow convergence term] [turbulence term]

The magnitude of the turbulence term is assumed to be small compared with the other terms. Three-dimensional effects due to the side wall boundary layer development in a confined channel flow configuration can be accounted for in the term $\theta/(x_c - x)$, where x_c, measured from the channel inlet, is the estimated point of convergence of the side wall boundary layers. The component of hydrostatic pressure force with streamwise direction for side wall boundary layer development is assumed to be negligible.

The flow measurement instrumentation available restricts the analysis to the case of two dimensional flow. Hence, for the analysis to be valid, the turbulent intensity of the flow must be such that the corresponding turbulence term is relatively small.

Typical parameters which are required in the flow analysis include x, U_e, R_c, θ, δ_1, H and C_f.

The distance x is measured along the channel length from the plane joining the outlet of the streamlined deturbulating tank to the parallel-sided channel. The free stream velocity U_e is measured on the channel centre line at a distance x and is used in the calculation of the value of the Reynolds number of the channel flow, R_c. The momentum thickness θ, displacement thickness δ_1 and shape factor H are determined for points along the centre line of the channel working surface using the respective boundary layer velocity distribution data. A computer program computes the values of θ, δ_1 and H from the formulae

$$\theta = \int_{z=0}^{\delta} \frac{u}{U_e} \left(1 - \frac{u}{U_e}\right) dz$$

$$\delta_1 = \int_{z=0}^{\delta} \left(1 - \frac{u}{U_e}\right) dz$$

$$H = \delta_1/\theta$$

Thus, using the computed values of θ and H and graphically determined values of dU_e/dx and $d\theta/dx$ over the work surface, a series of values of $C_{f(1)}$ are determined from the two-dimensional momentum integral equation.

Corresponding values of $C_{f(2)}$ are computed (see Appendix 4) assuming the validity of a logarithmic region in the boundary layer velocity distribution. Values of $C_{f(3)}$ are also computed by fitting the boundary layer velocity distribution to a logarithmic plus a wake relationship given by

$$\frac{\bar{u}}{u_\tau} = \underbrace{\frac{1}{\kappa} \log_e \frac{z u_\tau}{\nu} + B}_{\text{logarithmic function}} + \underbrace{\frac{\Pi}{\kappa} . W \left(\frac{z}{\delta}\right)}_{\text{wake function}}$$

Date

Chart No.

FIG. 2-1 THE FLOW SYSTEM

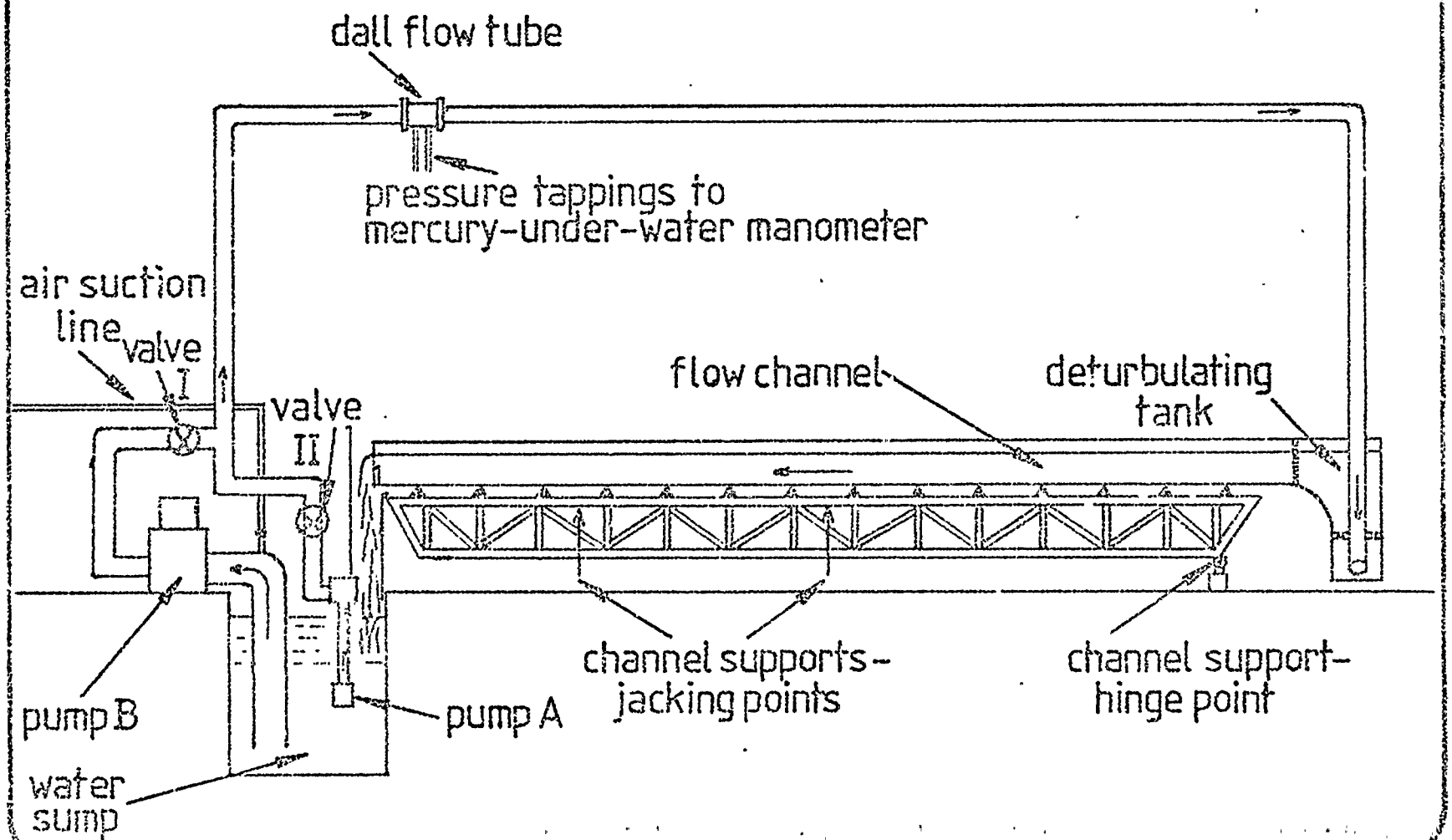

FIG. 2-2 THE FLOATING ELEMENT
SURFACE FRICTION BALANCE
(Karlsson, 1978)

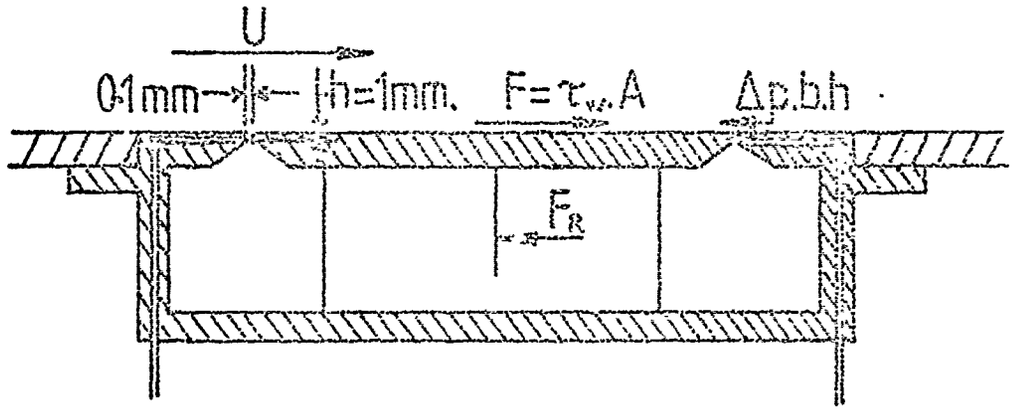

FIG. 2-3 THE LASER-DOPPLER ANEMOMETER

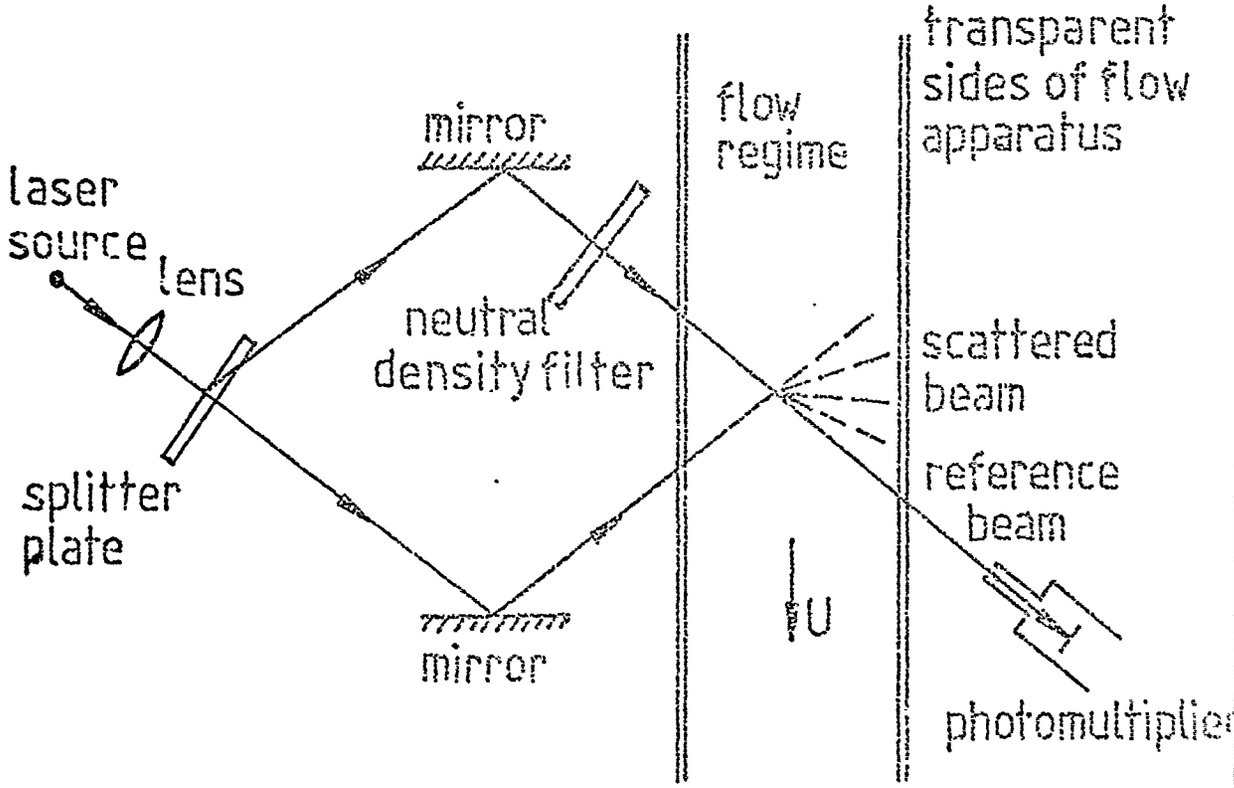

3. FLOW MEASUREMENT INSTRUMENTATION

3.1 Introduction

Preliminary measurements of the flow, where no great accuracy in the velocity readings near the solid boundaries is required, were carried out using a pitot-static tube and a propeller type current meter. Flow velocities in the case of the pitot-static tube were calculated using readings of stagnation and static pressures, resulting in an absolute measure of velocity.

The pitot-static tube is connected to a water manometer open to the atmosphere, the difference in the two pressures is measured in terms of the height difference in the manometer readings. The set up was such that the manometer readings for th' stagnation and static pressures could be measured separately using a depth gauge from the open top of the manometer tube. Arrangements were made to purge the pitot-static tube and manometer of air locks and obstructions using an air suction line and a pressurised water line (Figure 3-1). The pitot-static tube is held in position by a carriage arrangement which allows it movement in the x, y and z directions. A serious disadvantage of using the pitot-static tube in a liquid environment is the length of time that must be allowed for the manometer reading to settle down to an equilibrium position before a reading can be taken.

An alternative to the pitot-static tube is a water current meter. The current meter used consisted of a propeller unit, comprising the propeller, the shaft, the rotating sleeves and ball-bearings and a meter body, containing the electrical impulse generating unit plus

an electrical connection to an electrical counter which registers each revolution of the propeller. A stop-watch is used to register the number of revolutions per second, n, and the mean flow velocity computed from the calibration

$$U = K.n + \Delta_1$$

The constants K and Δ_1 are predetermined for the particular propeller used. The resulting velocity profiles were used to determine the approximate extent of the side wall shear layers.

The flow analysis used necessitated measuring the boundary layer velocity distribution very close to the work surface. Hence the measuring probe used must be as small as possible. This is especially so in the region near the surface where the gap between the probe and surface could act to accelerate the flow through the constriction so formed and hence produce a change in the flow pattern in the vicinity of the measuring probe. Both the current meter and pitot-static tube cannot be relied upon to give reliable velocity measurements close to a solid boundary due to their relative size. These instruments also have the disadvantage that they do not have an electrical output which can be electronically manipulated to provide the required fluid parameters. The hot-film anemometry has the advantage of an electrical signal and the measuring probe is relatively small.

3.2 The constant temperature anemometer

The use of hot sensors for the measurement of particle velocity in fluid flow relies on a relation similar to the formula derived by

King (1914) governing convective heat transfer from a cylinder in an incompressible potential flow. According to King, the rate of heat loss Q and flow velocity U are related through

$$Q = (A_1 + B_1 \sqrt{U}) \ (T - T_0)$$

where A_1 and B_1 are empirical constants, U is the flow velocity, T is the wire temperature and T_0 is the fluid temperature for thermal equilibrium conditions. The rate of heat loss from the sensor must equal the heating power produced in the wire by the electric current I.

Incorporating the temperature differences between the wire and fluid in the empirical constants A and B, the heat loss formula takes the form

$$I^2 R/R - R_o = A + B \ (U)^n$$

where R is the operating resistance of the hot-film, R_o is the resistance of the hot-film at fluid temperature and values of A, B and n are determined to give the best fit to the measured data within a selected velocity interval.

The anemometer output is a bridge voltage V, and the squared voltages V^2 and V_o^2, where V_o is the bridge voltage at zero velocity, are linearly related to the heat loss of the sensor at the velocity in question and at zero velocity respectively.

An analog computer is used to linearise the anemometer so that the meaurements of fluctuating velocities and velocity profiles are not

affected by amplitude distortion. The analog computer used has the following transfer function

$$V_{out} = K(V_{in} - V_{ino})^{m}$$

Thus, the non linear relationship,

$$V_B^2 = A + BU^n$$

between the output voltage V_B from the hot wire or hot-film anemometer and the measured flow velocity (U) can be linearised to read

$$V_{out} = KU$$

with good approximation down to velocities of 20 cm/sec.

3.2.1 Theory of operation of the CTA

Figure 3-2 shows a circuit diagram of the Disa CTA unit used. The sensing device used consists of a thin electrically heated metal film fused to a quartz fibre for support. The fibre plus film has a thin insulating coat of quartz and is suspended between the two probe supports.

The hot film probe forms one arm of a wheatstone bridge circuit, the other arm consisting of a 'non' inductive variable resistance box. The bridge is powered by an amplifier whose output voltage is controlled by the bridge imbalance. The system operates as a so-called null-seeking device. That is, if for instance, the probe resistance

is less than the resistance of the adjustable bridge arm, then an error voltage will be produced across the amplifier inputs. This voltage is applied across a very high gain amplifier and back to the bridge top so that the current through the bridge increases, causing the probe to heat up until its resistance is equal to the value of the variable resistance box, whereupon the bridge is again in balance.

Any flow over the probe will try to cool it, resulting in a small change in the probe resistance which in turn produces an error voltage across the bridge. This voltage is amplified in the servo amplifier and fed back to the bridge top, causing the bridge current to increase and the probe temperature to return to its original value. The voltage which is fed to the bridge top to maintain the probe temperature can be related to fluid velocity by calibration.

3.2.2 The probe operating resistance

The probe resistance is determined using the following procedure:

1. The probe cable and support are terminated using a shortening probe and the bridge is adjusted for balance with the feedback loop open by adjusting a potentiometer which is connected in series with the decade resistance box.

2. The shortening probe is then replaced by the actual probe to be used and again the bridge is adjusted for balance, this time by adjusting the resistance box. The resistance reading on the decade box corresponds to the cold resistance of the probe Rp (assuming a bridge ratio of 1:1) when

$Rp = R + R$

R_S = Sensor Resistance (at ambient temperature)

R_L = Resistance of probe leads

3. The required operating resistance (R_t) for the probe can now be set on the decade resistance using the formula

$$R_t = R_S + R_L (1 + \alpha (T - T_o))$$

where R_S is the sensor resistance at temperature T_o (ambient temperature), α = temperature coefficient of resistance of the sensor material and T = required operating temperature of sensor ($<150^oC$). The bridge is now balanced.

4. Turning the anemometer control switch to operate, which closes the feedback loop, causes the probe to heat up until its resistance reaches the required value and the anemometer is ready for use.

3.2.3 Frequency response

The anemometer is checked to make sure the instrument is not oscillating due to imbalance of the reactance on the two sides of the bridge. Moreover since the anemometer is designed to measure rapidly fluctuating velocities, the frequency response of the system is also checked.

The ideal way to check system stability and frequency response would be to place the probe in a flow and to subject it to a step change in velocity. By observing the anemometer output on an oscillo-

scope the impulse response of the system could be checked. In practice we simulate this by feeding an electrical square sine wave signal to the servo amplifier output. This causes a sudden increase in probe current and resulting bridge imbalance. The imbalance is amplified and fed back to the bridge top to restore balance. The anemometer output voltage meanwhile is monitored on an oscilloscope. Any instability in the system will result in oscillations on the anemometer response. Using the square wave generator, the frequency response of the CTA bridge is optimised with the bridge balanced.

3.2.4 Probe contamination

Before taking any measurements with the hot-film probe, it is lightly brushed with a dilutic solution of acetic acid to remove any impurities from its surface which may alter the heat transfer characteristics of the sensing element.

A filtration unit is incorporated in the flow system to remove any impurities which may enter the system via the channel's free surface or from corrosion of the connecting pipes. At low velocities, the probe is prone to air bubbles collecting on its surface which will lead to 'hot spots' on the sensing element which may cause it to burn out. In the case of air bubbles collecting on the probe surface, the probe current is switched off, the probe raised above the water, returned to its original position, and the measurements resumed.

3.2.5 Probe traversing technique

The hot-film is held in position using a carriage similar to that

used for the pitot-static tube and the current meter. A scale along the length of the channel plus scales on the vertical and cross-wise axis of the probe make it possible to relocate the sensing element to any point in the flow. The probe guide tube is earthed so as to prevent the build up of charge on the film sensor.

An off-set probe is used to take measurements very close to the channel floor; the orientation of the probe is such that the probe measures the velocity fluctuations in the x and z flow directions. The hot-film element is primarily sensitive to the component of flow velocity normal to the axis of the sensing element.

If the probe is yawed about an axis normal to the sensing element a progressively shorter length of the element will be exposed to the flow cooling effect and the sensitivity will fall. At a yaw angle of 90^{o}, that is when the flow is parallel to the sensing element, there will be a minimal cooling effect and therefore flow components along the sensor can be neglected. The sensitivity of a hot-film probe to variations in yaw angle is given by

$$U_{eff} = U \cos \alpha_1$$

where U = actual flow velocity, U_{eff} = effective cooling velocity and α_1 = yaw angle.

Considering the probe in a typical flow field, there will be a mean velocity $\overline{U}$ along the axis of the probe support and fluctuating velocity components u, v, w in the x, z and y directions. As has already been discussed, the effect of flow along the sensing element

has a negligible cooling effect and the component of velocity that the probe will measure is therefore

$$U_r = \left((\overline{U} + u)^2 + v^2 \right)^{\frac{1}{2}}$$

In a low turbulence flow field u and v are small, then

$$U_r = \overline{U} + u$$

3.2.6 Probe calibration

The experimental set up of the hot-film calibration rig is shown in Figure 3-3. The rig consists of a glass calibration tube 2.15 cm in diameter and 4.6 m long (≈ 200 diameters) connected via a globe valve to a constant head reservoir which is supplied with water pumped from the channel system. Hence, the hot-film probe is calibrated in a situation where the intensity of turbulence is at a minimum i.e. at the centre line into smooth turbulent pipe flow.

The calibration tube is slung between the sides of the flow channel above the level of water, so that the probe can be raised above the channel water level and inserted inside the outlet end of the calibration tube and a calibration performed without moving the probe from the channel system.

Various flow rates can be achieved by adjustment of the globe valve on the outlet of the constant-head tank. The flow rate in the calibration tube, and hence the mean velocity, are determined from the discharge rate measured over a minimum period of 30 seconds, the

water collected in a polythene bag and the volume measured. From a knowledge of the tube flow Reynolds number assuming the probe to be positioned on the calibration tube centre line, then the relation between the mean velocity and the centre line velocity (Figures 3-4 and 3-5) can be used to calculate the centre line velocity (NASA 1963). The centre line velocity is then related to the CTA bridge voltage and the probe calibrated. Typical calibration curves are shown in Figures 3-6 and 3-7. Calibrations are taken for each of the Linearliser unit exponent values and best fit lines by least squares fitted through each set of data. Thus the most appropriate exponent value for linear calibration can be determined. This value is then used for all the probe measurements.

3.2.7 Probe operation

After calibration the probe is immersed in the channel flow, and the operating resistance calculated and set for the existing water temperature. The probe is then ready for the measurement of water flow velocities at the same temperature. If the water temperature changes because of the heating effect of the pump or changes in the atmospheric temperature then the operating resistance must be re-calculated and reset on the CTA unit, thus providing a constant overheat ratio.

The probe is manually positioned for the first reading, the CTA unit and then the data logger switched on, and the linearised bridge voltage sampled at 0.33 second intervals over a period of 10 seconds. The sampled voltage is recorded on punched paper tape for a subsequent computer analysis. After the sampling period the data logger is switched off, the probe moved to the next measuring point and the

sampling procedure repeated. In the case of vertical velocity profile measurements the flow is sampled at points very close together (1 mm apart) in the floor shear layer region and at points further apart (1 cm) in the free-stream region. This is to enable an accurate measurement of the comparatively steep velocity gradients present in the shear layer.

For cross-channel constant depth flow measurements the probe is moved in equal comparatively larger (1 inch) steps across the channel width to gain a general picture of the side wall shear layer development and the central core flow. The resulting values of mean voltage for each of the measuring points at a station, along with a corresponding value of free stream velocity, are converted into mean velocities using the appropriate hot-film calibration.

The free stream velocity is measured using the Ott current meter which gives a value of velocity integrated over the area generated from the propeller radius, which is then assigned to the mean value of measured anemometer voltage in the same region of flow.

3.3 The Dall flow tube

A Dall tube measuring device is incorporated in the pipeline between the pumping station and the channel inlet to give a measure of the water flow rate through the channel at any particular set of flow conditions.

The Dall tube is a modified Venturi tube. The tube inlet incorporates a dam followed by the inlet converging cone and then a narrow

cylindrical section on either side of the throat slot. The flow then encounters the recovery diverging cone with an included angle of about 15 degrees after which the flow undergoes sudden enlargement to the pipe diameter. The cones are steep in addition to being truncated, and the whole device is only about 2 diameters long. There are no gradual curves as in Venturi tubes, and other devices which are intended to accelerate or decelerate a fluid with minimum loss.

The differential pressure produced by a Dall flow tube is much higher than that of a corresponding nozzle or Venturi tube. The flow rate, Q, is determined from the pressure differences created by the constriction in the meter, where Q is given by

$$Q = C_d A_2 \sqrt{2gH} / \sqrt{1 - m^2}$$

and which is valid for one dimensional flow as given by Bernoulli. Variations from the one-dimensional theory are all included in the particular value used for the coefficient C_d. A typical calibration curve of C_d values is shown in Figure 3-8 and values of C_d for different Dall flow tube, throat to pipe diameter ratios, β_1 , are plotted in Figure 3-9

Pipe Reynolds numbers of the order 3.5×10^5 and above need to be reached before the value of C_d can be assumed to be constant. In the calibration rig available the maximum obtainable Reynolds number is approximately 3.7×10^5 and therefore it was not possible to calibrate the Dall flow tube in its linear working region. The value of C_d for the Dall flow tube was therefore determined from Figure 3-9 for a pipe ratio, β_1 , of 0.643 and for Reynolds numbers greater than 3.5×10^5.

$$C_d \simeq 0.69$$

FIG.3-1 THE PITOT-STATIC TUBE MEASUREMENT SYSTEM

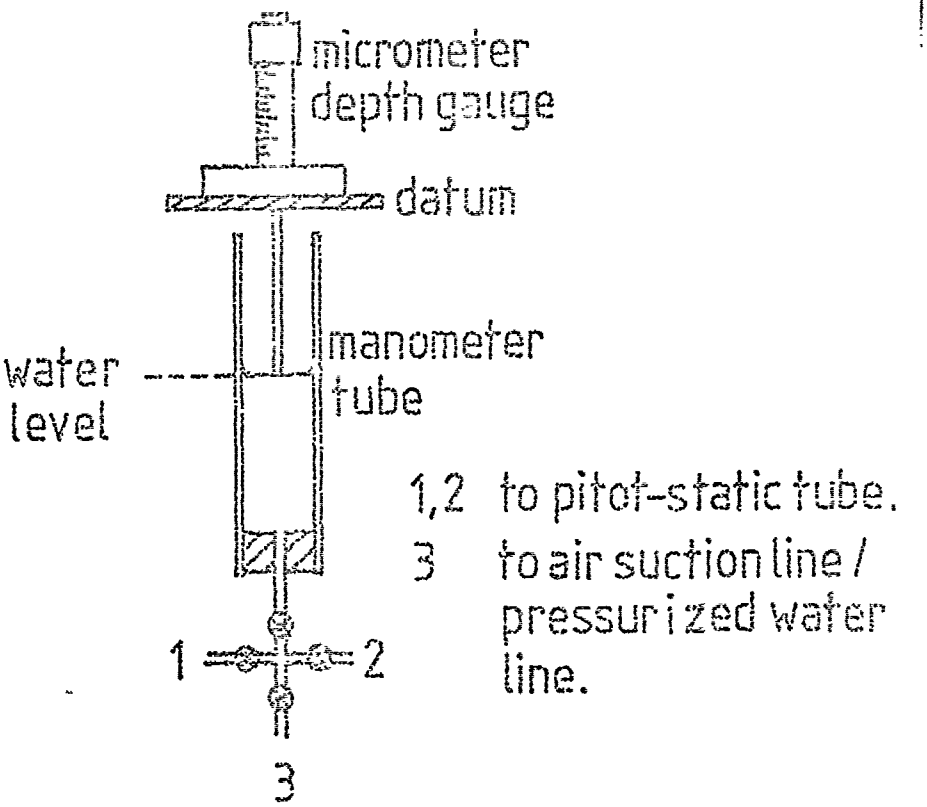

FIG.3-2 THE CONSTANT TEMPERATURE ANEMOMETER

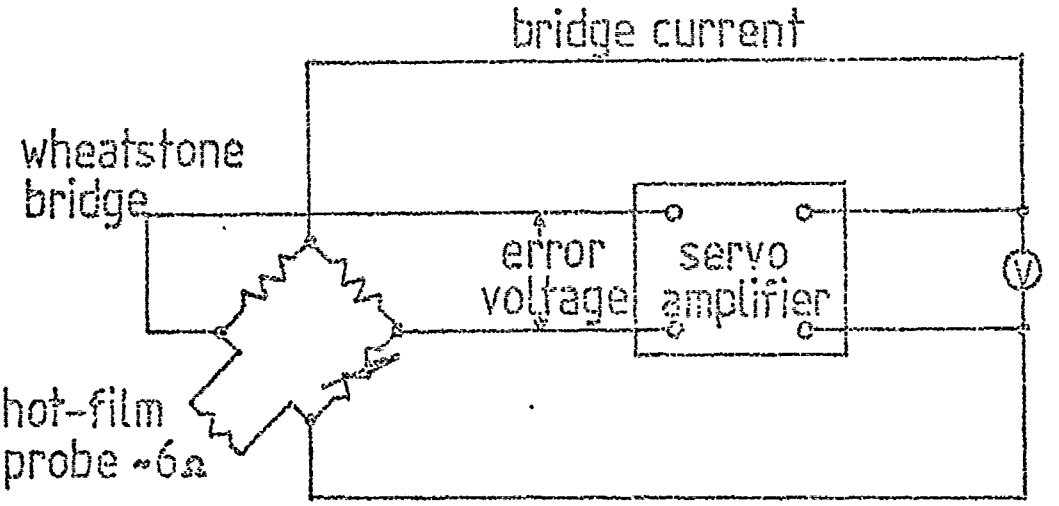

Date

Chart No.

FIG. 3-3 THE CTA CALIBRATION SYSTEM

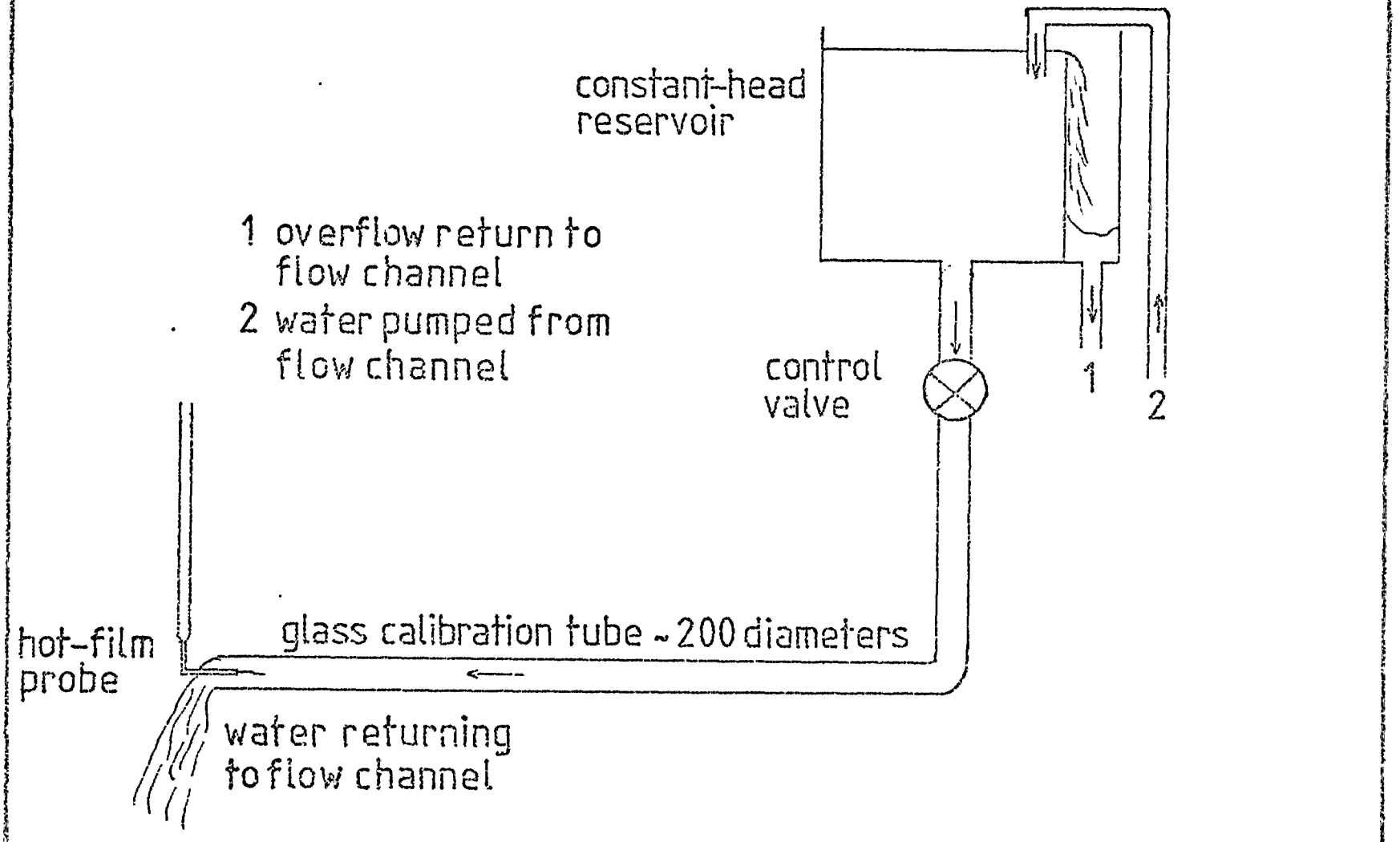

FIG 3-4 RATIO OF MEAN VELOCITY TO CENTRE-LINE VELOCITY VERSUS MEAN VELOCITY REYNOLDS NUMBER INCOMPRESSIBLE PIPE FLOW (NASA,19)

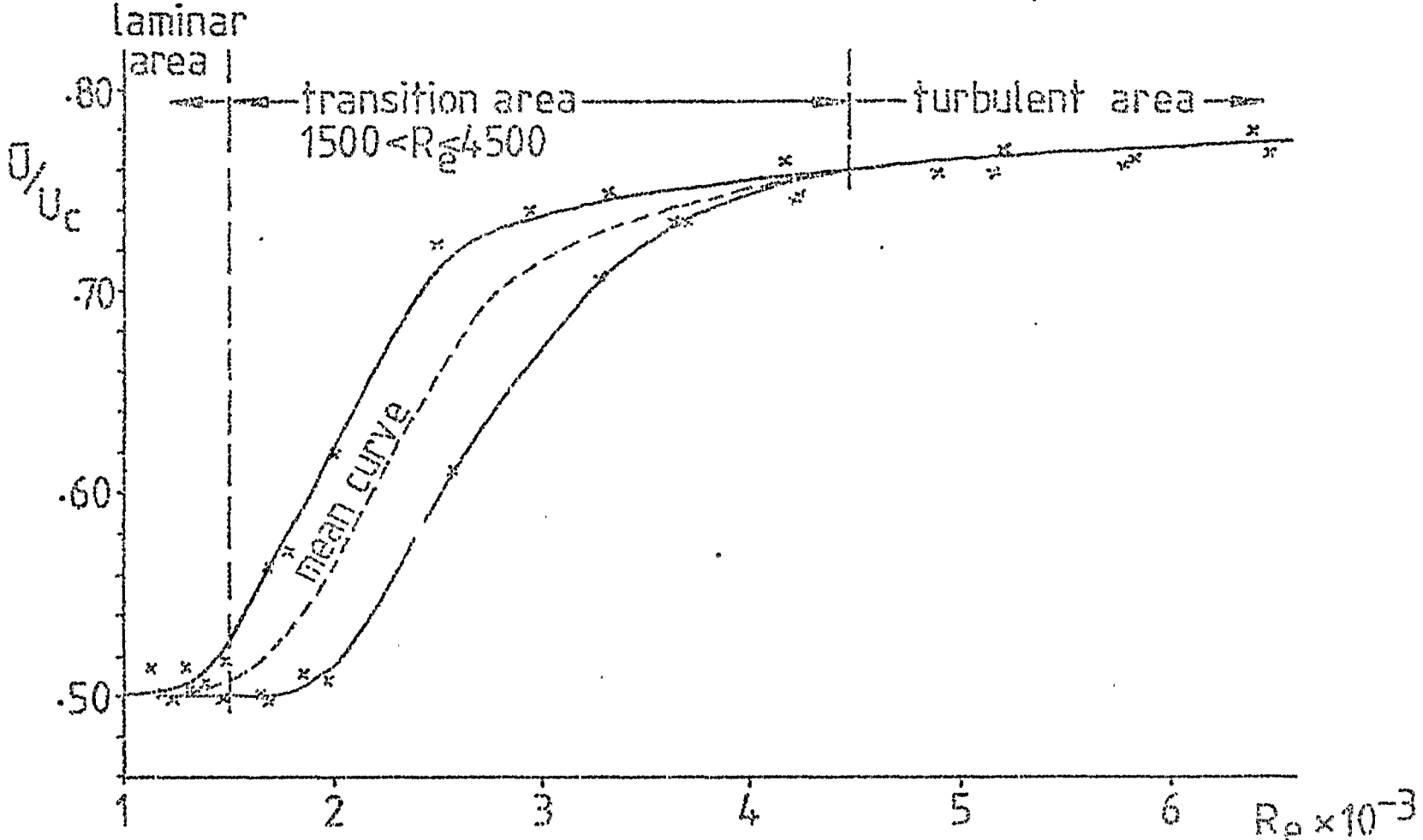

FIG 3-5 RATIO OF MEAN VELOCITY TO CENTRE-LINE VELOCITY VERSUS MEAN VELOCITY REYNOLDS NUMBER INCOMPRESSIBLE PIPE FLOW (TURBULENT) (NASA, 19)

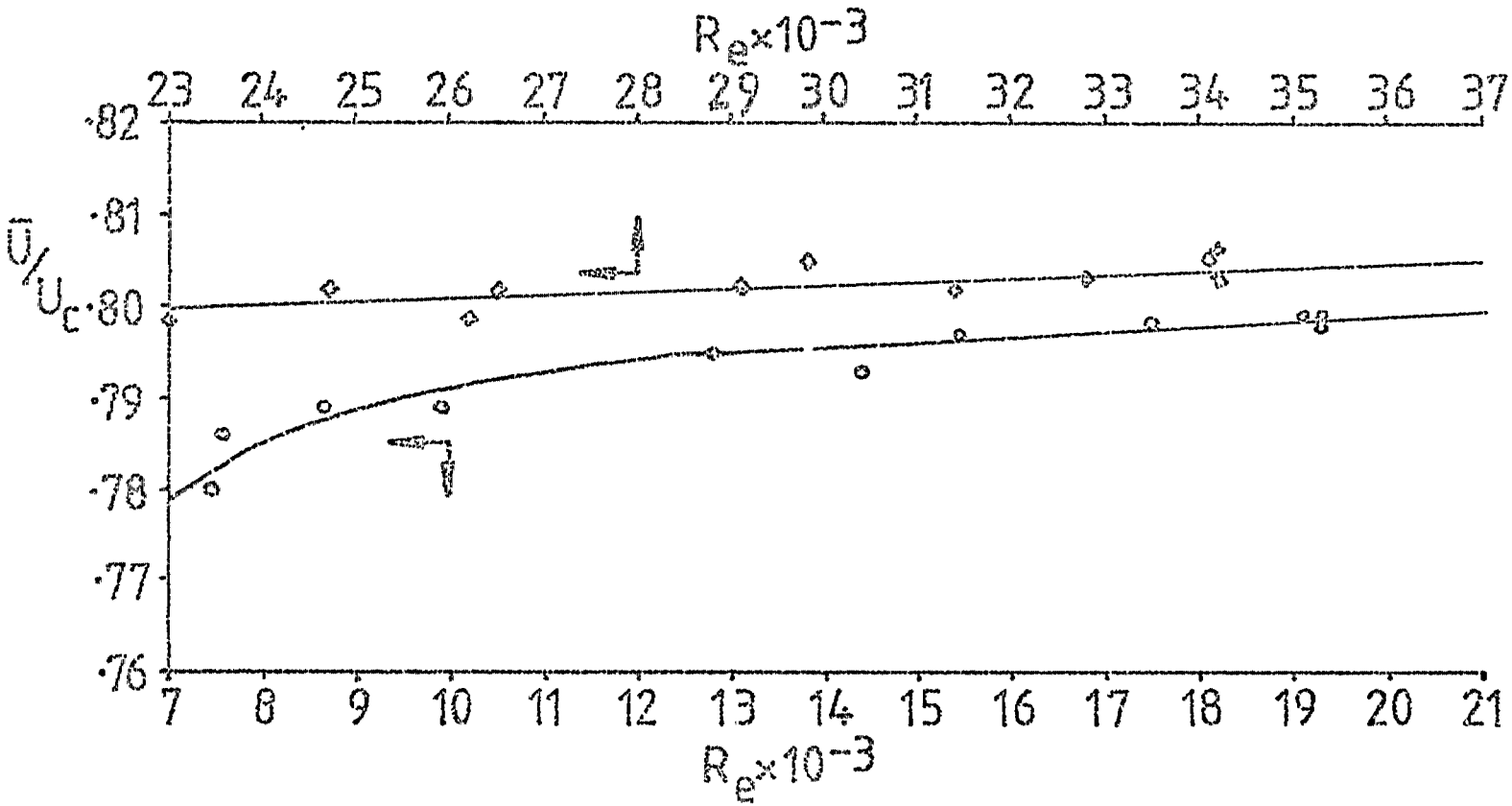

FIG 3-6 CTA BRIDGE VOLTAGE VERSUS CENTRE-LINE VELOCITY CALIBRATION

CTA lineariser exponent value = 4

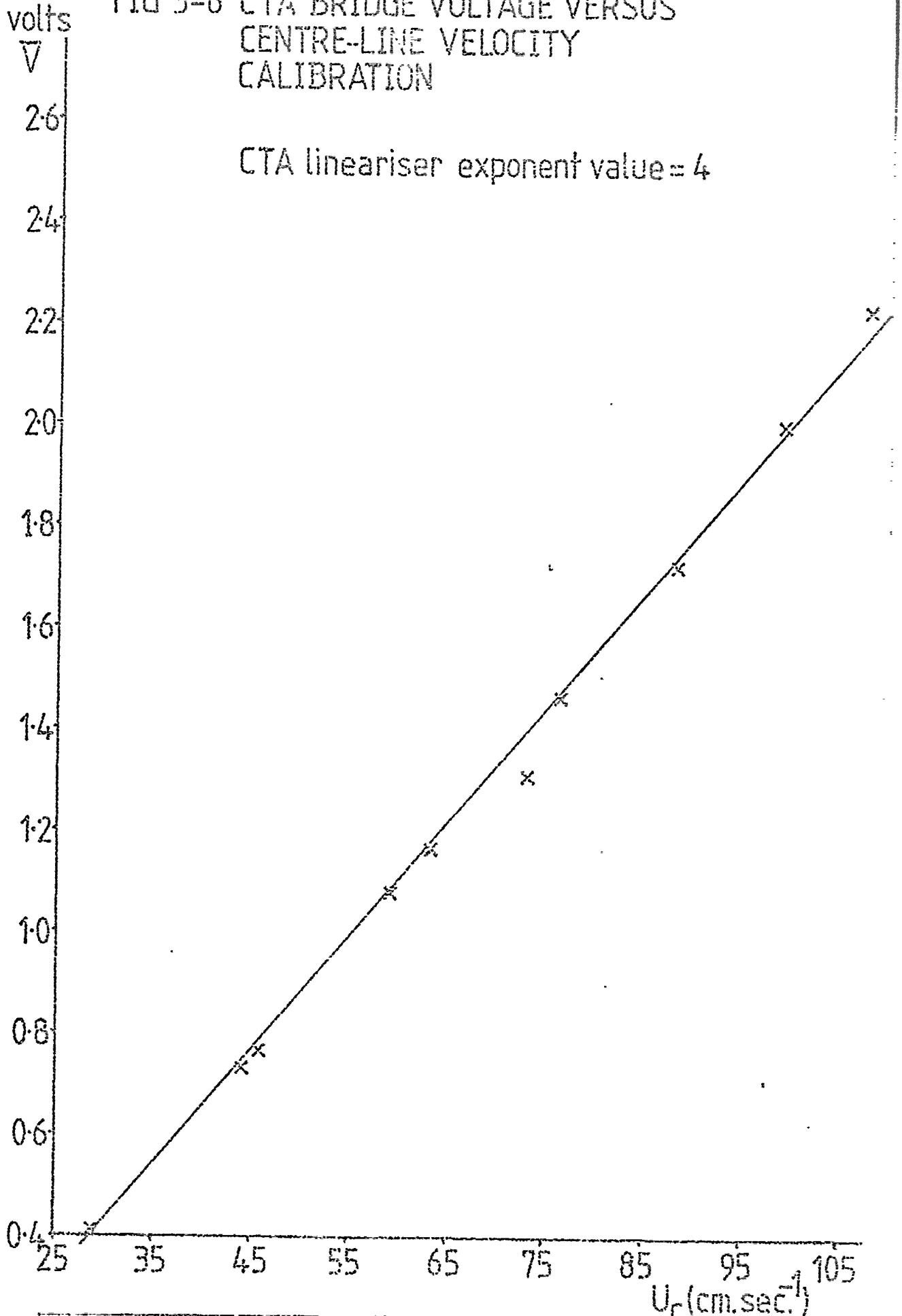

FIG 3-7 CTA BRIDGE VOLTAGE VERSUS CENTRE-LINE VELOCITY CALIBRATION

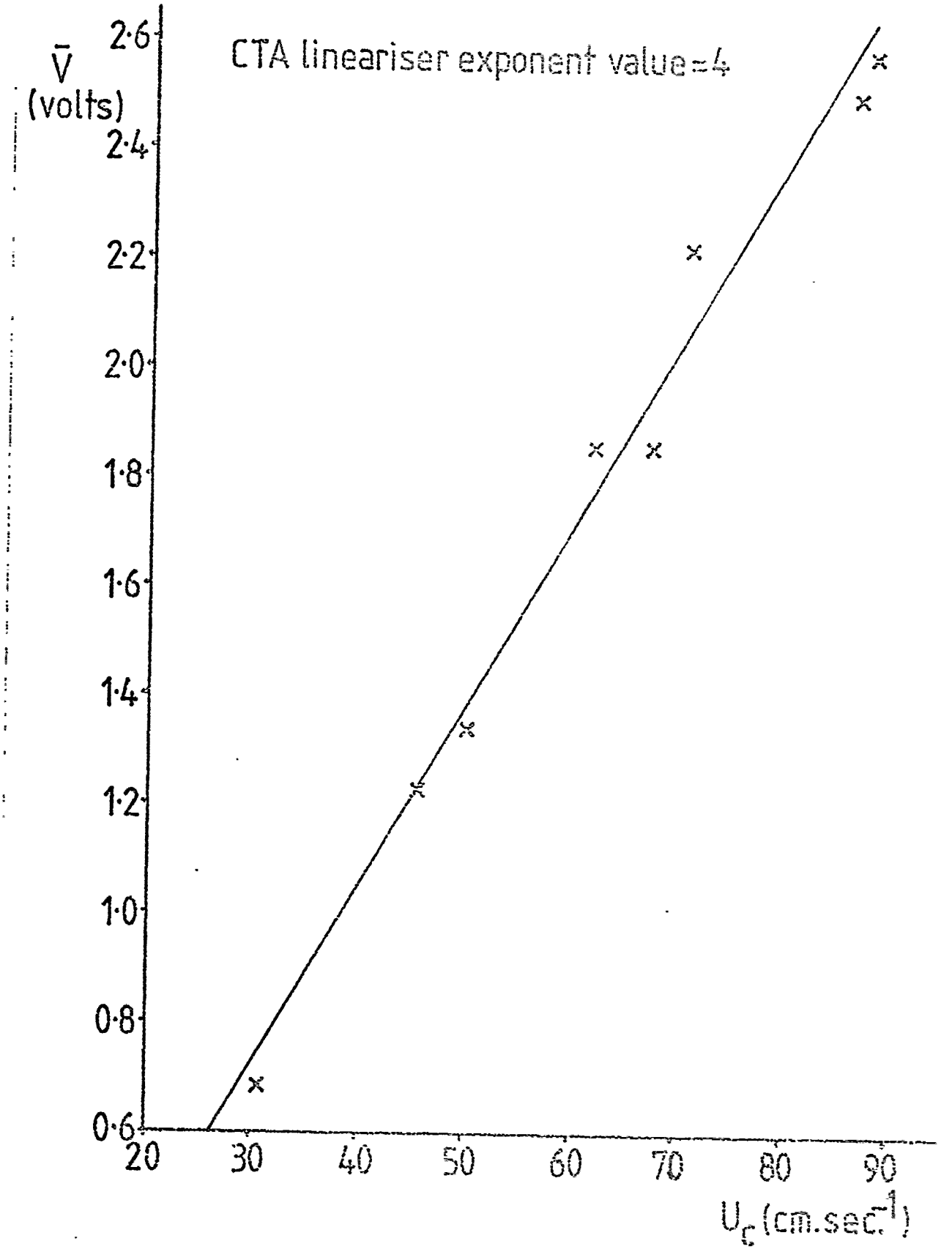

FIG 3-8 TYPICAL PLOT OF DALL FLOW TU[illegible] DISCHARGE COEFFICIENT VERSUS REYNOLD[illegible] NUMBER (Manufacturers details)

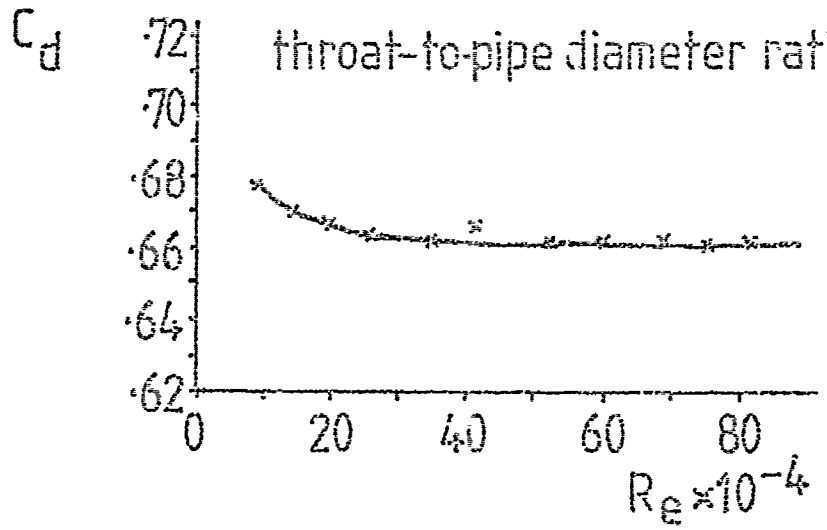

FIG 3-9 VALUES OF DISCHARGE COEFFICIENT FOR DIFFERENT THROAT TO PIPE DIAMETERS (Manufacturers details)

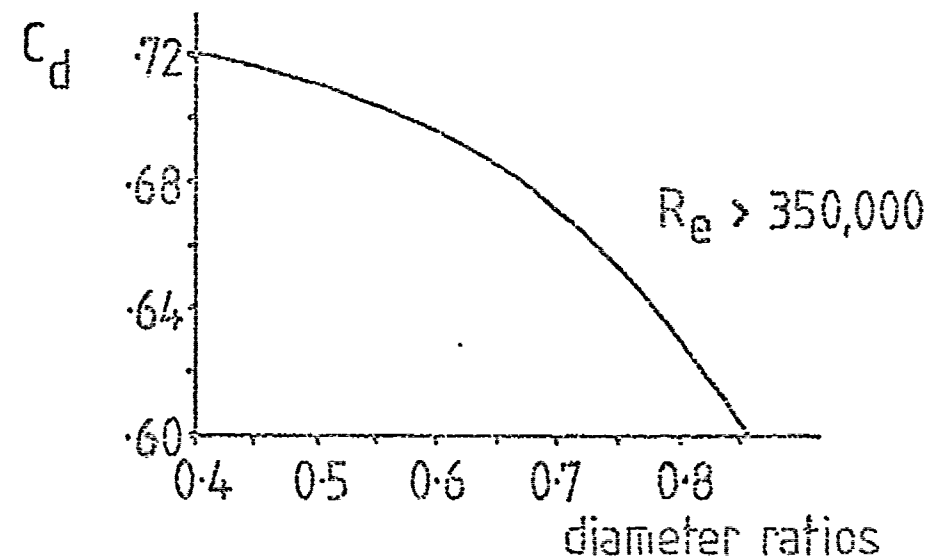

4. CONSIDERATIONS OF THE FLOW ANALYSIS

The flow analysis uses the momentum equation applied to a control volume bounded by: (1) the channel floor; (2) two vertical parallel planes, separated by a distance Δy, which coincides with the extremities of the side wall shear layers; (3) a plane parallel to the water surface but at a distance below the surface such that the water surface tension and interfacial shear effects can be neglected; (4) two vertical parallel planes across the flow channel separated by a distance dx Figure 4-1 gives a schematic diagram of the control volume.

The structure and the level of turbulence are assumed such that the contribution the resultant of the normal turbulent stress terms make to the momentum equation is deemed to be small by comparison with the other terms. For constant depth flow the resultant of the forces F_1 and F_2, on the ends of the control volume, which are equal and opposite, is zero, and the component of the normal forces in the direction of fluid motion is likewise negligibly small.

The weight W of the liquid in the control volume has a component $W \sin \alpha_2$ in the direction of motion, where α_2 is the angle of slope of the channel floor. The maximum slope encountered in the present investigation gives the maximum value of $\sin \alpha_2$ as 1×10^{-5}, hence the maximum value of the component of weight in the direction of motion is $1 \times 10^{-5} W$.

Consider that part of the control volume bounded by the outer edge of the channel floor shear layer (not a stream surface), and apply the continuity equation and momentum theorem to a stream-wise slice, of

unit traverse width, of the volume. The mass flow through the left hand end of the control volume is

$$\dot{m} = \int_0^{\delta} \rho u dz \tag{4-1}$$

and through the right hand boundary surface it is

$$\dot{m} + \frac{d\dot{m}}{dx} dx = \int_0^{\delta} \rho u dz + \frac{d}{dx}\left[\int_0^{\delta} \rho u dz\right] dx \tag{4-2}$$

The difference between the two,

$$\frac{d\dot{m}}{dx} dx = \frac{d}{dx}\left[\int_0^{\delta} \rho u dz\right] dx \tag{4-3}$$

must, by the continuity equation, be equal to the flow through the top boundary surface. The x component of momentum flux through the left hand side is

$$M_x = \int_0^{\delta} \rho u^2 dz \tag{4-4}$$

and through the right hand side it is

$$M_x + \frac{dM_x}{dx} dx = \int_0^{\delta} \rho u^2 dz + \frac{d}{dx}\left[\int_0^{\delta} \rho u^2 dz\right] dx \tag{4-5}$$

the difference being

$$\frac{dM_x}{dx} dx = \frac{d}{dx}\left[\int_0^{\delta} \rho u^2 dz\right] dx \tag{4-6}$$

The x component over the top surface is

$$(M_x)_{top} = U_e \frac{d}{d}\left[\int_0^{\delta} \rho u dz\right] dx \tag{4-7}$$

The only forces acting on the control volume are assumed to be shear forces at the plate ($-\tau_0 \ dx$) and the component of the weight $(W/\Delta z)\sin\theta$. The momentum law for steady flow states that the sum of all the forces acting on a volume in a given direction is equal to the next efflux rate of momentum from this volume in the same direction. Applying this law to the control volume, then in the x direction

$$\frac{d}{dx}\left[\int_0^{\delta}\rho u^2\,dz\right]dx - U_e\frac{d}{dx}\left[\int_0^{\delta}\rho u\,dz\right]dx = -\tau_0\,dx + (W/\Delta z)\,\text{Sin}\,\theta \qquad (4\text{-}8)$$

On substituting typical experimental values into the momentum equation, the effect of gravity on the control volume is found to be several orders of magnitude less than the other force components and is therefore neglected in the analysis.

For steady uniform incompressible turbulent flow, the streamwise boundary layer equations can be approximated by

$$\frac{d\bar{u}}{dx} + \frac{d\bar{v}}{dx} = 0 \qquad \text{continuity} \qquad (4\text{-}9)$$

$$\bar{u}\frac{d\bar{u}}{dx} + \bar{v}\frac{d\bar{u}}{dz} = U_e\frac{dU_e}{dx} + \frac{d}{dz}\left(\nu\frac{d\bar{u}}{dz} - \overline{u'v'}\right) + \frac{d}{dx}\left(\overline{v'^2} - \overline{u'^2}\right) \qquad (4\text{-}10)$$

x - momentum

The turbulent normal stresses, given by $\frac{d}{dx}\left(\overline{v'^2} - \overline{u'^2}\right)$, although commonly neglected can contribute as much as 10 per cent to the magnitude of the momentum equation at flow separation. Substituting $\tau = \mu(d\bar{u}/dz) - \rho\overline{u'v'}$ into the x momentum equation and neglecting the turbulent normal stress yields

$$\bar{u}\frac{d\bar{u}}{dx} + \bar{v}\frac{d\bar{u}}{dz} = U_e\frac{dU_e}{dx} + \frac{1}{\rho}\frac{d\tau}{dz} \qquad (4\text{-}11)$$

The continuity is used to eliminate $\bar{v}(x,z)$ in favour of $\bar{u}(x,z)$ and then the momentum equation integrated with respect to z across the entire boundary layer to give the ordinary differential equation

$$\frac{d\theta}{dx} + (2 + H)\frac{\theta}{U_e}\frac{dU_e}{dx} = \frac{\tau_\omega}{\rho U_e^2} = \frac{C_f}{2} \qquad (4\text{-}12)$$

since by definition $C_f = \frac{\tau_\omega}{\frac{1}{2}\rho U^2}$ (4-13)

where θ = momentum thickness $= \int_0^\delta \frac{\bar{u}}{U_e}\left(1 - \frac{\bar{u}}{U_e}\right) dz$ (4-14)

H = momentum shape factor $= \delta_1/\theta$ (4-15)

= displacement thickness $= \int_0^\infty \left(1 - \frac{\bar{u}}{U_e}\right) dz$ (4-16)

Thus, for the case of parallel side wall shear layers, the velocity distribution is measured perpendicular to the channel floor and at various stations along the channel centre-line in the control volume ABCD (Figure 4-1). From the velocity distributions the values of θ, δ_1, U_e and H are evaluated and these substituted into equation 4-4 to give the local values of the surface friction coefficient at each of the measuring stations in the control volume.

The analysis is modified to deal with the case of developing side wall shear layers by the addition of a convergence term, $\theta/(x_c - x)$* to the right hand side of equation 4. x_c is the location of the point, as measured from the channel leading edge, where the side wall shear layers merge. With the convergence of the control volume there will be a resultant streamwise hydrostatic pressure force; this is assumed to be neglifible.

---

* Proc. Computation of Turb. Bound Layers - 1968
AFOSR - IFP - Stanford Cont. Vol 1.

The results from the momentum integral analysis are compared with corresponding fluid parameters computed from the existence of a logarithmic relationship for boundary layer flow. The logarithmic region is formed by the overlap of the inner and outer laws for two dimensional turbulent boundary layer flow over smooth surfaces. The overlap between the two laws is given by

$$\frac{\bar{u}}{u_\tau} = \frac{1}{\kappa} \log_e \frac{z u_\tau}{\nu} + B \qquad (4\text{-}17)$$

The validity of the inner law, including the logarithmic overlap can be established by plotting velocity profile data in terms of the inner variables $\bar{u}/u_\tau$ and zu_τ/ν. A single plot of several sets of data produced by workers using widely different flow regimes (Figure 4-2) clearly shows the data with the exception of separating flow collapsing onto a single logarithmic relation in the overlap region $35 < \frac{zu_\tau}{\nu} < 350$, corresponding roughly to $0.02 < z/\delta < 0.2$, after which the individual data curves either veer off upwards in the outer (wakelike) layer or downwards in the inner viscous shear layer. The inner law is extended into the outer region of the boundary layer by the addition of the wake function (Coles 1956), thus

$$\frac{\bar{u}}{u_\tau} = \frac{1}{\kappa} \log_e \frac{z u_\tau}{\nu} + B + \frac{\Pi}{\kappa} W\left(\frac{z}{\delta}\right) \qquad (4\text{-}18)$$

For flow over smooth surfaces the surface roughness is entirely submerged in the viscous sublayer and the flow adjacent to the surface follows the contour of the surface roughness almost without separation. With 'increasing surface roughness' the roughness elements will begin to break through the viscous sublayer producing localised flow separation and eddy shedding. The viscous sublayer will become increasingly

less stable until the roughness elements are such that the sublayer will merge with the outer layers.

Thus, the effect of surface roughness on the shear flow is to modify the mean velocity distribution. The effect on the semilogarithmic plot of u/u_τ versus $\log_e zu_\tau/\nu$ is to displace it downwards from the smooth wall profile by an amount $\Delta u/u_\tau$. This downward shift of the logarithmic profile due to surface roughness had been noted by Nikuradse (1933) for the case of pipe flow.

For smooth surfaces a family of straight lines can be produced, each line corresponding to a given value of C_f. Hence, experimental points can be plotted on such a plot (Figure 4-3) and the line upon which they fall gives the appropriate value of C_f. The resulting value of C_f can be checked against both the slope and position of the line (Clauser 1954).

Extending this method to rough surfaces produces several difficulties, these being that the origin of z is not known and also, since the roughness causes a shift in the logarithmic profile, the value of C_f is confirmed only by the slope of the logarithmic line and not its position. By defining a height ε, measured from the crests of the roughness elements, where the logarithmic asymptote is located, Perry and Joubert (1963) were able to extend the method to the case of rough surfaces.

Using this method of shifting the origin of the mean velocity distribution to get the best fit line the the semilogarithmic plot, the relationship is given by

$$\frac{u}{u_\tau} = \frac{1}{\kappa} \log_e \left[\frac{z + \varepsilon}{k}\right] + g\left[\frac{ku_\tau}{\nu}\right] \qquad (4\text{-}19)$$

where the roughness function g is

$$g = \frac{1}{\kappa} \log_e \frac{ku_\tau}{\nu} + B - \frac{\Delta u}{u_\tau} \qquad (4\text{-}20)$$

for large values of the roughness Reynolds number R_k ($R_k = ku_\tau/\nu$).

In the search for a universal roughness function, the roughness Reynolds number R_k has been expressed in terms of various roughness height parameters. A characteristic roughness height in terms of the root mean squared roughness is used by Karlsson (1978), the mean apparent amplitude of the roughness and centre line average have been used by other workers (Musker et al 1976).

The inability of these parameters to provide a universal relationship between the roughness Reynolds number and the roughness function $\Delta u/u_\tau$ led to the use of various simple spatial parameters in the characterisation of the surfaces under investigation (Betterman 1966, Dvorak 1969, Simpson 1973). Several empirical relationships were subsequently produced, all applying to the special case of the fully rough flow regime.

In a study of flow through pipes lined with replicated ship hull surfaces Musker 1977 set out to determine a roughness function using parameters from a statistical analysis of the surfaces. The roughness Reynolds number is modified to

$$\frac{ku_\tau}{\nu} = \frac{\sigma u_\tau}{\nu} (1 + ASp)(1 + bS_k ku) \qquad (4\text{-}21)$$

(Musker & Lewkowicz 1978)

where σ is the standard deviation of the surface heights, Sp is the average slope based on a sampling interval equal to the correlation length and 'a' and 'b' are empirical constants. the parameter Sp is assumed to represent the degree of bluffness of the roughness elements, and S_K and K_U are the average skewness and kurtosis of the surface height distributions.

For the surface investigated an approximation to a universal curve for the roughness functions could be obtained if the short wavelength cut-off was set close to the extrapolated value of the average turbulence macro-scale in the vicinity of the roughness elements. Hence for a 2 mm cut-off wavelength the values a = 0.5 and b = 0.2 produce a nearly universal curve (Figure 4-4) for the roughness function, plotted against the modified roughness Reynolds number.

FIG 4-1 SCHEMATIC DIAGRAM OF THE CONTROL VOLUME USED IN THE FLOW ANALYSIS

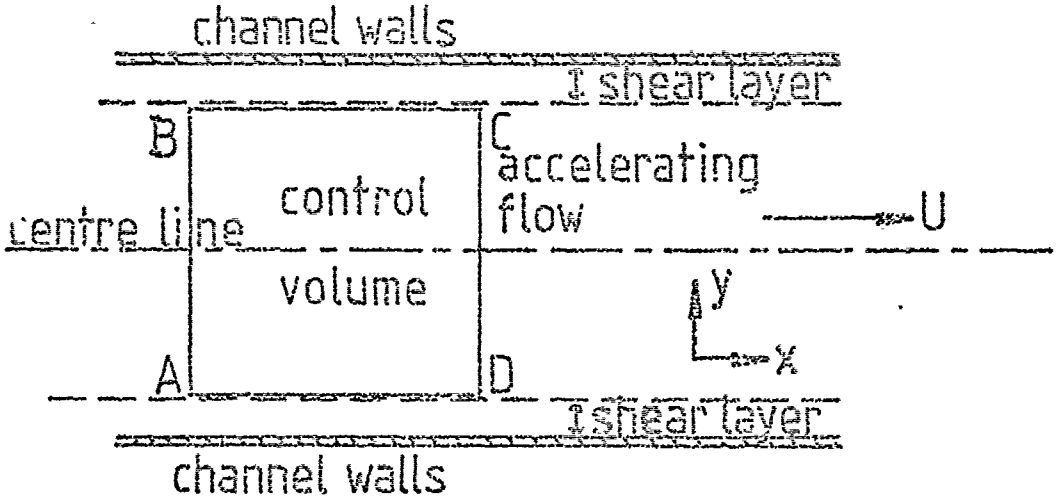

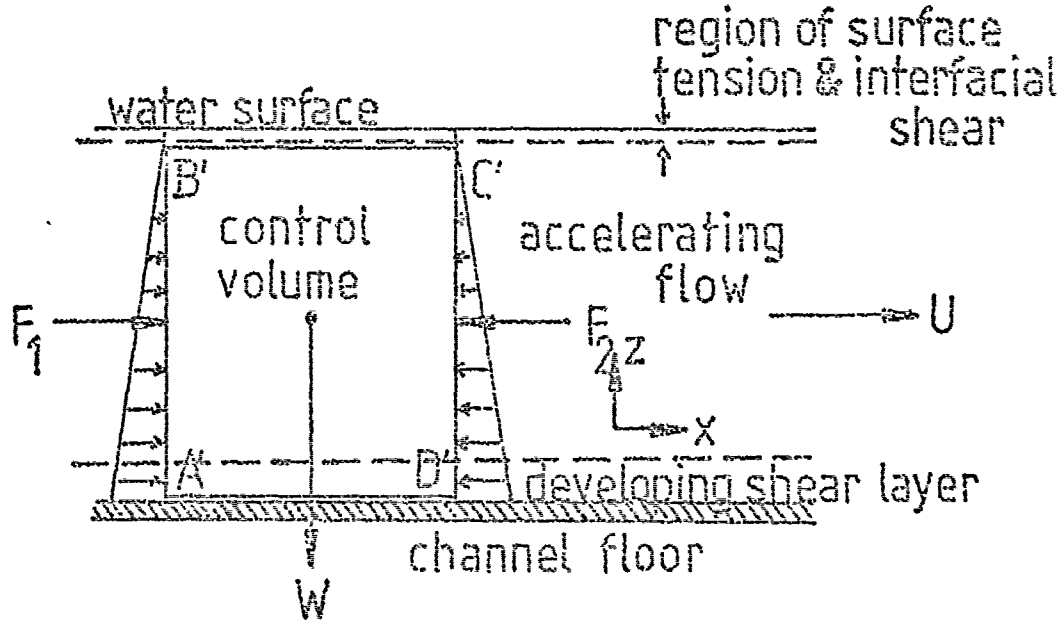

FIG 4-2 MEAN VELOCITY DISTRIBUTIONS IN TERMS OF THE LAW OF THE WALL, FOR WIDELY DIFFERENT FLOW REGIMES (White, 1974)

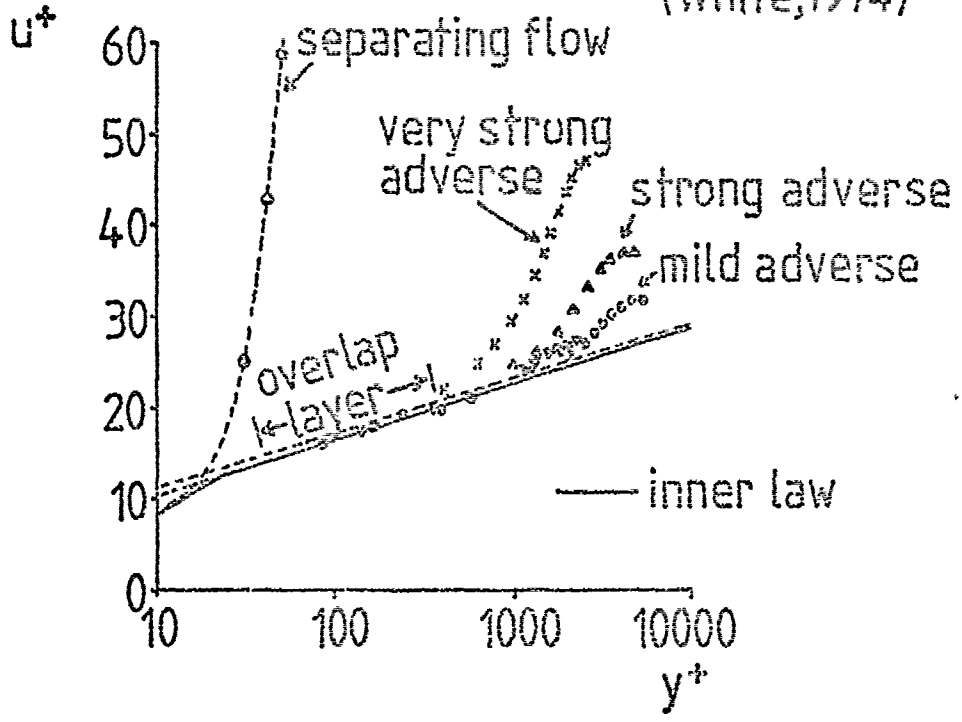

FIG 4-3 CHART FOR EXPERIMENTAL DETERMINATION OF TURBULENT SURFACE FRICTION (Clauser, 1954)

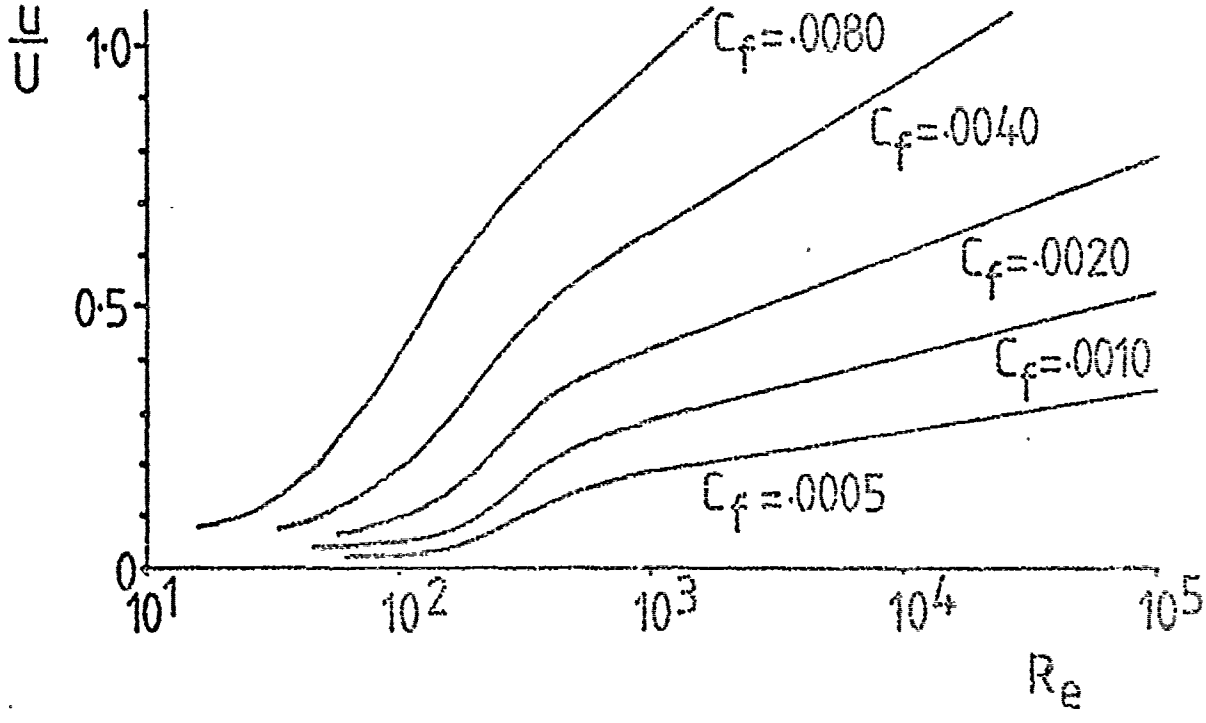

FIG 4-4 ROUGHNESS FUNCTION VERSUS ROUGHNESS REYNOLDS NUMBER (Musker & Lewkowicz, 1978)

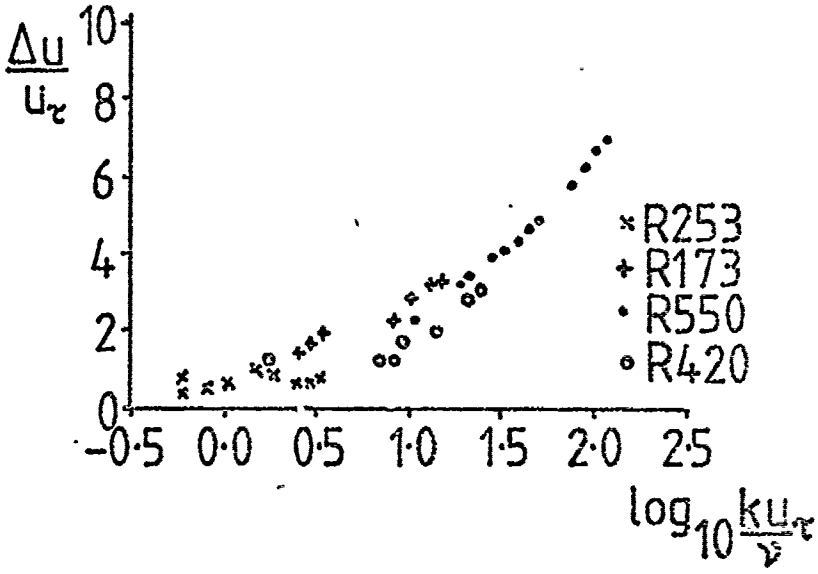

5. THE MEASUREMENT AND CHARACTERISATION OF SURFACES

5.1 Introduction to surface measurement

There are many instruments available for the measurement of surface geometry. These are capable of measuring surface features from meters in length as in the case of a surveyor's theodolite right down to looking at the molecular level as measured by the Scanning Electron Microscope. A state of the art review and bibliography of Surface Topography in Engineering is given by Thomas and King (1977).

For a successful analysis of surface roughness it is important that the measuring instrument used produces readily available quantitative information about the surface, it clearly being an advantage if the data is in the form of an electrical signal which lends itself to electronic manipulation and computer analysis.

It is, of course, important that the measuring device is capable of supplying information about surface parameters which together are capable of uniquely defining a particular surface.

5.2 Measuring techniques for surface microgeometry

The techniques available for looking at surface microgeometry, for example (1) Optical Methods; (2) Taper-Sectioning; (3) Pneumatic Gauging and (4) Stylus Instruments.

5.2.1 Optical methods

Optical methods include:

(a) Microscopic examination of the surface with normally incident illumination which at low magnifications gives a general picture of any trends in the surface features. At higher magnifications it becomes increasingly difficult to focus on the peak and valley features simultaneously thus severely restricting the scope of the microscope in the examination of surface roughness.

(b) The Light Section microscope partially overcomes the problem of focussing on the peak and valley features simultaneously by throwing light from a slit onto the surface at an incident angle of 45°. The reflected image of the slit is seen in effect as a section through the surface with the vertical scale magnified by a factor equal to the cosecant of the angle of incidence.

(c) The Interference microscope can be used for relatively smooth surfaces, it showing the surface height variations as light and dark interference fringes. Under suitable conditions it can give a complete contour map of the surface. None of these optical methods are capable of providing quantitative information without laborious processing.

(d) The Transmission Electron microscope has a much greater resolution and depth of field than its optical counterparts, but it requires a tedious, delicate two-stage replication technique, with a consequent danger of poor reproduction of the initial surface.

(e) The Scanning Electron microscope is a considerable improvement of the Transmission microscope. It is a reflection microscope in which an electron beam is modulated to scan the surface in a series of parallel traverses. The reflected beam is detected, amplified and displayed on a TV screen. Specimens can be examined directly; but the size of specimen is limited by the size of the specimen vacuum chamber.

(f) Various designs of glossmeter have been produced (Westburg 1967/8) to measure the reflectance of a surface to give a relative measure of the surface average roughness. A development of this technique is the laser scanning analyser (Clarke & Thomas 1979). A laser beam is reflected from a rotating polygonal mirror in order to scan the workpiece surface at high speed, where it is again reflected into a wide aperture photodetector which measures the reflected intensity. The detector output is amplified and applied to the vertical deflection coils of an oscilloscope whose time base is provided by the rotation of the mirror. Localised variations in the reflectance of the surface thus appear as changes in signal strength whose position on the workpiece can be established from the time elapsed since the start of the current scan. The laser beam spot diameter can be set from 200 μm upwards at 623 mm scan width, the angular traverse is $\pm 30^{o}$ and the scanning speed is 5 KHz maximum.

5.2.2 Taper sectioning

In taper sectioning the specimen is sectioned at a shallow angle to the surface and the section polished and examined microscopically. The result is a profile with its vertical scale exaggerated by a factor of cotangent α , thus emphasising the surface features. The method has the disadvantages of being destructive and time consuming.

5.2.3 Pneumatic gauging

In pneumatic gauging air is allowed to escape through the gaps between a flat nozzle and the surface it is in contact with. The back pressure is a function of the surface roughness. The gauge is insensitive to smooth surfaces and does not give quantitative information.

5.2.4 Stylus instruments

The basic form of the stylus instrument is that a fine stylus is drawn at a constant speed over an irregular surface and the variation of its vertical displacement with time will represent the variation in height of a section of the surface with horizontal displacement. As the average slopes of most surfaces are small, the vertical movement of the stylus is generally electronically amplified.

The one main advantage of the stylus instrument which makes it superior to the other surface instruments is the availability of an electrical signal which can be electronically manipulated to give any desired roughness parameter, displayed directly on a chart recorder, or analysed by computer.

5.3 Measuring techniques for surface macrogeometry

The previously mentioned instruments all measure surface features of horizontal dimensions up to a few millimetres. In the experimental set-up of this investigation the work surface is approximately 20 metres in length and therefore to characterise the surface, surface features of up to 20 metres must be measured. The techniques available to

measure the macrogeometry of the surfaces can be divided into (1) Optical techniques and (2) other techniques.

5.3.1 Optical techniques

Optical instruments for the measurement of surfaces include the auto-collimator and micro-alignment telescope. Both of these use a moveable target which is placed on the work surface and whose displacement relative to the sighting instrument, with distance between the two gives an indication of the surface geometry. The instrument's sampling interval and sample length are determined by the separation of the target's feet, the limit of angular deflection of the light source detectable by the sighting device, and the optical efficiency of the instrument.

5.3.2 Other techniques

The other methods include using instruments such as dial gauges which can be used to measure spot heights along the surface relative to a datum, such as an engineer's straight edge. An electronic level measures the inclination of the surface in steps equal to the separation of its feet, its range of surface feature measured being from the mean distance apart of its feet to as far as it is physically possible to move the instrument along the surface. The values of surface inclinations can then be easily converted into height readings.

Another instrument used for measuring surface 'macrogeometry' is a coarser version of the stylus measuring device used for measuring the microgeometry of a surface. BSRA have, for many years, used such an

instrument (Canham 1956) to take in-situ ship hull roughness records when ships undergoing trials are in dry dock. The instrument in question is called the BSRA Wall Roughness Gauge, a diagram of which is shown in Figure 5-1. The gauge consists of a measuring probe mechanically linked to a sapphire stylus which scratches the measured profile onto a graphitic coated glass slide. The measuring probe assembly is held in a carriage mounted on wheels and traversed across the hull surface on a track which is held in position on the surface by means of two magnets, one at either end of the track. The measuring probe which has a 1.6 mm diameter ball point is drawn over the surface in between each side of the track. The probe is constrained to move in a vertical direction and hence as it is drawn across the surface, its movement relative to the track-way is recorded by the sapphire stylus on the graphite coated glass slide. The vertical measurements on the recorded profile are equivalent to the vertical movement of the measuring probe, whilst the traverse distance has been reduced by a factor of approximately x10 to fit the profile onto the glass slide. Thus, the maximum length that can be traversed by the measuring probe is approximately 63.5 cm and the corresponding recorded profile is approximately 6.4 cm long.

The wall gauge records can be projected optically on to a screen and the Mean Apparent Amplitude (MAA) for a surface 'wavelength' of 2 inches (5.1 cm) manually determined and taken as a typical measure of the surface roughness. The reason for using a 2 inch length being that a statistical analysis of ship-model data (Chaplin 1967) seemed to indicate that a relationship exists between frictional resistance parameters based on the MAA per 2 inch length of hull surface and the corresponding computed ship-model correlation factor. The wall gauge surface profiles can also be digitised and statistically analysed by

computer. Prior to the analysis the optically enlarged profiles are projected onto a digitising table connected to a paper tape punch.

BSRA have recently produced an electronic Hull Roughness Analyser to replace the roughness gauge which has been in use for over 30 years. The new portable instrument provides a digital record on a strip-printer of peak to valley roughness amplitudes in alternate 50 mm lengths as the sensor is propelled manually over the work surface. The measuring probe has a vertical measuring range of between 15 μm and 2 mm.

5.4 Surface replication

The use of surface replication in the measurement of surface topography has been recently evaluated by George (1979). The investigation makes use of the power spectral density function to compare various replica materials and techniques. The requirement of the replica is that 'the geometric shape of the contact face should be as similar as possible to the parent surface'. Some replica materials, such as Acrulite Microtech type A, are known to distort as they set causing bowing of the replica. For many applications the bowing is relatively unimportant compared with the roughness replication. Bowing can however cause considerable inaccuracy when investigating the relatively long surface wavelengths.

It was found that for all the replica methods investigated, the replication resolution dropped off significantly for surface wavelengths less than 30 μm. Bowing of the replicas was considerably reduced by inserting a steel plate in the replica as it curved.

5.5 Surface characterisation

Surface topography is generally divided arbitarily into three classifications according to its scale (Figure 5-2). The largest wavelengths are classified as errors of form, intermediate wavelengths as waviness, and the short wavelengths form the surface roughness. Clearly the longest wavelength present can be attributed to the nominal size of the work surface. The shortest wavelength present is more difficult to define; theoretically it can be the atomic dimensions of the surface. The wavelength cut-offs of the measured profile must be taken into account in the subsequent analysis. The measured parameters of a surface are dependent both on the type of surface under investigation and on the wavelength cut-offs of the measuring instrument. For a stylus instrument the short wavelength limit is determined by the finite dimensions of the stylus, acting as a low-pass filter, and the long wavelength limit by the sampling length.

The surface parameters derived from a computer analysis of the surface profile are not intrinsic properties of the profile since all the digital computers in effect sample the profile at discrete intervals to obtain a discrete set of height readings defining the profile. Hence the computed surface parameters are a function of the finite dimensions of the measuring head, the sampling interval and the sampling length (Thomas & Sayles 1978).

The first task in analysing a surface profile is to define a mean line or datum from which parameters can be measured. This will make it possible to define the surface height variation, but a means is also required of defining how the heights vary in the plane of the surface.

Thus, to describe a surface at least two parameters are generally required, one defining the roughness height and the other, a spatial parameter, defining how the roughness varies along the surface. By assuming the surface profile to be tending to a straight line parallel to the measuring instrument's datum then a number of elementary parameters can be used to describe the roughness amplitude. For example, the maximum peak to valley height of the roughness, R_t, is defined as the vertical distance between the highest peak and lowest valley on the profile. It is easy to define but has the disadvantage of being sensitive to a typical surface event such as scratches. The highest peak and lowest valley on a profile as measured by a stylus instrument are not necessarily the highest and lowest points on the surface. It is unlikely that any peak on a profile will coincide with any summit of a surface asperity; the measuring instrument will probably follow a line that takes it over the shoulders of surface asperities. The two most widely used mean-line roughness parameters are the root mean square (RMS), R_q, and centre line average R_a, each of which can be used to define the mean line or plane through a profile. The rms mean line is produced by minimising the sum of the squares of the distances above and below the mean line. The rms roughness is defined by

$$\sigma = \left\{ \frac{1}{L_y} \int_0^{L_y} z^2 \, dy \right\} \qquad (5\text{-}1)$$

where z is measured from the mean line and L_y is the profile length.

The centre line average, R_a, is the most universally used roughness parameter because of its ease of measurement. The mean line or plane is defined by the condition of equal areas or volumes of surface and void, above and below the mean.

The R_a parameter is defined for a profile length L_y

$$R_a = \frac{1}{L_y} \int_0^{L_y} |z| dy \qquad (5\text{-}2)$$

Since the rms roughness is weighted by the square of the surface heights it tends to be more sensitive than R_a to large deviations from the mean line. In some cases this can represent an advantage in the rms over the R_a parameter.

A roughness measure used to specify ship hull roughness is the mean apparent amplitude, MAA (Chaplin 1967). Using the BSRA wall gauge a sample length of approximately 30 inches (76 cm) is recorded and divided into 2 inch (5.1 cm) lengths. The maximum and minimum points in the middle 13 x 2 inch lengths are then used to plot a peak to valley envelope over the total sample length. The MAA is the difference in height between the average of the 13 highest points on the envelope and the 13 lowest points.

Statistical techniques were used to evaluate such parameters as asperity peaks, curvatures, surface heights, slopes etc. and form probability distributions representing the frequency of occurence of each parameter (Greenwood & Williamson 1966). The parameters so obtained do not contain spatial information on the variation of surface properties about the plane of the surface. The representation of surface parameters spatially originated from random process theories developed for the analysis of random noise (Rice 1944/5). This technique was applied successfully to surface profile analysis by Whitehouse and Archard (1970) who express the spatial properties of the profile in terms of the autocorrelation function.

The use of statistical and random process theories for representing the surface as opposed to the profile was due originally to the classic work on sea waves by Longuet Higgins (1957, 1962). This was later adopted to solid surface topography by Nayak (1971).

The probability or distribution function $P(\zeta)$ represents the probability that the random variable $Z(y)$ takes a value less than or equal to ζ. The probability function is the integral of the probability density function $p(z)$,

$$P(\zeta) = \int_{0}^{\zeta} p(z)\, dz \qquad (5\text{-}3)$$

where ζ is the measured height and Z is the corrected profile height.

The shape of the probability density function in terms of the moments of the function can be used to provide information on the behaviour of the process under investigation. The first moment M_1, where

$$M_n = \int_{-\infty}^{\infty} z^n\, p(z)\, dz \qquad (5\text{-}4)$$

is the mean or DC level of the profile. This is generally removed prior to data processing and is therefore zero.

The second moment M_2 is the variance σ^2 which is the square of the rms value or standard deviation. It is a measure of the spread of the distribution and therefore of the data.

The third moment M_3 is the skewness, which is useful for defining variables with an asymmetric spread. It is conventional to normalise

M_3 thus

$$S = \frac{1}{\sigma^3} \int_{-\infty}^{\infty} z^3 \; p(z) \; dz \qquad (5\text{-}5)$$

where σ is the standard deviation of $p(Z)$. The symmetric Gaussian distribution, which is a good approximation for many surfaces' structures (Greenwood & Williamson 1966) has a skewness of zero.

The fourth moment M_4 is called the kurtosis and represents the peakedness of the distribution. Distributions having a kurtosis greater than $k = 3$ are called Leptokurtic and those with a kurtosis $k < 3$ are termed Platykurtic, where k is the normalised fourth moment

$$k = \frac{1}{\sigma^4} \int_{-\infty}^{\infty} z^4 \; p(z) \; dz \qquad (5\text{-}6)$$

The symmetric Gaussian distribution has a kurtosis of $k = 3$.

The use of these higher moments to characterise a height distribution is however limited because in assessing the significance of their numerical values it is necessary to remember that they are themselves distributed as the result of random sampling (Thomas & King 1978).

The statistical representation of the surface or profile heights in terms of the probability density function $p(Z)$ is known as the height distribution. In practice many surfaces have symmetrical Gaussian distributions of the form

$$p(Z) = \frac{1}{\sigma\sqrt{2\pi}} e^{-(z^2/2\sigma^2)} \qquad (5\text{-}7)$$

The distribution is constructed by plotting the number or proportion of surface heights lying in a height interval as a function of the height. A convenient method of testing for 'normal' or Gaussian height distributions is to plot the cumulative distribution on probability graph paper; this is scaled such that a Gaussian distribution will produce a straight line. The knowledge that a distribution is Gaussian is useful particularly when dealing with random process models. The 'asperities on asperities' model (Archard 1967) which accounts for both height and spatial properties of surfaces, combines the basic distributions in a random process theory approach.

The outstanding problem in surface analysis is the representation of spatial properties, i.e. how heights, slopes etc. vary with distance in the plane of the surface. The spatial functions, such as the autocovariance function or in its normalised form the autocorrelation function, the structure function and the power spectrum, offer a means of representing the properties of all the wavelengths present.

The autocorrelation function (ACF) is simply the autocovariance function (ACVF) normalised by the profile sample variance σ^2 (i.e. the square of the rms roughness). Thus

$$R(\tau) = C(\tau)/\sigma^2 \tag{5-8}$$

where τ = sampling interval, where the ACVF is given by

$$C(\tau) = \lim_{L \to \infty} \frac{1}{L} \int_0^L Z(y)\, Z(y + \tau)\, dy \tag{5-9}$$

where L is the sample length.

A model found to fit the autocorrelation function for many random surfaces is

$$R(\tau) = \exp(-\tau/\beta^*) \tag{5-10}$$

This has a correlation length of $\beta = 2.3\,\beta^*$ where $1/\beta^*$ is the decay rate of the function at the origin. The correlation length β was originally defined by Whitehouse and Archard as the distance over which the autocorrelation function $R(\tau)$ takes to decay to a value of 0.1.

The spatial variation can also be represented in the form of the structure or variance function (SF) (Whitehouse 1971, Sayles & Thomas 1977) defined for a surface as

$$S(r,\theta) = E\left\{(z(x,y) - z((x,y) + r(\theta))^2\right\} \tag{5-11}$$

where $E\{\ \}$ denotes expectation. $Z(x,y)$ is the surface height at coordinates (x,y) in the plane of the surface and $Z((x,y) + r(\theta))$ is the surface height at a radial distance (r) from (x,y) in a direction (θ). For a profile SF is simply

$$S(\tau) = E\left\{(z(y) - z(y + \tau))^2\right\} \tag{5-12}$$

which in an integral form is

$$S(\tau) = \underset{L \to \infty}{\text{Limit}}\ \frac{1}{L}\int_0^L (z(y) - z(y + \tau))^2\ dy \tag{5-13}$$

where (y) is the distance along the profile and τ the ordinate separation in the (y) direction.

The function represents the mean square of the difference in height expected over any spatial distance τ.

The power spectral density function (PSDF) or power spectrum represents the same information as the ACF or SF but in a different form. The PSDF is generally given in terms of the ACVF:

$$G(\omega) = \frac{2}{\pi}\int_0^\infty C(\tau)\ \cos\ (\omega\tau)\ d\tau \qquad (5\text{-}14)$$

where ω is a radial frequency $2\pi/\lambda$ and λ is the wavelength. The PSDF can also be obtained directly from the surface profile data through the equation

$$G(\omega) = \frac{1}{\pi}\int_{-\infty}^\infty Z(y)e^{-j\omega y}\ dy \qquad (5\text{-}15).$$

FIG 5-1 THE B.S.R.A. WALL GAUGE

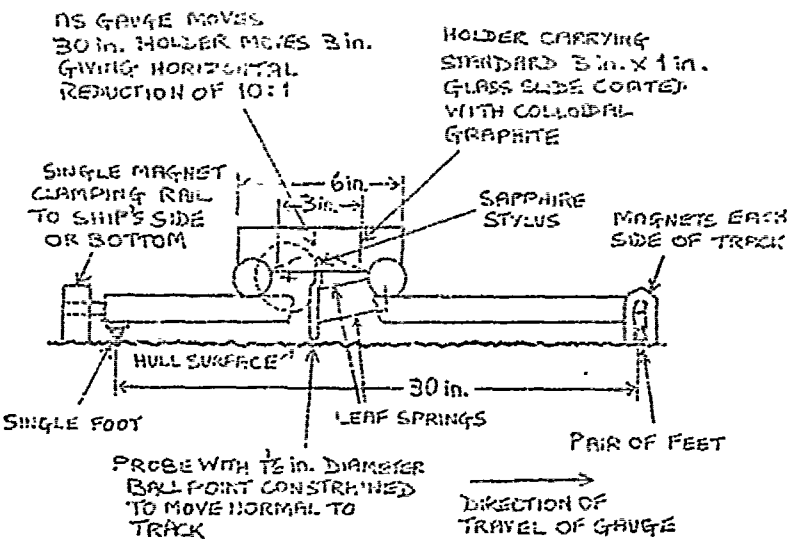

FIG 5-2 CLASSIFICATION OF TOPOGRAPHY

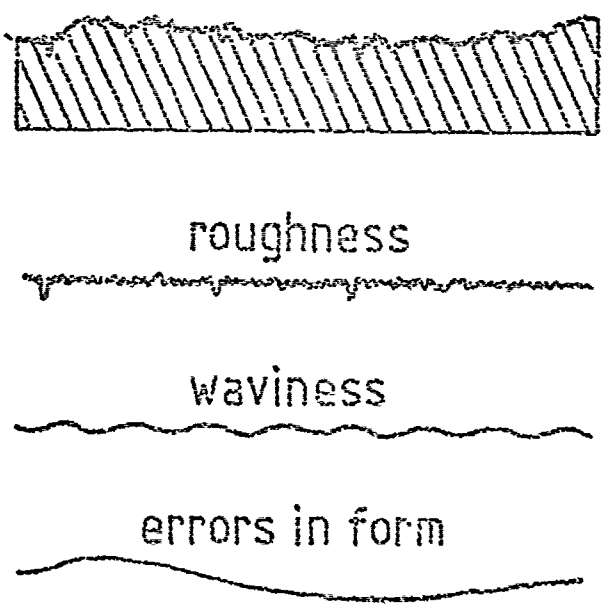

6. THE FLOW ANALYSIS

6.1 Introduction

The flow channel is 30.5 cm wide with a maximum flow depth of 30 cm and is supported at three points including two jacking points. The jacking facility can be used, along with a control valve on the channel inlet and a variable height weir on the channel outlet, to produce flows at varying mean velocity and mean depth in subcritical or supercritical regimes.

The regime of flow in a rectuangular channel is defined by the use of the non-dimensional Froude number, defined by $F = U/\sqrt{gh}$. where U is the mean flow velocity, g is the gravitational acceleration, and h is the depth of flow. From the dynamic considerations the Froude number may be shown to be proportional to the ratios of a representative inertia force to a representative gravity force. Hence for a liquid of constant density with a free surface the effects of gravity on the fluid inertia are expressed by the Froude number F where the fluid regime is defined as subcritical for F less than unity, and supercritical for F greater than unity.

For the purpose of this investigation the flow is maintained below its critical value in order to minimise flow instabilities and secondary flow effects which are produced by:

(1) Misalignments of the glass panels and the steel sections making up the sides and the floor of the channel respectively.

(2) Non-uniform or disturbed flow at the channel inlet.

(3) The introduction of flow measurement probes into the flow regime.

The joints between the side panels and the floor sections are made as unobtrusive as possible to the flow by careful alignment and subsequent smoothing out the joints with a filler.

6.2 The preliminary flow study

6.2.1 The flow at the channel inlet

The flow system was initially operated with the flow issuing into the channel directly from the deturbulating tank (Figure 2-1). An investigation of the flow conditions at various stations along the channel showed the existence of large scale eddies which were producing transverse instabilities.

These flow instabilities were thought to originate from swirl produced in the pipe upstream of the deturbulating tank in combination with the multi-orifice discharge apparatus through a blanked-off tee located near the bottom of the deturbulating tank. These were substantially reduced with the introduction of two honeycomb flow straighteners made from aluminium sheets, across the entire section of the deturbulating tank. The honeycomb flow straighteners are 5 cm thick with a honeycomb diameter of approximately 1 cm. One of the honeycomb flow straighteners is positioned horizontally in the deturbulating tank 40 cm above the inlet 'pepper pot' inverted T-piece whilst the

other honeycomb is positioned transversely at the channel inlet. The net effect of these flow straighteners is to break up any large scale eddies present in the deturbulating tank and produce pseudo two dimensional uniform flow at the channel inlet.

6.2.2 The side wall shear layers

The development of shear layers from the glass channel sides will significantly modify the flow in a narrow channel by producing a convergence effect on the free stream flow. Although a convergence term * can be introduced into the flow analysis it was found that the magnitude of the term, which is dependendent on measured transverse velocity profiles at various stations along the channel length, had an unacceptably high possible error. The convergence term is given a distance X_c measured from the channel inlet which is estimated to be the flow length over which the side wall shear layers develop and eventually merge. Thus, to graphically estimate the distance X_c from the appropriate transverse channel velocity profiles requires the flow to be uniform potential flow at the measurement datum (i.e. at the channel inlet) and also that the transverse profiles give a clear measurable representation of the state of the side wall shear layer development. Figure 6-1 shows a schematic representation of the procedure used to interpolate the distance X_c from transverse channel profiles. Typical measured transverse profiles are shown in Figures 6-2, 6-4 and 6-5.

6.2.3 The flow regime

An examination of the flow in the channel using the transverse velocity profile data from the hot-film anemometer (Figures 6-2, 6-4

---

* Proc. Comput. of Turb. Bound. Layers, Stanford Univ. 1968

and 6-5) showed there to be no appreciable growth of the side wall shear layers in a 2.4 m length of the channel chosen to be the test section for all subsequent measurements. Hence the flow analysis used assumes the growth of the shear layers over the channel's glass sides to be negligible. Hence from 4.5 m downstream of the channel inlet to 6.9 m from the inlet a series of boundary layer traverses were taken to determine the variation of C_f along the channel centre line, for a particular work surface and a particular set of flow conditions.

Thus from the initial investigation of the flow regime in the channel a test section was chosen such that the flow in a volume 2.4 m long, 30.5 cm wide and with a height bounded by the work surface and the open surface of the flow is assumed to be substantially an accelerating two-dimensional flow with a developing work surface shear layer and relatively unobtrusive parallel side wall shear layers.

6.3 The analysis

The flow analysis is divided into four sections, one section for each of the four surfaces investigated.

6.3.1 Flow over a painted steel surface

It was decided initially to carry out a study of the flow over a work surface consisting of three 6.1 m lengths of 0.5 inch thick shot-blasted steel plate butted up end-to-end on the channel floor. The surface finish consists of a brush-applied coat of marine paint* over a spray-applied coat of primer paint**.

---

* A thixotropic anticorrosion marine paint, Silver Primocon.

** A two-pack reinforced edge-type primer paint, Metagard G250.

The larger capacity pump B is connected into the channel system and the smaller axial flow pump isolated. The radial flow pump B which operates under conditions of a negative static suction head is primed using a vacuum line connected to a compressed air driven air ejector. Prior to taking any flow measurements the system is purged of air pockets and the hot-film sensor calibrated (see Chapter 3.2). By arrangement of the channel slope, weir height and pump outlet valve setting a number of flow conditions are set up in the channel. The flow analysis assumes the flow to be sub-critical at a constant depth, and substantially two-dimensional.

Three sets of flow conditions were analysed in the present section, namely flow conditions 1, 2 and 3. The flow parameters and values of C_f determined from measurements along the centre line of the channel flow control volume for each of these conditions are summarised in tables 6-1 to 6-3. Transverse flow profiles for the flow conditions are shown in Figures 6-2 and 6-3. The transverse profiles show a pseudo free stream region across the middle two-thirds of the flow where the measured mean flow velocities may fall off to 90 per cent of the maximum velocity recorded.

The range of Reynolds number over which the flow measurements could usefully be taken was limited chiefly by the constraining effect of the channel sides, causing significant departures from the assumed two-dimensional flow. Gravity surface waves were also encountered immediately downstream of the honeycomb sheet at the channel inlet. The amplitude of the surface waves, for a flow Reynolds number of 5.3×10^6 and a depth of flow of 24.5 cm was negligible over the test section, which corresponded to the maximum Reynolds number attained

in flow 3 (Table 6-3) with a Froude number of 0.53. A typical value of δ over the test section for flow 3 was 7 cm which leaves the remaining two-thirds or more of the flow to attenuate any surface wave effects on the boundary layer development. At Reynolds numbers much greater than 5.3×10^6 the flow regime begins to significantly break away from the simplified model which the flow analysis requires. The calculated values of the local coefficient of surface friction are consistent with those based on the momentum approach and are approximately equal in magnitude to the published values for hydrodynamically smooth surfaces (Schlichting, 'Boundary Layer Theory').

The scatter in the deduced values of the flow parameters and the low values of H, the shape factor, are thought to be a consequence of calibrating the flow measurement instrumentation in a flow environment dissimilar to the one in which it is to be operated. The hot-film probe is calibrated on the centre line in smooth turbulent pipe flow at pipe Reynolds numbers between 3.7×10^3 and 16.2×10^3 corresponding to a range of centre line velocities between approximately 25 cm/sec and 100 cm/sec. the hot-film probe is operated in open channel flow at varying distances from the work surface and therefore varying turbulent intensity at channel Reynolds numbers ranging from 2.3×10^6 to 5.3×10^6. The degree of turbulence will depend on the roughness of the wall and the distance from the wall.

The hot-film anemometer is assumed to have a linear response to values of mean streamwise flow velcities $\bar{u}$ measured at points ranging from adjacent to the channel floor to the free-stream region of the channel flow. The flow velocities, so determined, range from a minimum of approximately 10 cm/sec within 1 mm of the channel floor to a maximum of approximately 80 cm/sec in the free stream.

The determination of C_f using the momentum integral equation requires the evaluation of thw two integrals for momentum and displacement thickness over the boundary layer thickness δ . The integrals are inherently very sensitive to measurement inaccuracies in the inner regions of the boundary layer. With the instrumentation used, errors in the determination of z and $\bar{u}$ are unfortunately at a maximum in this critical region near the solid-liquid interface.

6.3.2. Flow over a gravel surface

The second surface flow regime to be examined consisted of flow over the channel floor covered with a closely packed layer of gravel. To reduce any movement of the gravel to a minimum the free stream velocity of the flow was reduced by isolating the larger capacity pump B and connecting into the channel system the smaller capacity axial flow pump A. Prior to any flow measurements the hot-film sensor is re-calibrated and the system purged of any air pockets by throttling back the flow at the channel inlet valve and opening vents in the overhead pipeline. the channel slope, weir height and channel inlet valve were readjusted to produce the desired flow conditions and then the boundary layer velocity profile sampled at 5 stations along the channel test section. The subsequent flow analysis is summarised in Table 6-4.

Transverse flow profiles are shown in Figure 6-4. These show a pseudo free stream region across the middle two-thirds of the flow where the measured mean flow velocity may fall off to 80 per cent of the maximum velocity recorded.

The flow parameters are determined for channel Reynolds numbers,

R_c, ranging from 1.5×10^6 to 2.4×10^6 corresponding to free stream velocities of 36.7 cm/sec to 38.8 cm/sec respectively. The flow was well below the critical Froude value and there were no detectable surface waves. The flow depth was 15.5 cm and the measured boundary layer velocities ranged from a minimum of 1 cm/sec adjacent to the gravel surface to 38.8 cm/sec maximum in the free stream. The determined shape factors H show the flow to be separated and the values of C_f from the momentum integral are consistant with flow over a sand roughened plate for $\chi/k_s = 1500$ (Schlichting) where k_s is the grain size. Hence for $x = 570$ cm this corresponds to a grain size of approximately 4 mm which is consistent with the surface analysis of the gravel (Chapter 7).

6.3.3 Flow over a ship hull replica

After removing the gravel from the channel floor the 4.8 m long replica of the hull surface, described in the surface analysis Chapter 7, was lifted into the channel and positioned on the channel floor with its upstream end 3.0 m from the channel inlet. The replica fitted tightly between the channel sides and any small gaps were filled with waterproof filler. An aluminium tapered leading edge similar to one positioned against the upstream end of the three steel plates was positioned at the upstream end of the replica. the tapered upstream insert caused a gradual change in the invert level, i.e. between the channel floor and the superposed replica. An abrupt change would undoubtedly cause a local disturbance with perhaps a separation bubble. A tapered section was also positioned downstream of the hull replica, again to obviate any abrupt changes in the flow which would engulf part of the flow over the replica.

The replica was positioned on the channel floor such that the test section was sufficiently downstream of the replica's leading edge and upstream of the trailing edge to eliminate any streamwise acceleration or deceleration effects. Transverse flow profiles were taken at stations along the replicas length (Figure 6-5) and these show a pseudo free stream region across the middle two-thirds of the flow where the measured mean velocities may fall off to 90 per cent of the maximum velocity recorded.

As with the steel plate surface the larger capacity radial flow pump B can be used for the flow over the replica surface and the smaller axial flow pump A isolated. With the possibility of precipitating disturbances at the leading edge of the replica's surface, it was deemed appropriate to investigate the flow conditions immediately downstream of the replica's leading edge (Table 6-5).

The preliminary study of the flow pattern on the upstream part of the replica's surface showed no measurable detrimental effects. Hence with the chosen flow conditions a series of 9 boundary layer profiles were recorded along the working surface test section. A summary of the subsequent flow analysis is given in Table 6-6. The determined values of the local coefficient of surface friction, using the momentum integral, approximate to published values for flow over hydrodynamically smooth surfaces (Schlichting 'Boudary Layer Theory'). The mean value of the shape factor, H, of 1.4 shows the boundary layer to be well below flow separation and the mean value of the Froude number of 0.4 agrees with the tranquil visual appearance of the flow.

6.3.4 Flow over a coated ship hull replica

The final surface/flow combination studied in this investigation used the 4.8 m long hull replica with its surface covered with a brush applied coat of thixotropic anti-corrosion marine paint* (See Chapter 7.6.1). The flow system was operated under identical conditions to the flow over the uncoated replica's surface and a series of transverse flow profiles are recorded (Figure 6-6). Boundary layer traverses were taken at the nine stations along the test section and the resulting flow analysis is summarised in Table 6-7. The magnitudes of the C_f values determined from the momentum integral approximate to those for the uncoated replica surface. An inspection of the surface analyses (Chapter 7) for these two surfaces shows there to be a relatively small difference in the surface geometry with respect to the overall geometry of the surfaces.

6.3.5 The determination of C_f

To determine the local values of the coefficient of surface friction it is necessary to determine the free stream velocity and momentum thickness gradients along the test section for each flow/surface investigated. Hence, best fit lines are drawn through the momentum thickness and free stream velocity data for each flow system, and the respective gradients used in the analysis. Plots of free stream velocity versus streamwise distance, x, and momentum thickness versus x, are shown in Figures 6-7 to 6-10.

The error bars on the free stream velocity plots show a total possible error of 2.5 cm/sec on the calculation of a free stream

---

* Silver Primocon marine paint

velocity value, taken as the maximum difference between five current meter readings. The error bars on the momentum thickness plots are made up of the errors derived from the integration-by-strips method of determining θ and the error derived from the location of the y origin on the velocity distribution. Hence each value of momentum thickness, so determined, has a possible error of 0.05 cm.

The plots force the experimental data onto best fit straight lines and hence make the assumption that both the free stream velocity and momentum thickness vary linearly along the channel length.

Variations in the boundary layer thickness and the possibility of deviations from two-dimensional flow will produce significant errors in the determination of the flow parameters. A simplified picture of the turbulence intensity across the measured boundary layers can be produced by displaying the alternating anemometer bridge voltage from the hot-film probe on an oscilloscope. The degree of turbulence will depend on the roughness of the wall and the distance from the wall.

An oscilloscope with triggering, storage and camera attachment facilities was used along with a polariod camera to record the alternating component of the CTA bridge voltage. Hence a series of pictures was taken of the alternating component of the CTA bridge voltage for the hot-film probe positioned at points across the working surface shear layer. The photographs were taken with the hot-film probe positioned 6.9 m from the channel inlet, above the coated replica work surface. The oscilloscope time base was set on 5 m sec and the vertical magnification on 0.1 volt/division. Hence Figures 6-11a to 6-11h show the low 'turbulence' level in the region very near to the solid

surface, the increased turbulence level further away from the wall in the turbulent shear layer, and the lower turbulence intensity in the free stream region. In contrast to the varying degree of turbulence in the channel flow, the hot-film anemometer probe is calibrated in a situation where the intensity of turbulence is at a minimum at the centre line in smooth turbulent pipe flow. Hence there will be an element of uncertainty in the interpretation of the anemometer bridge voltage as the probe is traversed through the channel floor boundary layer. This will add to uncertainty in the calculation of C_f.

The location of the origin of the z axis on the work surface is of special interest in this and other similar analyses. For set conditions of flow over a smooth flat surface, the plane of the surface can be used as a datum from which the boundary layer velocity profile can be measured. Since all points on the surface are on the datum, then the flow velocity at any point in the flow will be related to the distance z measured from the plane.

For a rough surface a best fit plane can be fitted through the surface, but not all the points on the surface will be on the plane. Hence, if the plane is used as a datum, the origin of the datum will not always coincide with points on the surface. The choice of reference plane must somehow be related to the interaction between the fluid flow and the rough surface. For example, a surface with a relatively large value of mean slope may have steep sided peaks between which the fluid will be relatively unaffected by the streamwise fluid motion. Pools of fluid will occupy the valleys between these steep sided peaks, with the bulk of the fluid shearing over the tops of the surface peaks and these pools. Hence, a suitable datum would seem to be definable by a

flexible plane or line which is forced to lie across the tops of the surface peaks. The problem then is to decide when the geometry of the surface is such that the fluid flow near the surface cannot be adequately represented by the viscous shear approach. The scale and intensity of turbulence near to the solid surface, the values of the local surface slopes and curvatures and the distance between the surface peaks may well be important in deciding the shape of the surface datum.

FIG 6-1 SCHEMATIC DIAGRAM OF METHOD USED TO DETERMINE THE APPROXIMATE CONVERGENCE POINT OF THE FLOW CHANNEL WALL SHEAR LAYERS

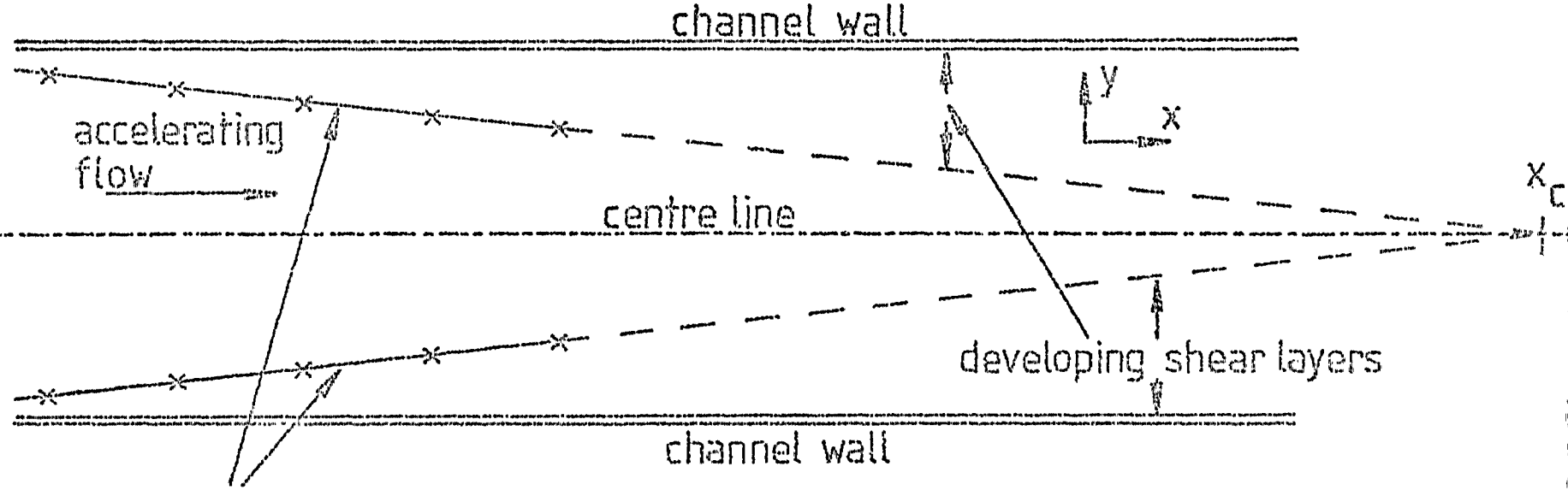

best-fit straight lines through experimentally determined cross channel velocity distributions at points on the 'boundary' between the free-stream accelerating flow and the wall shear layers. the lines are extrapolated to their cross-over point, x_c.

FIG 6-2 MEAN CTA BRIDGE VOLTAGE, NON-DIMENSIONLIZED WITH MAXIMUM VOLTAGE, VERSUS DISTANCE Y ACROSS CHANNEL FOR FLOW OVER PAINTED STEEL SURFACE (FLOW 1)

each plotted point represents the mean and standard deviation of readings taken at 2cm. intervals from z=2cm. to the fluid free surface

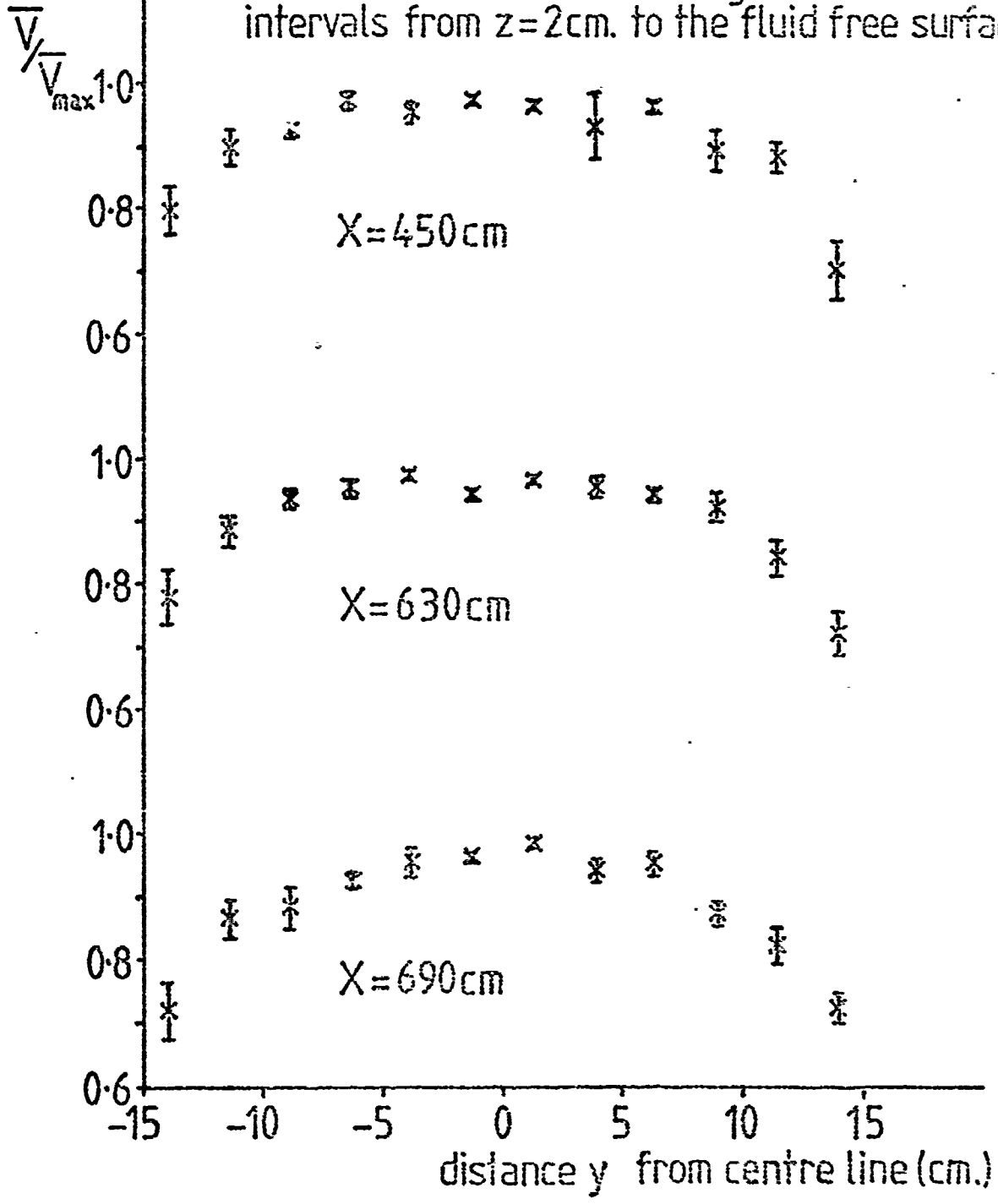

FIG 6-3 MEAN CTA BRIDGE VOLTAGE, NON-DIMENSIONLIZED WITH MAXIMUM VOLTAGE, VERSUS DISTANCE Y ACROSS CHANNEL FOR FLOW OVER PAINTED STEEL SURFACE (FLOW 2)

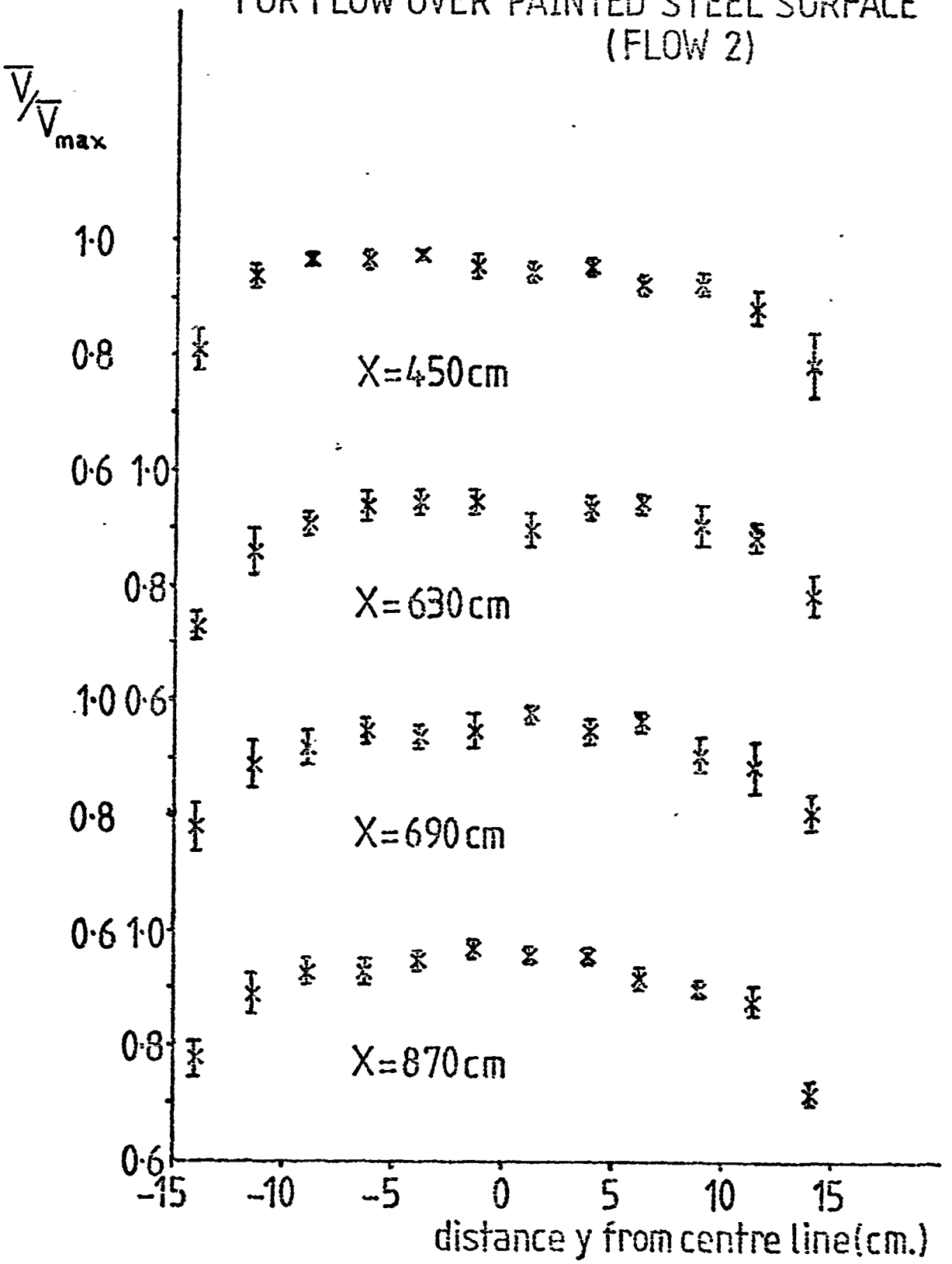

FIG 6-4 MEAN CTA BRIDGE VOLTAGE, NON-DIMENSIONLIZED WITH MAXIMUM VOLTAGE, VERSUS DISTANCE Y ACROSS CHANNEL FOR FLOW OVER GRAVEL SURFACE

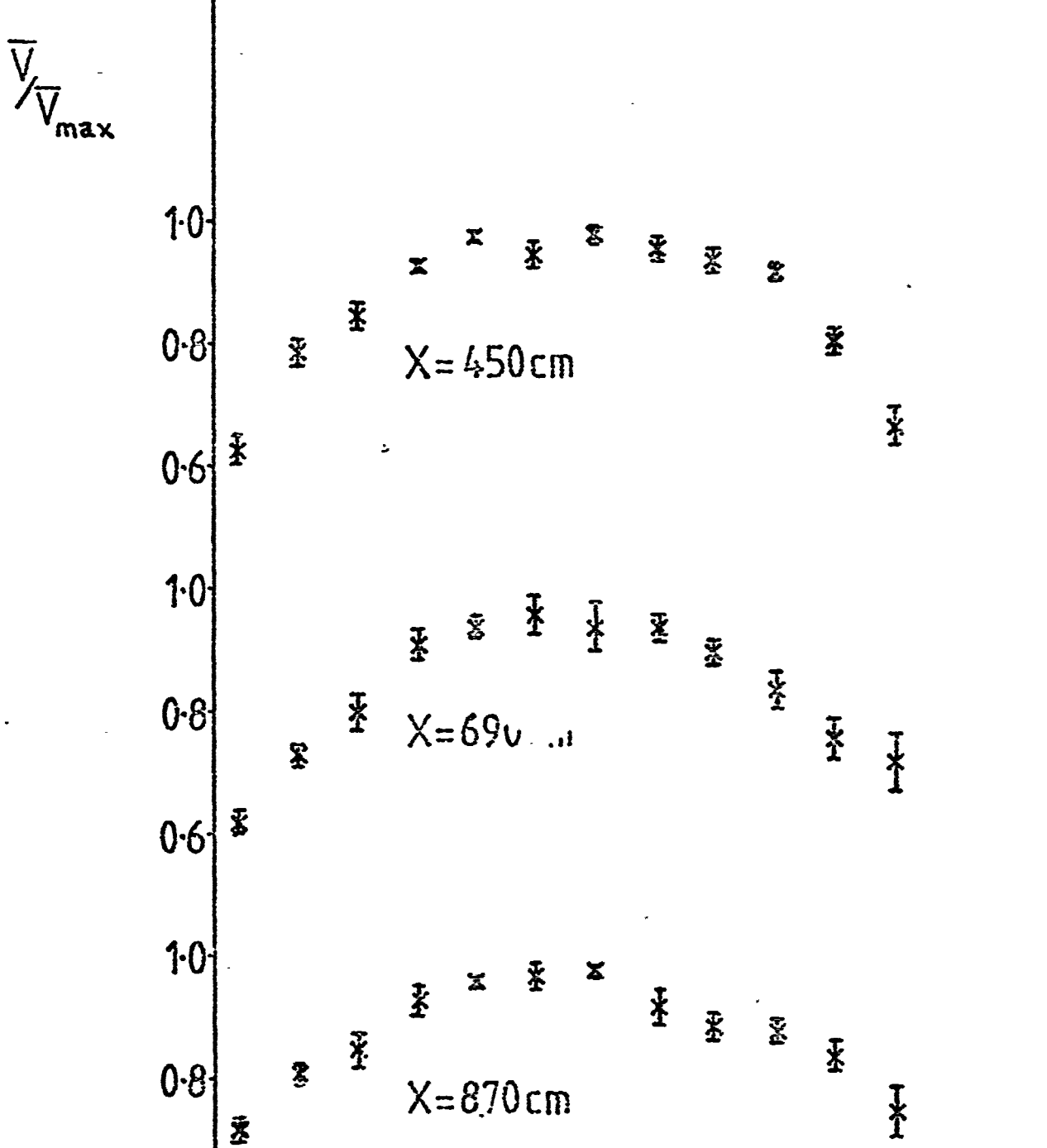

FIG 6-5 MEAN CTA BRIDGE VOLTAGE, NON-DIMENSIONLIZED WITH MAXIMUM VOLTAGE, VERSUS DISTANCE Y ACROSS CHANNEL FOR FLOW OVER REPLICA OF HULL SURFACE

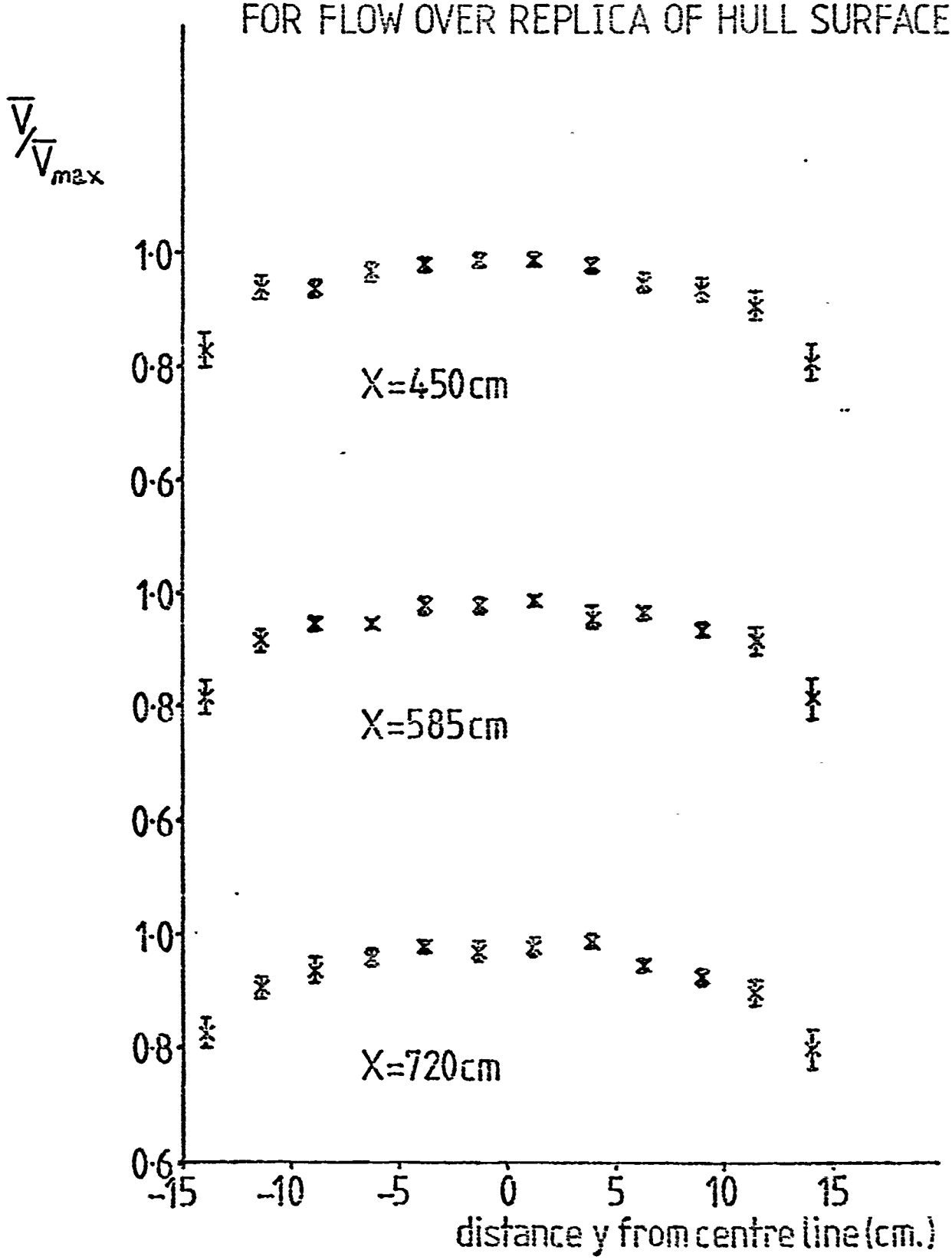

FIG 6-6 MEAN CTA BRIDGE VOLTAGE, NON-DIMENSIONLIZED WITH MAXIMUM VOLTAGE, VERSUS DISTANCE Y ACROSS CHANNEL, FLOW OVER COATED REPLICA OF HULL SURFACE

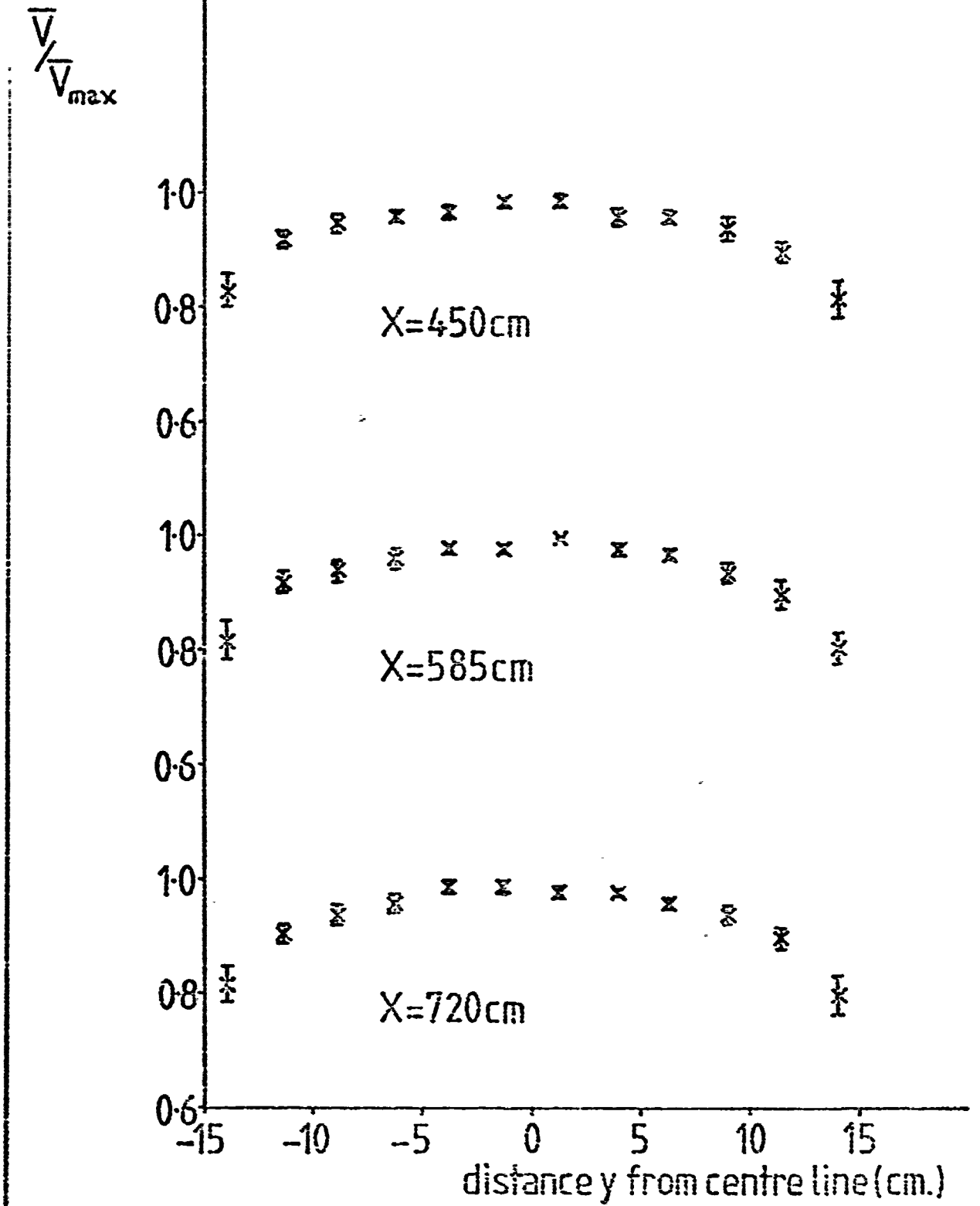

Date

Chart No.

TABLE 6-1 FLUID ANALYSIS1 OVER PAINTED STEEL SURFACE

Distanc Along x cm.	Freestr. Velocity cm/sec.	Reynold Number	Froude Number	Momentl Thickn. cm.	Displac Thickn. cm.	Shape Factor	$C_{f_{(1)}}$	$C_{f_{(2)}}$	$C_{f_{(3)}}$
450	56.30	2.3×10^6	0.37	0.36	0.67	1.84	.0032	.0023	.0031
510	56.90	2.6×10^6	0.38	0.55	1.00	1.83	.0034	.0020	.0027
570	57.40	3.0×10^6	0.38	0.56	0.81	1.45	.0034	.0026	.0029
630	57.53	3.3×10^6	0.38	0.51	0.73	1.44	.0033	.0024	.0028
690	58.13	3.6×10^6	0.39	0.59	0.84	1.43	.0034	.0026	.0029

Date

Chart No.

TABLE 6-2 FLUID ANALYSIS 2 OVER PAINTED STEEL SURFACE

Distance Along x cm.	Freestr. Velocity cm./sec.	Reynold Number	Froude Number	Moment. Thickn. cm.	Displace Thickn. cm.	Shape Factor	$C_{f(1)}$	$C_{f(2)}$	$C_{f(3)}$
450	70.92	2.9×10^6	0.47	0.09	0.11	1.18	.0030	.0049	.0030
510	71.15	3.3×10^6	0.47	0.07	0.08	1.13	.0030	.0052	.0033
570	71.09	3.7×10^6	0.47	0.04	0.04	1.10	.0030	.0056	.0035
630	72.64	4.2×10^6	0.48	0.10	0.11	1.08	.0030	.0053	.0035
690	73.43	4.6×10^6	0.49	0.16	0.18	1.17	.0031	.0045	.0033

Date

Chart No.

TABLE 6-3 FLUID ANALSIS 3 OVER PAINTED STEEL SURFACE

Distance Along x cm.	Freestr. Velocity cm./sec	Reynold. Number	Froude Number	Moment. Thickn. cm.	Displace Thickn. cm.	Shape Factor	$C_{f(1)}$	$C_{f(2)}$	$C_{f(3)}$
450	81.75	3.4×10^6	0.53	0.49	0.61	1.23	.0028	.0033	.0030
510	80.73	3.8×10^6	0.52	0.69	0.84	1.21	.0029	.0036	.0030
570	79.43	4.2×10^6	0.52	0.34	0.41	1.18	.0027	.0039	.0031
630	81.64	4.8×10^6	0.53	0.47	0.63	1.34	.0028	.0028	.0030
690	82.72	5.3×10^6	0.53	0.84	1.10	1.31	.0030	.0027	.0028

Date

Chart No.

TABLE 6-4 FLUID ANALSIS OVER GRAVEL SURFACE

Distance Along x cm.	Freestr. Velocity cm./sec	Reynold. Number	Froude Number	Moment. Thickn. cm.	Displace Thickn. cm.	Shape Factor	$C_{f(1)}$	$C_{f(2)}$	$C_{f(3)}$
450	36.69	1.5×10^6	0.30	1.03	3.86	3.75	.0058		
510	37.54	1.7×10^6	0.30	1.18	4.91	4.17	.0063		
570	38.14	2.0×10^6	0.31	1.23	4.26	3.48	.0061		
630	38.31	2.2×10^6	0.31	1.08	4.24	3.92	.0059		
690	38.82	2.4×10^6	0.31	0.95	4.11	4.32	.0057		

Date

Chart No.

TABLE 6-5 PRELIMINARY FLOW ANALYSIS OVER REPLICA SURF.

Distance Along x cm.	Freestr. Velocity cm./sec	Reynold. Number	Froude Number	Moment. Thickn. cm.	Displace Thickn. cm.	Shape Factor	$C_{f_{(1)}}$	$C_{f_{(2)}}$	$C_{f_{(3)}}$	$C_{f_{L-T}}$
390	61.79	2.2×10^6	0.44	0.50	0.71	1.41	.0033	.0026	.0031	.0032
420	62.13	2.4×10^6	0.44	0.53	0.74	1.39	.0033	.0027	.0031	.0033
450	62.01	2.6×10^6	0.44	0.61	0.84	1.38	.0034	.0027	.0030	.0032
480	62.81	2.8×10^6	0.44	0.69	0.95	1.37	.0035	.0026	.0031	.0032
510	62.41	2.9×10^6	0.44	0.53	0.73	1.37	.0033	.0029	.0031	.0034

Date

Chart No.

TABLE 6-6 FLOW ANALYSIS OVER REPLICA SURFACE

Distance Along x cm.	Freestr. Velocity cm./sec.	Reynold. Number	Froude Number	Moment Thickn. cm.	Displace Thi'dsn. cm.	Shape Factor	$C_{f_{(1)}}$	$C_{f_{(2)}}$	$C_{f_{(3)}}$	$C_{f_{L-T}}$
450	60.63	2.5×10^6	0.43	0.47	0.63	1.34	.0031	.0030	.0032	.0037
480	61.75	2.7×10^6	0.44	0.47	0.69	1.45	.0032	.0026	.0031	.0031
510	62.44	2.9×10^6	0.44	0.50	0.68	1.36	.0032	.0029	.0032	.0035
540	62.54	3.1×10^6	0.44	0.47	0.65	1.36	.0031	.0029	.0032	.0036
570	62.78	3.3×10^6	0.44	0.57	0.76	1.34	.0033	.0028	.0031	.0035
600	63.22	3.5×10^6	0.45	0.53	0.71	1.34	.0032	.0030	.0031	.0035
630	63.80	3.7×10^6	0.45	0.60	0.82	1.37	.0034	.0027	.0030	.0033
660	64.24	3.9×10^6	0.45	0.59	0.79	1.35	.0033	.0028	.0030	.0034
690	64.34	4.1×10^6	0.45	0.70	0.98	1.39	.0036	.0025	.0029	.0030

Date

Chart No.

TABLE 6-7 FLOW ANALYSIS OVER COATED REPLICA SURFACE

Distance Along x cm.	Freestr. Velocity cm./sec.	Reynold Number	Froude Number	Moment. Thickn. cm.	Displace Thickn. cm.	Shape Factor	$C_{f_{(1)}}$	$C_{f_{(2)}}$	$C_{f_{(3)}}$	$C_{f_{L-T}}$
450	60.82	2.5×10^6	0.43	0.47	0.65	1.39	.0031	.0029	.0032	.0034
480	61.79	2.7×10^6	0.44	0.50	0.71	1.42	.0032	.0027	.0031	.0032
510	62.41	2.9×10^6	0.44	0.51	0.72	1.41	.0032	.0029	.0031	.0032
540	62.98	3.1×10^6	0.44	0.55	0.78	1.40	.0032	.0026	.0030	.0032
570	63.21	3.3×10^6	0.45	0.59	0.83	1.40	.0033	.0025	.0030	.0031
600	63.92	3.6×10^6	0.45	0.53	0.74	1.41	.0032	.0027	.0031	.0032
630	64.26	3.7×10^6	0.45	0.67	0.95	1.41	.0035	.0027	.0029	.0030
660	64.34	3.9×10^6	0.45	0.59	0.81	1.38	.0033	.0028	.0031	.0032
690	64.45	4.1×10^6	0.45	0.66	0.89	1.35	.0034	.0027	.0030	.0033

FIG 6-7 PLOT OF FREE-STREAM VELOCITY VERSUS DISTANCE ALONG FLOW CHANNEL FOR REPLICA OF HULL SURFACE

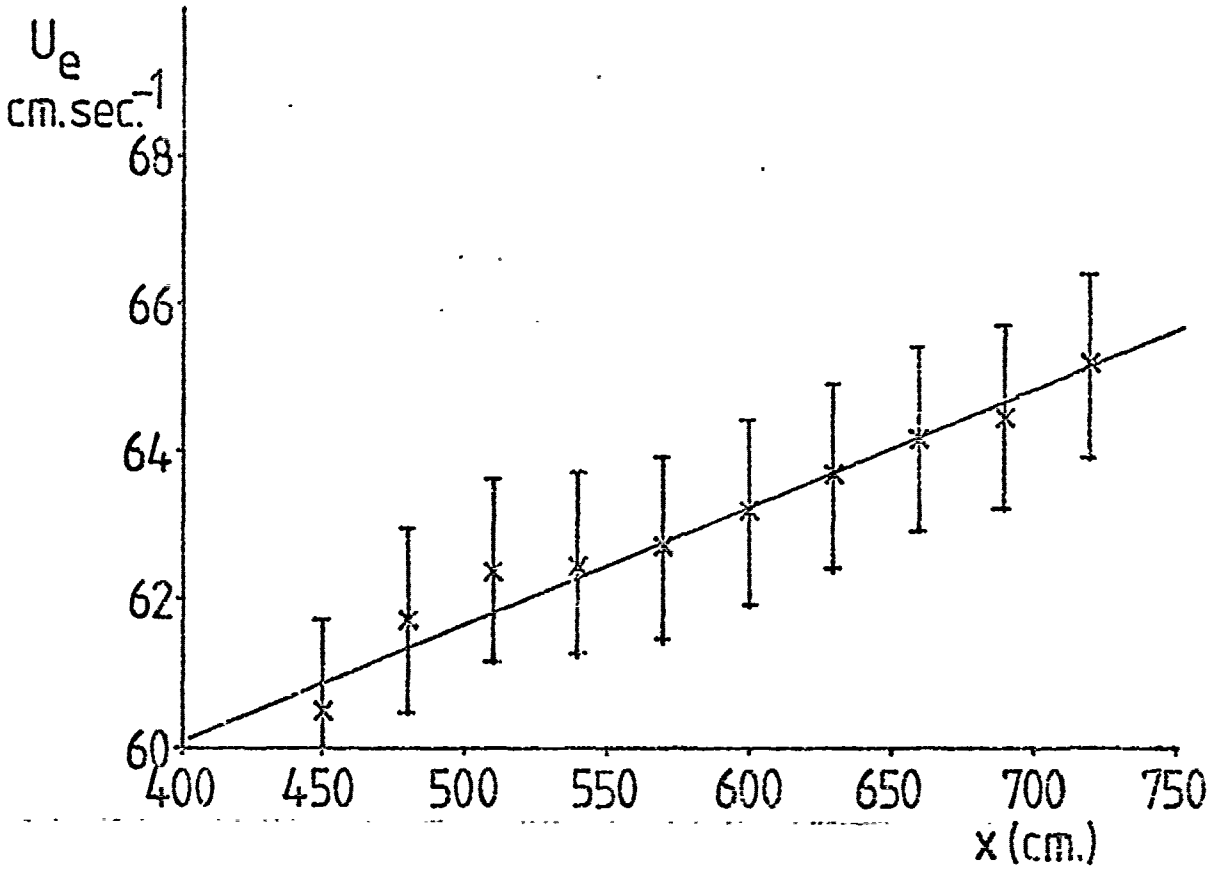

FIG 6-8 PLOT OF MOMENTUM THICKNESS VERSUS DISTANCE ALONG FLOW CHANNEL FOR REPLICA OF HULL SURFACE

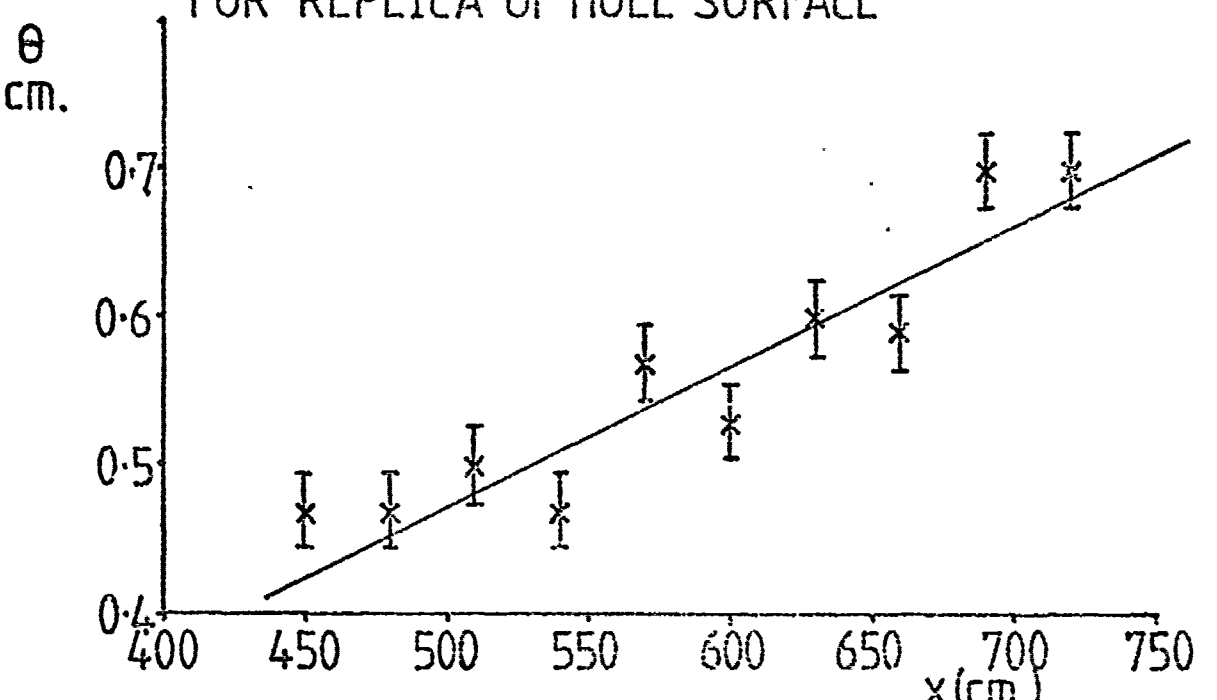

FIG 6-9 PLOT OF FREE-STREAM VELOCITY VERSUS DISTANCE ALONG FLOW CHANNEL FOR COATED REPLICA OF HULL SURFACE

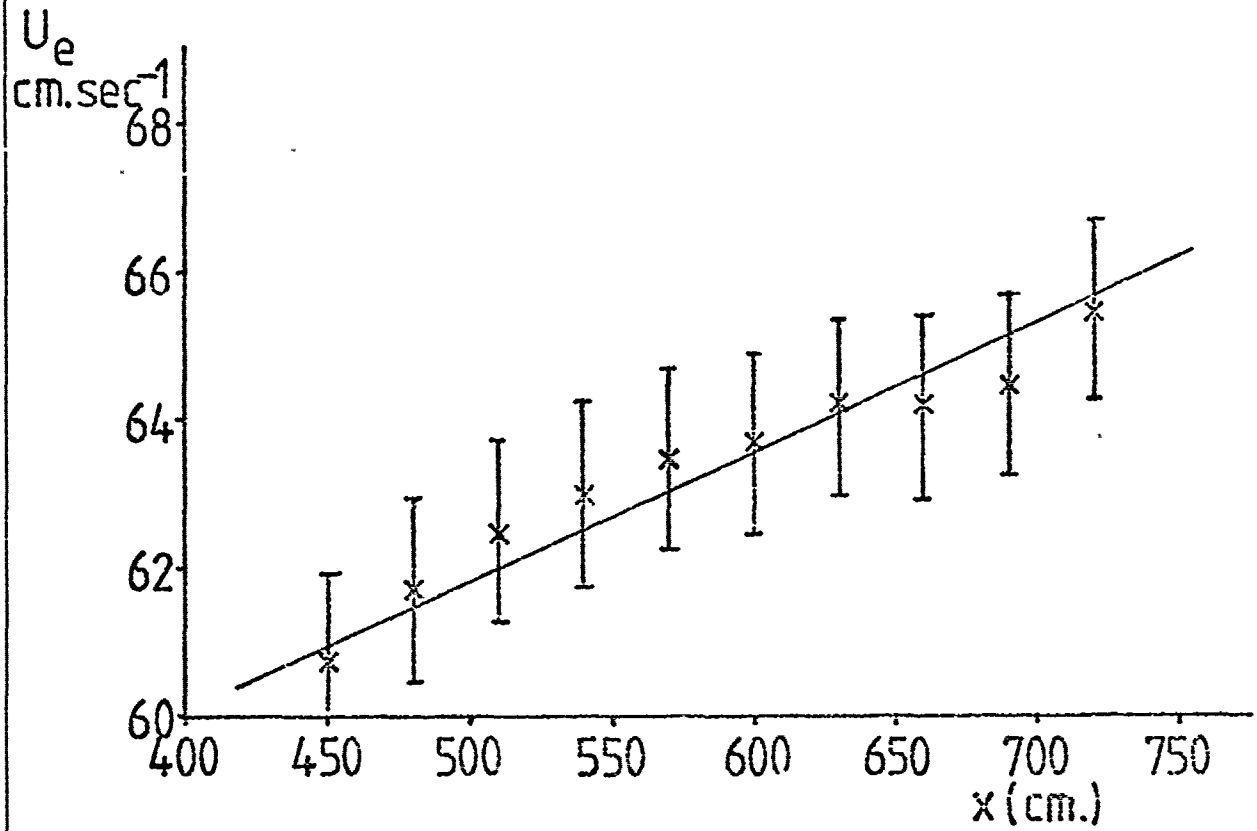

FIG 6-10 PLOT OF MOMENTUM THICKNESS VERSUS DISTANCE ALONG FLOW CHANNEL FOR COATED REPLICA OF HULL SURFACE

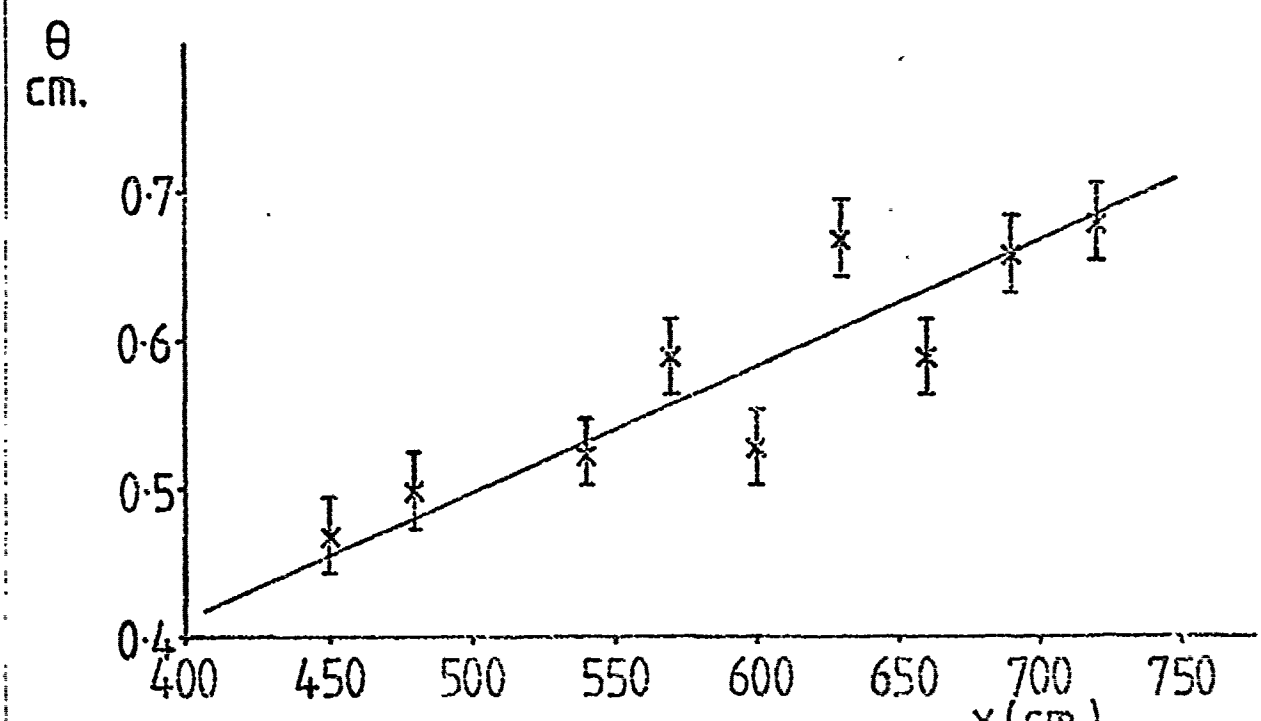

FIG 6-11a OSCILLOSCOPE TRACE OF C.T.A. BRIDGE VOLTAGE FOR PROBE POCITIONED 6·9m. FROM CHANNEL INLET, OVER COATED REPLICA SURFACE

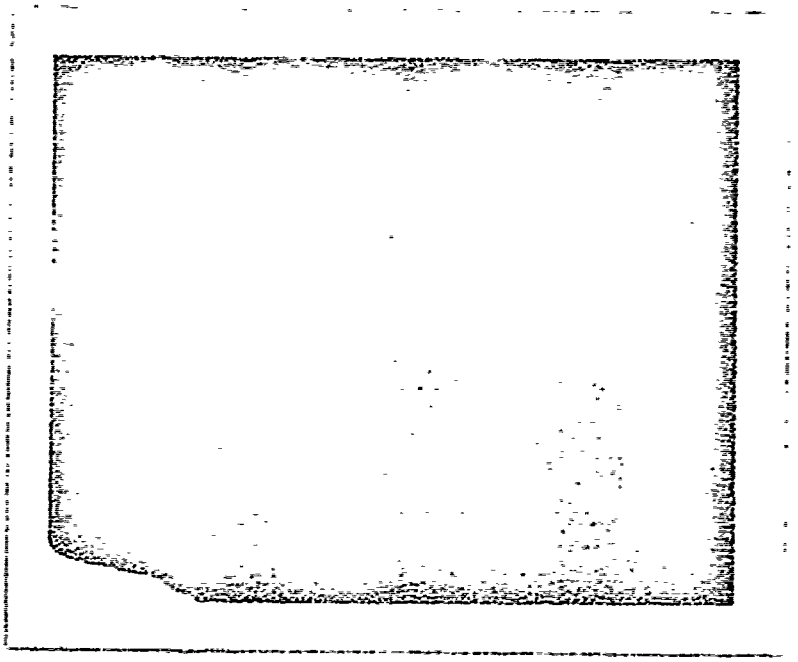

z ≃ 0·5mm.; 0·1 volt/division; time base = 5 m.sec.

FIG 6-11b

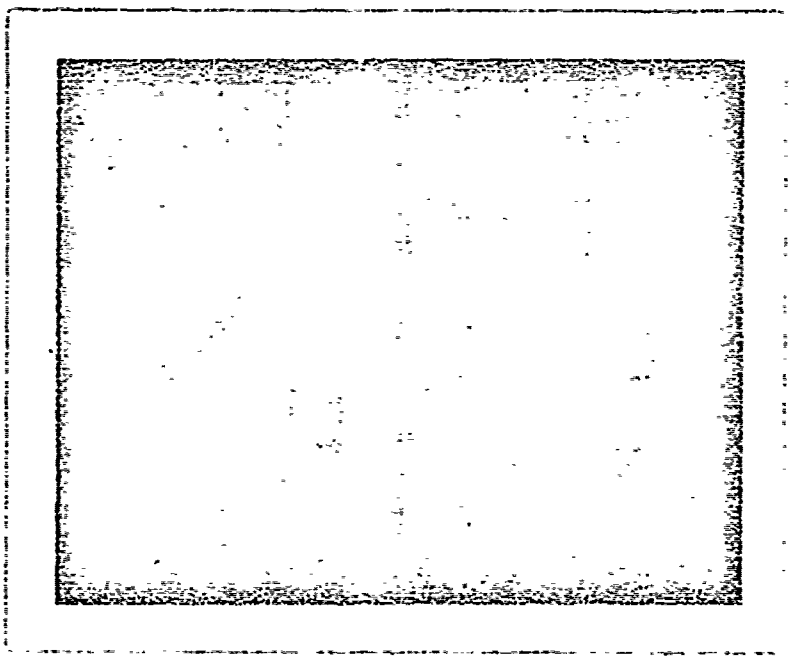

z = 1·0mm.; 0·1 volt/division; time base = 5 msec.

FIG 6-11c

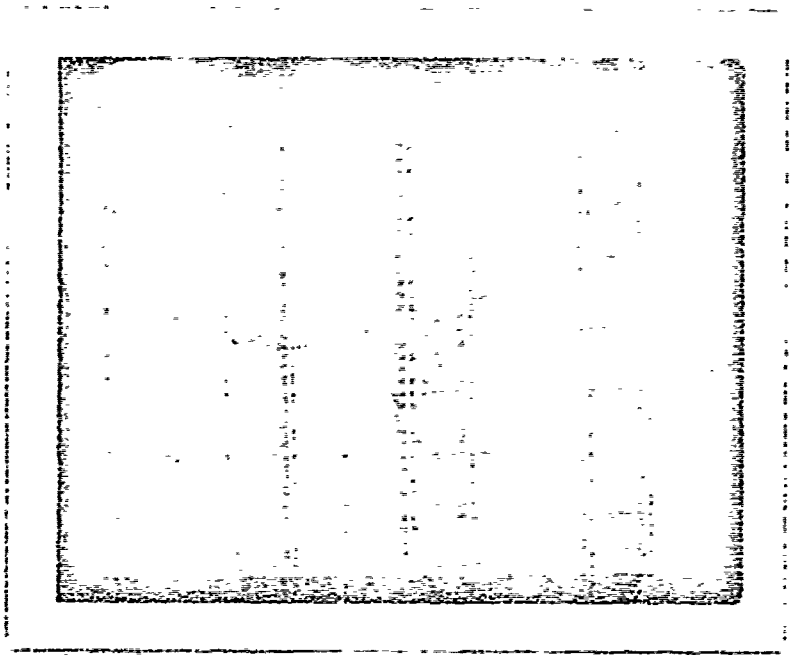

z = 1·2 cm.; 0·1 volt/division; time base = 5 msec.

FIG 6-11d

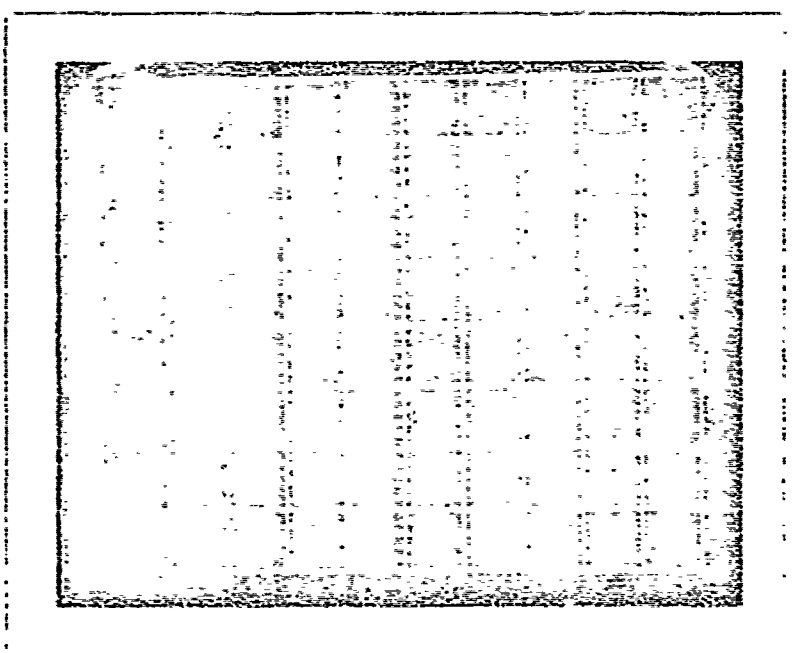

z = 2·3 cm.; 0·1 volt/division; time base = 5 msec.

FIG 6-11e

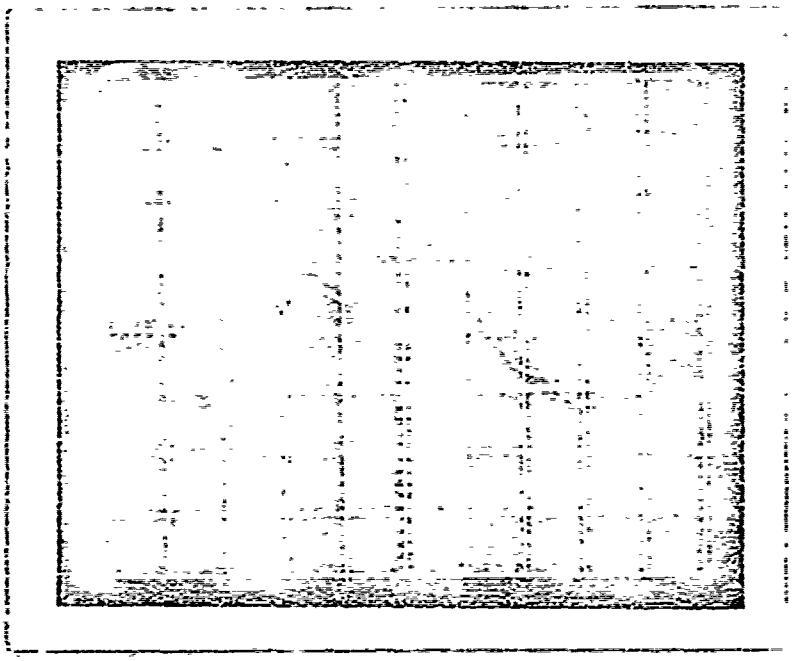

z = 4·5 cm; 0·1 volt/division; time base = 5 msec.

FIG 6-11f

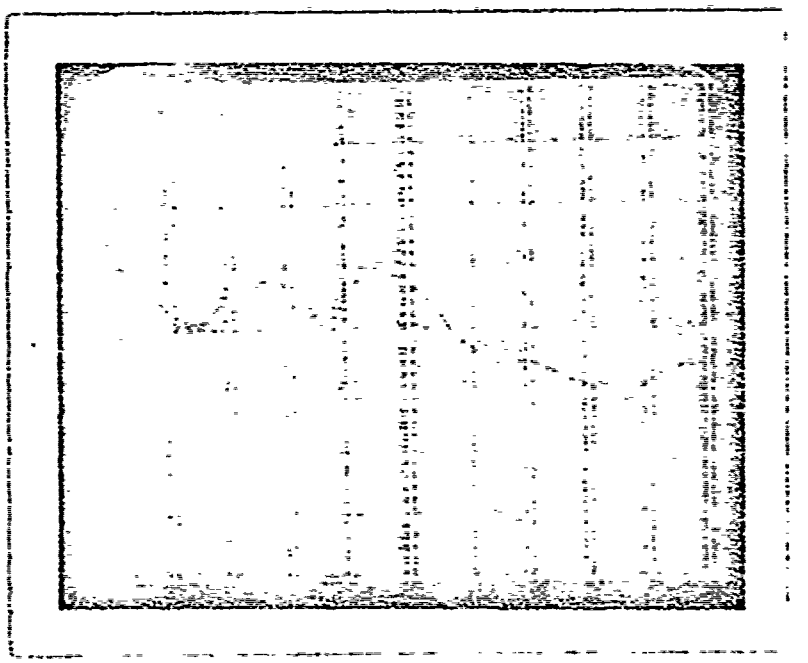

z = 6·7 cm.; 0·1 volt/division; time base = 5 msec.

FIG 6-11g

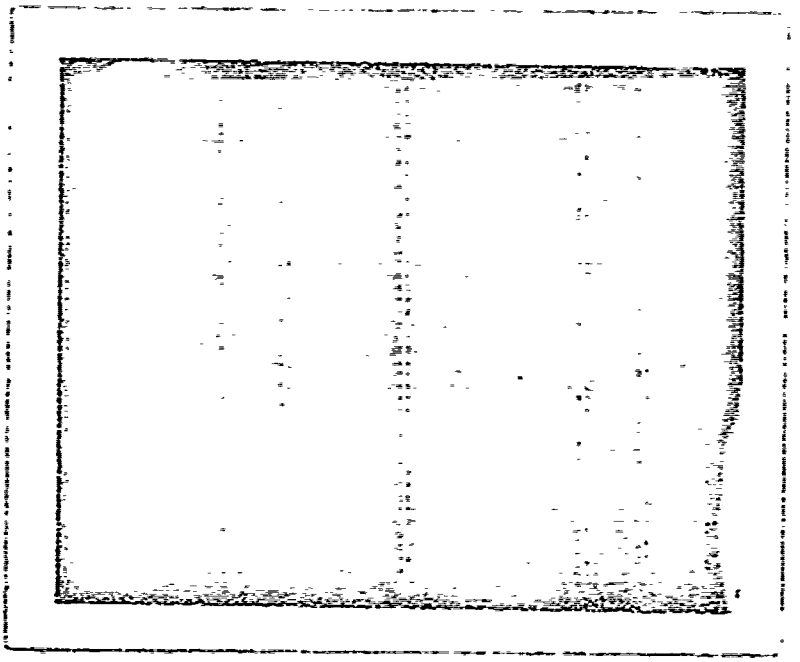

z = 8·9 cm.; 0·1 volt/division; time base = 5 msec.

FIG 6-11h

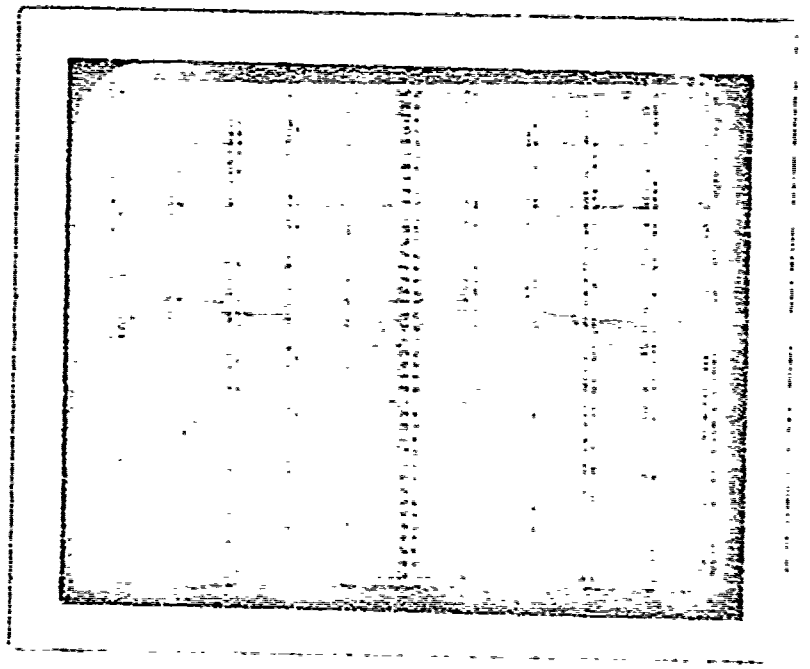

z = 13·3 cm.; 0·1 volt/division; time base = 5 msec.

7. THE SURFACE ANALYSIS

7.1 Introduction

In this investigation tests have been carried out on various surface geometries which make up the floor of a 17.4 m long glass-sided flow channel (Figure 2-1). An attempt is made to relate a section or sections of the spectrum of surface wavelengths present to changes in the flow regime resulting in relatively large increases in the surface frictional resistance. The study is divided into two main sections: the measurement and analysis of the channel floor surface geometry and the measurement and analysis of the fluid flow over the channel floor. The results of both sections are then brought together and the inter-relation of the surface geometry and frictional resistance deduced.

7.2 Preliminary roughness measurements on ship hull surface replicas

Surface measurements were taken on two surface replicas and the subsequent statistical analyses of the surface were used to help identify significant characteristics of the type of surface under investigation. The first of these replicated surfaces was a positive acrylic replica taken from a heavily corroded ship hull by the British Ship Research Association (BSRA).

A network of 50 mm long surface profiles was recorded using the Talylin stylus instrument connected to a data logging system. The surface measured approximately 15 cm by 30 cm. A specially designed stylus is used for these relatively rough surfaces, the stylus having

an included angle of 30 degrees and a tip width of 460 μm. The electrical output from the stylus instrument is digitised and recorded on punched paper tape for computer analysis, the results of which are given in Tables 7-1 to 7-8 and Figures 7-1 to 7-3. The analyses show the surface peaks to have a much higher radius of curvature than the valleys and the height distributions to be negatively skewed. These results are typical of a profile which has lost its peaks in some way. The most common explanation for the removal of peaks is given in terms of some kind of wear mechanism (Thomas 1972). The peaks will be worn down towards their broader bases increasing the distance across the peak, whilst the valley will be relatively unaffected. The peaks' higher radius of curvature and the negatively skewed height distribution can also be explained by the modification of the surface by the replication process. The physical properties of the replication material may be such that it cannot exactly follow the contours of the specimen surface, bridging valleys or building up on the shoulders of peaks.

The second replica surface consisted of a positive resin replica taken from the hull of a Shell oil tanker. The amplitude of the surface features was such that the Talylin instrument using both the standard stylus and the specially designed stylus was incapable of recording the large height variations encountered on the surface. Hence an extension stylus with a ball end of 1.6 mm was constructed producing a 2:1 lever reduction on the standard stylus. The maximum stylus traverse length was reduced by half to 50 mm which coincided with the reference length used by the BSRA Wall Gauge (Canham 1956). The stylus was used to record ten 50 mm profiles from the surface. The measurements consisted of two parallel traverses along the length of the replica each made up of five consecutive 50 mm sample lengths.

A summary of the analyses of the ten sample lengths is given in Tables 7-9 and 7-10. The results again show the mean peak radius of curvatures to be greater than the mean valley radius of curvatures, hence the peaks are more rounded than the valleys.

The measurement of replicated surfaces is often found to be the only practical method of carrying out a comprehensive analysis of a surface, as has been the case for ship hulls, whose inaccessibility and surface condition is such that the necessary delicate electronic surface measuring equipment is generally inoperative in such conditions. The need for measurements on actual ship hull surfaces is underlined here by the inconclusive analyses of the replicated surfaces. Hence new surface measuring instruments are required which are capable of working in various orientations, unaffected by possible contact with salt water and marine growths, and capable of providing the information necessary for a comprehensive surface analysis.

7.3 Surface measurements on detachable ship hull plates

Surface measurements were carried out on four specially painted steel plates before and after their attachment to the bilge keel of a supertanker for the duration of a 6 month deep sea voyage. These measurements were primarily to investigate the surface properties of a specific marine paint under the action of fluid flow. The paint used, produced by Internation Marine Coatings, is specified as a 'self-polishing' marine paint. Under the action of fluid flow over the coated surface, the tops of the highest surface peaks are 'polished' down whilst the valleys, protected by adjacent peaks, are relatively unaffected, resulting in an overall reduction of the surface roughness.

The specimen plates used were 100 cm long by 70 cm wide. Three of the plates were roughly painted to simulate a typical in-service re-painting whilst the fourth plate was smoothly painted. Two traverses using a Talylin stylus instrument were taken on each plate as shown in Figure 7-4. Each traverse is made up of between 9 and 11 consecutive 50 mm gauge lengths which are analysed separately. The standard Talylin stylus, a steel chisel with a radius of curvature of 0.6 - 1.2 mm could be used on the smoothest plate whilst for the other three roughly painted plates the coarser stylus with a ball end of 1.6 mm diameter was used (see previous surface measurements, Section 7.2). A summary of the subsequent surface analysis is given in Tables 7-11 to 7-14. In each column the first figure is the average for all the 500 mm gauge lengths in that traverse; the second figure (in parentheses) is the standard error of the mean; the third figure is the number of gauge lengths averaged over. The results from the two parallel traverses on each plate are reasonably self-consistent on all plates except MB1. This is true both for the initial and later results, and is a good indication that the surfaces are homogenous.

The smoothest plate, MB2, does not appear to become any smoother, in fact its CLA roughness has increased (Table 7-11), while the peak and valley radii of curvature increased by between 1½ and 3½ times. The figures for the slopes are not very informative, since one has increased while the other has decreased. The other three plates (Tables 7-12 to 7-14) become smoother by a consistent 70 to 80 per cent. Each of the three roughness parameters CLA, RMS and MAA show this effect to nearly the same degree. Their mean slopes are lower by 70 to 80 per cent and the peak and valley radii of curvature are higher by factors of between 1½ and 8.

In Figure 7-5 cumulative surface height distributions are plotted on a normal probability scale and it can be seen that the earlier distribution is much rougher over the upper portion of the surface than over the lower. This result agrees with its visual appearance as a relatively smooth plane covered with raised droplets of dried paint. The later distribution, though overall much smoother, shows a similar trend, suggesting that the loss of roughness is not necessarily all at the peaks. Other evidence which suggests this is that the increases in peak radii of curvature are no greater than the increases in the valley radii of curvature. The computed values for the power spectral density functions, derived from the autocovariance function are shown in Figure 7-6. The figure shows the drop-off in power of the wavelengths present on one of the roughly painted plates, MT1, after the ocean voyage in comparison to before the voyage.

The above results show that the marine coating used has the useful hydrodynamic property of its surface becoming smoother with the action of fluid motion. Thus, a hull surface may be rapidly recoated in dry dock and the resulting uneven surface finish will become smoother whilst the ship is in service. This is a much more economic method of providing a smooth surface finish than by producing the same surface in dry dock.

The afore-mentioned results from the coated detachable ship hull plates can be explained by the following hypothesis: When the roughly coated surfaces are placed in situ on the ships hull, the highest peaks of the coating may protrude through the quiescent inner region of the ship's boundary layer. The summits of the highest peaks will subsequently be exposed to the relatively violent action of the outer turbu-

lent flow. The smaller peaks and the surface depressions, enveloped by the inner viscous layer, are protected from the wearing action of the turbulent outer flow and so will remain unchanged. The properties of the coating are such that the fluid action will produce a surface with an overall reduction in the mean value of roughness.

This implies that the viscous layer adjacent to the specimen surface has a thickness comparable to the surface roughness amplitude. In fact, the final value of the average or rms roughness amplitude will, if the polishing mechanism is correctly explained, give an indication of the thickness of the viscous layer adjacent to the specimen surface. The mean value of the rms roughness of the surfaces after the ocean voyage is approximately 15 μm, hence if all the surface features protruding through the viscous layer have been removed then the thickness of the viscous layer is in the region of 15 μm.

7.4 Introduction to the measurement of the channel test surface geometry

The initial channel floor working surface consisted of three lengths of half inch thick shot-blasted steel plate butted up end to end along the flow channel. A selection of surface measuring instruments were used to record as wide a spectrum of surface features as possible. In this way as much information as possible about the surface geometry can be made available for an analysis of the work surface.

7.5 Surface measurement instrumentation

The measurement procedure was such that the longer surface fea-

tures were investigated initially and then instruments capable of recording surface features of decreasing dimensions were employed.

(a) The Talyvel* electronic level is used to record profiles along the entire length of the channel floor. The Talyvel has a sampling interval of a few centimetres and a sampling length of up to the total length of the work surface. The instrument measures the inclination of a surface, upon which its feet are resting, by means of a suspended pendulum whose flat top rests against two variable inductance transducers. The transducers provide an electrical displacement signal, related to the tilt of the pendulum, which is amplified and applied to a centre-zero meter. The instrument is traversed along the channel centre line in steps equal to the mean separation of the feet, 9 cm. The inclination of the surface is measured in units of inches of inclination per inch and a small computer program is used to convert these into height readings.

(b) A dial gauge, held in a magnetic clamp with its measuring probe perpendicular to the work surface, is used to record spot heights on the surface relative to a 122 cm long straight edge laid lengthwise along the centre line of a section of the work surface. The dial gauge is used to record surface features of horizontal dimensions from a few millimetres to tens of centimetres in length.

The dial gauge has a ball end measuring head with a diameter of 2 mm. One small division on the dial scale represents a vertical movement of 2.54 μm.

---

* Talyvel is a Rank Taylor Hobson instrument.

(c) Measurements can also be taken along the entire length of the work surface using a mechanical stylus instrument, the BSRA wall gauge. The gauge consists of a metal stylus, in contact with the surface, connected by mechanical linkage to a smaller stylus. The smaller stylus duplicates the motion of the larger stylus by scratching its path onto a graphite coated glass slide. the length of the recorded profile is reduced by a factor of 10, whilst the transverse motion remains at unity. The motion of the stylus is relative to a track-way magnetically clamped to the work surface upon which the gauge, mounted on wheels, is manually propelled.

The recorded surface profile can be analysed by projecting the magnified image of scratched profile onto a digitising table connected to a paper tape punch. The sampled height readings can then be computer analysed to give a measure of the surface roughness.

(d) A Ferranti three-axis measuring table is used to measure spot height profiles for surfaces which have a variation in heights too great to be recorded by the afore-mentioned instruments. The tapered steel measuring probe has a tip radius of approximately 500 μm. The probe is held in a chuck along the vertical axis of the measuring table. The probe can then be traversed along the three axes manually to any position on the work surface placed on the measuring table below the probe. A series of traverses can be taken across the work surface, for which the probe is moved horizontally in convenient step lengths and the probe lowered to come into contact with the surface at each measuring point. The orientation of the probe relative to the three axes can be read off from three digital displays which are connected to a print-out unit which automatically records the relative position of the probe on punched paper tape.

(e) Three electronic stylus instruments* were available to measure the relatively small surface wavelengths in the range from a few micrometres to a few centimetres in length. A typical stylus instrument (Figure 7-7) consists of a pick-up driven by a gear box which draws the stylus across the surface at a constant speed. The stylus is connected to a transducer which converts its vertical movement, relative to some datum, into an oscillating electrical signal which is then electronically amplified. The output can then be either fed to a chart recorder for a profile trace to be made, or it can be digitised and stored on punched paper tape for a subsequent computer analysis.

The Talysurf and Surfcom stylus instruments are such that for this investigation they can not be used in situ on the channel floor and hence a representative piece of the channel floor surface had to be brought to the instruments for measurements to be taken.

7.6 The measurement and analysis of the surfaces under investigation

7.6.1 A preliminary study of the means available to alter the geometry of a surface

In order to correlate surface parameters with related flow parameters it is essential to have a means of producing a variety of work surfaces with predictable trends in their overall geometry. Applying successive coats of paint to a surface was though to be a possible way of producing a number of surfaces with differing surface features.

---

* The Talylin 1 and the Talysurf 3 stylus instruments produced by Rank Taylor Hobson and the Surfcom produced by Ferranti.

Hence a study was carried out to examine the changes in the statistical microgeometry of a steel surface with successive coats of paint, using a stylus instrument. Preliminary measurements on the coating material* showed the stylus instrument to be capable of recording accurate profiles of the coating surface. The subsequent measurements showed that on the application of the initial coat of paint the surface roughness decreased substantially, whereas on further application of paint the surface roughness does not change by anywhere near the initial amount.

The results are given in full in Appendix 3, as published in the Journal of Coatings Technology, August 1978.

7.6.2 Looking into the possibility of damage caused by stylus instruments on coated surfaces

The diamond stylus of a Talysurf 3 instrument was drawn across the surface of a coated** glass slide and a Vickers high power microscope used to view the area of the surface traversed by the stylus. A mark left by the stylus could be detected and an approximate value of its depth was obtained using the microscopes calibrated micrometer scale. By focussing on the top and bottom of the stylus mark the depth of which was found to be approximately 1 μm.

A light-section microscope set on x400 magnification is used to view the section of surface over which the stylus has passed. Any

---

* Silver Primocon marine paint.

** The coating consisted of a dip-applied coating of Silver Primocon paint, applied twenty four hours previous to the investigation.

mark left by the stylus was undetected, hence from a knowledge of the resolution of the microscope it is possible to approximate the depth of the previously detected stylus mark. Assuming the resolution of the microscope is limited by the thickness of the light image line, then the depth of the stylus mark must be less than the microscope's resolution for the mark to be undetected, that is, less than 2 μm.

The coating thickness was measured using a Talysurf 4 stylus instrument connected to a chart recorder. The stylus was traversed across the surface of a glass slide, half of which is coated. The traverse was taken in order to record on the chart recorder the path of the stylus across the coated surface and onto the uncoated part of the slide, from which the coating thickness was found to be approximately 13 μm.

The Vickers hardness of the coating, determined using a Leitz Wetzlar Hardness Tester was approximately 50 on the hardness scale.

7.6.3 The painted steel surface

The surface consists of three, 0.5 inch thick, shot-blasted steel plates with a spray-applied coat of primer paint* and a subsequent brush applied coat of marine paint**.

The Talyvel electronic level is used to record a profile along the centre line of the channel floor. The surface is sampled along

---

* A two pack reinforced edge type primer paint, Metagard G250.

** A thixotropic anticorrosion marine paint, Silver Primocon.

its entire length of 17.4 m at sampling intervals of 9 cm, 203 samples in all. The statistical analysis of the sampled heights is summarised in Table 7-15. The recorded profile is shown in Figure 7-8.

The dial gauge, held in a magnetic clamp, is traversed across a section of the work surface and the surface heights sampled at 5 mm intervals. A 122 cm long engineering straight edge laid along the specimen section of the surface is used as a datum for the dial gauge readings. The magnetic clamp holding the dial gauge in contact with the surface is moved along the length of the datum and the sampled heights recorded manually on punched computer cards. The dial gauge ball end measuring probe, 2 mm in diameter, is traversed over a total sample length of 114 cm resulting in 228 sample heights. A visual inspection of the surface showed it to be sufficiently homogenous, within the range of surface features measured by the dial gauge, to allow a measured section of the surface to be treated as representative of the surface as a whole. The subsequent statistical analysis is summarised in Table 7-15.

The BSRA wall gauge is used to record a series of 26 consecutive surface profiles. The sample length of each profile is 63.5 cm and the measuring probe has a diameter of 1.6 mm. The surface profiles are recorded on standard glass slides coated with colloidal graphite, the profiles having a 10:1 horizontal reduction. The results of an analysis of the profile data is given in Table 7-16.

The Talylin stylus instrument is used to record profiles at a number of positions on the work surface (Figure 7-9). The stylus is conical hardened silver steel with a tip diameter of 0.46 mm. A sample

length of 10.2 cm is used with a sampling interval of 190 μm for each of the recorded profiles. A summary of the statistical analysis for the surface is given in Table 7-15.

A small sample of the painted steel surface, approximately 15 cm^2, is produced so that it can be fixed to the bed of the Talysurf 3 stylus instrument for subsequent measurement. A single sample is taken from the downstream end of the steel plates due to the destructive nature of this measurement. The measurement on the sample is assumed to be representative of the surface as a whole and this is to some extent justified by the homogenous appearance of the painted steel surface. The Talysurf stylus, in the form of a truncated diamond pyramid of tip dimensions 8 μm by 2.5 μm, is traversed across the surface for a sample length of 8 mm. The analysis of the measured profile is summarised in Table 7-15.

Figure 7-10 shows a single plot of the power spectral density functions computed from the measurements made by the various surface instruments used on the painted steel surface. The curve is a reasonable fit to the inverse-square law for a surface with a gaussian height distribution.

The analyses as a whole (Table 7-15) show the measured peak and valley curvatures and surface slopes to decrease with increasing sampling interval and sample length. This is because unlike true random data which has limits of plus and minus infinity, surface heights are distributed within a relatively narrow band governed by the mechanical properties of the constituent material and the surface function. Similarly the RMS roughness increases with increasing sampling interval and sample length.

7.6.4 The gravel surface

A specimen of the gravel surface was made up by bonding a closely packed layer of gravel to a rigid backing surface producing a surface 30 cm^2. It was not posssible to record the relatively large surface slopes present on the gravel surface with the conventional surface measurement instrumentation. Hence, the specimen surface was placed on a Ferranti three-axis measuring table and a profile of the surface recorded on punched paper tape. The sample length used is 27 cm with a sampling interval of 1 mm. A summary of the statistical analysis of the recorded profile is given in Table 7-17. The recorded profile is shown in Figure 7-11. The distribution of surface slopes is shown in Figure 7-13 and the distribution of curvatures in Figure 7-12.

7.6.5 The ship hull replica surface and the coated replica surface

The replica of the ship hull surface was produced using a two-stage replication process perfected by Shell Research Ltd.

The technique involves clamping a framework, to retain the replication material, against a vertical flat section of the dry docked ship hull. Neoprene rubber solution is poured into the space between the hull and the framework and cures whilst constrained to take up the geometry of the hull surface. The surface replicated was taken from the side of a badly corroded hull.

The resulting 'negative' replica of the surface, approximately 3 cm thick by 5 m long by 0.4 m wide, is peeled away from the mating hull surface after removing the constraining framework. The first

stage of the replication process can then be transported from the dry dock to the laboratory containing the flow analysis equipment. A flat, levelled, wooden base was made up on the laboratory floor and the neoprene sheet, replicated surface upwards, placed on it. A closely fitting framework was bolted around the edges of the neoprene replica to form the sides of an open-topped reservoir into which a layer of resin* is poured. The resulting resin cast (Figure 7-14), approximately 1.5 cm thick by 483 cm long by 30.5 cm wide, is allowed to harden for 7 days and then carefully pulled away from the neoprene negative.

The underside of the resin cast forms the positive replica of the hull surface, hence the up-turned cast can be lowered into the flow channel to form the work surface. The mass of the replica plus its flexibility allowed it to take the form of the channel floor, producing a rigid surface.

A statistical analysis of the replica surface is computed for each of four instruments capable of recording a wide range of the surface features. The hull replica is investigated both for its untreated surface and with a coat of paint applied to the surface (see Chapter 7.6.1). Hence for each surface, digitised profiles were recorded using:

(1) A Talyvel electronic level is used to record 3 parallel profiles along the entire length of the surface. The traverses are taken 8 cm and 17 cm from the front channel side (see Figure 2-1) and 6 cm from the rear side of the channel. The recorded profiles are shown in Figure 7-15 for the virgin replica surface and the analyses for the virgin replica surface and the coated replica surface are summarised in Tables 7-18 and 7-19.

---

* Shell Chemicals: Epikote 816 with Epikure RTV.

(2) The dial gauge plus datum are used to record three 118 cm long profiles spaced out along the length of the work surface, moving towards the channel inlet. The first profile started at the outlet end and 15.9 cm from the front side of the flow channel. The second profile started 192.7 cm from the outlet end of the replica and 11.1 cm from the front side of the channel. The third profile was taken 360.7 cm from the outlet end of the replica and 9.5 cm from the front side of the flow channel.

The recorded profiles for the untreated replica surface are shown in Figure 7-16 and a summary of the analyses for the untreated replica surface and the coated replica surface is given in Tables 7-18 and 7-19.

(3) The Talylin instrument is used to record surface features measuring from a few millimetres in length to a few centimetres. The standard Talylin stylus cannot faithfully reproduce the relatively rough surface of the replica. Although the standard stylus could not be used, the specially constructed extension stylus (Chapter 7.2) could be successfully traversed across a specimen piece of the replica approximately 15 cm^2. Prior to the measurements the specimen surface was securely mounted on a relocation table (Williamson & Hunt 1968). The relocation table allows repeat profiles to be recorded along the same section through a surface and hence record the changes in the surface with the application of paint (Figure 7-17). The paint is applied by brush, hence profiles were also recorded across and along the visible brush marks (Table 7-20). The results of the analysis of the relocated profiles are summarised in Table 7-21.

(4) The Surfcom stylus instrument is used with the relocation table to record relocated profiles of the changes in geometry of a section through the replica surface with the application of paint (Figure 7-18). Two profiles are also recorded along and across the brush marks left in the coated surface. The results of the analysis for the relocated profiles are summarised in Table 7-22.

The measuring head of the Surfcom consists of a diamond stylus with a 3 μm tip and a loading of 0.5 gram. The instrument is used with a sampling interval of 100 μm and a sample length of 2.5 cm. The vertical magnification is on its lowest setting of x200 and the horizontal magnification is x10.

The combined analyses for the replica surface and coated replica surface data are shown in Tables 7-18 and 7-19 respectively. The results show the RMS roughness of the coated surface to have increased by approximately 5 per cent for sample lengths of 2.5 mm and 10.2 cm. Since a reliable and rapid measure of the change in roughness of a surface can only be gained from repeat measurements through the same section of the surface, the measurement results for sample lengths of 1.18 m and 4.83 m can be neglected in a comparison of the surface roughness. The measurements in fact show a RMS roughness increase of 10 per cent and a decrease of 10 per cent for the sample lengths of 1.18 m and 4.83 m respectively.

The values of the measured slopes and curvatures for each surface decrease with increasing sampling interval and sample length, with the exception of the 2.5 mm sample measurements. The maximum vertical movement of the 2.5 mm cut-off instrument is such that a relatively

smooth section of the surface had to be chosen for a complete profile to be successfully recorded, hence the artificially low values for the surface slopes.

The distributions of profile slopes and curvatures are shown in Figures 7-19 and 7-20 respectively. The distributions are for a sample length of 5 cm and the solid lines show the uncoated replica surface whilst the broken lines show the coated surface. There is little difference between the distributions for the coated and uncoated surface.

Date

Chart No.

TABLE 7-1 SURFACE ANALYSIS OF REPLICA FROM CORRODED HULL

RMS μm.	CLA μm.	Highest peak μm.	Lowest valley μm.	Difference μm.	Skewness	Kurtosis	Mean peak curvature $10^{-4}\mu m^{-1}$	Highest peak curvature $10^{-4}\mu m^{-1}$	Mean valley curvature $10^{-4}\mu m^{-1}$	Mean absolute slope degrees	Highest absolute slope radians	No. of peaks per mm.	
72.5	58.2	209	135	344	.198	2.73	4.79	12.4	9.89	10.8	.698	.817	
90.0	75.6	132	236	368	.704	2.44	5.27	16.3	8.21	11.0	.716	.844	
158	123	267	391	658	1.03	3.49	3.36	8.53	7.14	20.2	1.31	.703	
107	84.8	185	365	550	1.07	4.06	3.77	25.6	6.09	25.8	.944	.941	
159	135	369	305	674	.027	2.11	5.81	33.7	8.73	34.8	1.48	.857	
117	95.3	232	286	519	.527	2.97	4.60	19.3	8.01	20.5	1.03	.832	MEAN
35.4	29.0	80.0	92.7	140	.521	.712	.914	9.16	1.31	9.11	.315	.077	STANDARD DEVIATION

Date

Chart No.

TABLE 7-2 SURFACE ANALYSIS OF REPLICA FROM CORRODED HULL

RMS μm.	CLA μm.	Highest peak μm.	Lowest valley μm.	Difference μm.	Skewness	Kurtosis	Mean peak curvature $10^{-4}\mu m^{-1}$	Highest peak curvature $10^{-4}\mu m^{-1}$	Mean valley curvature $10^{-4}\mu m^{-1}$	Mean absolute slope degrees	Highest absolute slope radians	No. of peaks per mm.	
63.5	50.8	140	153	293	.507	2.73	5.61	17.1	7.74	12.4	.559	.871	
53.7	40.6	124	174	298	.378	3.56	5.86	18.6	7.83	6.79	.396	.897	
95.1	73.5	143	294	437	1.11	4.12	5.70	14.4	7.99	17.8	1.09	.881	
124	99.5	333	227	560	.254	2.82	4.65	11.6	6.65	25.8	1.35	.901	
60.1	50.5	124	130	254	.164	2.17	4.85	12.4	6.80	17.1	.632	.897	
79.3	63.0	173	196	368	.381	3.08	5.33	14.8	7.40	16.0	.805	.889	MEAN
26.5	21.2	80.5	58.7	114	.447	.683	.488	2.68	.561	6.30	.357	.011	STANDARD DEVIATION

Date

Chart No.

TABLE 7-3 SURFACE ANALYSIS OF REPLICA FROM CORRODED HULL

RMS μm.	CLA μm.	Highest peak μm.	Lowest valley μm.	Difference μm.	Skewness	Kurtosis	Mean peak curvature $10^{-4}\mu m^{-1}$	Highest peak curvature $10^{-4}\mu m^{-1}$	Mean valley curvature $10^{-4}\mu m^{-1}$	Mean absolute slope degrees	Highest absolute slope radians	Number of peaks per mm	
62.7	49.5	153	147	300	.496	2.68	5.49	19.0	7.16	10.9	.563	1.00	
84.2	68.6	228	229	457	.044	2.84	5.61	15.5	7.96	10.4	.655	.988	
65.0	53.3	177	141	318	.104	2.59	6.46	29.9	8.42	7.97	.459	.841	
52.1	43.2	142	158	300	.136	2.71	4.57	10.9	6.88	7.62	.500	.821	
107	91.3	203	273	476	.448	2.26	5.68	20.6	7.17	22.0	.916	1.04	
74.2	61.2	181	190	370	.204	2.62	5.56	19.2	7.52	11.8	.619	.938	MEAN
19.4	17.2	31.7	52.3	79.1	.232	.195	.602	6.31	.577	5.27	.163	.089	STANDARD DEVIATION

Date

Chart No.

TABLE 7-4 SURFACE ANALYSIS OF REPLICA FROM CORRODED HULL

RMS μm.	CLA μm.	Highest peak μm.	Lowest valley μm.	Difference μm.	Skewness	Kurtosis	Mean peak curvature $10^{-4}\mu m^{-1}$	Highest peak curvature $10^{-4}\mu m^{-1}$	Mean valley curvature $10^{-4}\mu m^{-1}$	Mean absolute slope degrees	Highest absolute slope radians	No. of peaks per mm.	
78.8	65.8	161	111	272	.072	2.12	5.16	16.3	10.4	9.79	.494	.953	
87.5	69.7	210	248	458	.386	3.24	5.07	11.3	11.6	10.9	.632	.881	
88.6	74.4	181	206	387	.365	2.29	5.53	14.0	9.96	13.0	.625	.961	
85.0	70.0	184	188	372	.274	2.55	5.25	13.8	10.7	11.2	.584	.932	MEAN
4.38	3.52	20.1	57.3	76.6	.143	.493	.199	2.06	.693	1.33	.063	.036	STANDARD DEVIATION

Date

Chart No.

TABLE 7-5 SURFACE ANALYSIS OF REPLICA FROM CORRODED HULL

RMS μm.	CLA μm.	Highest peak μm.	Lowest valley μm.	Difference μm.	Skewness	Kurtosis	Mean peak curvature $10^{-4}\mu m^{-1}$	Highest peak curvature $10^{-4}\mu m^{-1}$	Mean valley curvature $10^{-4}\mu m^{-1}$	Mean absolute slope degrees	Highest absolute slope radians	No. of peaks per mm.	
90.8	74.7	151	223	374	.659	2.58	6.09	14.4	11.3	11.0	.613	.837	
62.2	48.2	191	180	371	.055	3.57	6.04	14.0	11.3	7.77	.558	.817	
106	87.8	199	239	438	.490	2.44	6.20	13.6	10.7	26.1	1.00	.797	
86.3	70.2	180	214	394	.401	2.86	6.11	14.0	11.1	15.0	.724	.817	MEAN
18.2	16.5	21.0	24.9	30.9	.254	.503	.067	.327	.283	7.99	.197	.016	STANDARD DEVIATION

Date

Chart No.

TABLE 7-6 SURFACE ANALYSIS OF REPLICA FROM CORRODED HULL

RMS μm.	CLA μm.	Highest peak μm.	Lowest valley μm.	Difference μm.	Skewness	Kurtosis	Mean peak curvature $10^{-4}\ \mu m^{-1}$	Highest peak curvature $10^{-4}\ \mu m^{-1}$	Mean valley curvature $10^{-4}\ \mu m^{-1}$	Mean absolute slope degrees	Highest absolute slope radians	No. of peaks per mm.	
58.9	47.8	116	163	279	.691	2.74	5.34	22.5	6.88	7.09	.497	.897	
121	103	234	293	527	.504	2.39	5.19	15.1	7.12	25.2	1.05	.804	
106	83.6	292	202	494	.272	2.89	6.44	40.7	10.7	25.4	.982	.957	
95.3	78.1	214	219	433	.308	2.67	5.66	26.1	8.23	19.2	.843	.886	MEAN
26.5	22.9	73.2	54.5	110	.417	.209	.557	10.8	1.75	8.58	.246	.063	STANDARD DEVIATION

Date

Chart No.

TABLE 7-7 SURFACE ANALYSIS OF REPLICA FROM CORRODED HULL

RMS μm.	CLA μm.	Highest peak μm.	Lowest valley μm.	Difference μm.	Skewness	kurtosis	Mean peak curvature $10^{-4}\mu m^{-1}$	Highest peak curvature $10^{-4}\mu m^{-1}$	Mean valley curvature $10^{-4}\mu m^{-1}$	Mean absolute slope degrees	Highest absolute slope radians	No. of peaks per mm.	
75.4	63.6	153	144	297	.050	1.97	5.29	14.7	8.21	14.4	.644	1.02	
65.6	54.9	171	130	301	.080	2.37	4.34	26.4	6.24	16.3	.738	.988	
68.9	53.9	124	215	339	.576	3.40	5.70	30.3	8.65	8.91	.477	.910	
70.0	57.5	149	163	312	.182	2.58	5.11	23.8	7.70	13.2	.620	.973	MEAN
4.07	4.36	19.4	37.2	18.9	.284	.602	.570	6.63	1.05	3.13	.108	.046	STANDARD DEVIATION

Date

Chart No.

TABLE 7-8 SURFACE ANALYSIS OF REPLICA FROM CORRODED HULL

RMS μm.	CLA μm.	Highest peak μm.	Lowest valley μm.	Difference μm.	Skewness	Kurtosis	Mean peak curvature $10^{-4}\,\mu m^{-1}$	Highest peak curvature $10^{-4}\,\mu m^{-1}$	Mean valley curvature $10^{-4}\,\mu m^{-1}$	Mean absolute slope degrees	Highest absolute slope radians	No. of peaks per mm.	
114	91.2	247	327	574	.235	2.77	7.84	38.4	10.2	16.7	.879	1.06	
68.1	54.1	146	192	338	.220	2.87	7.54	18.2	10.6	12.9	.589	.807	
126	97.2	387	276	663	.500	3.97	5.53	29.9	7.89	20.6	1.03	.897	
103	80.8	260	265	525	.015	3.20	6.97	28.8	9.56	16.7	.833	.921	MEAN
25.0	19.1	98.8	55.7	137	.343	.544	1.03	8.28	1.19	3.14	.183	.105	STANDARD DEVIATION

Date

Chart No.

TABLE 7-9 SURFACE ANALYSIS OF REPLICA FROM OIL TANKER HULL

RMS μm.	CLA μm.	Highest peak μm.	Lowest valley μm.	Difference μm.	Skewness	Kurtosis	Mean peak curvature $10^{-4}\ \mu m^{-1}$	Highest peak curvature $10^{-4}\ \mu m^{-1}$	Mean valley curvature $10^{-4}\ \mu m^{-1}$	Mean absolute slope degrees	Highest absolute slope radians		
37.8	29.7	100	89.8	190	.435	3.14	1.78	6.99	2.71	1.69	.145		
55.2	43.8	88.8	125	214	.691	2.67	1.40	5.20	2.28	1.73	.140		
35.0	28.2	80.9	96.7	178	.192	2.79	1.07	2.51	2.07	1.30	.161		
42.8	31.1	102	94.9	197	.525	3.55	1.17	3.05	3.02	1.56	.166		
36.7	30.7	87.8	57.4	145	.447	2.25	1.17	2.87	2.16	1.21	.184		
41.5	32.7	91.9	92.8	185	.105	2.88	1.32	4.12	2.45	1.50	.159		MEAN
7.33	5.64	7.94	21.5	23.1	.474	.439	.255	1.71	.361	.208	.016		STANDARD DEVIATION

Date

Chart No.

TABLE 7-10 SURFACE ANALYSIS OF REPLICA FROM OIL TANKER HULL

RMS μm.	CLA μm.	Highest peak μm.	Lowest valley μm.	Difference μm.	Skewness	Kurtosis	Mean peak curvature $10^{-4}\mu m^{-1}$	Highest peak curvature $10^{-4}\mu m^{-1}$	Mean valley curvature $10^{-4}\mu m^{-1}$	Mean absolute slope degrees	Highest absolute slope radians		
53.4	45.1	91.5	107	199	.004	1.98	1.21	3.05	2.49	1.77	.203		
61.6	45.1	138	123	261	.194	3.18	1.44	4.48	3.30	2.02	.278		
30.7	23.5	63.8	89.6	153	.428	3.45	1.01	2.69	2.15	1.30	.111		
56.4	37.9	72.3	192	264	1.76	6.24	1.13	2.33	1.20	1.22	.306		
39.9	32.0	102	107	209	.123	3.01	3.21	4.66	2.85	1.67	.294		
48.4	36.7	93.5	124	217	.375	3.57	1.60	3.44	2.40	1.60	.238		MEAN
11.4	8.20	26.0	35.7	41.5	.725	1.42	.817	.950	.710	.298	.073		STANDARD DEVIATION

FIG 7-1 CUMULATIVE SLOPE DISTRIBUTIONS FROM SURFACE ANALYSIS OF REPLICA FROM CORRODED SHIP HULL

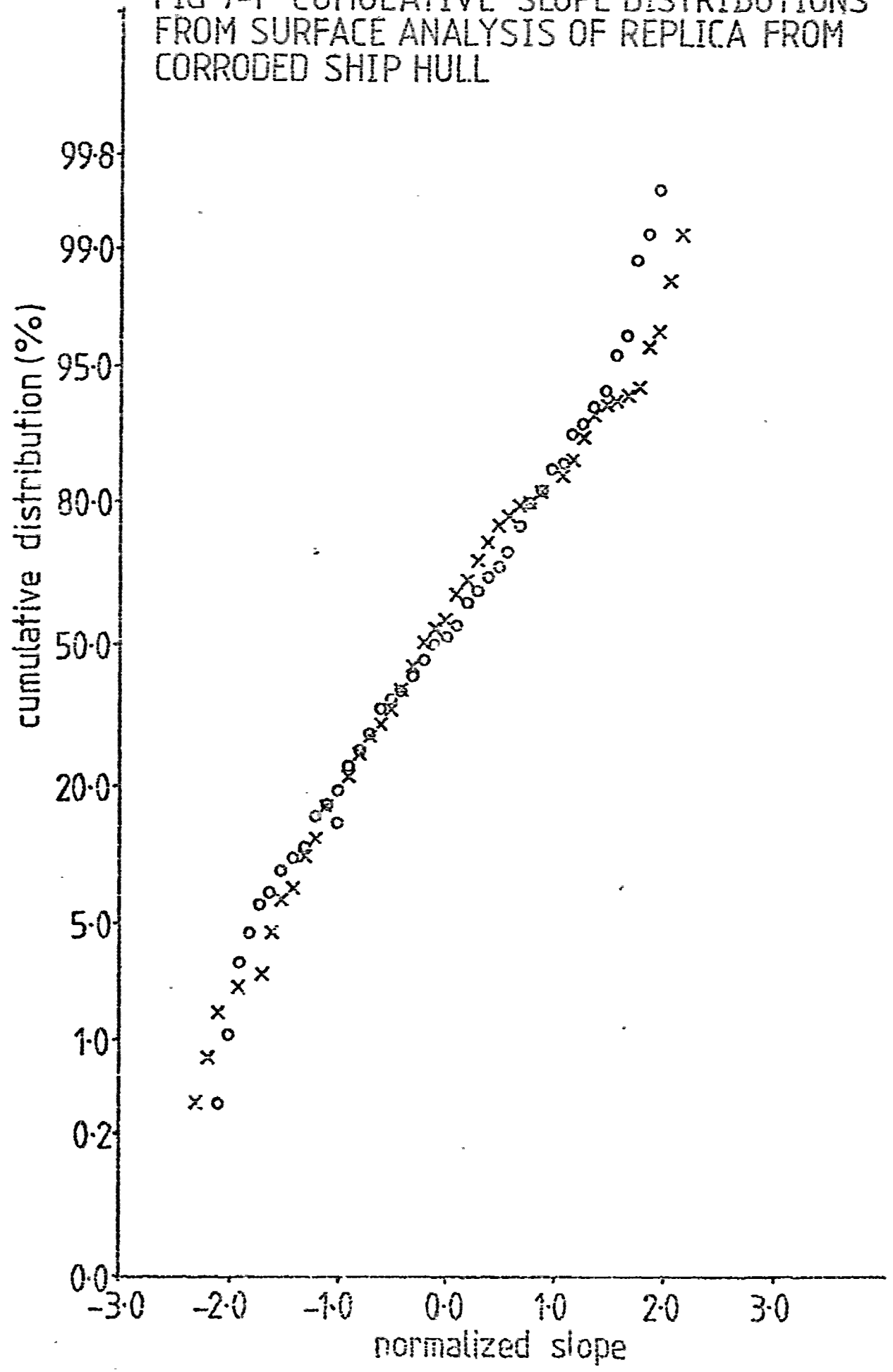

FIG 7-2 PLOT OF POWER SPECTRAL DENSITY VERSUS SURFACE WAVELENGTH FOR REPLICA FROM CORRODED SHIP HULL

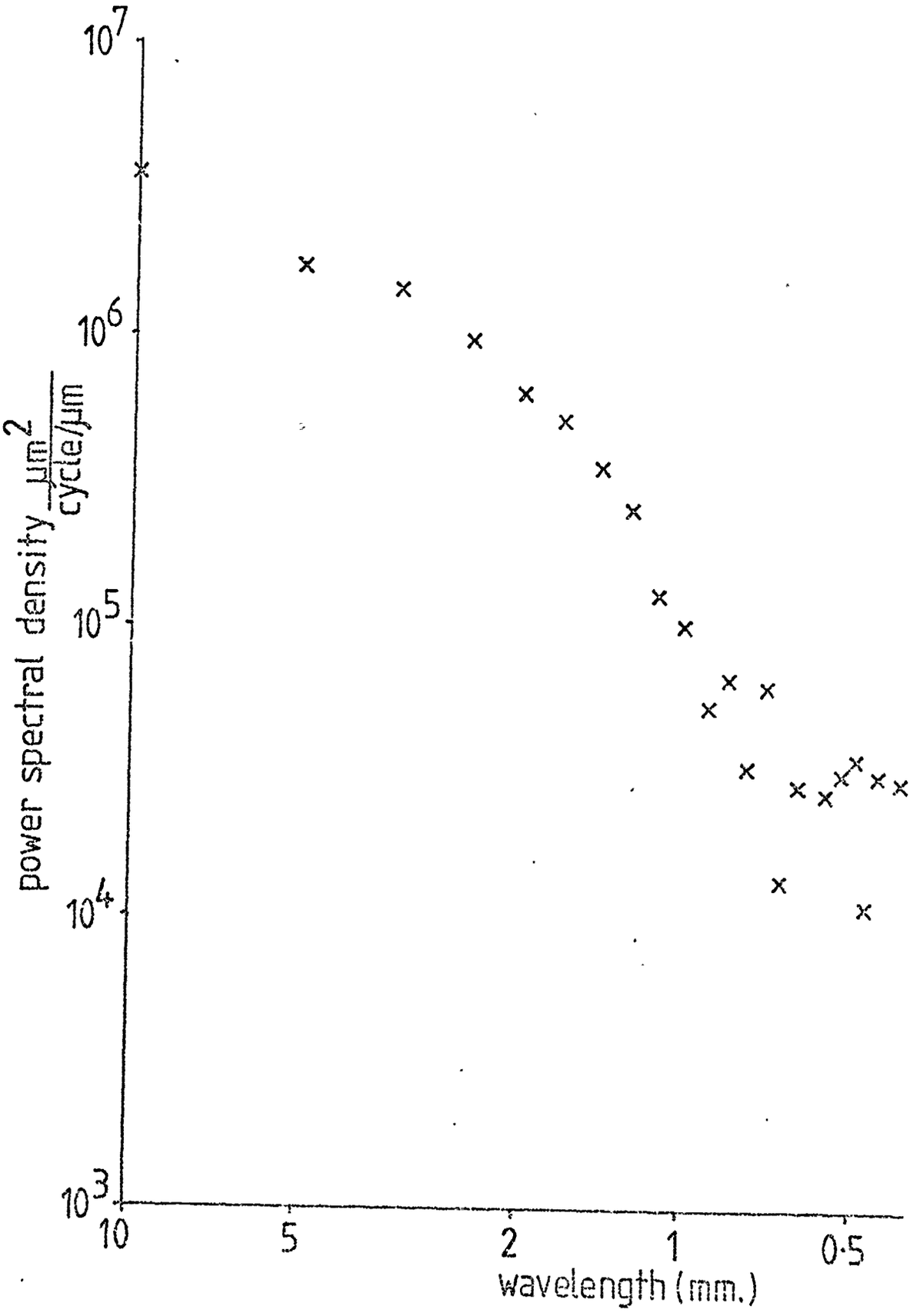

FIG 7-3 CUMULATIVE HEIGHT DISTRIBUTION FROM SURFACE ANALYSIS OF REPLICA FROM CORRODED SHIP HULL

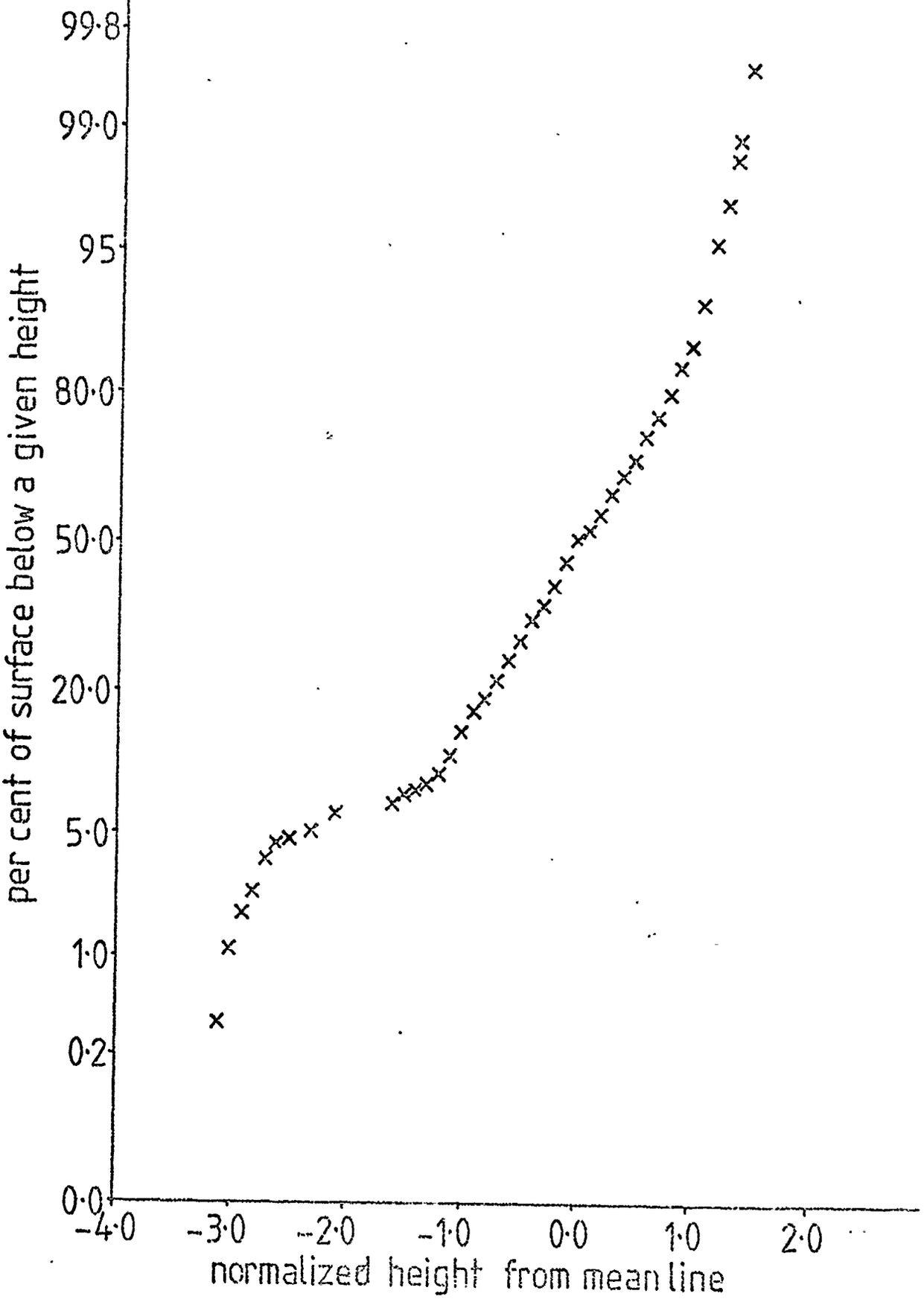

FIG 7-4 DETACHABLE SHIP HULL PLATE

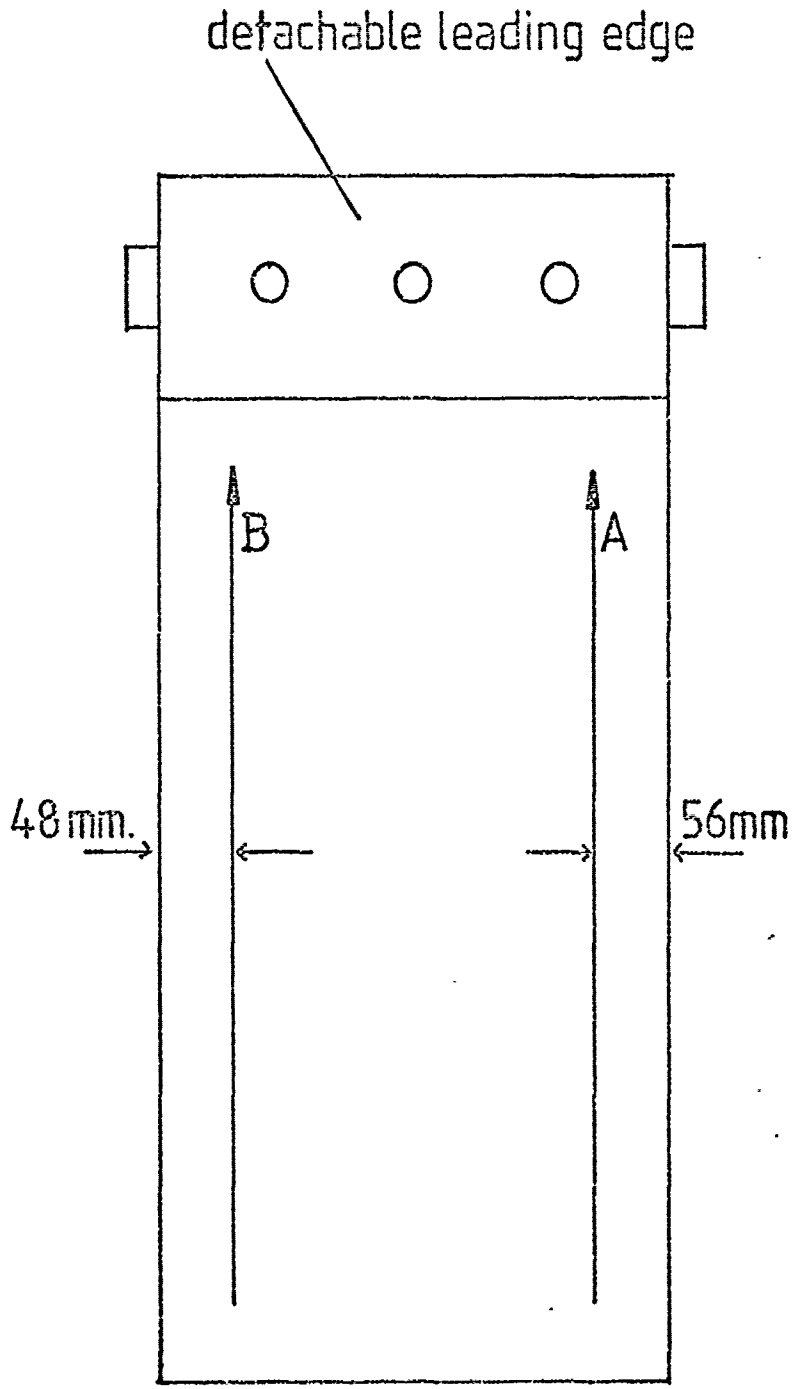

Date

Chart No.

TABLE 7-11 SURFACE ANALYSIS OF DETACHABLE HULL PLATE MB2

Parameter	traverse A before voyage	traverse A after voyage	% change	traverse B before voyage	traverse B after voyage	% change
RMS roughness (μm.)	16·0 (4·2) 9	16·8 (2·5) 12	+5	14·0 (2·4) 10	12·7 (1·2) 11	−9
CLA roughness (μm.)	10·0 (1·4) 9	14·3 (2·2) 12	+43	9·3 (3·1) 10	10·5 (1·0) 11	+13
Mean apparent amplitude (μm.)	47·0 (6·8) 8	60·0 (7·1) 12	+28	45·0 (6·0) 8	48·5 (4·1) 11	+7
Mean peak rad. of curvature(mm.)	27·0 (·28) 8	67·0 (3·3) 11	+149	20·0 (4·9) 10	60·6 (3·1) 11	+203
Mean valley rad. of curvature(mm.)	−26·0 (1·0) 8	−45·7 (3·1) 11	+76	−12·5 (6·6) 9	−43·2 (3·7) 11	+246
Average slope (degrees)	·549 (·073) 7	·79 (·17) 10	+44	·83 (·24) 10	·558 (·054) 11	−33

Date

Chart No.

TABLE 7-12 SURFACE ANALYSIS OF DETACHABLE HULL PLATE MT3

Parameter	traverse A before voyage	traverse A after voyage	%change	traverse B before voyage	traverse B after voyage	%change
RMS roughness (μm.)	51·0 (7·0) 10	16·1 (1·4) 9	-68	61·0 (6·3) 10	17·4 (2·6) 9	-71
CLA roughness (μm.)	35·0 (3·3) 10	10·6 (·74) 9	-70	42·0 (3·2) 10	11·5 (1·6) 9	-73
Mean apparent amplitude (μm.)	323·0 (49·0) 10	108·0 (12·0) 9	-67	379·0 (47·0) 10	117·0 (18·0) 9	-69
Mean peak rad. of curvature(mm)	2·13 (·068) 10	6·4 (2·6) 9	+200	1·82 (·061) 10	5·1 (2·0) 9	+180
Mean valley rad. of curvature(mm)	-1·82 (·093) 10	-9·62 (·59) 9	+428	-1·54 (·051) 10	-5·81 (·81) 9	+277
Average slope (degrees)	5·81 (·59) 10	1·77 (·22) 9	-70	7·05 (·46) 10	2·10 (·30) 9	-70

Date

Chart No.

TABLE 7-13 SURFACE ANALYSIS OF DETACHABLE HULL PLATE MT1

Parameter	traverse A before voyage	traverse A after voyage	% change	traverse B before voyage	traverse B after voyage	% change
RMS roughness (μm.)	52·0 (2·8) 9	12·3 (1·1) 10	−76	68·0 (9·0) 10	17·3 (2·5) 10	−75
CLA roughness (μm.)	32·0 (4·2) 9	8·8 (·78) 10	−73	45·0 (4·7) 10	12·5 (1·7) 10	−72
Mean apparent amplitude (μm.)	390·0 (115·0) 9	83·2 (8·8) 10	−79	439·0 (77·0) 10	106·0 (16·0) 10	−76
Mean peak rad. of curvature(mm)	1·47 (6·36) 9	11·4 (·43) 10	+676	2·00 (·061) 10	10·6 (1·4) 10	+430
Mean valley rad. of curvature(mm)	−1·59 (·19) 9	−10·4 (·56) 10	+554	−1·07 (·093) 10	−7·1 (1·3) 10	+325
Average slope (degrees)	6·08 (·97) 8	1·24 (·11) 10	−80	7·30 (·73) 10	2·20 (·28) 10	−70

Date

Chart No.

TABLE 7-14 SURFACE ANALYSIS OF DETACHABLE HULL PLATE MB1

Parameter	traverse A before voyage	traverse A after voyage	%change	traverse B before voyage	traverse B after voyage	%change
RMS roughness (μm.)	87.0 (5.1) 10	16.2 (0.76) 9	-81	159.0 (19.0) 11	34.8 (5.1) 9	-78
CLA roughness (μm.)	64.0 (3.8) 11	11.0 (.66) 9	-82	122.0 (16.0) 11	25.8 (3.8) 9	-79
Mean apparent amplitude (μm.)	502.0 (83.0) 11	89.9 (3.4) 9	-82	806.0 (81.0) 11	181.0 (24.0) 9	-78
Mean peak rad. of curvature(mm)	1.49 (.34) 11	2.90 (.31) 9	+95	1.25 (.17) 11	5.62 (.42) 9	+350
Mean valley rad. of curvature(mm)	-1.54 (.16) 11	-2.73 (.25) 9	+77	.77 (.11) 11	-2.72 (.54) 9	+253
Average slope (degrees)	9.28 (.81) 10	2.66 (.11) 9	-71	17.3 (2.1) 11	3.98 (.64) 9	-77

FIG 7-5 CUMULATIVE HEIGHT DISTRIBUTIONS FROM SURFACE ANALYSIS OF DETACHABLE SHIP HULL PLATES

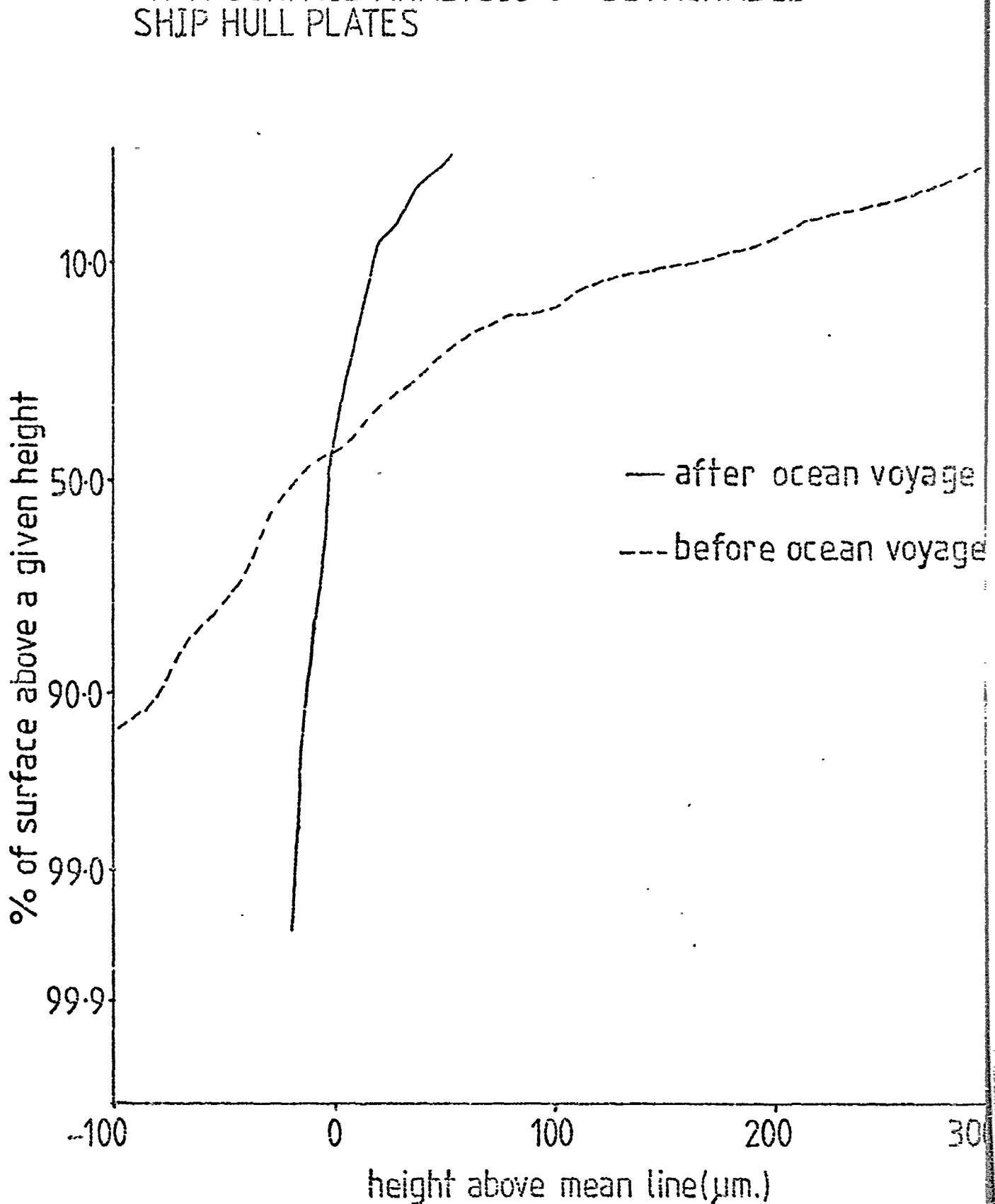

FIG 7-6 POWER SPECTRAL DENSITY VERSUS SURFACE WAVELENGTH FOR DETACHABLE SHIP HULL PLATE MT1 BEFORE AND AFTER AN OCEAN VOYAGE

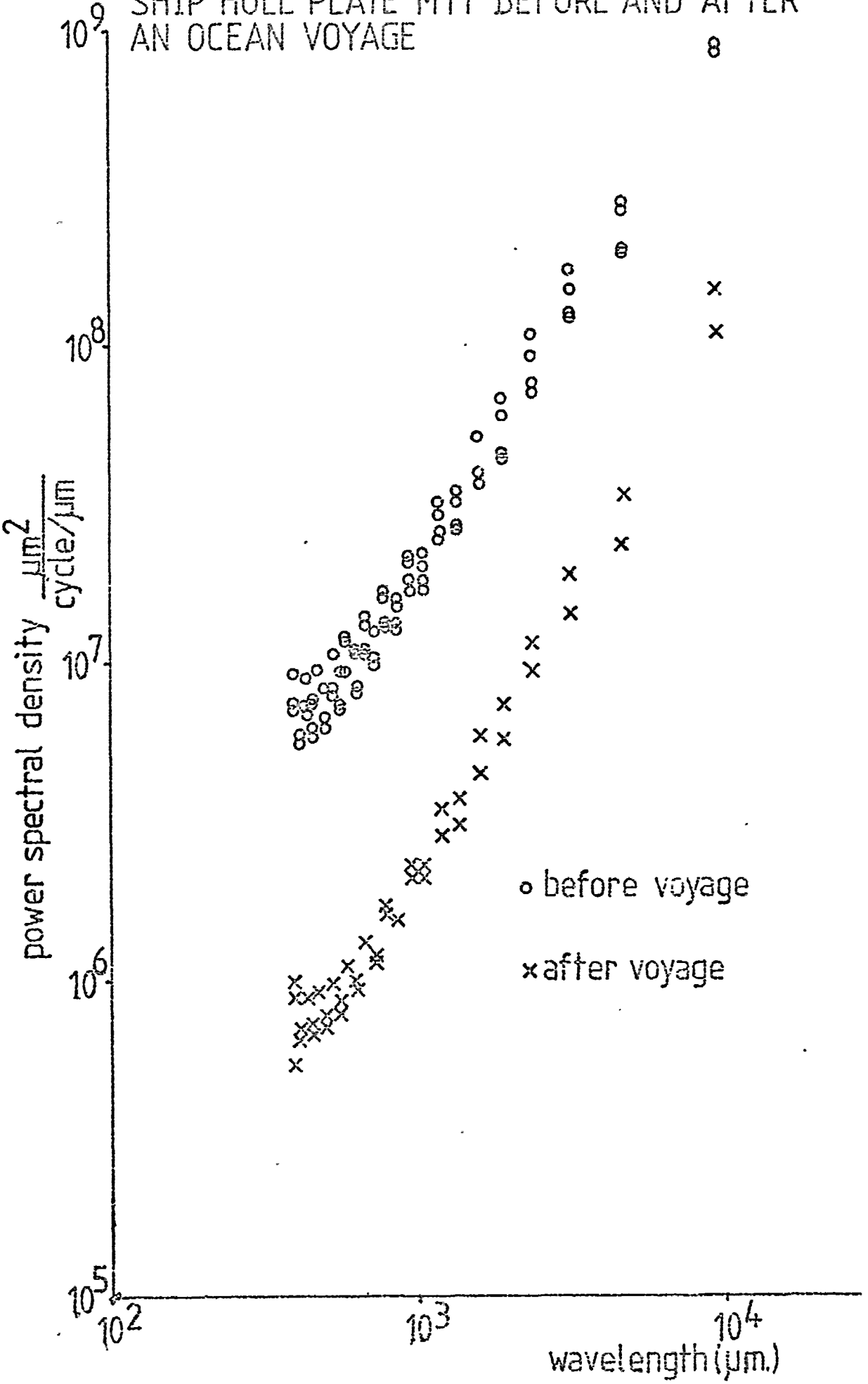

Date

Dwg. No.

FIG 7-7 SCHEMATIC DIAGRAM OF A TYPICAL STYLUS INSTRUMENT

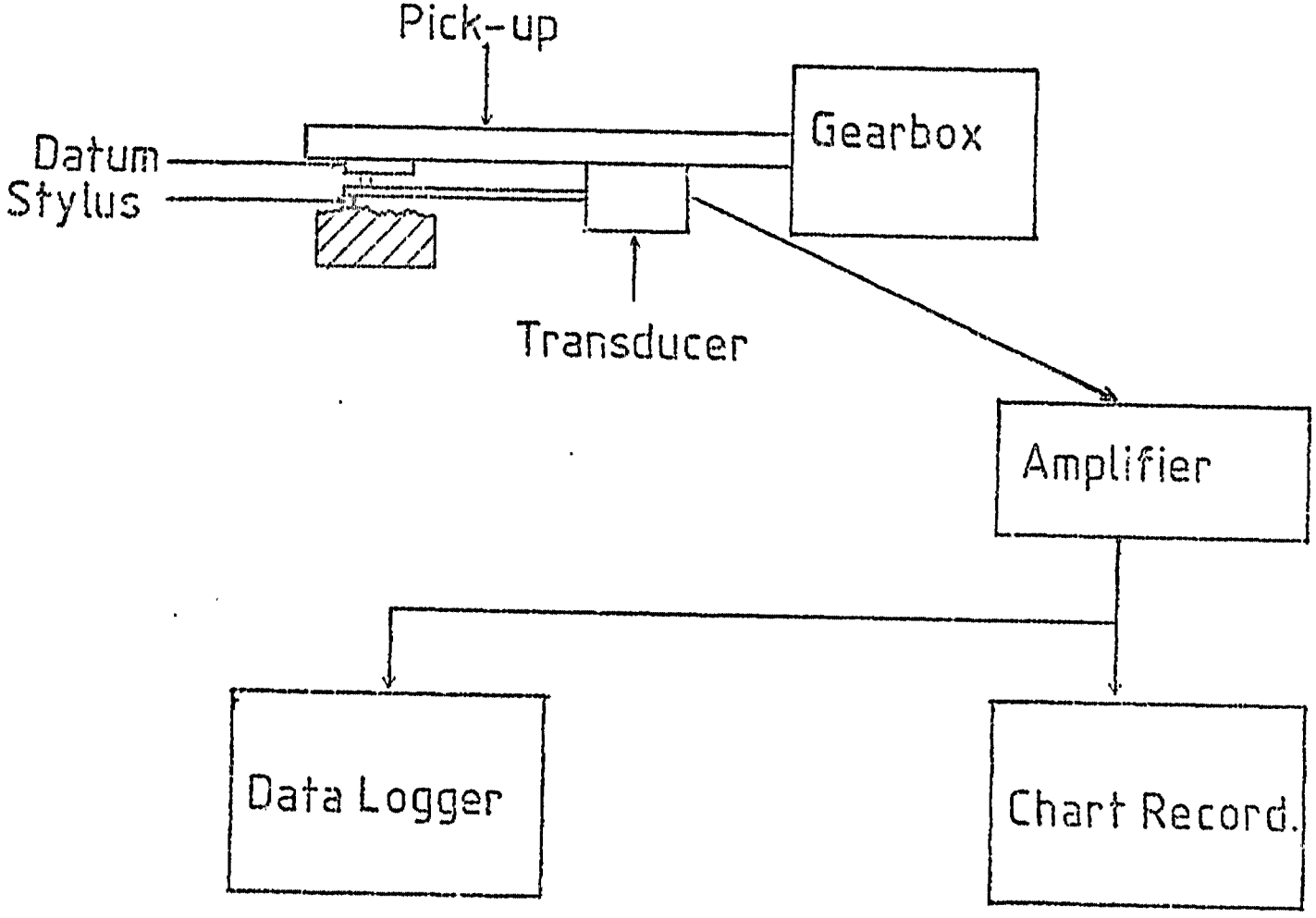

Date

Chart No.

TABLE 7-15 SURFACE ANALYSIS OF PAINTED STEEL PLATES

Sample length m.	Sampling Interval μm.	RMS μm.	CLA μm.	High. Peak μm.	Low. Valley μm.	Diff. μm.	Skewness	Kurtosis	Mean Peak Curv. 10^{-4} μm^{-1}	High. Peak Curv. 10^{-4} μm^{-1}	Mean Valley Curv. 10^{-4} μm^{-1}	Mean Abs. Slope degs	High. Abs. Slope rads
17·4	90000	311	238	1143	−1023	2166	−·321	3·94	·0004	·002	−·0004	·063	·007
1·14	5000	80·4	63·0	139	−202	341	−·947	3·07	·009	·021	−·01	·079	·006
·102	190	13·4	10·9	39·9	−38·4	78·2	−·155	2·89	3·51	10·8	−3·54	1·22	·102
·008	2	7·00	5·90	22·7	−14·5	37·2	·055	2·24	494	4523	−506	6·42	·71

FIG 7-8 SURFACE PROFILE OF PAINTED STEEL PLATES

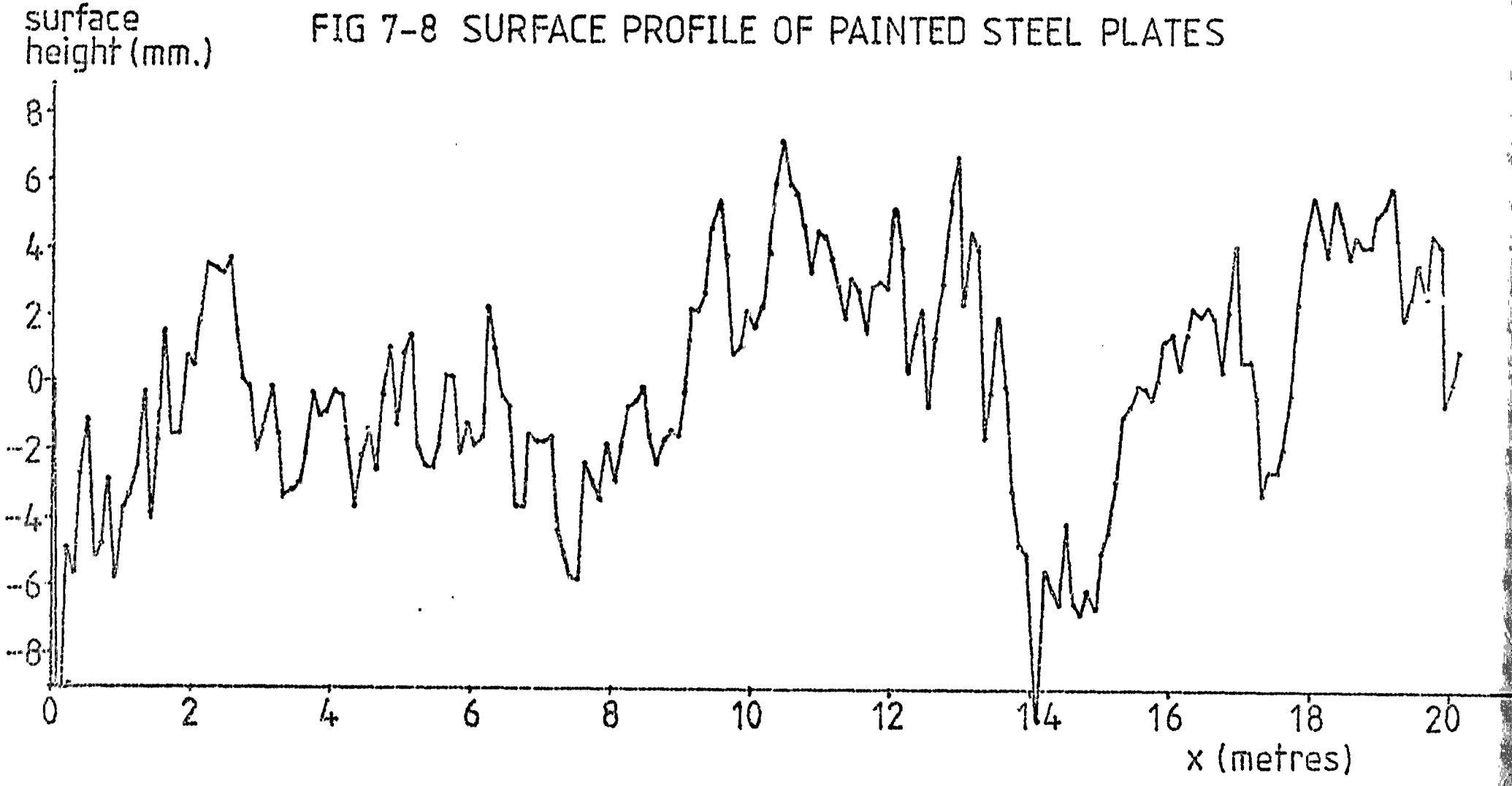

TABLE 7-16 ANALYSIS OF SURFACE RECORDS FROM TRAVERSING THE B.S.R.A. WALL GAUGE OVER THE PAINTED STEEL SURFACE

record number	Mean Apparent Amplitude MAA (μm)	
1	56	
2	69	
17	71	
18	69	
19	83	
20	60	
21	27	
22	39	
23	47	
24	30	
	55	mean
	19	standard deviation

sample length = 50mm.
ball-ended probe, 1·6mm. diameter

FIG 7-10 PLOT OF POWER SPECTRAL DENSITY VERSUS SURFACE WAVELENGTH FOR PAINTED STEEL SURFACE

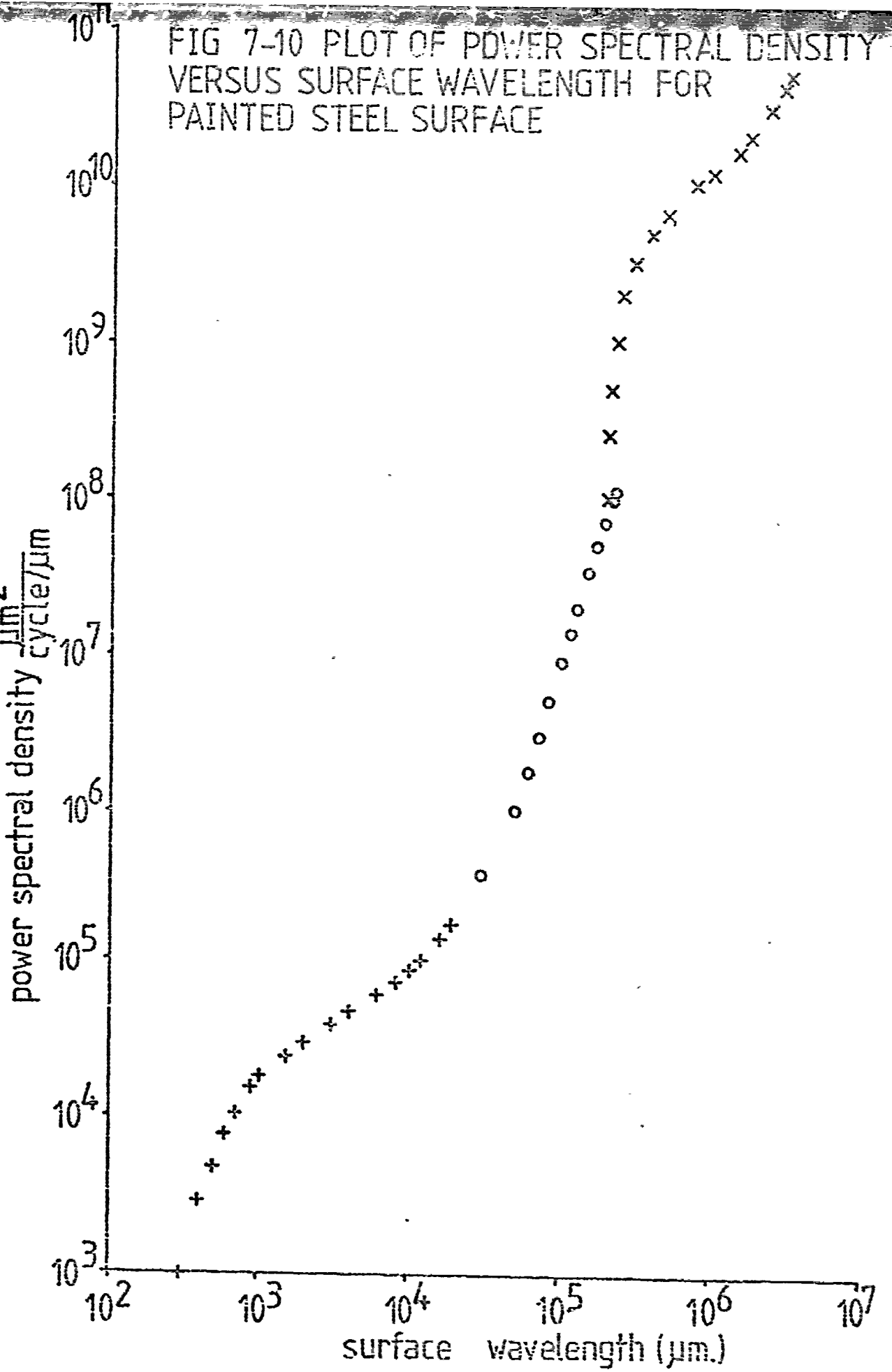

FIG 7-9 LOCATION OF PAINTED STEEL PLATES IN FLOW CHANNEL AND LOCATION OF MEASURED SURFACE PROFILES ON PLATES

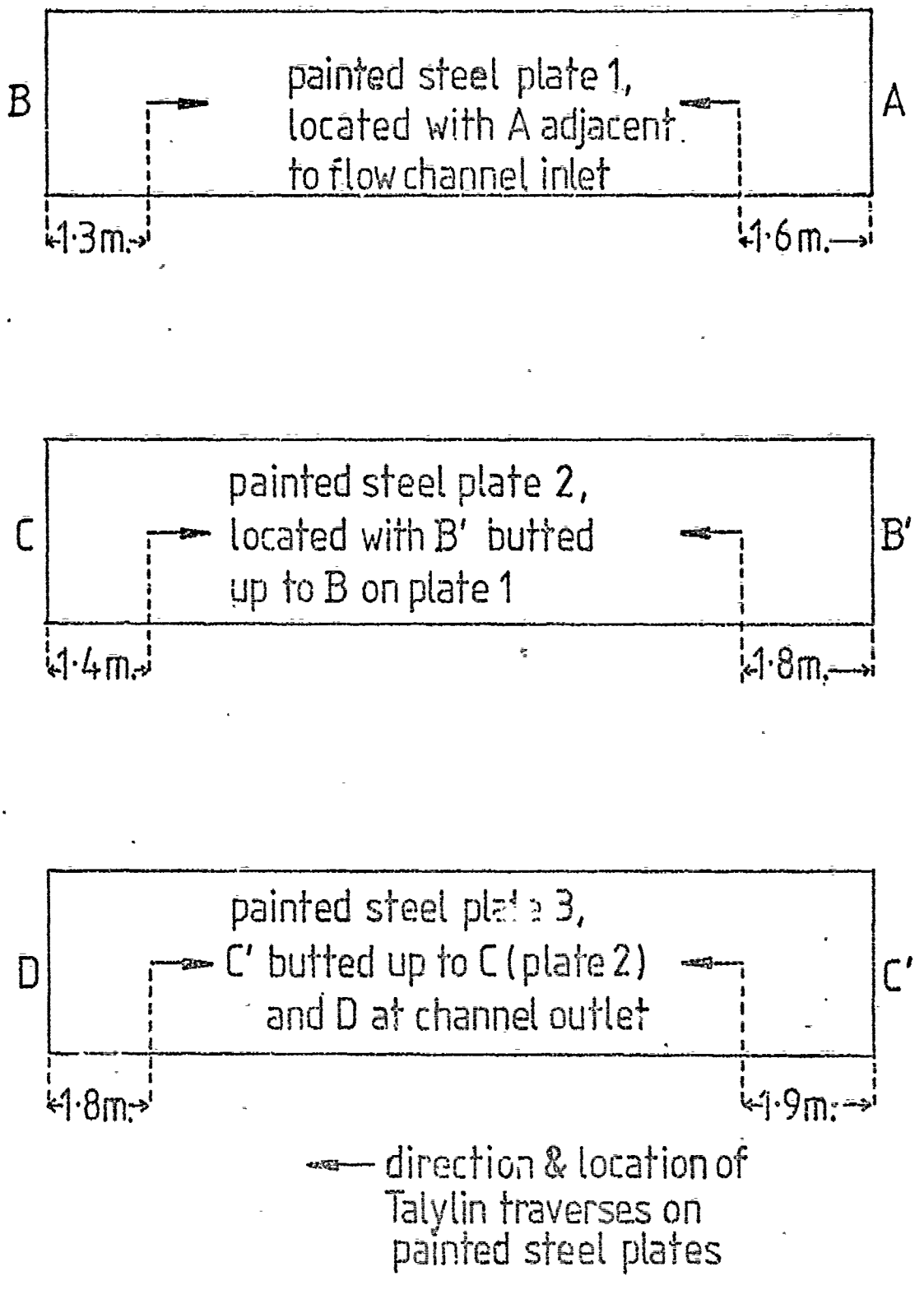

Date

Chart No.

TABLE 7-17 SURFACE ANALYSIS OF GRAVEL SURFACE

Sample length m.	Sampling Interval μm.	RMS μm.	CLA μm.	High. Peak μm.	Low. Valley μm.	Diff. μm.	Skewness	Kurtosis	Mean Peak Curv. 10^{-3} μm^{-1}	High. Peak Curv. 10^{-3} μm^{-1}	Mean Valley Curv. 10^{-3} μm^{-1}	Mean Abs. Slope degs.	High. Abs. Slope rads.
0·27	1000	959	754	2768	-2485	5253	-·074	2·95	11·39	24·8	-6·03	17·14	·895

FIG 7-11 PROFILE FROM GRAVEL SURFACE

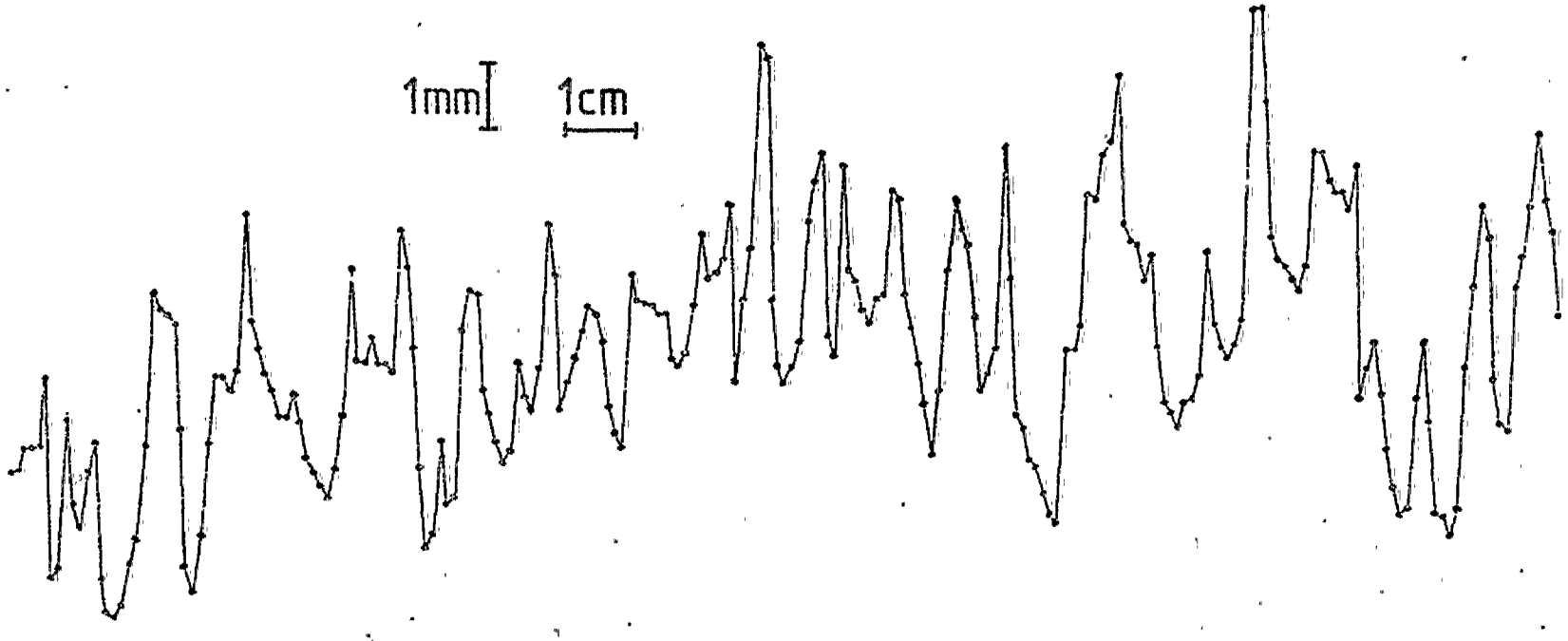

FIG 7-12 DISTRIBUTION OF CURVATURES FOR GRAVEL SURFACE

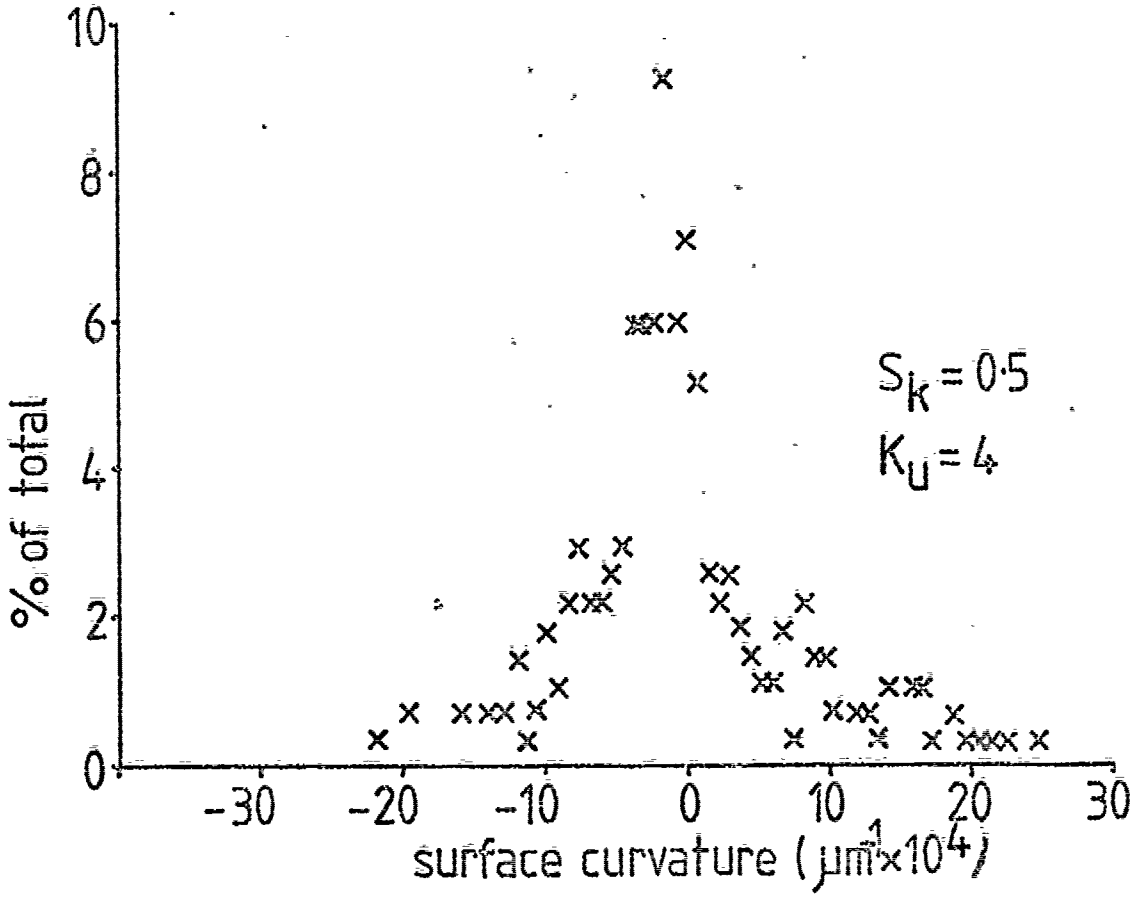

FIG 7-13 DISTRIBUTION OF SLOPES, FOR GRAVEL SURFACE

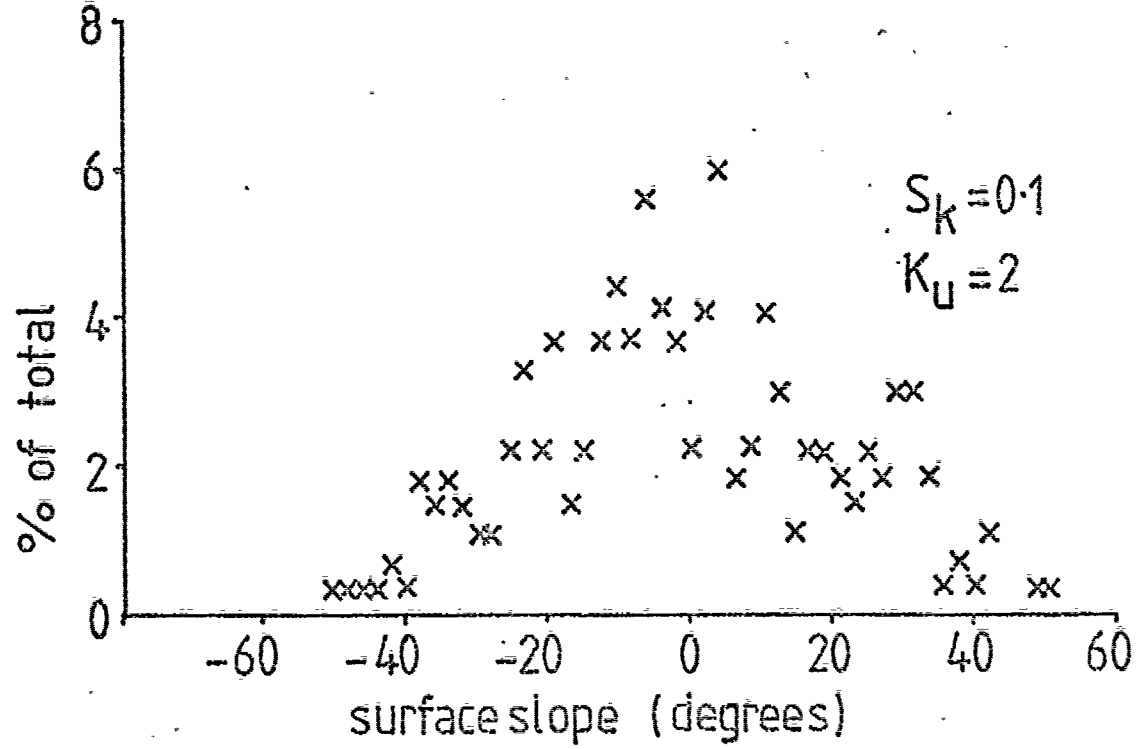

FIG 7-15 SURFACE PROFILES FROM REPLICA OF PART OF A SHIP HULL SURFACE

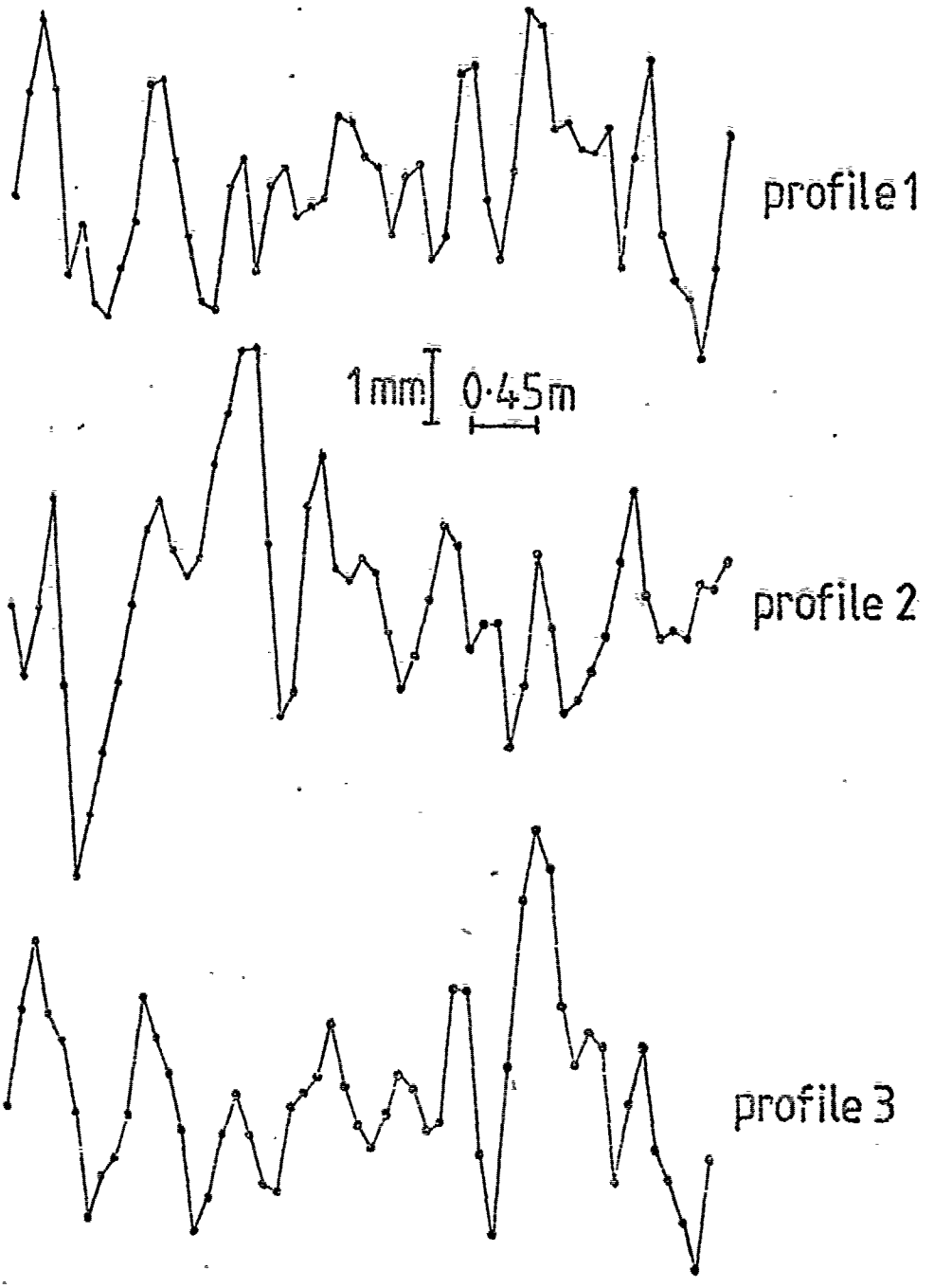

Date

Chart No.

TABLE 7-18 SURFACE ANALYSIS OF REPLICA OF HULL SURFACE

Sample length m.	Sampling Interval μm.	RMS μm.	CLA μm.	High. Peak μm.	Low. Valley μm.	Diff. μm.	Skewness	Kurtosis	Mean Peak Curv. $10^{-4}\mu m^{-1}$	High. Peak Curv. $10^{-4}\mu m^{-1}$	Mean Valley Curv. $10^{-4}\mu m^{-1}$	Mean Abs. Slope degs.	High. Abs. Slope rads.
4·83	90000	1308	1031	3296	−2968	6264	·128	3·15	·002	·004	−·002	·464	·026
1·14	5000	653	551	1498	−1315	2813	·100	2·38	·161	·539	−·154	1·22	·105
·05	190	145	106	578	−318	896	−·919	5·26	4·96	18·35	−8·83	6·53	·653
·025	100	41·1	33·1	115	−74·3	189	·595	3·11	22·5	49·1	−22·5	5·75	·342

Date

Chart No.

TABLE 7-19 SURFACE ANALYSIS OF COATED REPLICA OF HULL SURFACE

Cut-Off m.	Sampling Interval μm.	RMS μm.	CLA μm.	High. Peak μm.	Low. Valley μm.	Diff. μm.	Skewness	Kurtosis	Mean Peak Curv. 10^{-4} μm^{-1}	High. Peak Curv. 10^{-4} μm^{-1}	Mean Valley Curv. 10^{-4} μm^{-1}	Mean Abs. Slope degs.	High. Abs. Slope rads.
4·83	90000	1189	977	2644	-2201	4845	-·081	2·34	·002	·004	-·002	·446	·023
1·18	5000	725	619	1472	-1425	2897	·039	2·18	·144	·506	-·138	1·16	·095
·05	190	155	111	610	-321	931	-1·10	5·80	4·95	15·2	-8·04	6·63	·682
·025	100	43·3	36·0	112	86·1	198	·075	2·22	10·5	25·8	-8·35	4·29	·329

FIG 7-16 SURFACE PROFILE OF REPLICA FROM SHIP HULL

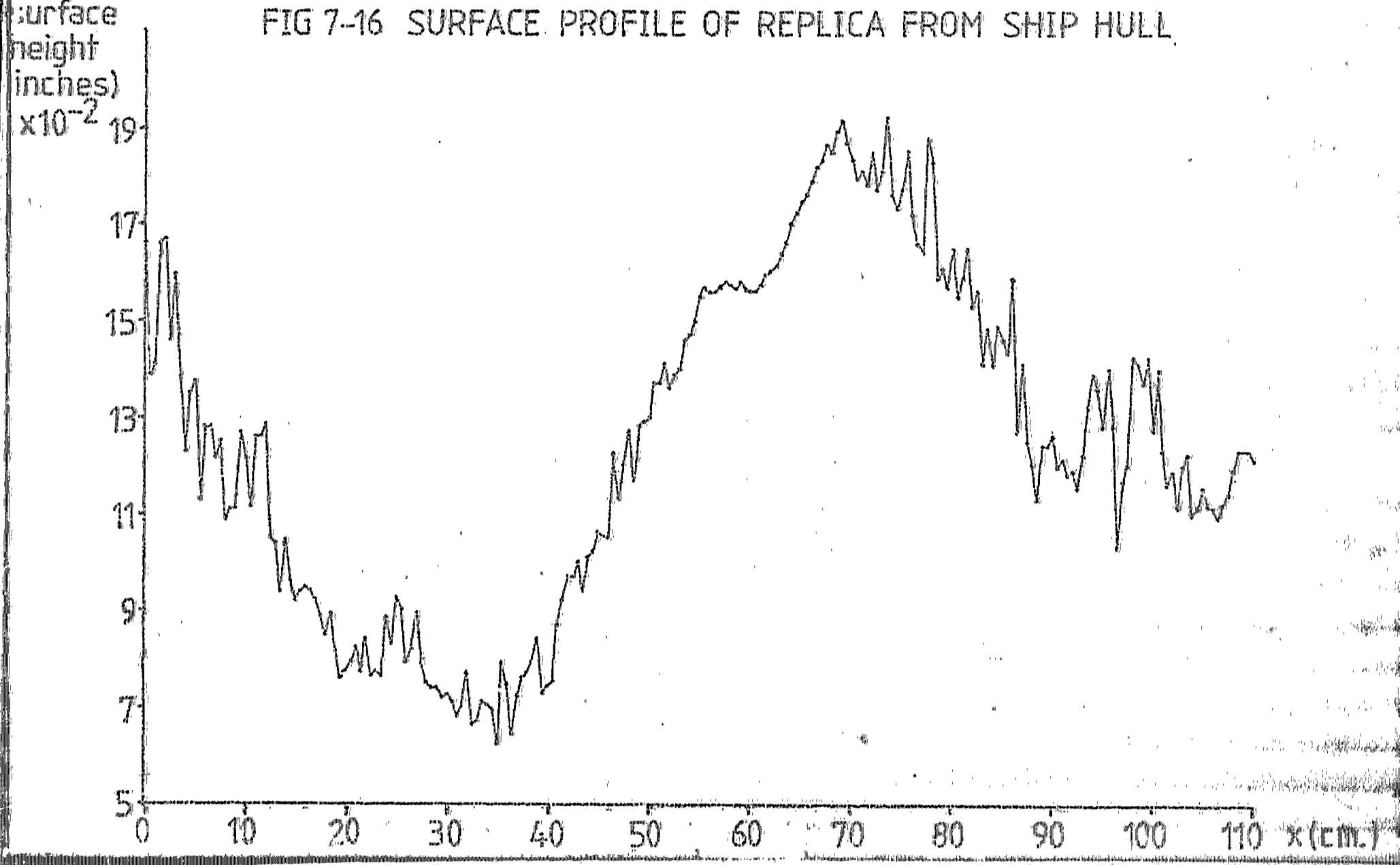

FIG 7-17 PROFILES FROM RELOCATED MEASUREMENTS ON THE REPLICA, FROM PART OF A SHIP HULL SURFACE, FOR SUCCESSIVE COATS OF MARINE PAINT

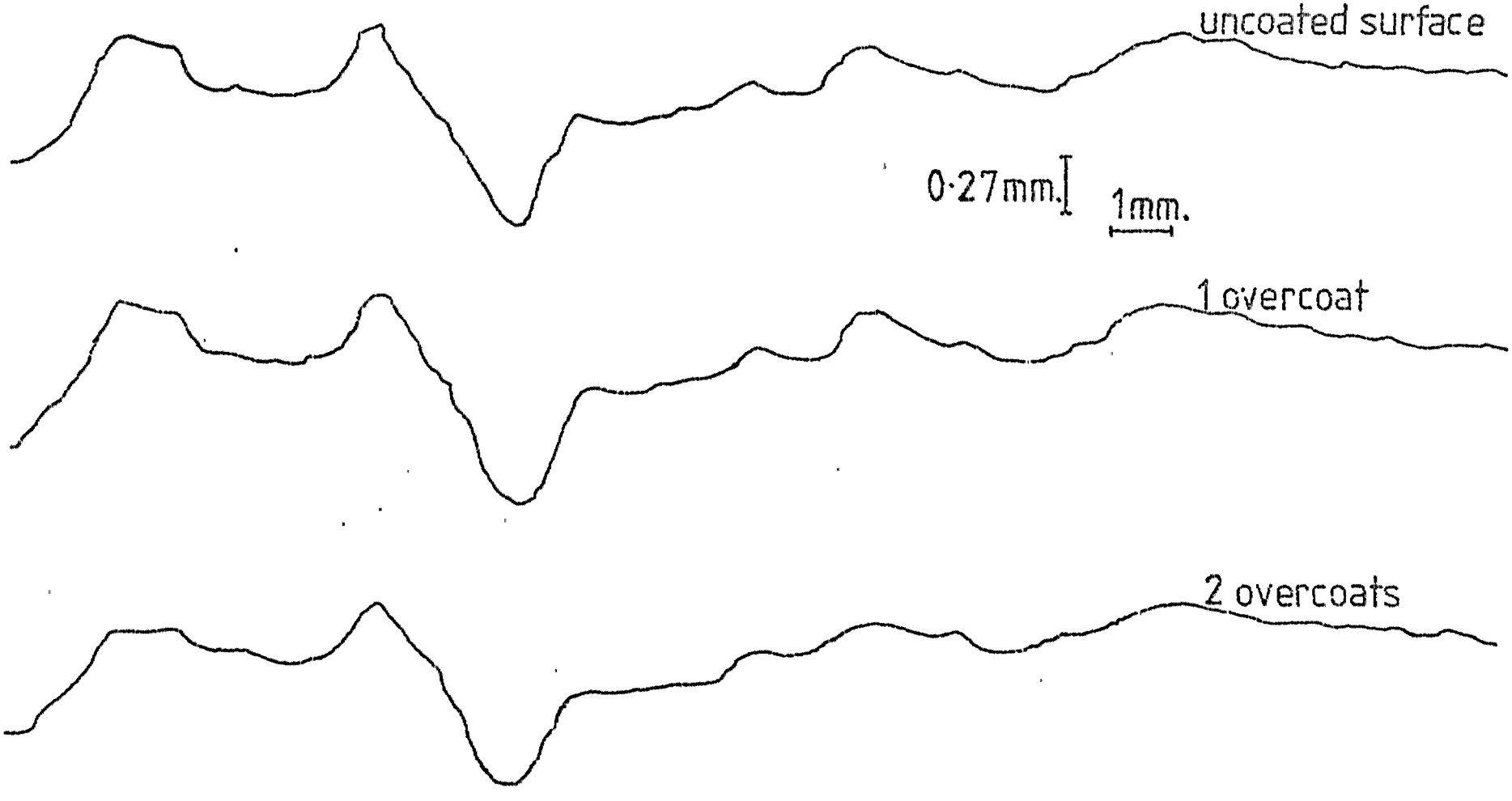

Date

Chart No.

TABLE 7-20 SURFACE ANALYSIS FOR COATED REPLICA

RMS μm.	CLA μm.	High. peak μm.	Low. valley μm.	Diff. μm.	S_k	K_u	Mean peak curv. $10^{-3}\mu m^{-1}$	High. peak curv. $10^{-3}\mu m^{-1}$	Mean valley curv. $10^{-3}\mu m^{-1}$	Mean abs. slope degrees	High. abs. slope degrees	
210	166	648	-368	1016	-0·8	3·4	5·0	13·3	-6·6	6·12	0·53	(1) parallel to brushmarks
182	148	439	-368	807	-0·2	2·6	3·9	11·4	-5·0	4·07	0·36	(2) parallel to brushmarks
196	157	544	-368	912	-0·5	3·0	4·5	12·4	-5·8	5·1	0·45	mean values
118	97	276	-249	525	-0·5	2·4	3·2	9·5	-6·1	4·30	0·48	(1) perpendicular to brushmarks
189	143	532	-389	921	-0·8	3·6	3·9	11·4	-5·5	6·02	0·66	(2) perpendicular to brushmarks
154	120	404	-319	723	-0·7	3·0	3·6	10·5	-5·8	5·16	0·57	mean values

Date

Chart No.

TABLE 7-21 SURFACE ANALYSIS FOR REPLICA WITH SUCCESSIVE COATS OF MARINE PAINT

RMS μm.	CLA μm.	High. peak μm.	Low. valley μm.	Diff. μm.	S_k	K_u	Mean peak curv. $10^{-1}\mu m^{-1}$	High. peak curv. $10^{-1}\mu m^{-1}$	Mean valley curv. $10^{-1}\mu m^{-1}$	Mean abs. slope degr.	High. abs. slope rad.	
145	106	578	-318	896	-0·9	5·3	4·9	18·4	-8·8	6·53	0·65	uncoated
155	111	610	-321	931	-1·1	5·8	4·9	15·2	-8·0	6·63	0·68	1 overcoat
140	106	537	-271	808	-1·2	5·4	3·1	8·2	-6·3	5·42	0·62	2 overcoats

FIG 7-18 PROFILES FROM RELOCATED MEASUREMENTS ON REPLICA FOR SUCCESSIVE COATS OF MARINE PAINT

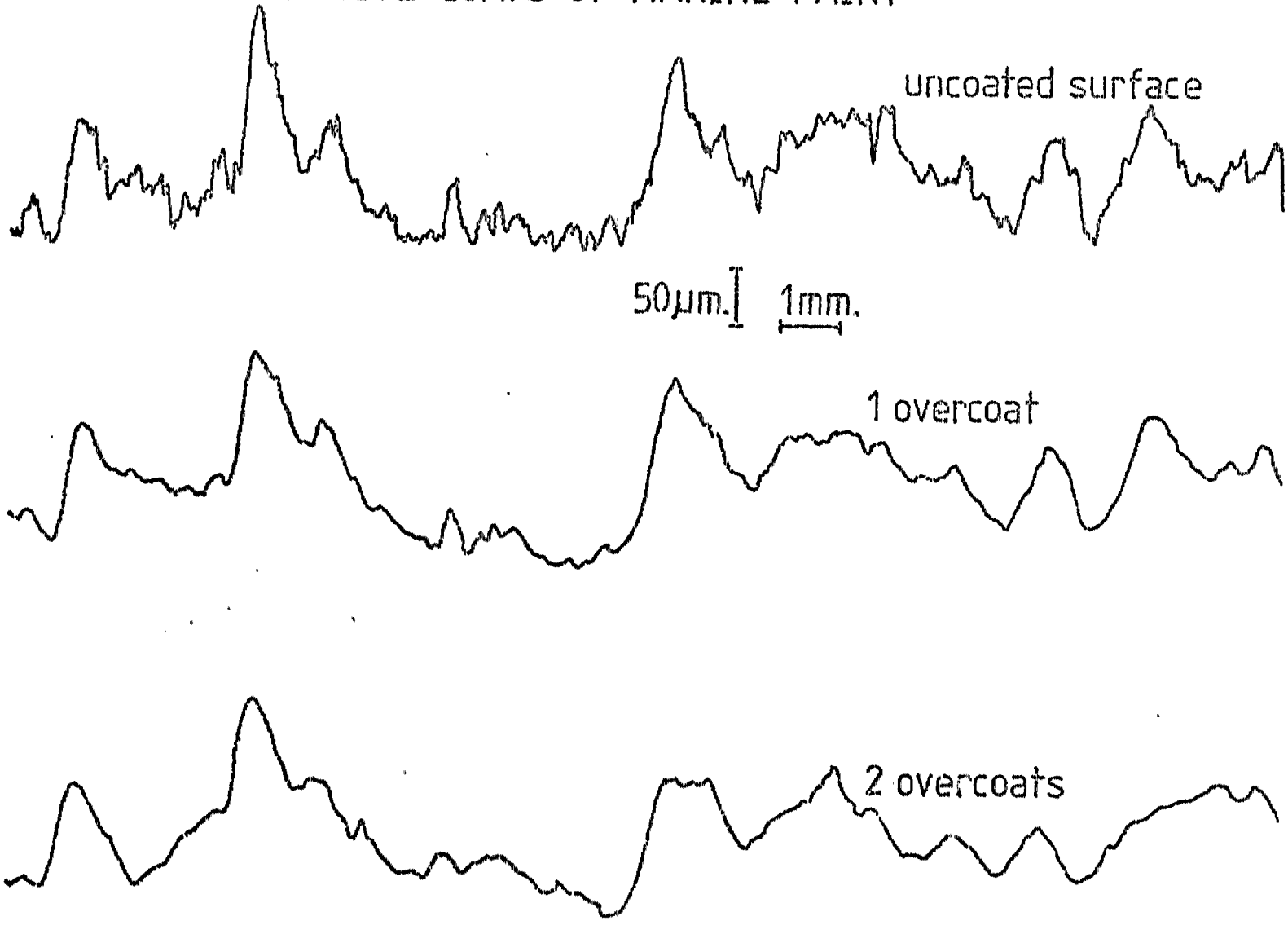

Date

Chart No.

TABLE 7-22 SURFACE ANALYSIS FOR REPLICA WITH SUCCESSIVE COATS OF MARINE PAINT

RMS μm.	CLA μm.	High. peak μm.	Low. valley μm.	Diff. μm.	S_k	K_u	Mean peak curv. 10^{-3} μm^{-1}	High. peak curv. 10^{-3} μm^{-1}	Mean valley curv. 10^{-3} μm^{-1}	Mean abs. slope degr.	High. abs. slope rad.	
41	33	115	-74	189	0·6	3·1	22·5	49·1	-22·5	5·75	0·34	uncoated
43	36	112	-86	198	0·1	2·2	10·5	25·8	-8·3	4·29	0·33	1 overcoat
35	28	115	-71	186	0·4	3·0	7·7	25·6	-6·6	3·45	0·30	2 overcoats

PLOTS OF THE DISTRIBUTIONS OF SURFACE SLOPES, FIG 7-19, AND SURFACE CURVATURES, FIG 7-20, FOR THE REPLICA AND COATED REPLICA

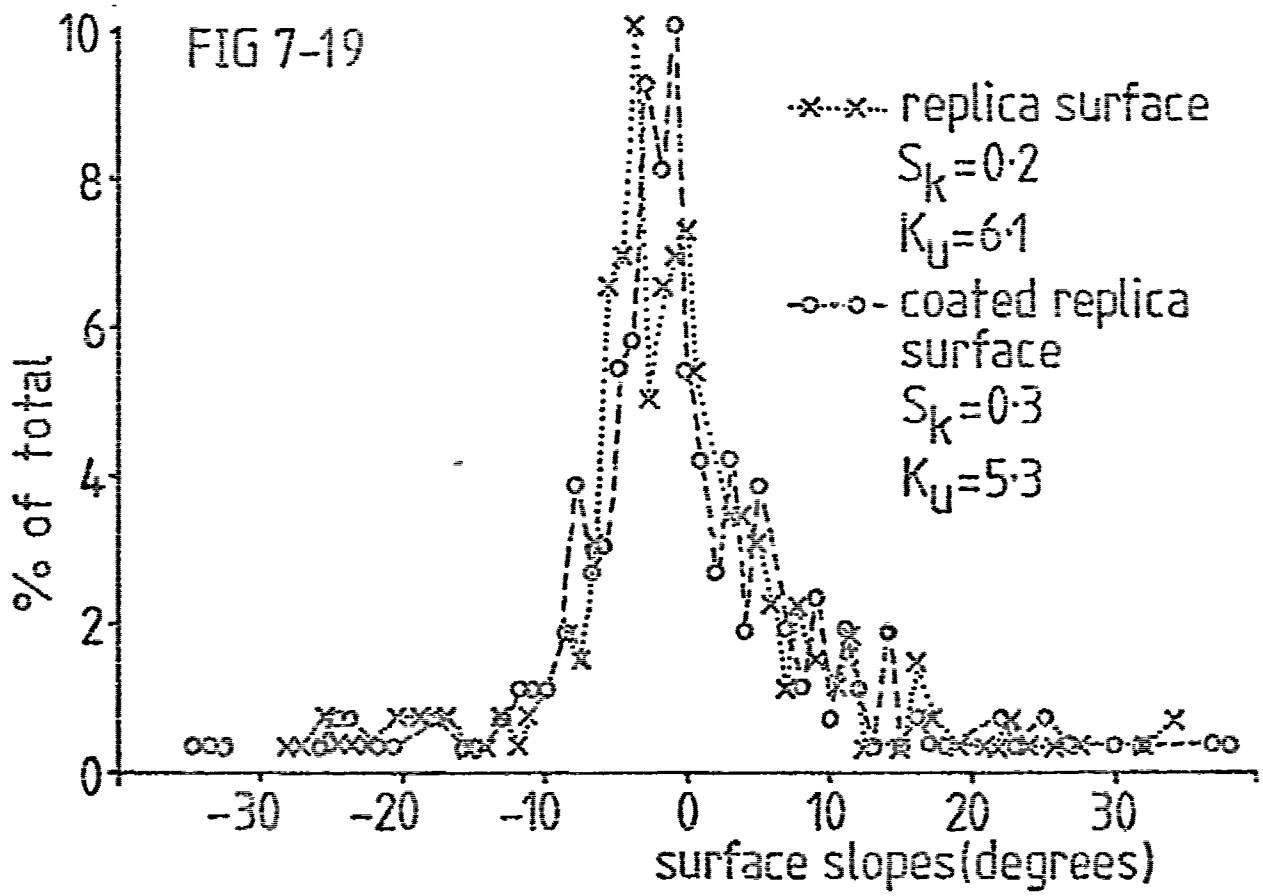

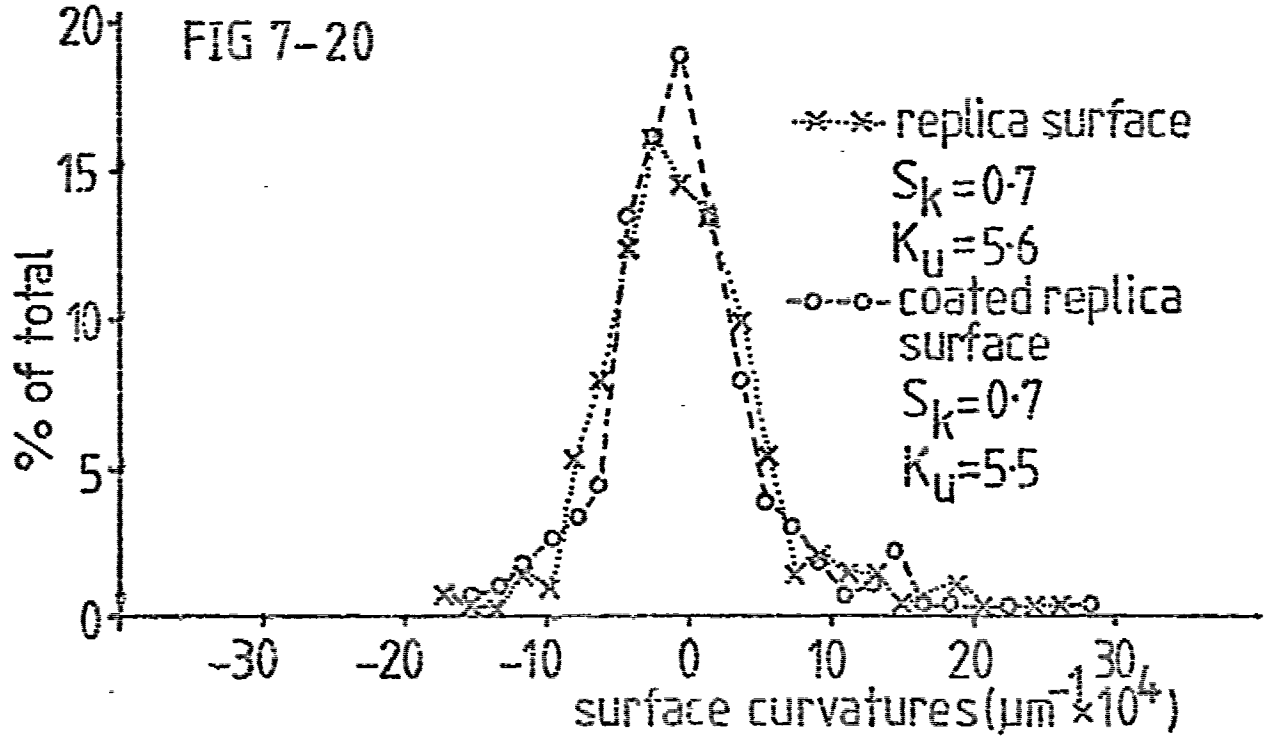

8. THE SURFACE ANALYSIS/FLOW ANALYSIS CORRELATION

The experimental flow data for the test surfaces is plotted using the inner law for the boundary layer velocity distribution (Figure 8-1). The plot shows the existence of the logarithmic region in the mean velocity distributions. The gravel surface data is displaced downwards by an amount $\Delta\bar{u}/u_\tau$, dependent on the roughness Reynolds number (Musker ewkowicz 1978). The painted steel surface and replica surfaces both lie on the well known universal curve for smooth walls (Clauser 1954). The values of C_f determined for the paint steel and replica surfaces agree with the inner law plot, but the surface analyses show the replica surfaces to have R_a values for a sample length of 1.14 m, of approximately 10 times that of the relatively smooth painted steel surface (Table 7-15). The curvatures and slopes for the replica profile are approximately 20 times the magnitude of the curvatures and slopes for the painted steel surface.

The gravel surface has a CLA roughness of approximately equal magnitude to the replica surface for comparable sample lengths. The mean peak curvature for the gravel profile measurement is 70 times that of the replica profile for a sample length of 1.14 m, whilst the grand profile mean valley curvature and profile slopes are 40 times and 10 times respectively the values for the replica. The local coefficients of surface friction, C_f, determined for the gravel surface are approximately 2 times the magnitude of the C_f values for the replica surface at comparable Reynolds numbers. Therefore the difference in the values of the local coefficient of surface friction for the gravel and ship hull replica surfaces is clearly bound with the magnitude of the surface curvatures and slopes, in particular to the peak curvatures.

The profile slope distribution for the gravel surface (Figure 7-13) has a kurtosis of 2.44 whereas the replica surface and coated replica surface have profile slope distributions of kurtoses 5.32 and 6.08 respectively (Figure 7-20).

The profile slope distribution obtained for the gravel surface shows there to be a relatively large proportion of high angled slopes present on the surface. The profile curvature distributions for the replica surfaces show there to be a relatively large proportion of small curvature slopes present on the surfaces. Hence the gravel surface has a relatively large proportion of high angled slopes and high surface curvatures with respect to the replica's surfaces.

As can be seen, this analysis uses a very simplified approach to the determination of flow parameters in a not so simply defined flow regime. Added to this are the complex specimen surfaces, such as the replica surface with its relatively long surface wavelengths, which will affect the boundary layer development and hence the flow parameters in a random manner.

The results of the flow and surface analysis for the painted steel surface are consistent with published results for hydrodynamically smooth surfaces. The gravel surface gives results comparable to published sand-grain surface friction results.

The replica surfaces have values of the local coefficients of surface friction which are comparable with those for a smooth surface. The replica surface analyses show them to have CLA values comparable

with that for the gravel surface, but with shallower slopes and smaller surface curvatures.

Whilst it is feasible that the magnitude of the local coefficients of surface friction for the replica's surface is less than that for the gravel surface, it is not possible to justify the result that the replica's surface has C_f values comparable to a hydrodynamically smooth surface.

The inability of the flow analysis to detect the effect of the smaller changes in the geometries of the surfaces on the C_f values is attributed to an over-simplification of the flow in the open-channel. The single sensor hot-film anemometry used in the investigation is found to give reasonably reproducable values for the local coefficients of surface friction along the centre line of the test section surfaces.

The instrumentation and techniques available for the measurement and analysis of the test surfaces are such that the surfaces can be analysed to a much greater degree of accuracy than the analysis of the corresponding fluid motion. Hence, to obtain a realistic correlation between fluid parameters and surface parameters, the flow analysis must be refined to obtain a fuller picture of the fluid/surface interaction. In order to achieve this a more sensitive and reliable flow measuring instrument, in the form of a laser doppler-shift instrument, is to be incorporated into the flow system.

Thus the present work has shown the feasibility of using open-flume flow in an investigation of the surface frictional resistance of

nominally flat surfaces. The results are plotted using the semi-empirical formula in terms of the centre-line average roughness height, CLA.

$$\chi_{CLA} = 5.62 \log_{10} \left| \frac{7.752\ ku_\tau/\nu}{e^{-0.005\ ku_\tau/\nu} + 0.44\ ku_\tau/\nu} \right| \quad \text{(Musker et al 1976)}$$

where k is the CLA roughness parameter. Figure 8-2 shows the results from the painted steel, gravel and replica surfaces plotted in terms of the roughness function, χ_{CLA}, versus the roughness Reynolds number, R_k. The plot shows good agreement with the results of Musker et al (1976). The results are also plotted using the modified roughness Reynolds number,

$$\frac{ku_\tau}{\nu} = \frac{\sigma u_\tau}{\nu} (1 + aS_p)(1 + bS_k K_u) \quad \text{(Musker \& Lewkowicz 1978)}$$

Figure 8-3 shows the results plotted along with data from Musker & Lewkowicz (1978). The results from the present work, for the painted steel and replica surfaces, correlate to some extent with the published data, whilst the gravel surface data lies well clear of a mean curve fitted by eye through the published data. It has been found that no reasonable curve fit could be produced for a surface sample length higher than 10 mm regardless of the values assigned to the empirical constants a and b (Musker & Lewkowicz 1978). Hence, Figure 8-3 is included merely to give an indication of any trend in the present data. The local surface friction coefficient was also calculated using the surface friction law by Ludwieg and Tillman (1950),

$$C_{f_{L-T}} = 0.246.10^{-0.678H} (R\theta)^{-0.268}$$

for the replica and coated replica surface (Tables 6-5 to 6-7). The values are compared with the values of C_f calculated using the momentum and inner law equations.

FIG 8-1 INNER LAW PLOT USING THE FLOW ANALYSES FOR THE TEST SURFACES

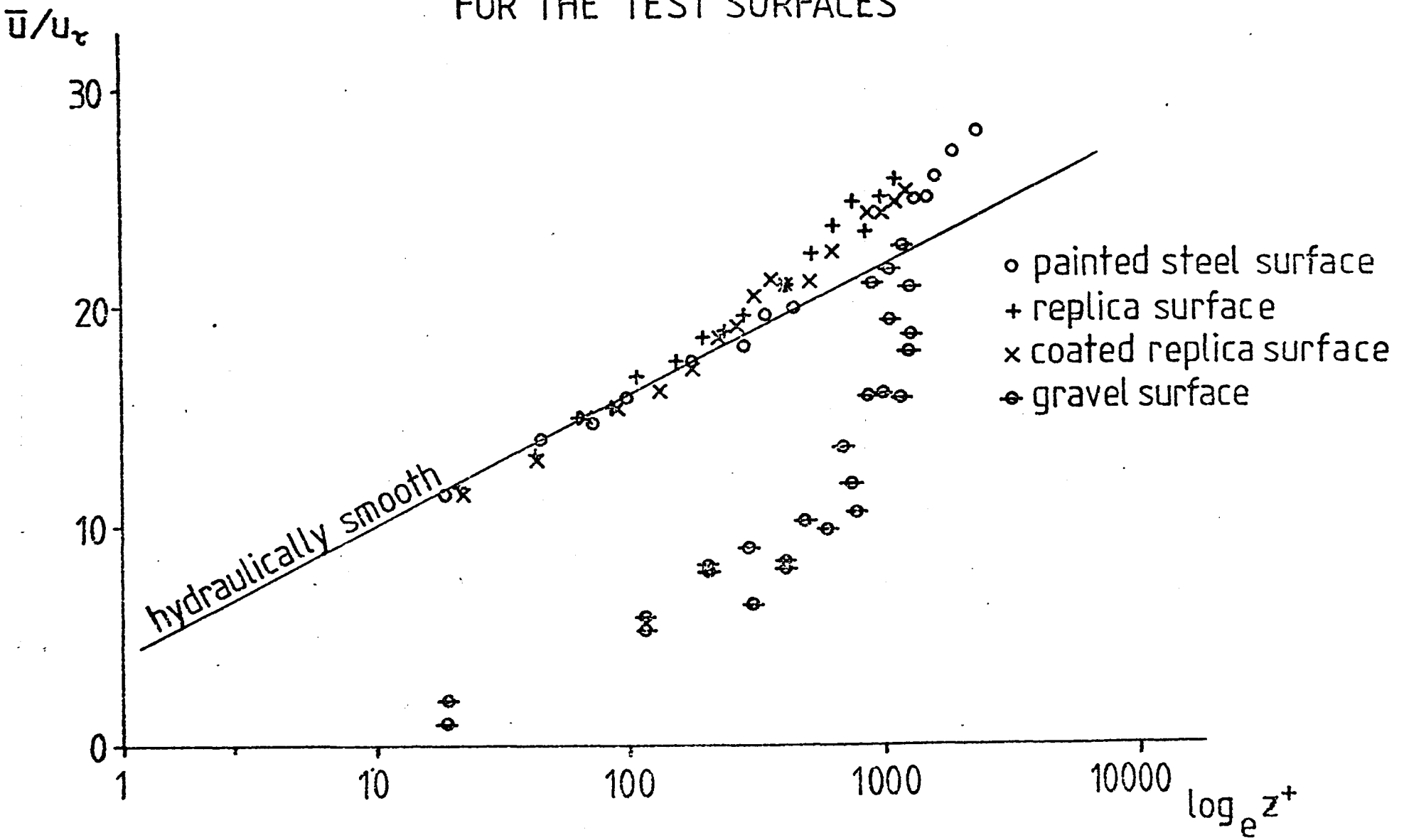

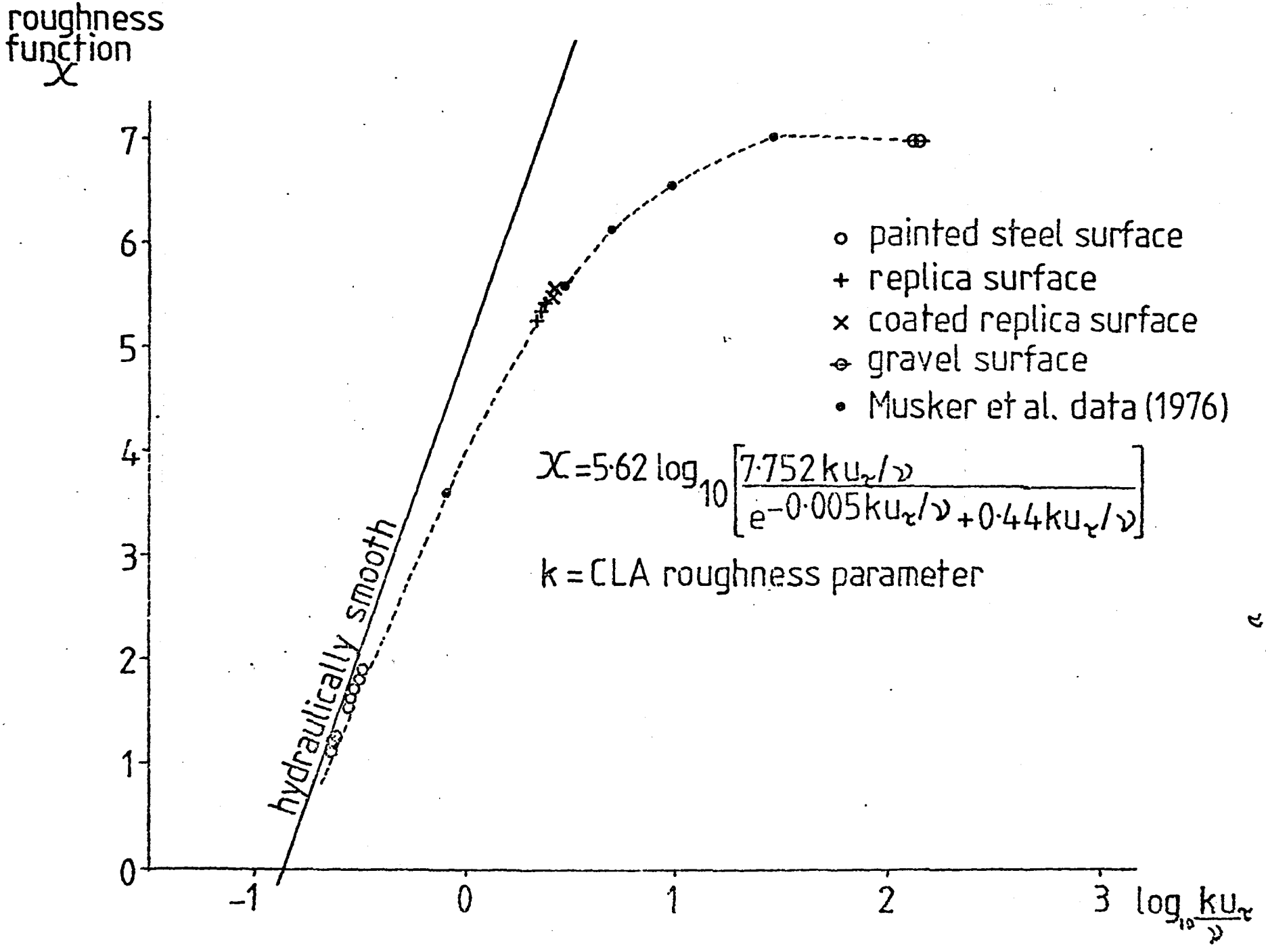

FIG 8-2 ROUGHNESS FUNCTION $\mathcal{X}$ VERSUS ROUGNESS REYNOLDS NUMBER $\frac{ku_\tau}{\nu}$

FIG 8-3 ROUGHNESS FUNCTION VERSUS ROUGHNESS REYNOLDS NUMBER

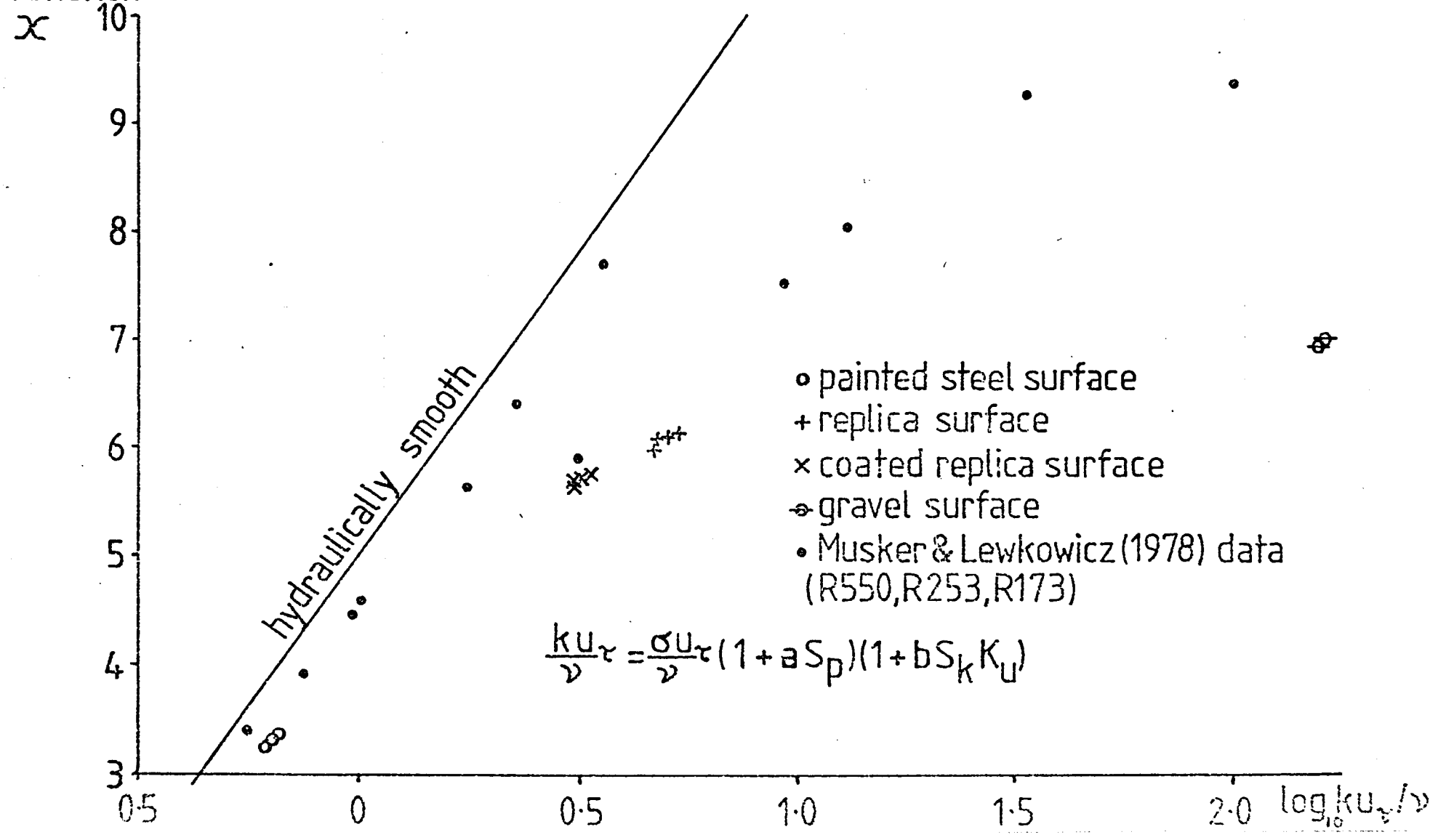

RELATION BETWEEN THE SURFACE FRICTION OF PLATES AND THEIR STATISTICAL MICROGEOMETRY

BY

M.J. KING

(Thesis submitted to Teesside Polytechnic for the degree of Master of Philosophy)

January 1980

CONTENTS

CONTENTS (continued) PAGE NO.

APPENDIX 1: LITERATURE SURVEY

1.1 Introduction

The resistance of a ship in steady motion in calm water can be resolved into the following principal components: (a) Surface-frictional resistance; (b) Wavemaking resistance; (c) Eddy-making resistance; and (d) Wind and air resistance.

The ship is generally assumed to be in steady motion in order to simplify the resistance analysis.

The surface friction is made up of the summation of the components in the direction of motion of the tangential stresses which the water produces on the hull surface, and apart from the viscosity and density of the water, it depends primarily on the area, length and roughness of the wetted surface of the hull, as well as the speed of the vessel.

The wavemaking resistance consists of the summation of the components, in the direction of motion, of the normal pressures on the hull due to the surface wave systems set up by the action of the hull on the water. Wavemaking resistance, apart from the density of the water, is primarily effected by geometrical features such as proportions, fineness and shape of hull, as well as the strength of the gravity field.

The third component, that is, resistance due to eddying wakes, is associated with energy losses due to, firstly, the formation of eddies behind the stern of the ship; more especially these associated with the rudder and stern post and the propeller shaft supports. Under certain

adverse pressure gradients, the formation of vortices and separation eddies can also be associated with contracting flow in the after-body of the ship. This type of resistance can also manifest itself in the form of normal pressures on the hull but is generally of viscous origin. It is often referred to as the form resistance.

The fourth component is the resistance due to the relative wind acting on the above-water part of the ship. Due to the low density of air compared with that of water, this resistance is generally quite small compared with the water resistance.

Therefore it can be said that there are two principal components of resistance, namely, surface friction and wave-making (Figure A1-1).

Of the two principal components, the surface friction resistance is predominant at low Froude numbers, that is for relatively low speeds such as for tankers. At higher speeds the wave-making component becomes predominant.

1.2 Ship-Model correlation

The inability to calculate these resistances directly from hydrodynamic theory led to the use of tests on models geometrically similar to the ship.

Typically a ship will have a resistance comprising of up to 85 per cent frictional (Schoenherr 1932). Methods of measuring the resistance of ships were originally based on the determination of the power required to propel a ship at a certain speed and then comparison with past results.

A more convenient and much used method in the early 1900's was the Froude Method. This assumed that the frictional component of the total resistance could be determined independently and subtracted and that the remaining residuary resistance is free from viscous effects and is subject to the laws of dynamical similitude. The residuary resistance is related to inertia and gravitational forces only, and determinable by ship-model experiments using Froude's law of dynamical similarity.

1.2.1 Flat plate analysis

In 1872 Froude carried out a series of experiments to investigate the influence on the surface friction of the velocity and the dimensions of a flat plate towed edgewise through still water, in particular the length of the plate in the direction of motion. The first known tests on the surface friction of flat surfaces in fluids were those of Beaufoy in 1793. In 1880 Froude and Tideman, using the experimental data of Froude's earlier towing experiments, proposed a formula of the form $F = CAU^m$ for the frictional resistance of plates. That is, the surface friction was assumed to vary jointly as the wetted surface area A, and the speed, U, raised to some power m.

Thus, in the analysis of the surface friction of a ship, it was found convenient initially to consider the surface friction of a flat surface moving in its own plane. It was found that the above relation held quite well for a given plate but that C and m varied from one plate to another.

1.2.2 Friction lines

When the experimental results of Froude were re-analysed on the more acceptable basis of Reynolds number and due account taken of laminar flow on the smaller planes (Lackenby 1937), the results could then be fitted with a universal curve, or friction line (Figure A1-2). With the theory of the boundary layer as proposed by Prandtl in 1904 it was now possible to define a characteristic length for the flow along a plane surface which corresponded to the radius in the case of developed flow in pipes. This characteristic length was called the "boundary layer thickness". Thus with the flow in cylindrical pipes and the flow along plane surfaces being reduced to a common base, Von Karman and Prandtl showed independently how experimental data obtained by measuring pressure losses in smooth pipes could be used to deduce a formula for the frictional resistance of smooth plane surfaces. (The investigations were extended to rough pipes by Nikuradse who successfully correlated the frictional data of dense sand-grain roughnesses of different sizes in various diameter pipes.) This formula and other subsequently produced formulae were experimentally and not theoretically derived and hence they were no more accurate than formulae based on direct measurements of the resistance of plates towed through still water or suspended in a wind tunnel. This led back to various experimental work on towing plates through water as Froude had done in 1872. The first investigation of the resistance of plane surfaces in air was carried out by Zahm, in 1903.

Each of these individual experiments covered only a limited range of length and speed and hence produced a series of equations for the frictional resistance of plane surfaces deduced from mean lines drawn through each of the plots of results.

Schoenherr (1932) collected together all the existing sets of experimental data for the frictional resistances of smooth, flat surfaces, each set being for a limited range of length and speed. Experiments were carried out at low Reynolds numbers (2×10^5 to 2×10^6) to provide new data where existing data was widely scattered. The kinetic viscosity was varied in addition to the length and speed. The whole of the existing data was then used to produce a single plot of surface friction coefficient versus Reynolds number.

Bearing in mind that these tests were made at different times, in different media and with widely different apparatus, the plot showed that on the whole the results were in fairly good agreement, and that an average curve would be representative for all the tests (Figure A1-3). Accordingly the best representative mean curve was fitted to the data. It was found that, on attempting to fit an equation to this mean curve, none of the existing formulae fitted over the entire range. From an extension of the work done by Von Karman, an equation of the form

$$K/\sqrt{C_f} = \log (RC_f) + M \qquad \text{Schoenherr (1932)}$$

was applied to the mean line through the data.

It was found that with the following values for the constants K and M, M = 0 and K = 0.558, the equation coincided almost exactly with the mean line over the whole range of Reynolds numbers.

1.2.3 Ship hull resistance

The extension of the flat plate analysis to the frictional resistance of the uneven and curved surfaces of ships' hulls has been attempted by various workers. Several of these set out to determine the influence on drag of different types of roughness to be found on a typical ships hull, and also to produce a parameter for the effect of curvature of a ships surface. But, in order to be of value these attempts had to be checked against actual frictional resistance of the ship itself. Hence, it was necessary to have a method of measuring the frictional resistance of ships to a fair degree of accuracy. For this purpose, it was proposed to tow ships, as had been done previously by Froude, at low speeds where the wave-making resistance was considered small. Such tests however, are expensive and the results are of limited value. Hence from Froude's method of calculating ship resistance which is denoted by the equation

$$r/au^2 - R/\gamma AU^2 = f/au^2 - F/AU^2$$

where ship units are denoted by capital letters and ship-model units by small letters; total resistance = r,R; frictional resistance = f,F; area of wetted surface = a,A; velocity = u.U; specific gravity of salt water = γ

Hence the frictional resistance of the ship can be determined when the total resistance is known.

It was shown that the relation between the resistance of a ship and the propeller thrust to overcome this resistance involves the so-

called thrust deduction coefficient, which could be approximately obtained from the self-propelled tests of the ship's model. Methods had also been developed for determining the wind resistance of ships' superstructure. From these considerations the total water resistance of a ship could be obtained.

It was usually assumed that the frictional resistance of the model is equal to that of a smooth plane surface of equal length and area, and the frictional resistance of the ship is equal to that of a smooth plane surface of equal length and area increased by an allowance for the resistance of the butt straps, laps and other projections on the ship's hull. Although the correlation of the resistance of ship models of different sizes and the reliable prediction of actual ship resistance from model results is of fundamental importance, it was not possible to accurately predict the frictional resistance of a ship model from the results of another model to a different scale.

Later work by Froude on plates coated with fine, medium and coarse sand was re-analysed by Telfer (1951) giving

$$C_F = \left[1.2 + 75\left(\frac{k_s}{L}\right)^{1/3}\right] \times 10^{-3}$$

where k_s is the sand grain size and L the ship length.

1.2.4 Geometrical similarity between ships and their models

The chief criticism made against the use of the Schoenherr (1932) curve fit (friction line) was not so much against the line itself but that the data producing the line shows such a large spread of values

so invalidating the use of a mean line, making prediction by extrapolation to ship values uncertain. The range of variation of value in the Schoenherr plot was of the order of 20 per cent in the range of Reynolds numbers from on million to twenty million. Hughes (1952) decided to examine critically the basis of the existing data and to determine the possible reasons for these large variations. Differences in the experimental conditions were thought to be the most likely cause of these variations. It was found from this examination that there was a promise of a high degree of consistency (and hence conformity to Reynold's Law) if proper account was taken of variations in the ratio of length to breadth of the plane surfaces used by the various experimenters, or in other words if proper respect were given to the condition of geometrical similarity implicit in any dynamic similarity law. Hence, the lack of geometrical similarity appeared to be one of the major causes of 'apparent' inconsistencies revealed by the survey of the data, as verified by Figure A1-4. Other major causes appeared to be due to the additional effect of wave-making resistance, pressure resistance, and transitional flow phenomena.

Thus, before any new data was obtained it was decided that firstly flat surfaces having a range of values of the length to breadth proportions would be used. Secondly, the plates were made as thin as possible so that both form resistance and wave-making resistance would be minimised. This had to be balanced against preserving the flatness of the surface, the flatness becoming more difficult to achieve as the thickness of the plate is decreased.

It was also realised that it was essential that the flow over the test surface must be fully turbulent from as near the leading edge as possible and at the lower speeds (Figure A1-5).

With the increased interest in the prediction of the resistance of ship forms from tests on models a review of the subject was carried out by Granville in 1956. It became apparent that when plotting the total-resistance coefficients of a family of geometrically similar vessels, it is necessary to specify non-dimensional ship lengths to satisfy dynamical similarity. A graphical method of analysing the resistance of geometrically similar forms was developed in terms of flat-plate resistance.

On examination of the existing experimental data for families of geometrically similar models it was found that there was insufficient accuracy to establish definitely the superiority of any one prediction method. Furthermore, a lack of tests on hydrodynamically smooth full-scale vessels prevents verification of full-scale predictions.

1.2.5 Ship-Model flow regime

For drag measurements in general to be useful it is necessary to have a means of determining the type of flow present, whether it be laminar, transitional, or fully turbulent. In the case of ship models it had been established that some of the models have a laminar region of flow during testing (Figure A1-6). It was decided that ships models, for reasons of comparing results, should be operated with fully turbulent boundary layers. The techniques that became available for examining the state of the boundary layer flow were in general cumbersome, requiring special and often very extensive tests, in addition to the resistance measurements.

In 1960 Townsin used a technique for flow detection which did not obstruct the flow in any way, the sensing elements forming part of the model surface; hence simultaneous flow observations and resistance measurements could be made. The method used was similar to hot wire anemometry, but instead of using wires, which are easily broken in water and need a probe to hold them in position, it used platignum hot film sensors.

Flow measurements were made over the forward end of three models of different lengths, two of which with turbulence stimulators in the form of studs. The third one was a 9 foot model of the ship Lucy Ashton tested both with a trip wire as a stimulator and with no stimulator at all. Studs are the generally accepted form of turbulence stimulator.

It was found that, even at the top end of the speed range, a laminar region persisted behind the studs on the largest of the models (15.4 feet in length) covering half to one per cent of the wetted surface. The smaller the length to breadth ratio of the vessels tested, the more prone they were to laminar flow.

The model of the Lucy Ashton (1953), which has a relatively large length to breadth ratio, was found to be free of laminar flow even at the lowest speeds when the trip wire was used. Without the trip wire, a laminar region covering some 5 per cent of the model surfaces persisted up to the higher speeds used. The results showed conclusively the need to study the flow regime during the testing of ship models.

1.2.6 Full-scale ship trials

Ship trials at sea are used to evaluate the accuracy with which prediction of the full-scale resistance of vessels can be made from tests on models. Thrust or torque measurements on the propeller shafts are related to ship resistance on the basis of additional tests on models. The usual result from sea trials was that the resistance so determined is greater than the predicted resistance, the difference between them, the correlation coefficient, being made up of the hull roughness and errors due to scale effects in the propeller allowances and errors in the prediction method.

The most recent extrapolation methods for ship-model tests (ITTC, September 1978) are good for most classes of vessel and the correlation coefficient is now almost entirely due to hull roughness. Differences between the prediction method and the ship trial results give rise to the following roughness allowance

$$\Delta C_f \times 10^3 = 105 (k_{MAA}/L)^{1/3} - 0.64$$

where k_{MAA} is the BSRA mean apparent amplitude (MAA).

To eliminate the uncertainties due to the action of the propellers, more difficult and costlier tests were performed on hulls without propellers, the propulsion being achieved by a towing vessel or more recently by aircraft engines. The classical test of this kind is that of the Greyhound by William Froude. More recently BSRA carried out an investigation in which a former Clyde steamer, the 'Lucy Ashton', (1953) was propelled by aircraft jet engines. The combined measured thrusts

of the jet engines gave a measure of the ship's resistance which was free from the difficulties inherent in towing the vessel (Figure A1-7). In these trials the effect of different hull surface conditions was measured. A noticeable difference was found in the total resistance and estimated surface friction between using a red oxide paint and sharp seams, and a slightly smoother aluminium paint with faired seams (Figure A1-8). On allowing the hull to foul, the surface resistance increased by about 50 per cent. The fouling consisted of scattered small barnacles about 1/8 inch high on the hull bottom, together with a band of fine grasses on the sides. Thus, the trials showed the surface friction to be very sensitive to small roughnesses, and more so to fouling (Figure A1-9).

1.2.7 Analysis of the ship hull surface

In an attempt to throw more light on the 'Lucy Ashton' results, records of the hull surfaces were taken with a wall gauge on the two painted surfaces used. Analysis of these showed that the nature of the roughness was a complex function of superimposed undulations, the mean amplitude depending on the wavelength, and there seemed to be no simple parameter which could be used to define the surface. A form of harmonic analysis was used which showed that the amplitude decreased with decreasing wavelength and that over most of the range the aluminium paint surface was smoother, the amplitudes being about two-thirds those of the red oxide paint which agreed with the measured resistances. From this work BSRA realised the importance of the effect of hull roughnesses on the performance of ships and decided to make hull roughness surveys on all subsequent ship trials in the hope of explaining differences in performance between sister ships: there could be as much as 23 per cent

variation in the performance figures for sister ships. A statistical analysis was used to look at the separate factors affecting trial performance and this showed, as expected, that plate roughness is by far the most significant factor. The greater part of the variation in the hull surface roughness seemed to be due to the uneven application of paint.

In order to look at the effect of deterioration of hull surface due to breakdown of the paint system, formation of corrosion products and organic fouling, BSRA in conjunction with Shell Tankers carried out a series of repeat trials on two sister ships after various periods in service (Figure A1-10). The dry dock inspections showed that there was little or no organic fouling and that the deterioration of the hull surface was primarily due to corrosion. The plot of measured shaft horse powers against corresponding hull roughness (Figure A1-11) shows considerable scatter but has a marked trend of shaft horse power increasing with hull surface roughness.

1.3 Ship hull roughness/fluid flow considerations

1.3.1 Tests on the effects of different types of structural hull roughness, painting, corrosion and fouling, on fluid flows

In an attempt to determine the influence of the various types of roughness likely to occur on a ship's hull, Kempf (1937) ran three comparative sets of tests on pontoons whose flat bottoms were covered with the types of surface under examination. The first set of tests comprised two different conditions of paint-roughness and investigated the influence of butt weld joints. The second set of tests was to

study the additional influence of rivets, straps and butt weld joints on the resistance of a surface with various finishes. The third set of tests were run with the pontoon bottom covered with roughened paint. The results of the tests showed that a poor condition of a coat of paint can affect the resistance of a surface far more than the constructional protuberances. Interpreting the results suggests that a ship operator could expect to save 3 per cent on fuel consumption at a given speed with a smoothly coated hull in comparison to a badly painted hull surface.

Kempf then went on to measure the additional roughness-resistance of ships using two new approaches. In the first case Froude's method of measuring the total resistance of a towed ship and of her model was adopted by using the Prandtl-Schlichting formula for minimum frictional resistance for the model to calculate the coefficient of frictional resistance for the ship. The second method was based on the measurement of the local resistance of a certain small piece of the hull surface from the paralle middle body part of the ship (Kempf 1929), and provided a direct measure of local frictional resistance.

The results produced C_F values for the ships which were too high at the lower Reynolds number, i.e. at lower speeds. This discrepancy was explained as the result of there being laminar flow round the models which would make the measured model resistance at lower speeds too small, and as the turbulent frictional resistance is subtracted, the residual resistance for the ship will be calculated too small.

Kempf then went on to look at the effect of fouling on the resistance of ships. Included in this category: (1) rusting, (2) growth

of shell, (3) growth of seaweed. He formulated the following conclusions regarding the above aspects:

(1) Rusting is a gradual process over the years, affecting the whole bottom of the ship. The equivalent sand roughness may be doubled or more by rusting producing 10 per cent to 20 per cent more frictional resistance.

(2) The resistance of ship hull surfaces fouled with shells can be evaluated using an equivalent sand grain roughness, where the shells are assumed to be similar in shape to the sand grains. A comparison was made of the experimental data obtained for a clean ship hull bottom and for one covered with a growth of shells. The shells were of 'medium' height (approximately 4.5 mm) with a density on the surface producing a maximum resistance to the flow. The results showed that frictional resistance of the shell coated surface could be as much as 85 per cent more than the clean surface.

(3) The resistance of seaweed which mostly covers a small strip under the water-line was not tested, but from ship trials it seemed that smooth seaweed did not affect the resistance very much in comparison to the sharp-edged roughness of shells.

Telfer (1969) considered the problem of fouling in the case of tankers and found that owing to their quick turn-round in port they do not usually suffer badly from fouling, but in the event of fouling being present the ship's frictional resistance could be substantially increased.

At the present time toxic anti-fouling is applied to the hull in the form of a paint. The anti-fouling system must adhere well to the underlying anti-corrosive coatings or else tie coats and barrier coats may be required. Removal of the anti-fouling coat due to it becoming ineffective can seriously increase the surface roughness, resulting in an expensive blasting procedure to renovate the surface. In practice anti-fouling coatings have to be renewed frequently, at say, one to two year intervals.

Allan and Cutland (1956) looked at the problem of the effect of hull roughness on the ship resistance, by studying separately the various structural roughnesses occurring on a ship's hull. Full scale experiments were carried out on pontoons with the various roughnesses on plates fixed to their undersides. The results from these tests were then applied to a number of representative ships in the large cargo ship range (450 feet to 620 feet long).

It was found that the local velocities at the edge of the boundary layer calculated in the fore-body of the ship were above that for the flat surface, whereas those in the after-body were below that for the flat surface. Thus, it was thought probable that the effect of roughness in the front quarter length of the ship was substantially underestimated, whereas the opposite was probably happening for the last quarter length, so the two effects tended to balance out. Contrary to belief, the middle quarters of the ship's length were found found to be as important as the leading quarter in their contribution to the overall resistance.

In conclusion it was thought that even when care is taken to ensure that the local small-scale roughness does not exceed a few thousandths of an inch, the effect of resistance will still be considerable at ship Reynolds number. The effect on resistance of roughness arising from bad paintwork was shown to increase the surface friction by as much as 100 per cent, thus again showing the need to ensure a smooth hull finish.

Results derived from measurements of ship hull roughness and performance on ship trials collected over a period of years by the BSRA (1977) showed that a one per cent increase in power is required to maintain speed for every 10 μm (0.0004 inch) increase in the mean apparent amplitude (Chaplin 1965) of the hull roughness. Hence, the bad surface in Figure A1-12 would be expected to require 17 per cent more power than the average surface, whilst the good surface would require 8 per cent less power than the average hull surface.

A typical new ship has a hull roughness equivalent to 130 μm (0.005 in) mean apparent amplitude, whereas an old ship in poor condition can exceed 1,000 μm (0.04 in). Whilst it is thought possible that improvements of 100 μm (0.004 in) and more could be made for older ships, the finish on a newly built ship is unlikely to be better than 80 μm (0.003 in).

A study by Townsin et al. (1976) found that the condition of a ship's bottom and the effect it has on the ship's performance could be particularly important in the economic operation of the ships studied. Weld beads could contribute to the increase in power by 1 per cent or more. Hence, buffing off the butt welds seemed in some cases to be

economically attractive. On several ships a large increase in the hull roughness was observed after recoating in dry dock. The popular method of recoating by rapid application of the paint using a high pressure spray was found to give an uneven 'over-sprayed' surface which could be rougher that the uncoated surface.

Frequent underwater scrubbing of the ship hull to remove marine growths such as weeds gave worthwhile short term improvements in the ship performance, but fouling should be eliminated completely if large increases in fuel consumption are to be avoided (Townsin 1978).

1.3.2 The initial preparation of the hull surface

Hudson et al. (1959) studied the effect of surface preparation on the performance of the subsequently painted surface of ships' bottoms, in an attempt to provide a common procedure on surface preparation for the shipbuilding and shipping industries as a whole. The experimental work consisted of producing specimens of ship plate, in both the as-rolled and the descaled conditions, exposing them to weathering for various periods of up to 12 months. the weathered plates were then treated by several accepted practical methods of surface preparation, before being painted with three coat bottom painting schemes and immersed in the sea for one year.

It was found that the paint did not adhere well to freshly descaled, unrusted steel. Adhesion was greatly improved by a chemical surface treatment and allowing the plate to rust a little after pickling or grit blasting, provided that the plate is wire-brushed immediately before painting.

The surface preparation of steel by abrasive blast cleaning methods is a well established procedure with both technical and economic advantages. The technology of abrasive blast cleaning had been investigated by many workers whilst the effect of the resulting surface roughness on the thickness of paint coatings applied to such surfaces had received very little attention. Daniel (1969) investigated the importance of film thickness in relation to the anti-corrosive properties of paint coatings. On a rough surface, the minimum film thickness will be present over the largest 'peaks' of the surface, hence this minimum thickness will largely determine the initial protective properties of the coating. In other words, an abrasive blasted surface will require more paint to keep it free from corrosion than a smooth surface. The basic problem is, how much more paint is required and can this extra paint be estimated by a consideration of the properties of the paint and of relevant measurements carried out on the substrate. In order to help solve the problems, methods for predicting and measuring minimum paint thickness were required. The investigations were restricted to a consideration of surfaces produced by the abrasive blasting of fairly smooth steel surfaces.

The characterisation of blast cleaned surfaces in terms of the volume per unit area bounded by the metal surface and a plane located by the summits of peaks (i.e. surface volume) was examined and a method of measurement was developed. The effects of surface roughness upon paint thickness was investigated, the most significant parameter of a blast cleaned surface being the 'surface volume'. Variations in paint thickness shown by paint/substrate systems were experimentally measured on cross-sections of the test surfaces. A method of estimating the minimum paint thickness over peaks was proposed for systems when the

volume of dry paint present per unit area is much greater than the surface volume. Instruments were used to measure paint film thickness and it was shown that an approximate measure of the volume of dry paint present per unit area, and a very approximate indication of minimum thickness could be achieved, with certain limitations.

1.4 General surface roughness/fluid flow considerations

1.4.1 Practical aspects of surface frictional resistance

In the field of aerodynamics, Young (1950), for instance, looked at the particular problem of the effect of camouflage paint on profile drag of aeroplanes, and thus, assessed the effects on their performance. This problem was of some importance during the 1939-45 war and the results were of general interest for workers in the field of surface frictional drag. The profile drag is assumed to be the sum of the surface frictional drag and the form drag.

Measurements were made in a high speed wind tunnel of the drag of a wing with various grades of surface roughness in the form of camouflage paint. The drag effect of each roughness tested was such that an equivalent size of sand-roughness could be associated with it. An analysis of roughness records taken with a roughness gauge, developed by Tomlinson of NPL, showed that the equivalent sand roughness heights for each of the surfaces were about 1.6 times the arithmetic mean of the roughness heights $\bar{k}$, and in general had similar amplitudes to the largest roughness elements occurring with moderate frequency. Estimates were then made of the effects, of the various surface finishes tested, on the aircraft drag for different values of wing chord or body length,

forward speeds and heights. The results were then used to assess the effects on the performance of representative aircraft.

More recently, Reda (1974) carried out experimental work in connectic. with a missile development program. During flight test, the missiles were suffering from a reduction in range which could not be accounted for in the original drag calculations. It was thought that the surface of the missile motor casing was in some way amplifying the surface-frictional drag levels beyond the estimated values. On inspecting the motor casing surfaces, which were constructed from fibre glass-wound material, they were found to have a large percentage of their surface covered with ridges and grooves formed during fabrication. These surface undulations were in a transverse direction to the local flow direction, and it was thought that the resulting random rough/wavy surface was, in some way, increasing the surface frictional resistance levels beyond the estimated levels which were based on the smallest roughness dimension, the fibre material filament radius.

In the resulting investigation, surface contour traces, using a stylus instrument, were taken from an actual motor case section, and these showed the existence of three scales of roughness i.e. (1) a roughness scale, (2) a short wavelength scale and (3) a long wavelength scale.

Several rough/wavy patterns were fabricated in an attempt to simulate the different types of surface features. The most complex was a roughness scale superimposed on a short wavelength waveform, both of which were superimposed on a long wavelength waveform.

Three types of models were tested: (1) sand grain models for comparison with previous results, (2) machined models formed by impressing the desired surface patterns on aluminium plates and (3) a mould of the roughness pattern taken directly from a full-scale motor casing. The results of the investigation showed that:

(a) Superposition of a given roughness dimension on a surface which already possesses long and short periodic waveforms increases the surface shear above the levels measured for identically rough surfaces possessing only one, or none, of these same periodic waveforms.

(b) Equivalent sand-grain roughnesses for the random rough/wavy wall (motor case material) were of the order of four to eight times the physical roughness scale attributed to it, the physical roughness scale used being peak to valley height.

(c) Velocity profiles measured over rough/wavy surfaces, including random rough/wavy and rough/multiple periodic waveform surfaces, were found to possess logarithmic regions for which the law-of-the-wall is valid.

(d) When plotted in terms of velocity defect coordinates (White 1974), the smooth, rough and rough/wavy profile data collapsed onto a near universal curve in outer portions of the layer, in agreement with previously published results, verifying that, even for complex surface patterns, roughness effects are localised deep within the boundary layer.

1.4.2 Relating surface roughness to frictional resistance

There have been a number of other experiments on various types of roughness carried out in various flow configurations. Open-channel flow, for instance, has been used in several investigations of the frictional resistance of rough surfaces. Powell (1946) carried out tests in a rectangular flume on various types of roughness made up of different arrangements of square steel strips layed at right angles to the flow and extending down the sides and across the bottom of the flume. Measurements were also carried out in a smooth flume. The analysis of the results were based on the fundamental work on open channels by Keulegan in 1938. The roughness effect was found to depend both on the height of the roughness elements and their spacing. Einstein and Banks (1950) carried out a series of tests to determine the total resistance of different types of roughness opposing the flow of water through an open channel. Previous work had mainly been confined to the effect of uniform roughness elements, whereas here the roughness was made up of various densities, patterns and combinations of different shaped roughness elements. The aim of the investigation was to find if the total roughness frictional resistance could be expressed as the sum of the individual resistances. On a much larger scale, this type of argument had been suggested in a study of the Salinas river where the total force opposing the flow was thought to consist of the superimposed resistance exerted by the river bed and sides, the sand bars, and the vegetation. An analysis of the experimental results of the investigation showed that it was possible to express the total resistances as the sum of the individual resistances as long as the separation between the roughness elements was sufficiently large so that individual roughnesses did not exert any mutual interference on one another.

In the paper by Morris (1954), friction factor equations which were derived for uniformly rough surfaces in conduits were found to be valid for surfaces with variable roughness if the roughness dimensions were averaged. Separate friction factor equations were derived for three distinct types of flow regime occurring in rough pipes and channels. Thus, if for a particular rough surface, more than one of the flow regimes were to be produced, then the friction factors calculated for each regime present could be added to give the apparent friction factor for the surface as a whole.

Perry and Joubert (1963) showed that the effect of roughness in the outer flow can be accounted for using an equivalent viscosity which is assumed to be dependent only on the variables at the wall, such as shear stress, fluid density, viscosity and the roughness size and geometry. Using a wind tunnel, flow measurements were taken over roughness elements consisting of timber strips. The work surface could be adjusted in the tunnel to produce various pressure gradients. The resulting velocity distributions were used, along with a modified graphical method, to determine the local boundary layer parameters for each of the flow regimes. The graphical method used in the analysis was primarily for hydrodynamically smooth surfaces in flows with and without pressure gradients. For rough surfaces the origin of z is not known and there is a shift in the logarithmic profile, hence in using the logarithmic line to accurately calculate C_f, only the slope of the line and not its position might be used. The logarithmic asymptote is assumed to be located at a distance ε below the roughness crests. Hence to use the position of the line in calculating C_f the value of ε must be estimated an error in the value of the z origin distorting the logarithmic line into a curve.

1.4.3 Frictional resistance considerations of surfaces treated as random processes

An attempt was made to treat the surface roughness as a random process (Nayak 1971) by Singh and Lumley (1971) who examined the problem of steady incompressible flow past a semi-infinite rough wall whose roughness was randomly distributed in a way which can be described. Assumptions were made in the analysis which linked the average size and extent of the roughness. The average slope of the roughness was assumed to be very much less than 1 and it was therefore expected that the additional mean velocity and pressure due to the roughness would be small compared with those corresponding to a smooth wall. The problem was then to calculate the contribution made by wall roughness in modifying the mean velocity profile in the laminar boundary layer. Calculations were made to find the roughness-induced velocity in terms of the spectral density of the roughness and an influence factor. It was concluded that flows over rough surfaces invariably become less stable, probably because in a wide spectrum of roughness there will always be some roughness wavelengths present which will make the shear layer unstable and increase the surface friction.

Monzavi (1972) investigated the relation between natural roughnesses and their frictional resistance. It had already been shown that characterising the surface roughness by the height of the roughness elements alone is insufficient to uniquely define a surface, therefore in this investigation nine roug surfaces were tested, flow measurements taken and the surfaces statistically evaluated. Experimentally determined frictional resistance values were correlated with possible hydromechanical significant statistical parameters of the surface geometry. From

the investigation three main statistical surface parameters seemed to correlate with surface frictional resistance values. These were:

(a) The Standard Deviation σ of the roughness heights, which gives a measure of the roughness intensity.

(b) The Half-Width Value γ_δ which is a measure of the mutual top distance of roughness elements in the flow direction.

(c) The absolute mean value of the surface slope, S_{abs}.

In two papers presented by Leukowicz and Musker at the 1978 International Symposium on ship viscous resistance at Goteborg the results from study of the effect of ship hull surfaces on fully developed pipe flows were presented. A replication technique was used which allowed cylindrical replicas of ship hull roughnesses to be tested in a pipe line with compressible fully developed turbulent air flow. The replicas form the internal surface of the pipe line. Dynamic similarity is used to achieve a comparison between the fully developed pipe flow and the inner regions of the turbulent boundary layer over a flat plate which is assumed to be equivalent to the flow over a ship surface. The flow analyses were correlated to statistical analyses of the respective surface roughness (Thomas 1975). It was noted that marine rough surfaces like engineering surfaces are unlikely to have a surface texture similar to Nikuradse's tightly packed 'equivalent' sand grain roughnesses (Nikuradse 1933). Engineering surfaces are generally random and have average slopes of a few degrees. Marine surfaces are more likely to have randomly positioned areas of different roughnesses with abrupt

changes in roughness caused by areas of paint breaking away from the substrate due to corrosion or attachment of marine creatures to the surface, producing relatively large average surface slopes.

Surface height parameters such as MAA were found to be incapable of producing a universal correlation between a surface roughness Reynolds number and frictional resistance.

Manning (1979) investigated the influence of surface roughness on the gas flow through cracks. Gas flow rates were measured through a number of idealised cracks whose surfaces were roughened by grit-blasting. Crack surfaces were used with roughnesses between 0.7 and 13 μm R_a, and with a number of different widths. The results were analysed in terms of friction-factor/Reynolds number plots. The power spectral density function was used in the analysis of the surface topography. The computer power spectrums showed the surfaces could be approximated to bandwidth-limited white noise.

1.4.4 Flow over curved surfaces

The work so far reviewed has been, in the main, limited to analysing the friction effect of the relatively short surface wavelengths. Since a considerable amount of work correlates the flow measurements over flat surfaces with the flow over the curved hull of a ship it is of considerable interest to investigate the effect of curved surfaces on fluid flow.

Meroney and Bradshaw (1975) investigated turbulent boundary layers over convex and concave surfaces. The experimental set-up consisted

of a curved test section with static pressure taps on both its concave and convex sides. The test section had a radius of curvature of 2.54 m on its convex side. The ratio of boundary layer thickness to radius of curvature (δ/R) was between 0.01 and 0.02.

The growth rate of the boundary layer along the convex surface decreased to about half of what would be expected for a corresponding flat surface and the surface friction decreased by about 10 per cent. For the concave surface there was an increase in the boundary layer growth with a corresponding increase in the surface friction. The concave surface produced significant lateral variations in all the observed flow parameters.

1.5 Roughness characterisation

1.5.1 Characterising surfaces comprising easily defined elements

In order to determine the roughness allowance which must be applied to data from model tests in order to make it possible to accurately predict the resistance of the ship, it is essential to have a means of characterising a rough surface.

From the classic work of Nikuradse (1933), whose rough surfaces were made of closely packed sand grains, a great deal of subsequent work was concerned with establishing an equivalent sand roughness for each surface considered, so that the resistance could be obtained from Nikuradse's results. Simple averages and root-mean-square (RMS) values of the roughness amplitude were used and interpreted in terms of equiv-

alent sand roughness. As the work progressed it became clear that many forms of roughness could not be defined satisfactorily by an equivalent sand roughness.

1.5.2 Characterising surfaces of non-uniform dimensions

In most practical cases, the roughness elements are of non-uniform size, so that the 'completely rough' regime obtained by Nikuradse in which the surface friction is independent of Reynolds number and dependent only on the relative roughness, is not valid. For example, Todd (1951) has shown that ship hulls are hardly ever 'completely rough' in this sense.

In attempting to characterise practical rough surfaces it became clear that a statistical description of the surface by centre line average (CLA) or RMS roughness amplitudes and other similar parameters was not adequate. For example, two surfaces could have the same CLA or RMS roughness amplitudes but have completely different textures and probably produce different amounts of frictional resistance to fluid flow over them (Eisenberg 1950). This need to have a more comprehensive method of surface characterisation was also true in the case of engineering surfaces (Peklenik 1968) where the interest is in the study of a number of interfacial phenomena such as friction and wear, and electrical and thermal contact resistance.

Returning to the problem of the frictional resistance of rough surface (Eisenberg 1950), on looking at simple cases of surfaces with the same average amplitude parameters (Figure A1-13) it is clear that

an additional parameter to correlate the surface with its frictional resistance is the slope or slope distribution.

Thus, an adequate description for the uniform two-dimensional roughness could be built up using the averages or frequency distributions of the amplitudes, slopes and curvatures (Posey 1946). In addition to the above geometrical properties, for rough surfaces in practice, it was thought necessary to specify the roughness distribution in the direction of motion and the traverse direction, and the roughness density in the direction of motion. It was also thought prudent, in these early stages of characterising surfaces, to look at the spectral distributions and correlations (as between the longitudinal and traverse distribution) of the above parameters,

1.5.3 Roughness measurement and analysis

To help in the characterisation of practical surfaces, a surface measuring instrument was developed in order to make it possible to produce chart recordings of surface profiles from the movement of a probe which follows the surface. The movement of the probe is fed through a linkage system to strain gauges. The resulting electrical signal is suitably processed and used to drive a pen in the recorder. The instrument was designed in order to be usable in situ on ships hulls (Todd 1951, Hama 1954).

A surface roughness measuring device was developed by the British Ship Research Association (BSRA) (Canham 1956) in order to enable them to take comprehensive roughness records of ship hulls. These records

could then be used alongside the ship trial data. The roughness measurements are made in dry dock shortly before, or immediately after trials and involve the recording of roughness profiles at a number of positions on the hull (Deer 1977).

A statistical analysis was used to examine the various factors affecting the trial performance and it was found, as expected, that the hull plate roughness was by far the most significant factor. The nature of the roughness varies in different parts of a hull (for example, paint drops tend to accumulate on the flat of the bottom) and alternatively, the same degree of roughness may well have different effects on resistance according to the position on the ship's hull.

A technical memorandum by Canham (1961) set out to give some guidance on the selection or recording positions and the number of records required to be taken with the BSRA wall roughness gauge in order to make a satisfactory hull roughness survey. A hull roughness survey is required to establish whether the surface of a hull has a roughness within predetermined limits, or to determine the average roughness of the hull surface, or to make an accurate assessment of the frictional resistance of the hull. The hull surface is divided into definite areas in each of which there is a significantly different type of surface roughness. It is therefore essential to survey as much as possible of the hull before deciding on the number of records and the location of the recording positions required. The number of records to be taken should increase with increasing average roughness and with increasing non-uniformity of the roughness, and should not be less than fifty for a 'reasonably concise' hull survey.

Roughness records were taken on a sample of 68 new ships (Lackenby 1962) and the resulting distribution of average roughness was found to approximate to a normal gaussian distribution with a mean roughness value of 0.0074 inch (18.8 μm) (Figure A1-14). Typical roughness tracers for these surfaces are shown in Figure A1-12.

In a subsequent BSRA report dealing with the various methods of analysing hull surface roughness records, Chaplin (1965) proposed that spectral analysis could be successfully used as a method of obtaining alternative roughness parameters to those currently in use. It was also shown that commonly used parameters such as the mean apparent amplitude and the centre line average could be deduced from the spectral analysis. The previously accepted method of analysis of hull surface roughness records had been to determine the mean apparent amplitude for a sample length of 2 inches. Statistical analysis of numerous ship trial and corresponding model test results indicated the existence of a significant relationship between frictional resistance parameters based on the mean apparent amplitude per 2 inch length of hull surface and the corresponding derived ship-model correlation factor. It was clear that alternative methods of analysing roughness records had to be considered in the hope of throwing more light on the relationship between surface roughness and ship resistance and in improving the ship-model correlation factors. The records obtained showed the profile to be nearly always random in nature (Nayak 1971) making it impossible to represent the profile by any simple mathematical function. Much the same sort of problem existed in the study of the sea surface and electrical 'noise', and this resulted in the development of the technique of spectral analysis to a high degree. Thus, Chaplin went on to represent the

profile by the sum of a large number of harmonic components in which the amplitudes and phase angles were random variables. These quantities could be estimated by suitable numerical techniques and an amplitude spectrum constructed.

Just as the energy spectrum can be used to resolve white light or a complex sound into a sum of pure colours or tones, so a roughness profile can be resolved into a series of component sine waves each with a definite frequency and contributing a definite proportion of the total variance in the profile.

Apart from providing a distribution of the amplitudes and frequencies of the component waves in the profile, several useful measures of roughness, including the mean apparent amplitude and centre line average, and other statistical properties can be derived from the spectrum.

FIG A1-1 SHIP RESISTANCE - RESULTS FROM WIND-TUNNEL TESTS AND TANK TESTS ON A 20 FT. LONG MODEL (Lackenby 1962)

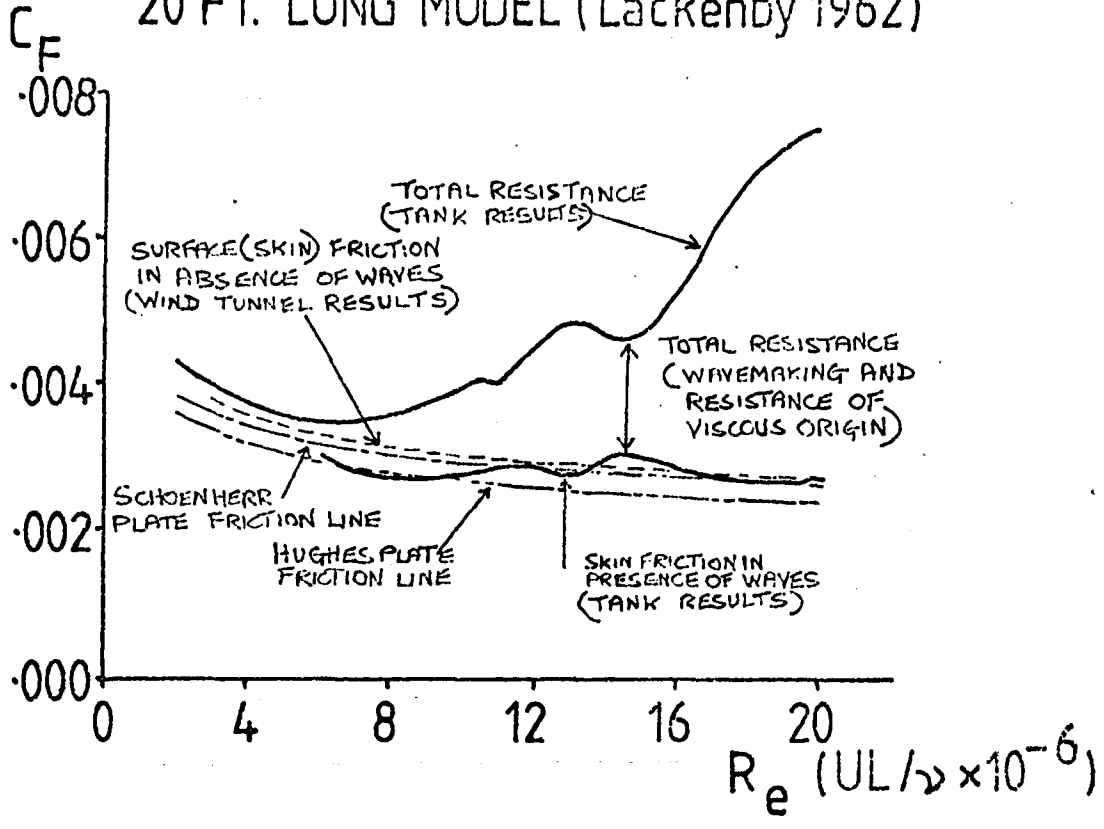

FIG A1-2 FROUDES RESULTS, FROM TOWING WOODEN BOARDS IN A TANK, ANALYSED ON A REYNOLDS NUMBER BASE (Lackenby 1962)

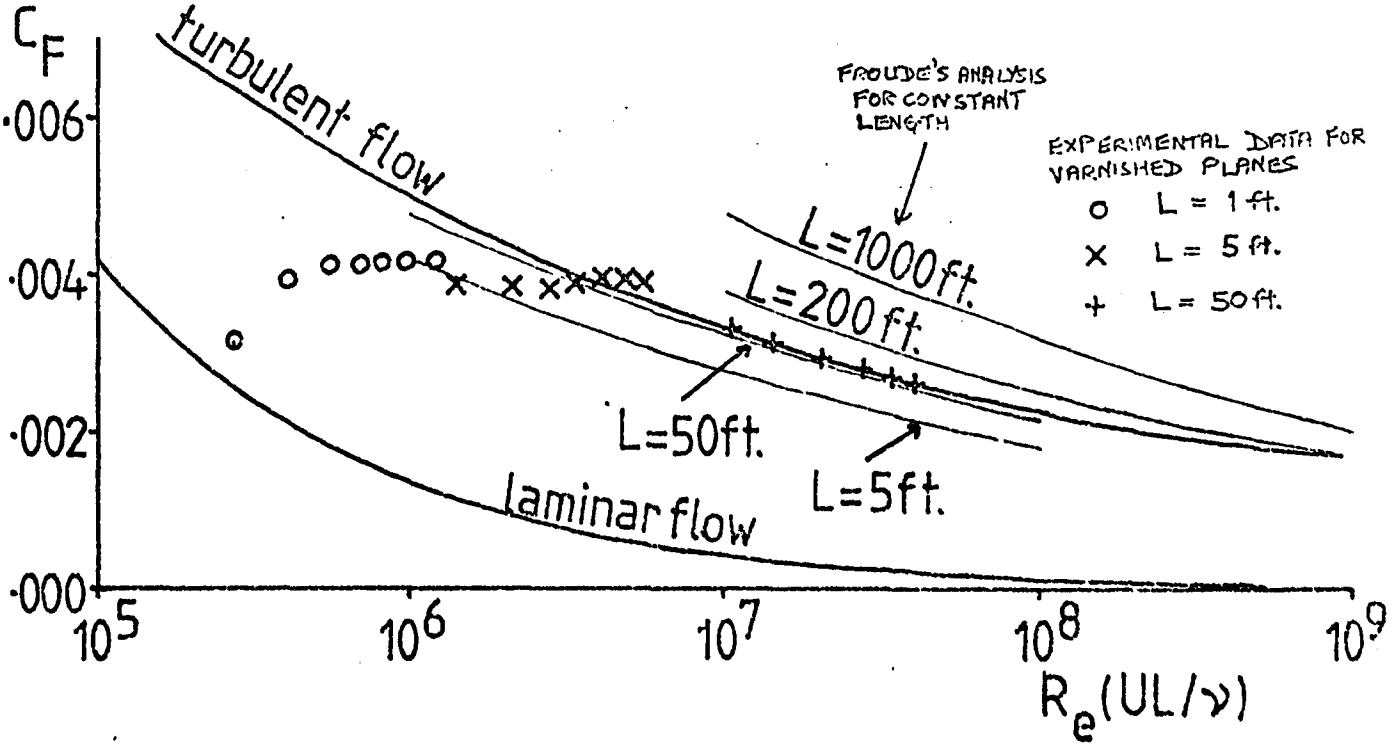

FIG A1-3 COMPILED EXPERIMENTAL DATA ON THE FRICTIONAL RESISTANCE OF PLANE SURFACES (Schoenherr 1932)

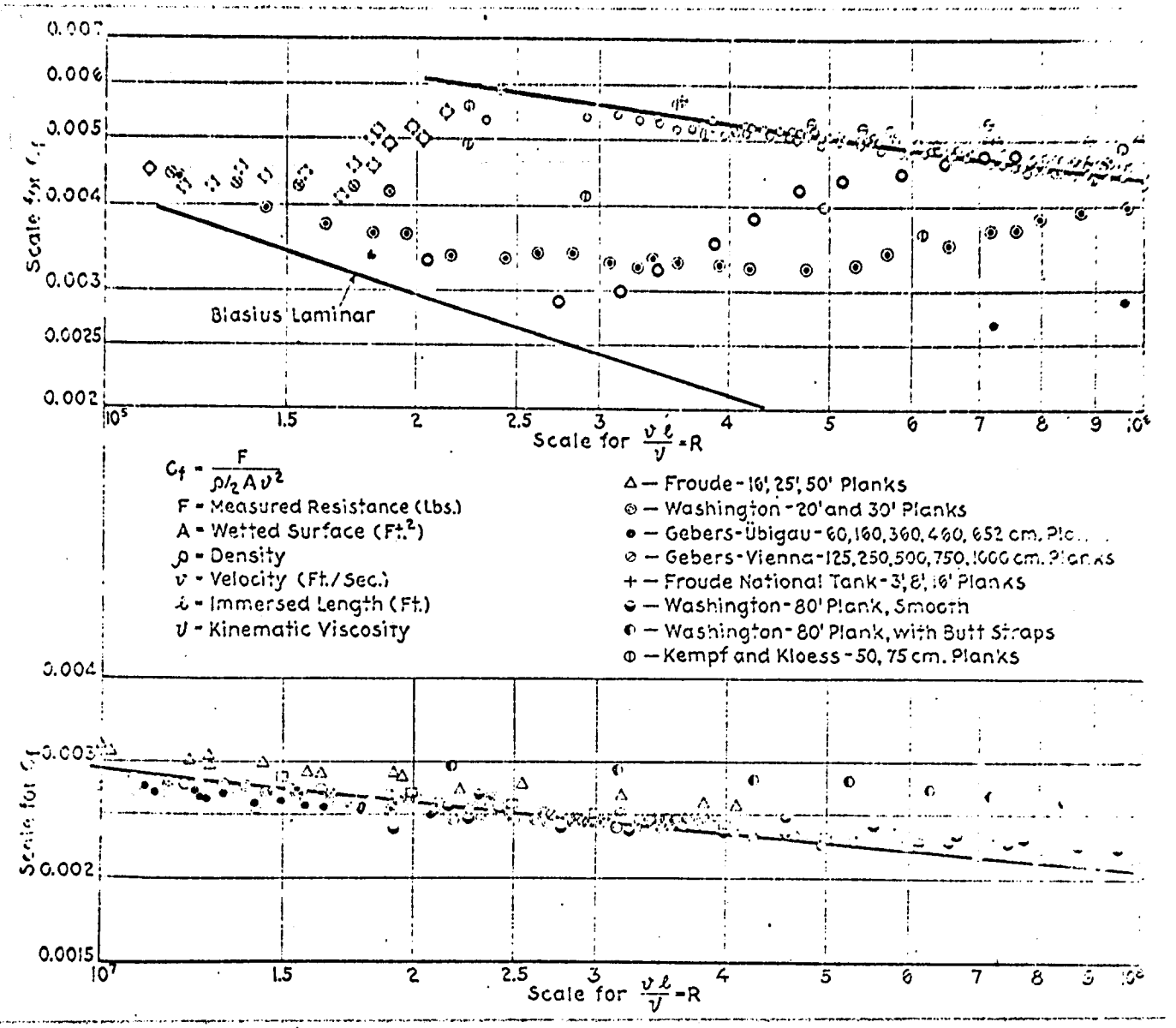

FIG A1-3 COMPILED EXPERIMENTAL DATA ON THE FRICTIONAL RESISTANCE OF PLANE SURFACES (Schoenherr 1932)

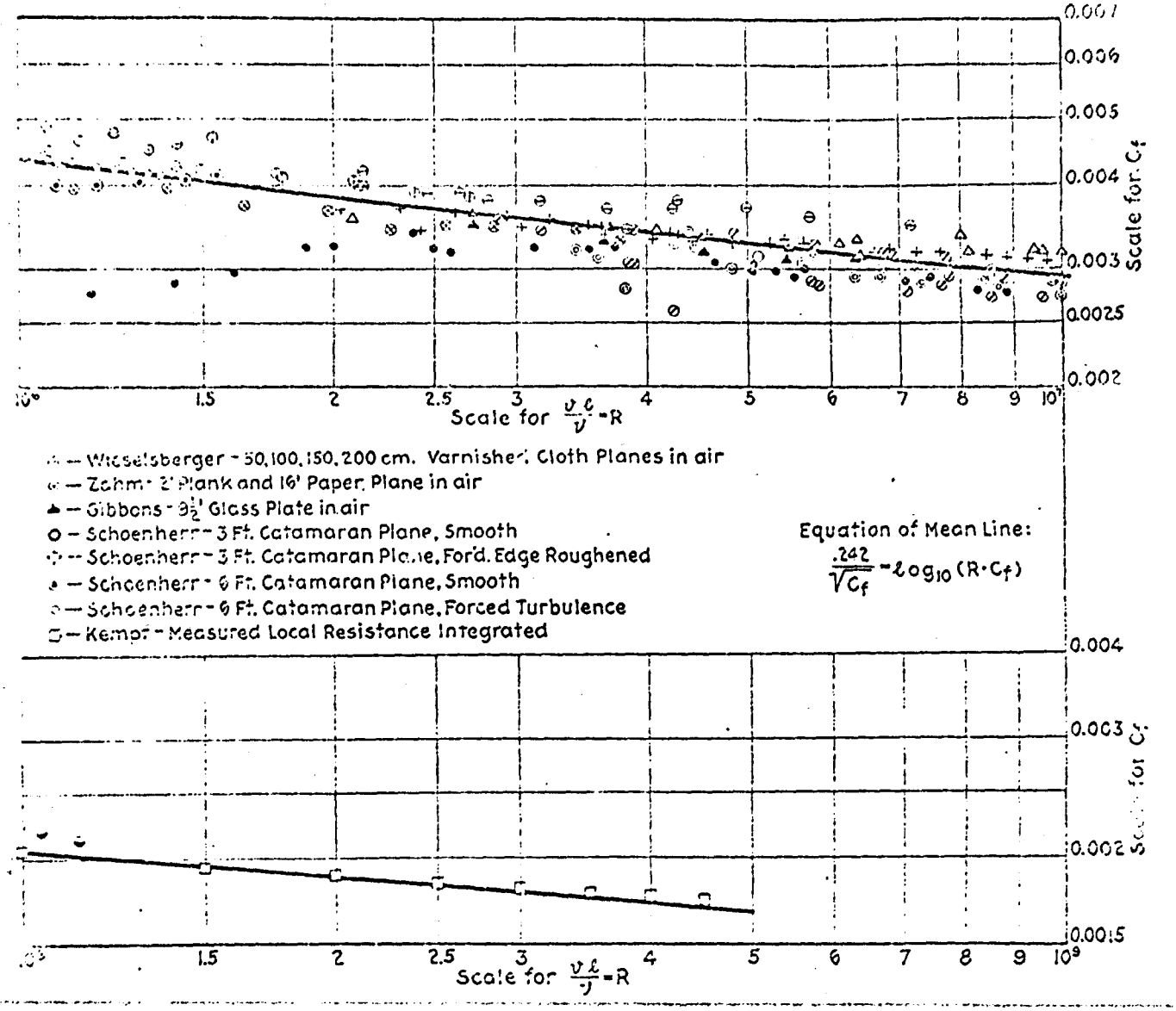

FIG A1-4 PLOT OF NEW AND OLD FRICTIONAL RESISTANCE DATA, PLOTTED TO A BASE OF LENGTH/BREADTH RATIO (Hughes 1952)

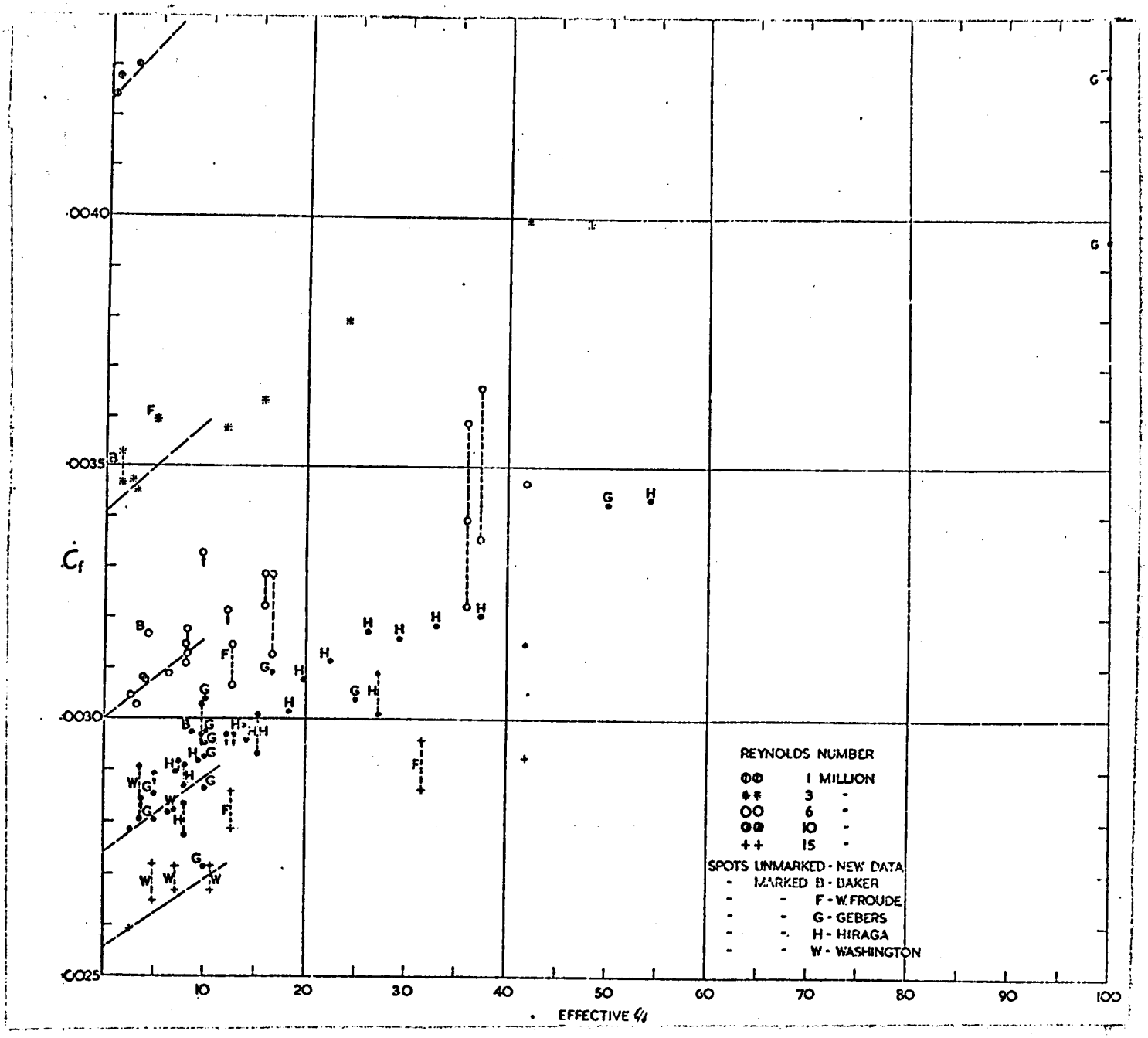

FIG A1-5 PLOT SHOWING THE EFFECT OF NON-FULLY TURBULENT FLOW ON THE FRICTION DATA FROM PLANE SURFACES (Hughes 1952)

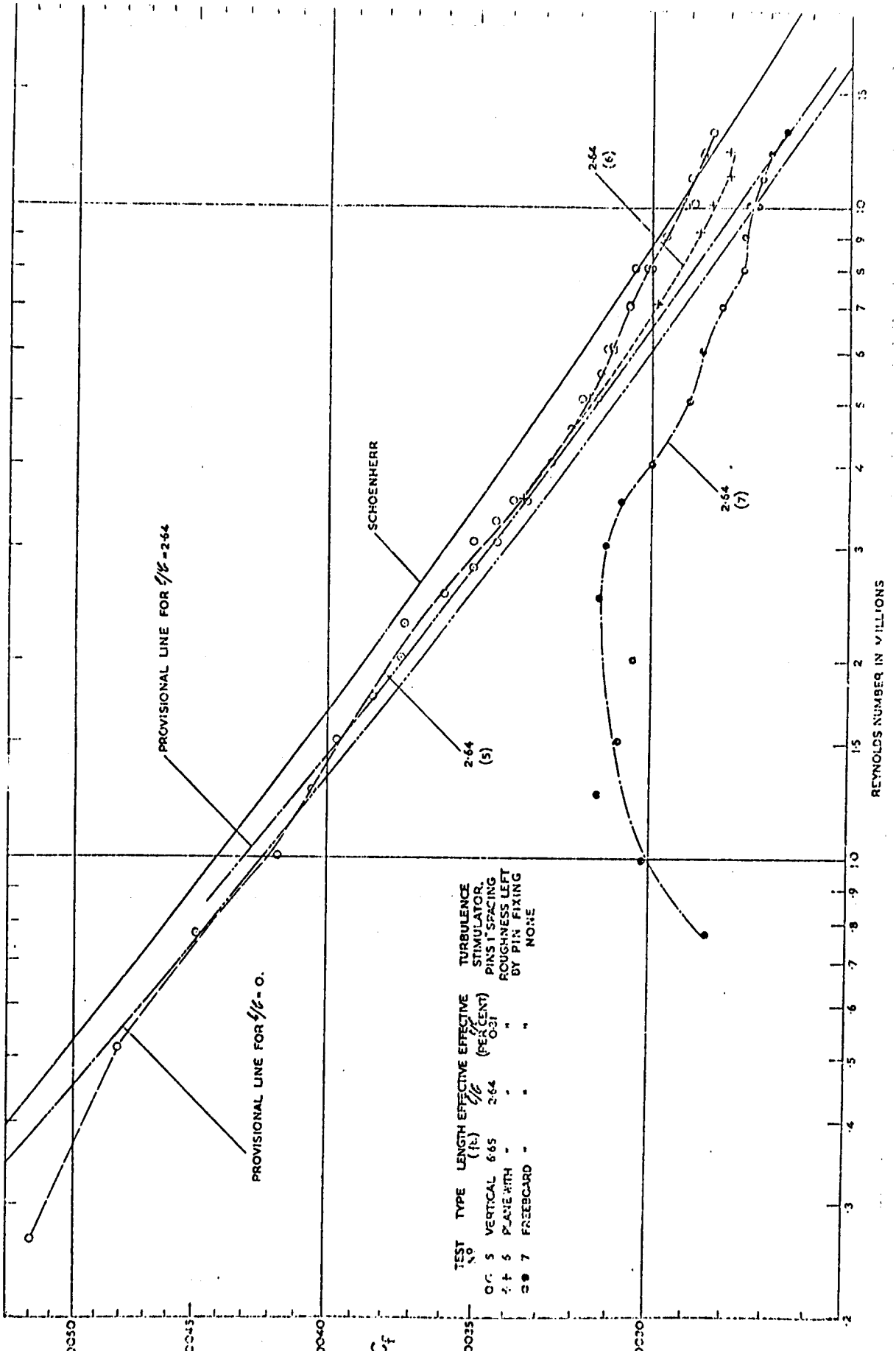

FIG A1-6 CURVES OF FRICTIONAL RESISTANCE COEFFICIENT (Lackenby 1962)

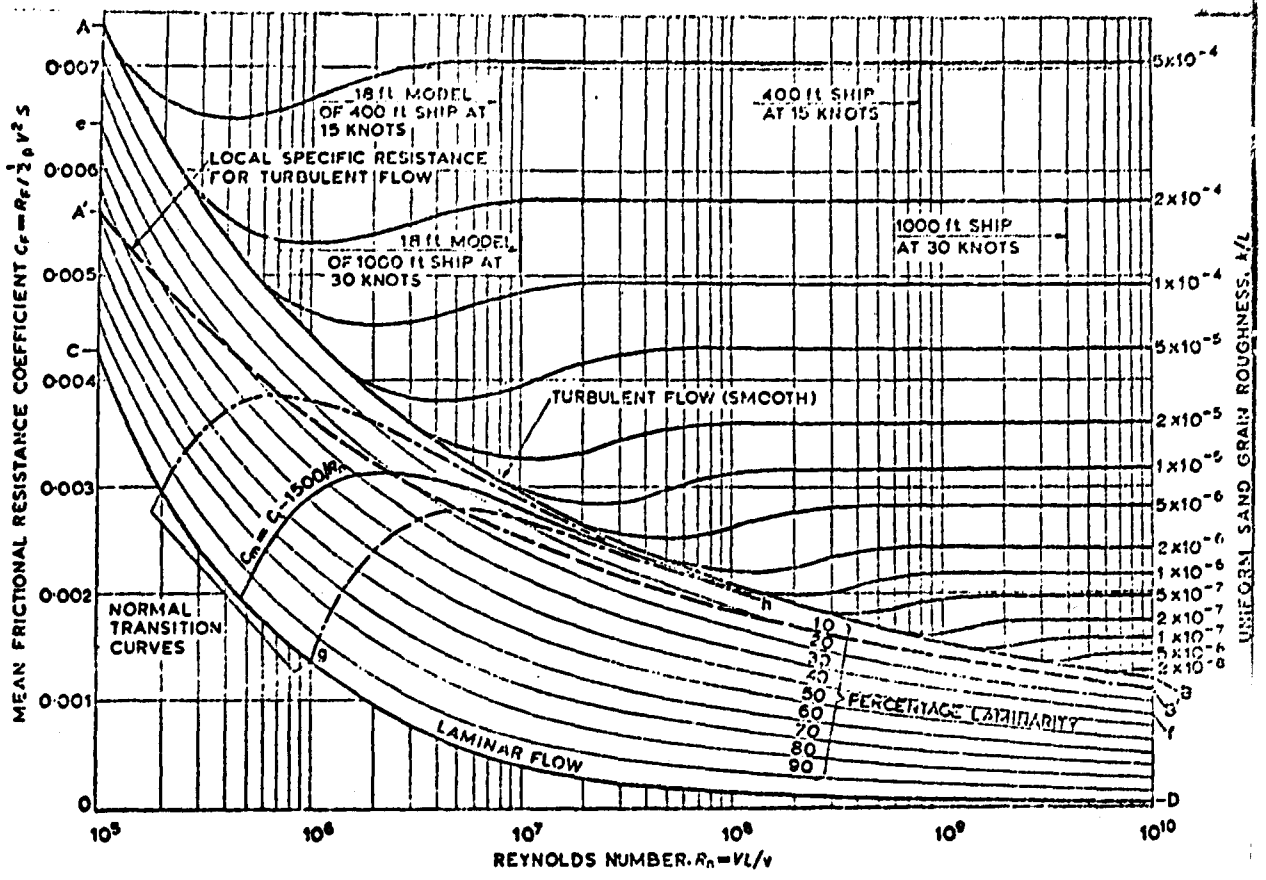

a Mean.

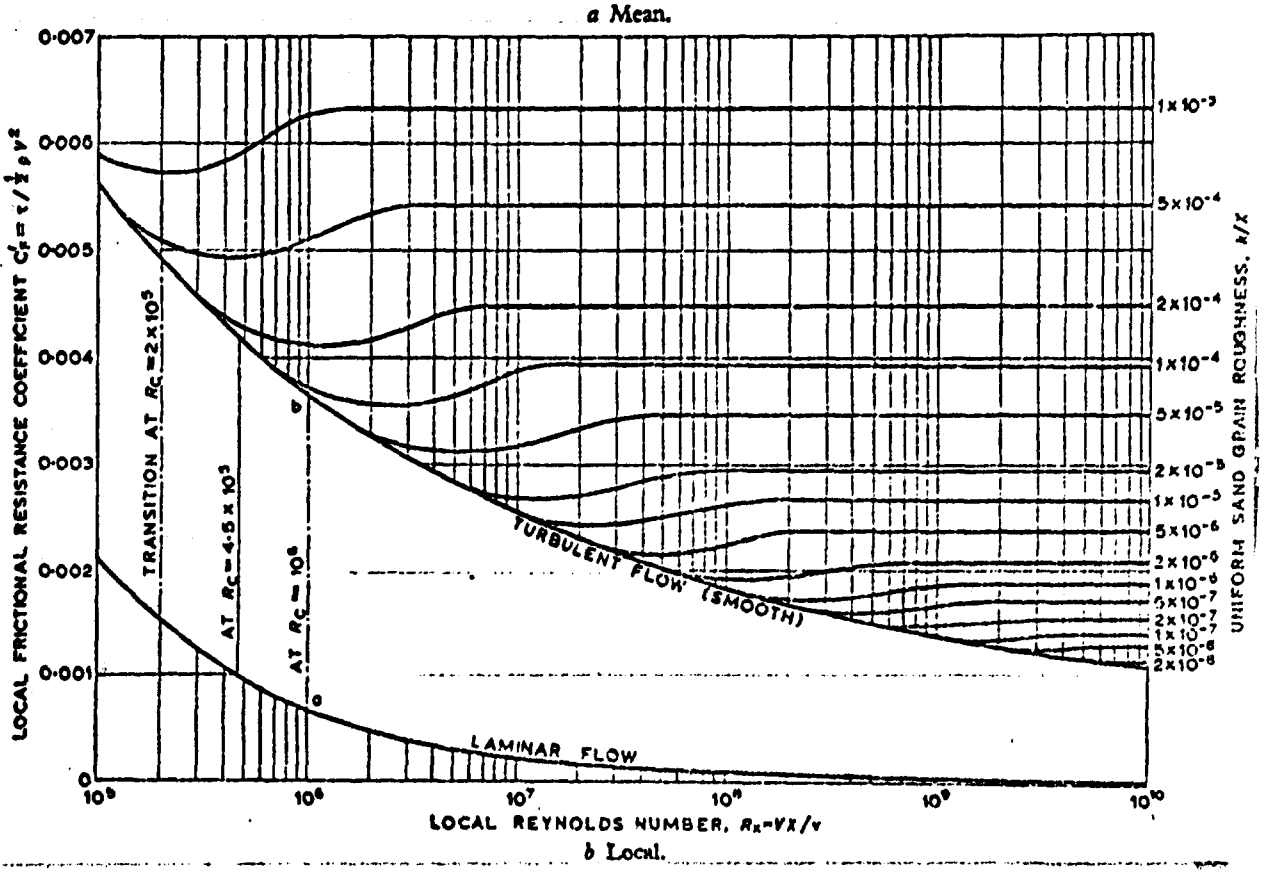

b Local.

FIG A1-7 CORRELATION OF SHIP AND MODEL RESULTS FOR LUCY ASHTON (Lackenby 1962)

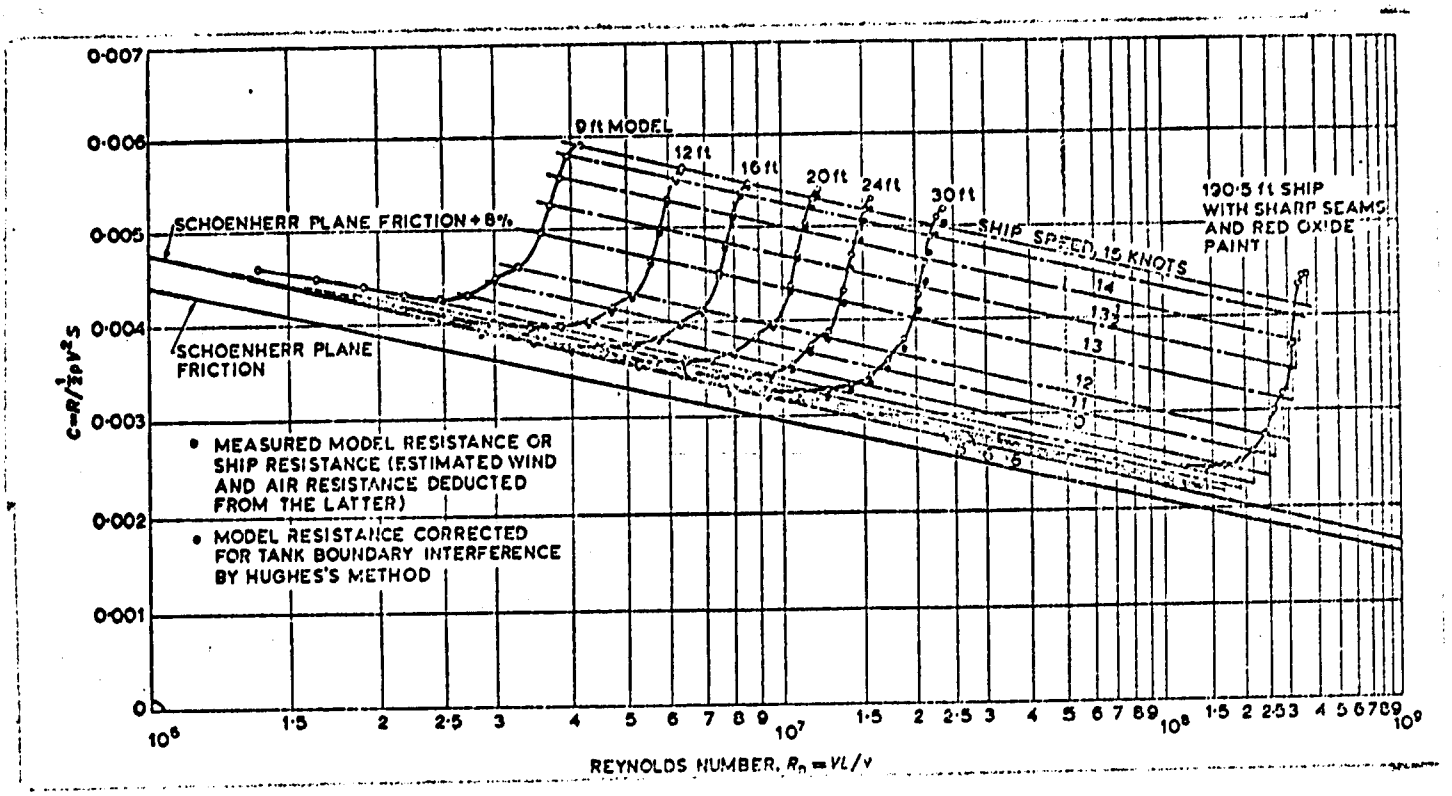

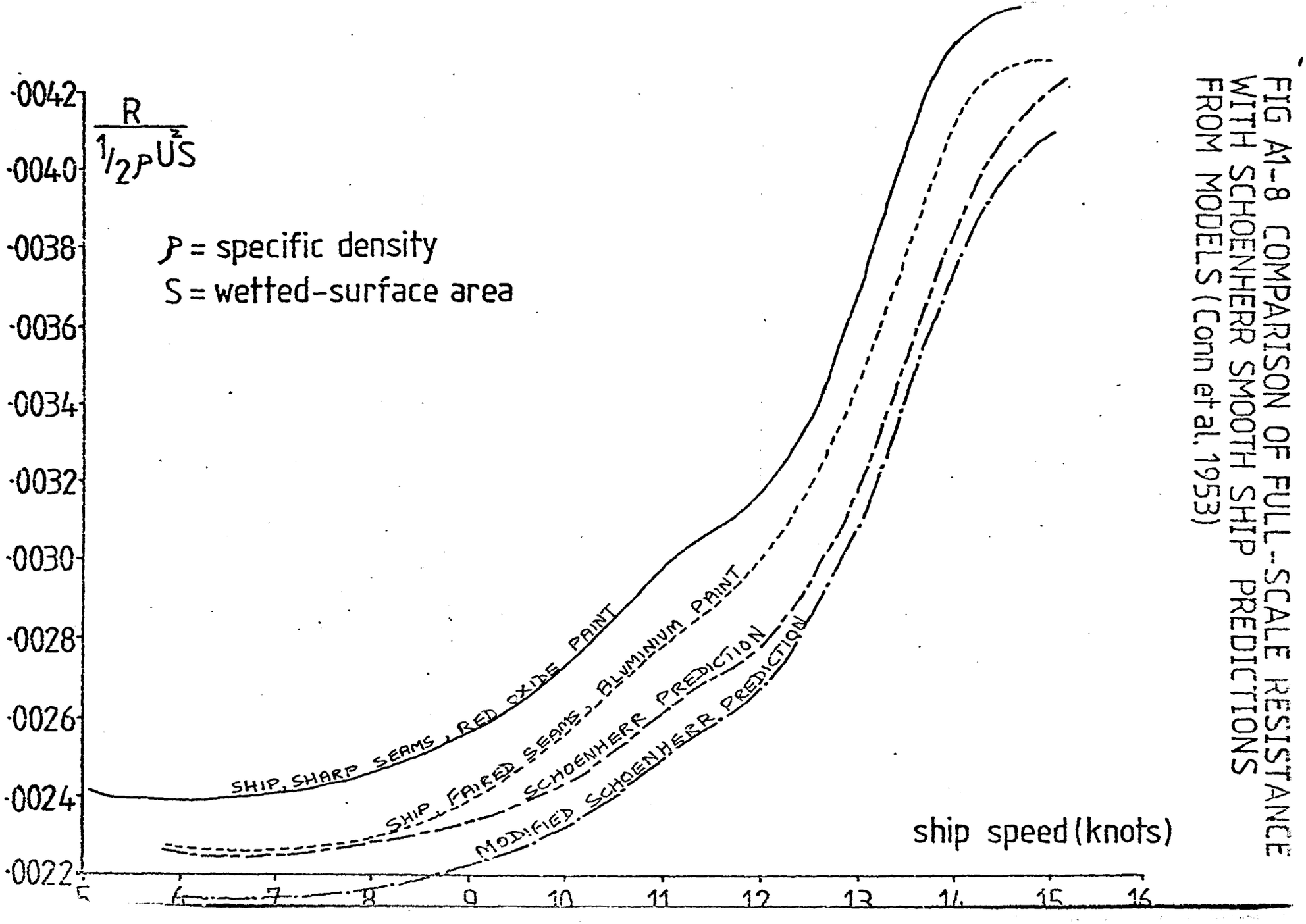

FIG A1-8 COMPARISON OF FULL-SCALE RESISTANCE WITH SCHOENHERR SMOOTH SHIP PREDICTIONS FROM MODELS (Conn et al. 1953)

FIG A1-9 LOSS IN PERFORMANCE WITH TIME IN SERVICE FOR THE CROSS-CHANNEL SHIP KONINGEN ELISABETH (Lackenby 1962)

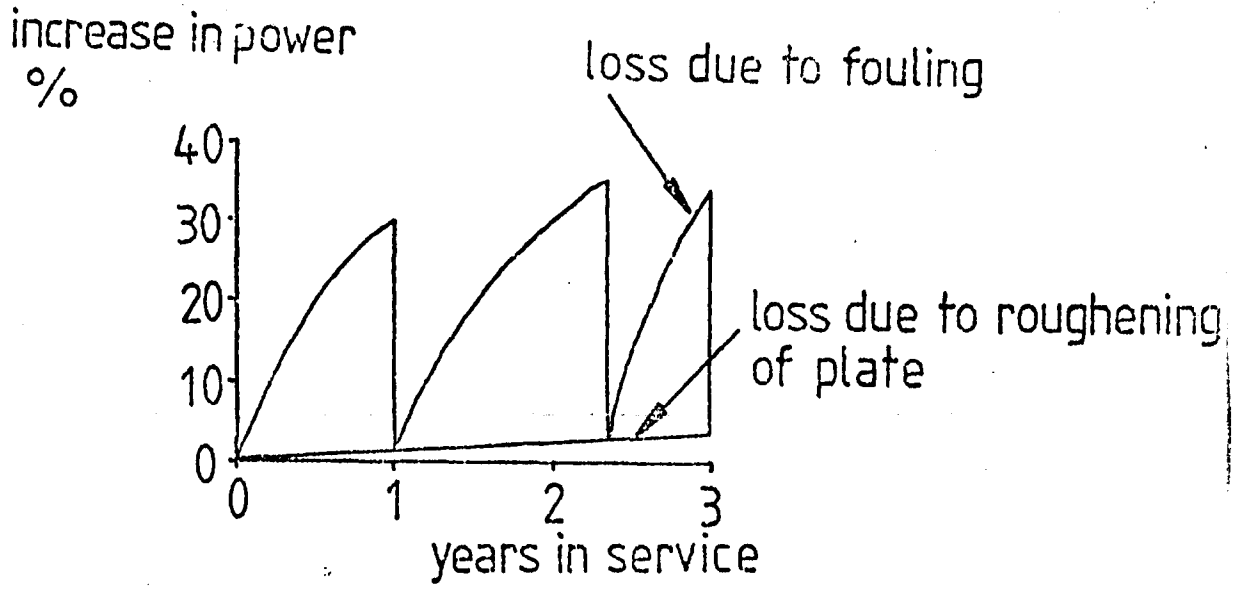

FIG A1-10 PERCENTAGE INCREASE IN TRIAL SHP OVER THE ORIGINAL TRIAL (Lackenby 1962)

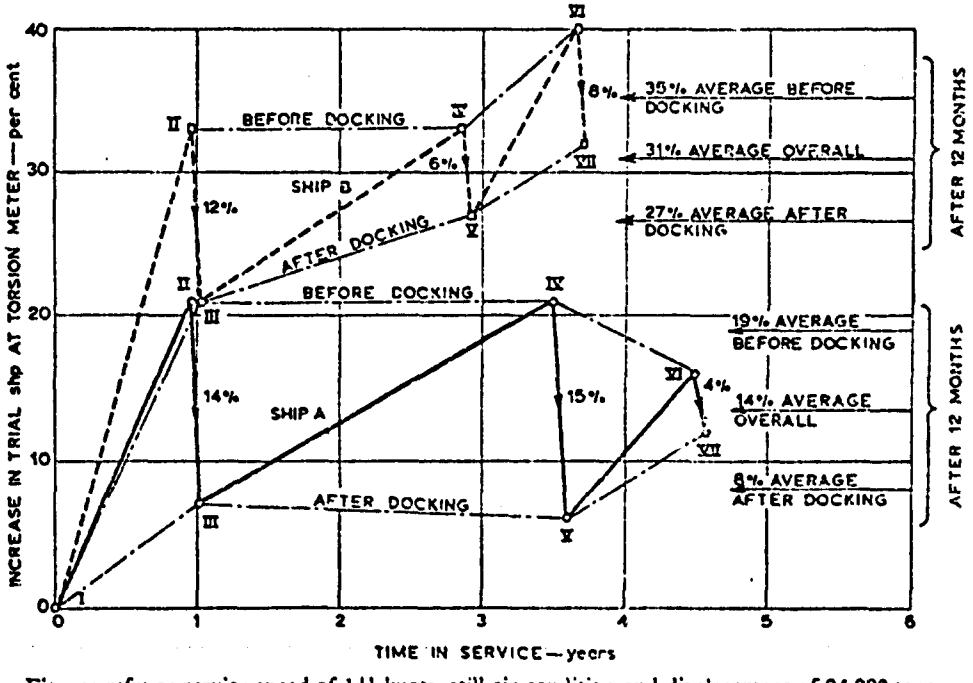

Figures refer to service speed of 14½ knots, still air condition and displacement of 24 282 tons.

FIG A1-11 PERFORMANCE OF 18 000-TON DEADWEIGHT TANKERS. VARIATION IN TRIAL SHP WITH HULL ROUGHNESS (Lackenby 1962)

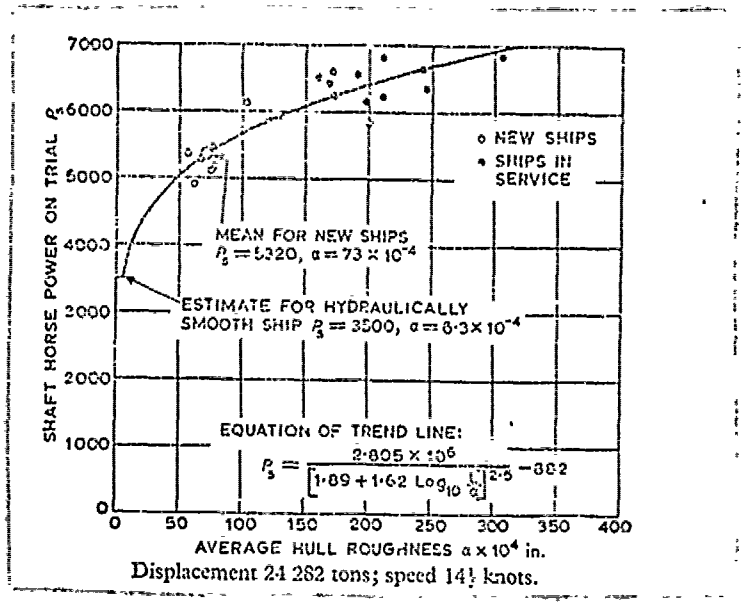

Displacement 24 282 tons; speed 14½ knots.

FIG A1-12 SURFACES WITH GEOMETRIES WHICH CANNOT BE DEFINED BY AMPLITUDE PARAMETERS ALONE (Eisenberg 1950)

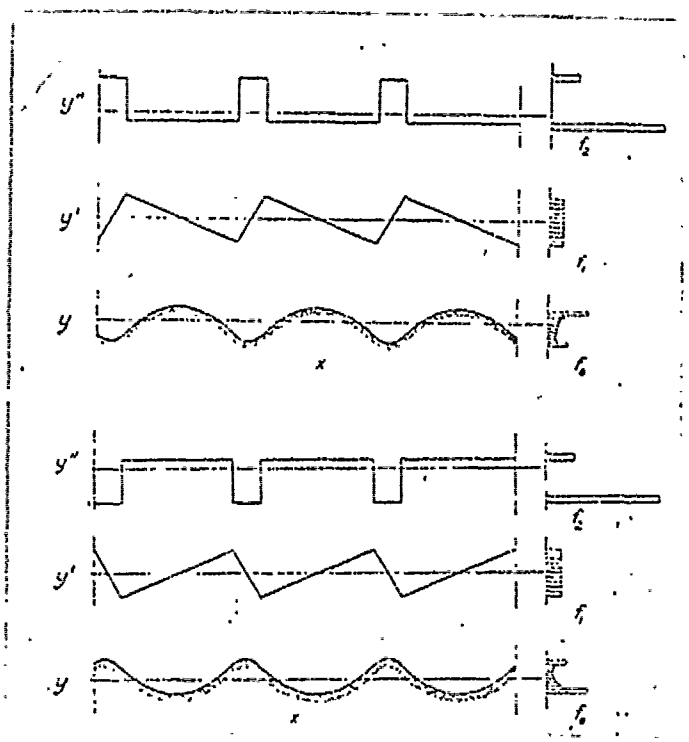

FIG A1-13 DISTRIBUTION OF HULL ROUGHNESS AMONG CLEAN NEW SHIPS (Lackenby 1962)

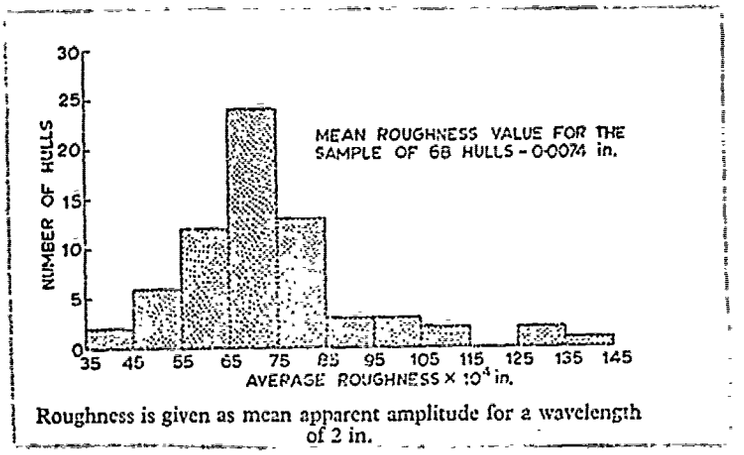

Roughness is given as mean apparent amplitude for a wavelength of 2 in.

FIG A1-14 TYPICAL RECORDS OF HULL ROUGHNESS (Lackenby 1962)

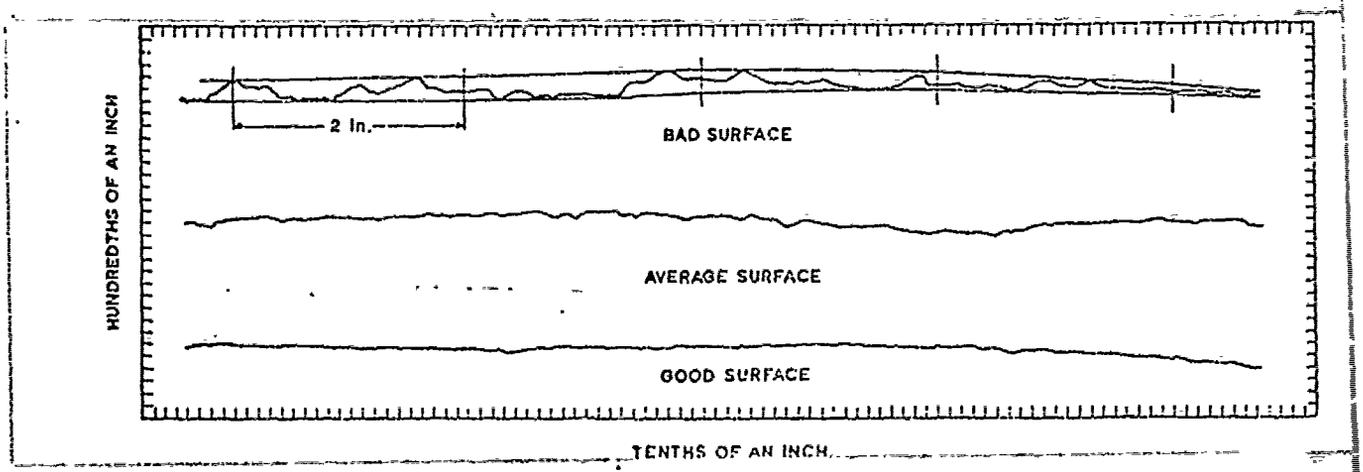

APPENDIX 2: FLUID THEORY

2.1 Introduction

In analysing the effect of surface roughness on the surface frictional resistance coefficient C_f, a number of fundamental relations are available to predict the motion of a fluid flowing over a solid surface. In fact the fundamental equations of viscous flow have been known for more than a hundred years. At low Reynolds numbers (laminar flow) the equations are very difficult to solve, even on digital computers, and at high Reynolds numbers (turbulent flow) the equations are, at present, unsolvable because of the random nature of flow fluctuations, in particular the boundary conditions.

Although the exact solutions to the fundamental equations of compressible viscous flow cannot be obtained, a great deal of useful information can be released from simplified solvable forms of these exact equations. A pioneer in this field was Prandtl, who using the boundary layer concept, which stated that the viscous effects are confined to a very thin layer near the solid surface, gave approximate solutions of the three laws of conservation for the case of two-dimensional flow over a plane surface.

2.2 The three laws of conservation

The number of viscous flow equations used is generally reduced to the three laws of conservation:

(1) Conservation of mass (continuity).

(2) Conservation of momentum (Newton's second law).

(3) Conservation of energy (first law of thermodynamics).

The exact number of basic flow equations depends on personal preference, some relations being more basic than others. Truitt, for example, used nine basic equations relating to nine unknowns (White 1974). In the present investigation the flow is assumed to be incompressible and isothermal, hence the three laws of conservation, for fluid flow, reduce to:

(1) The equation of continuity, which in its commonest form is given by:

$$\frac{D\rho}{Dt} + \rho \text{div } V = 0 \quad \text{or} \quad \frac{d\rho}{dt} + \text{div } \rho V = 0 \tag{2-1}$$

where V is the three-dimensional velocity vector, $V = iu + jv + kw$ and $\text{div } V = \frac{du}{dx} + \frac{dv}{dy} + \frac{dw}{dz}$

If the density, ρ, is constant (incompressible flow) the equation of continuity reduces to

$$\text{div } V = 0 \tag{2-2}$$

(2) The conservation of Momentum equation, commonly known as Newton's second law, is given by

$$\rho \frac{DV}{Dt} = \rho g + \nabla . \tau_{ij} \tag{2-3}$$

where g = gravitational acceleration and $\nabla.\tau_{ij} = d\tau_{ij}/dx_j$

∇ is the gradient operator, τ_{ij} is the stress tensor, which for a Newtonian viscous fluid is given by the general deformation law

$$\tau_{ij} = -p\delta_{ij} + \mu\left(\frac{du_i}{dx_j} + \frac{du_j}{dx_i}\right) + \delta_{ij}C_{bv}\ \text{div}\ V \qquad (2\text{-}4)$$

where λ is called the coefficient of bulk viscosity. Thus, the momentum equation for viscous Newtonian flow is obtained by substituting the general deformation law (equation 2-4) into Newton's second law (equation 2-3). The resulting equation of motion originally given by Navier and Stokes can be written as

$$\rho\frac{DV}{Dt} = \rho g - \nabla p + \frac{d}{dx_j}\left|\mu\left(\frac{dv_i}{dx_j} + \frac{dv_i}{dx_i}\right) + \delta_{ij}C_{bv}\ \text{div}\ V\right| \qquad (2\text{-}5)$$

For incompressible flow, the density is constant and div V vanishes from the Continuity equation (2-2) and the coefficient C_{bv} vanishes from Newton's law. Also assuming that viscosity is constant, the Navier-Stokes equations can be considerably simplified to

$$\rho\frac{DV}{Dt} = \rho g - \nabla p + \mu\nabla^2 V \qquad (2\text{-}6)$$

Summarising, the two laws of conservation of mass and momentum, as used for fluid motion are

$$\frac{d\rho}{dt} + \text{div}\ \rho V = 0 \qquad (2\text{-}1)$$

$$\rho\frac{DV}{Dt} = \rho g + \nabla.\tau_{ij} - \nabla p \qquad (2\text{-}3)$$

where for Newtonian fluid, the viscous stresses are

$$\tau'_{ij} = \mu \left(\frac{du_i}{dx_j} + \frac{du_j}{dx_i} \right) + \delta_{ij} C_{bv} \text{ div } V \qquad (2\text{-}4)$$

Equations 2-1 and 2-3 involve four variables, of which p and V are assumed primary, and the remaining two variables are assumed known from auxiliary relations and data of the form:

$$\rho = \rho(p, T) \; ; \quad \mu = \mu(p, T)$$

2.3 Approximate solutions of the laws of conservation using the boundary layer hypothesis

As can be seen, the equations to be solved are a formidable set of non-linear partial differentials equations. No method of solving these equations for an arbitary viscous flow problem exists, although digital computer numerical techniques using finite-difference approximations show considerable promise. Thus, approximate solutions are obtained using generalised forms of the exact equations.

Several exact solutions have been obtained for specific types of Newtonian viscous flow (White 1974). The high Reynolds number flows considered are explainable using a boundary layer hypothesis. The boundary layer theory states that the viscous effects are confined to relatively thin layers adjacent to solid boundaries. In the remaining region away from the wall the influence of viscosity is assumed to be unimportant and the flow is frictionless and potential. Hence Prandtl (1904) simplified the Navier-Stokes equations to provide approximate solutions for two dimensional incompressible boundary layer flow on a plate.

Thus, the boundary layer equations, in dimensional form, for steady isothermal two-dimensional incompressible flow are

$$\frac{du}{dx} + \frac{dv}{dz} = 0 \qquad (2\text{-}7)$$

$$\frac{du}{dt} + \frac{udu}{dx} + \frac{vdu}{dz} = \left(\frac{dU}{dt} + \frac{dU}{dx} \right) + \frac{\nu d^2 u}{dz^2} \qquad (2\text{-}8)$$

These are numerically solvable, for practically any distribution of free stream velocity. The solution of the boundary layer equations involves a great deal of labour, and so the introduction of digital computer techniques lightened the burden in this respect. A number of finite-difference solutions are available using both explicit and implicit methods. The methods involve examining the flow at the different stations in the x-direction. The explicit methods (Gortler 1939) have the advantage of simplicity but give inconsistent results unless small steps Δx are used, usually meaning excessive computation time. The implicit methods (Smith & Clutter 1963) are relatively complicated but give more stable results.

2.4 Integral forms of the basic boundary layer equations for laminar isothermal two-dimensional incompressible flow

Turning our attention to more approximate, rapid and simpler techniques we consider the integral equations of the boundary layer. The basic boundary layer equations:

$$\text{Continuity} - \frac{du}{dx} + \frac{dv}{dz} = 0 \qquad (2\text{-}9)$$

$$\text{Momentum} - \frac{du}{dt} + \frac{udu}{dx} + \frac{vdu}{dz} = \left(\frac{dU}{dt} + \frac{UdU}{dx} \right) + \frac{1}{\rho} \frac{d\tau}{dz} \qquad (2\text{-}10)$$

where buoyant forces are neglected. τ is used for the shear stress, and hence the equations are valid for both laminar and turbulent boundary layers. For laminar boundary layers,

$$\tau_\omega = \mu \frac{du}{dz}$$

Thus to compute the values of total momentum etc. over the boundary layer, they are integrated from $z = 0$ to $z = \infty$, using the boundary conditions and the continuity relation.

The momentum integral relation is obtained by multiplying the continuity equation by $(u - U)$ and subtracting from the momentum equation. The resulting equation is integrated from $z = 0$ to $z = \infty$, and are seen to vanish at infinity, for the boundary layer approximation.

Hence

$$\frac{\tau_\omega}{\rho} = \frac{d}{dt} \int_0^\infty (U - u)\,dz + \frac{d}{dx} \int_0^\infty u(U - u)\,dz + \frac{dU}{dx} \int_0^\infty (U - u)\,dz - U.v_\omega$$

where $v_\omega(x)$ allows for instabilities in the flow and for the possibility of a porous wall.

The integrals $(U - u)$ and $u(U - u)$ are equivalent to the displacement and momentum thicknesses δ_1 and θ respectively where

$$\delta_1 = \int_0^{z \to \infty} \frac{1}{U} (U - u)\,dz \qquad (2\text{-}12)$$

$$\theta = \int_0^{z \to \infty} \frac{u}{U^2} (U - u)\,dz \qquad (2\text{-}13)$$

Hence the momentum relation can be reduced to

$$\frac{C_f}{2} = \frac{d\theta}{dx} + (2 + H)\frac{\theta}{U}\frac{dU}{dx} \qquad (2\text{-}14)$$

for the case of steady flow over an impermeable wall.

The H or shape factor is always greater than unity (Figure A2-1), and for laminar flows varies from a value of about 2 at the stagnation point to about 3.5 at separation. In turbulent flow, the variation is between about 1.3 to 2.5.

Continuing with the derivation of the integral relations, the mechanical-energy integral formed by multiplying continuity by $u^2 - U^2$ and momentum by 2u, subtract, and integrate as before to get

$$\frac{2}{\rho}\int_0^\infty \tau\frac{du}{dz}\,dz = \frac{d}{dt}\int_0^\infty u(U - u)\,dz + U^2\frac{d}{dt}\int_0^\infty (1 + \frac{u}{U})\,dz \qquad (2\text{-}15)$$

$$+ \frac{d}{dx}\int_0^\infty u(U^2 - u^2)\,dz - U^2 v_\omega$$

which can be reduced to

$$C_D = \frac{2D}{\rho U^3} = \frac{1}{U}\frac{d}{dt}(\theta + \delta_1) + \frac{2\theta}{U^2}\frac{dU}{dt} + \frac{1}{U^3}\frac{d}{dx}(U^3\delta_3) - \frac{v_\omega}{U} \qquad (2\text{-}16)$$

where D is the shear dissipation term, $D = \int_0^\infty \tau\frac{du}{dz}\,dz$ (2-17), δ_3 is the kinetic energy thickness or dissipation thickness, $\delta_3 = \int_0^\infty \frac{u}{U}(1 - \frac{u^2}{U^2})\,dz$ (2-18) and C_D is the energy dissipation coefficient.

Thus, equations 2-11 and 2-16 are the basic integral relations for isothermal laminar two-dimensional incompressible flow.

2.5 Turbulent boundary layer equations

Laminar flow is inherently unstable and above a critical .olds number there is an abrupt change to turbulent flow. Turbulence is an experimentally observed phenomenon and there is no existing theory which states that turbulent flow should occur at high Reynolds numbers. The transition process can be made to occur earlier by the introduction of an obstruction or obstructions at the wall such as roughness elements, causing additional disturbances in the boundary layer, which distort the velocity profile and lower the critical Reynolds number. The transition can also be affected by pressure gradients, wall cooling, or free stream turbulence. Thus, for the majority of cases of low-viscosity fluids (water, mercury, gases ....) the flow is normally turbulent, not laminar.

Using the assumption that fluid is in a randomly unsteady turbulent state the time-averaged or mean equations of motion can be used to approximate the flow. Thus

$$\frac{d\bar{u}}{dx} + \frac{d\bar{v}}{dy} + \frac{d\bar{\omega}}{dz} = 0 \qquad (2\text{-}19)$$

$$\rho\frac{D\bar{V}}{Dt} + \rho\frac{d}{dx_j}\left(\overline{u'_i\, u'_j}\right) = \rho g - \nabla\bar{p} + \mu\nabla^2\bar{V} \qquad (2\text{-}20)$$

where the turbulent inertia term $\overline{u'_i\, u'_j}$ is dependent on not only the physical fluid properties but also on local flow conditions (velocity, geometry, surface roughness, and upstream history).

Thus, the time-averaging process has introduced nine variables for which there is no available means of defining their values. On assuming that the turbulent inertia terms can be looked upon as stress terms the mean momentum equation simplifies to

$$\rho\frac{D\bar{V}}{Dt} = \rho g - \nabla\bar{p} + \nabla.\tau_{ij} \qquad (2\text{-}21)$$

(White 1974) where $\tau_{ij} = \mu\left(\frac{du_i}{dx_j} + \frac{du_j}{dx_i}\right) - \overline{u'_i\, u'_j}$

The turbulent shear $-\rho\overline{u'v'}$ is the dominant term in any attempt to resolve the momentum equation in the boundary layer. In attempting to resolve the turbulent flow momentum equation it is far simpler initially to look at the case of two-dimensional boundary layers. One method of resolving the term $-\rho\overline{u'v'}$ is to assume the term to be a function of local geometry and flow conditions, whilst another is to look at the local velocity profile itself.

Using the first of these approaches, Prandtl (1926) related the turbulent shear to the local mean fluctuations using an eddy-transport theorem based on the much smaller scale kinetic theory molecular transport model. The local RMS fluctuations were related to the local velocity gradient through a turbulent length scale ℓ,

$$\sqrt{\overline{u'^2}} \propto \ell_1 \frac{d\bar{u}}{dz} \qquad (2\text{-}22)$$

$$\sqrt{\overline{v'^2}} \propto \ell_2 \frac{d\bar{u}}{dz} \qquad (2\text{-}23)$$

where ℓ_1 and ℓ_2, called the mixing lengths, are analogous to the mol-

ecular mean free path. Prandtl's mixing-length model can then be written as

$$\tau_t = \mu_t \frac{d\bar{u}}{dz} \quad \text{where} \quad \mu_t = \rho \ell^2 \left| \frac{d\bar{u}}{dz} \right| \tag{2-24}$$

Other approaches included the introduction of an eddy viscosity ε_1 by setting $-\overline{u'v'} = \varepsilon_1 \, d\bar{u}/dz$ or by utilising the process by which the boundary layer acquires additional turbulent fluid, entrainment (Proc. comput. of Turb. Boundary Layers 1968).

2.6 The general form of the boundary layer velocity distribution

The velocity profile across the boundary layer can be split into three regions: The region next to the wall where viscous shear dominates, and an overlap region where both types of shear are present. Relationships have been put forward to predict the shape of the profile in these regions.

Prandtl in 1933 deduced that in the inner region the mean velocity depends upon the wall shear stress, the fluid properties, and the distance z from the wall: Thus the law of the wall is of the form

$$\frac{\bar{u}}{u_\tau} = f\left(\frac{z u_\tau}{\nu} \right) \tag{2-25}$$

For the outer region, Karman in 1930 deduced that the wall acts only to retard the flow, reducing the local velocity u below the free stream value U_∞ independently of viscosity but dependent upon the wall shear stress and the distance z over which the flow is affected.

Thus, the outer, or velocity defect law is given by

$$(U_\infty - \bar{u})/u_\tau = g(z/\delta) \qquad (2\text{-}26)$$

For the overlap region, the two functions are merged together over some finite region between the inner and outer (Millikan 1938). Overlap law:

$$\frac{\bar{u}}{u_\tau} = f\left(\left(\frac{\delta u_\tau}{\nu}\right)\left(\frac{z}{\delta}\right)\right) = \frac{U_\infty}{u_\tau} - g\left(\frac{z}{\delta}\right) \qquad (2\text{-}27)$$

For the inner part of the overlap region the relation is given by

$$\frac{\bar{u}}{u_\tau} = \frac{1}{\kappa}\log_e\left(\frac{zu_\tau}{\nu}\right) + B$$

and for the outer part

$$\frac{U_\infty - \bar{u}}{u_\tau} = -\frac{1}{\kappa}\log_e\left(\frac{z}{\delta}\right) + A$$

where κ is Von Karman's constant and A and B are constants.

For the inner region, the form of the law of the wall can be solved by assuming that the total shear is constant very near the wall and that the eddy viscosity follows a cubic relation near the wall and an exponential relation further out (Spalding 1961) to produce a formula for the inner law which was found to be equally valid in the logarithmic overlap region (Figute A2-2).

2.7 The effect of pressure gradients and surface roughness on the boundary layer

Although all the profiles for the inner law collapse onto a universal curve (Figure A2-3) it can be seen that at the top end of the curve i.e. in the overlap region, there are increasing deviations from the predicted curve. Thus the outer law is much more sensitive to external influences, such as pressure gradients. The addition of a parameter involving pressure gradient to the outer law was first attempted by Clauser (1954, 1956).

The work previously done on the problem of the turbulent boundary layer had, in the main, been directed towards looking at the simplest of cases, such as flow over a smooth surface with zero pressure gradient. Only a few empirical methods existed for predicting the effect of pressure gradients on turbulent boundary layers and these were unreliable, doing little more than to correlate the set of data on which they were based originally.

For some time it had been realised that the state of the turbulent boundary layer depended not only upon the local environment such as the local values of pressure gradient, the wall shear, the surface roughness, the boundary layer thickness, etc, but also upon the previous history of the layer. Thus, when Clauser (1954) carried out his research on the turbulent boundary layer he began by attempting to study in detail a few cases that had simple and well defined pressure histories. The work was carried out on boundary layers having relatively constant histories, which provided a particularly simple and well defined case to study. The resulting set of profiles for these so defined pressure histories were called "equilibrium" profiles.

Thus, trial pressure distributions would be set up and the velocity profiles at a number of stations would be measured. The surface-friction coefficients were determined and $(u - U_e)/u_\tau$ plotted against z/δ for each station. If the velocity profiles were not similar, the pressure distribution was altered and the procedure repeated until similar profiles were obtained.

Clauser found that the plots of $(u - U_e)/u_\tau$ against z/δ produced a universal curve which showed an expected difference from the universal curve at constant pressure (Figure A2-4). Next it was decided to experiment with a steeper dimensionless pressure distribution. When analysing the results it was found that many of the previously used boundary layer parameters were unsatisfactory. The boundary layer thickness has the difficulty that the outer edge of the turbulent layer is ill-defined. The displacement thickness

$$\delta_1 = \int_0^\infty \left(1 - \frac{u}{U_e}\right) dz \qquad (2\text{-}28)$$

and the momentum thickness

$$\theta = \int_0^\infty \frac{u}{U_e}\left(1 - \frac{u}{U_e}\right) dz \qquad (2\text{-}29)$$

could not be obtained directly from the universal plot that formed the basis of the correlation of turbulent profiles.

Thus, parameters were required which did not need additional data for their specification. The simplest universal thickness so defined was

$$\Delta = \int_0^\infty \frac{U_e - u}{u_\tau}\, dz = \delta \int_0^\infty f(\eta)\, d\eta \qquad (2\text{-}30)$$

For constant pressure profiles the integral has the value 3.6, and for each set of equilibrium profiles there was a different value for the integral.

In addition to the defect thickness Δ, a suitable parameter was required to characterise the various members of the universal family of profiles. A ratio of moments on the universal plot was used,

$$G = \int_0^\infty \left(\frac{U_e - u}{u_\tau}\right)^2 dz \quad \int_0^\infty \frac{U_e - u}{u_\tau}\, dz = \int_0^\infty \left(\frac{U_e - u}{u_\tau}\right)^2 d\left(\frac{z}{\Delta}\right) \qquad (2\text{-}31)$$

The new thickness Δ, and the integral family parameter G, were related to θ and δ as follows

$$\delta_1 = \sqrt{\frac{C_f}{2\Delta}} \qquad (2\text{-}32)$$

$$\theta = \sqrt{\frac{C_f}{2}} \left(1 - G\sqrt{\frac{C_f}{2}}\right)\Delta \qquad (2\text{-}33)$$

The assumption that the entire profile is represented by the universal function of $(u - U)/u_\tau$ versus z/δ was known to be not true near the wall. The calculated values of the integrals for Δ and G for a given distribution of $(u - U)/u_\tau$ versus z/δ in the outer portion of the layer were applicable only as long as the surface roughness elements are small compared with the thickness of the viscous sublayer. Pressure gradients were found to have an unexpectedly large effect on surface friction. By combining his work with the results of previous researchers (Ludwieg & Tillman 1950, Schubaner & Klebanoff 1950) a more complete picture of turbulent surface friction was produced.

The universal velocity distribution for turbulent velocity profiles near smooth walls (Figure 2-3) showed a region outside the viscous sublayer in which the velocity distribution could be represented by

$$\frac{u}{u_\tau} = 5.6 \log_{10} \left(\frac{zu_\tau}{\nu}\right) + 4.9 \qquad (2\text{-}34)$$

even when pressure gradients are present.

For the case of a rough wall, it had already been shown by Prandtl that the semilogarithmic part of the curve was displaced downward parallel to itself by an amount $\Delta u_1/u_\tau$, which depends on the roughness Reynolds number ku_τ/ν . Plots of experimental data on the relations between these two parameters for various types of roughness showed that when ku_τ/ν is greater than approximately 100, the asymptotic form is

$$\Delta u/u = 5.6 \log(ku_\tau/\nu) + \text{constant} \qquad (2\text{-}35)$$

Assuming that zu_τ/ν at the outer edge of the viscous sublayer is approximately 50, then, when the roughness is greater than about twice the thickness of the viscous sublayer, the universal law for the turbulent region near the wall becomes

$$u/u_\tau = 5.6 \log(z/k) + \text{constant} \qquad (2\text{-}36)$$

The above result held for smooth, moderately rough, and extremely rough walls without pressure gradient and for smooth walls with pressure gradients. Using dimensional reasoning showed that the effects of

pressure gradients on conditions near the wall should be small, it then followed that the results were true for rough walls with pressure gradients. For all these cases, there existed a turbulent region next to the wall for which u/u_τ is linearly related to log z.

Looking at the universal plot of $(u - U)/u_\tau$ versus z/Δ it was seen that for the inner portion of the plot, $(u - U)/u_\tau$ should be linearly proportional to log z/Δ. Further the slope of this semilogarithmic curve should be 5.6, the same as that on the plot of u/u_τ versus log zu_τ/ν or log z/k (Figure A2-5). Thus, there is a region of overlap between the two plots for which data for the inner and outer portions of the layer may be correlated and used to establish surface friction laws for turbulent layers.

An analysis along these lines produced a universal surface friction law for all turbulent boundary layers having constant pressure gradients. It includes the effects of Reynolds number, pressure gradient, and surface roughness. Thus,

$$\sqrt{\frac{2}{c_f}} = 5.6 \log R_e - \left(\frac{\Delta u_1}{u_\tau}\right) R_k \sqrt{\frac{c_f}{2}} + \left(\frac{\Delta u_2}{u_\tau}\right) G + 4.3 \qquad (2\text{-}37)$$

The effects of pressure gradient on surface friction were found to be large, both for laminar and turbulent layers. Gradients considerably smaller than those required to produce separation being effective in reducing the surface friction.

On comparing these results with those of previous authors it was

found that they showed little agreement. Since these methods did not agree with the relatively simple experimental results obtained in this analysis it was concluded that a reliable method of predicting the behaviour of turbulent layers under the influence of pressure gradients was still required.

2.8 The law of the wake

Carrying on from the work of Clauser (1954), Coles (1956) represented the turbulent boundary layer velocity profile by a linear combination of two universal functions, one being the law of the wall and the other the law of the wake.

The law of the wake is characterised by the profile at a point of separation or reattachment. The development of the turbulent boundary layer was interpreted in terms of an equivalent wake profile, which supposedly represents the large eddy structure and is a consequence of the constraint provided by inertia. This equivalent wake profile is modified by the presence of a wall, at which a further constraint is provided by viscosity. The wall constraint, although it affects the entire boundary layer, is effective mainly in the sublayer and in the logarithmic profile near the wall.

Thus, the main part of Coles' work was the study of the function $h(x,y)$ in the general mean-velocity formula

$$u/u_\tau = f(zu_\tau/\nu) + h(x,y) \qquad (2\text{-}38)$$

An examination of existing experimental data led to the conclusion that the function $h(x,z)$ could be reduced to a second universal similarity law. That is, the general mean-velocity formula could be written in the form

$$u/u_\tau = f(zu_\tau/\nu) + \frac{\Pi}{\kappa} W(z/\delta) \qquad (2\text{-}39)$$

where Π is a profile parameter which independent of x and y, and the function $W(z/\delta)$ is supposedly common to all two-dimensional turbulent boundary layer flows.

Coles noticed that when the deviations of the velocity above the overlap region on the plot of u/u_τ versus zu_τ/ν (Figure 2-6) were normalised by the maximum deviation (at $z = \delta$) the result would be a single wakelike function of z/δ. The deviations were correlated using

$$\frac{u^+ - 2.5 \log_e z^+ - 5.5}{U_e^+ - 2.5 \log_e \delta^+ - 5.5} \approx 0.5\, W\left(\frac{z}{\delta}\right) \qquad (2\text{-}40)$$

The function W is called the wake function and is normalised to be zero at $z = 0$ and have a value $W = 2$ at $z = \delta$. From plots of W against z/δ (Figure A2-6), W has a point of inflection about the region of $z = \delta/2$, $W = 1$. Thus, the following curve fit approximation for the wake function was proposed

$$W\left(\frac{z}{\delta}\right) \approx 2 \sin^2\left(\frac{\pi}{2}\frac{z}{\delta}\right) \qquad (2\text{-}41)$$

The law of the wake can be used in both the overlap and outer layers and is given by

where Π, the wake parameter, is directly related to the outer variable overlap constant A. Thus, $\Pi = A/2$ where $A \simeq 2.35$ for boundary layer flow (flat plate) and $A \simeq 0.65$ for pipe or channel flow. The parameter Π is assumed constant in an equilibrium boundary layer; e.g. for flat plate $\Pi \simeq 0.5$. For other equilibrium layers, it is assumed that $\Pi = \Pi(\beta)$ where Clauser's equilibrium parameter, $\beta = \frac{\delta_1}{\tau_\omega}\frac{dp_e}{dx}$ (2-43) (Clauser 1954, 1956).

Data from near equilibrium flows (Coles & Hurst 1968) was plotted along with some typical non-equilibrium data as shown in Figure A2-7 (White 1974) and a reasonable fit to the equilibrium points is given by

$$\Pi \simeq 0.8(\beta + 0.5)^{0.75} \qquad (2\text{-}44)$$

which is not too bad a fit even for the non equilibrium flows. Coles and Hurst (1968) recommended that the fit of the law of the wake to velocity profiles should be confined to the range of $0.1 < z/\delta < 0.9$, there being discrepancies near the wall and near the edge of the boundary layer.

It was also suggested that three-dimensional flows could be usefully represented by the same two universal functions, considered as vector rather than scalar quantities. When the wall component was defined to be in the direction of the surface shearing stress, then the wake component, in the cases studied, was found to be very nearly parallel to the gradient of the pressures.

Schofield and Perry (1972) in proposing a new wake hypothesis noted that previous integral methods were developed without any knowledge of the shear stress behaviour. This meant that the moment of momentum and the mean kinetic energy integral equations could not be used as sources of information. Thus, the analysis proposed a new wake hypothesis which had some physical basis and led to a relationship between the mean velocity and the shear stress distribution through the layer.

The model fitted the experimental data satisfactorily in the region adjoining the logarithmic law of the wall and implied a half power distribution in the mean velocities in this region for the experimental data. The model also gave a universal description of the data at the outer edge of the layer. Thus, although the proposed outer flow defect lane was not valid over as wide a range of pressure gradients as the Coles wake hypothesis, the model afforded a more accurate description of the experimental data and showed a connection between the mean flow and Reynolds stress fields.

2.9 The linear momentum equation applied to an inertial control volume

A closer look is now taken at the momentum equation as developed for a control volume.

The net force F on a particle or system or particles of fixed mass is given by the law of conservation of momentum (Newton's second law),

$$F = dM/dt \qquad (2\text{-}45)$$

where M is the total linear momentum of the system. If the force is assumed to be constant over a time Δt, then $F.\Delta t = \Delta M$ (2-46)

Referring to Figure A2-8 we consider a certain quantity of matter at some time t enclosed by the solid line. At some time $t + \Delta t$, the boundary of the system has a new physical location as represented by the dotted line.

Considering the regions denoted by A, B and C, the system occupies region A at time t and regions B + A - C at time $t + \Delta t$. If m represents the mass contained in the different regions and at different times, then

$$m_A(t) = m_A(t + \Delta t) - m_C(t + \Delta t) + m_B(t + \Delta t) \qquad (2\text{-}47)$$

Hence the change in the total momentum of the system is given by

$$\Delta M = M_A(t + \Delta t) - M_C(t + \Delta t) + M_B(t + \Delta t) - M_A(t)$$

Rearranging and dividing by Δt gives,

$$\frac{M}{t} = \frac{M_A(t + \Delta t) - M_A(t)}{\Delta t} + \frac{M_B(t + \Delta t) - M_C(t + \quad t)}{\Delta t} \qquad (2\text{-}48)$$

Taking the limit as $\Delta t \to 0$, the first term on the right of equation 2-48 becomes

$$\lim_{\Delta t \to 0} \frac{M_A(t + \Delta t) - M_A(t)}{\Delta t} = \frac{d}{dt}(M)_{c.v.} = \frac{d}{dt}\int_{c.v.} \rho V dv$$

and the second term becomes

$$\lim_{\Delta t \to 0} \frac{M_B(t+\Delta t) - M_C(t+\Delta t)}{\Delta t} = \lim_{\Delta t \to 0} \frac{(\Sigma \Delta M(t+\Delta t))_B - (\Sigma \Delta M(t+\Delta t))_C}{\Delta t}$$

$$= \underset{B}{\Sigma \Delta \dot{M}} - \underset{C}{\Sigma \Delta \dot{M}}$$

$$= \left[\Sigma \Delta \dot{m} V\right]_{out} - \left[\Sigma \Delta \dot{m} V\right]_{in}$$

$$= \int_{c.s.} V \rho V . dA$$

c.v. designates the control volume fixed in space and bounded by the control surface (c.s.) where $\underset{B}{\Sigma \Delta M}(t+\Delta t)$ is the momentum associated with the mass that has crossed the boundary into region B in time Δt. $\underset{B}{\Sigma \Delta \dot{M}}$ is the time rate at which the momentum is crossing the surface into region B at time t. Thus, equation 2-46 becomes

$$F = \frac{d}{dt} \int_{c.v.} V \rho dv + \int_{c.s.} V \rho V \, dA \qquad (2\text{-}49)$$

The total force F is made up of the total surface force F_s (pressure and shear) and a body force B which is a force per unit volume. Hence, the momentum equation for a control volume becomes,

$$F_s + \int_{c.v.} B dv = \frac{d}{dt} \int_{c.v.} V \rho dv + \int_{c.s.} V \rho V \, dA \qquad (2\text{-}50)$$

This equation is valid only for an inertial system, such that Newton's laws of motion apply.

FIG A2-1 PLOT OF u/U, 1-u/U and u/U(1-u/U) VERSUS DISTANCE FROM WALL

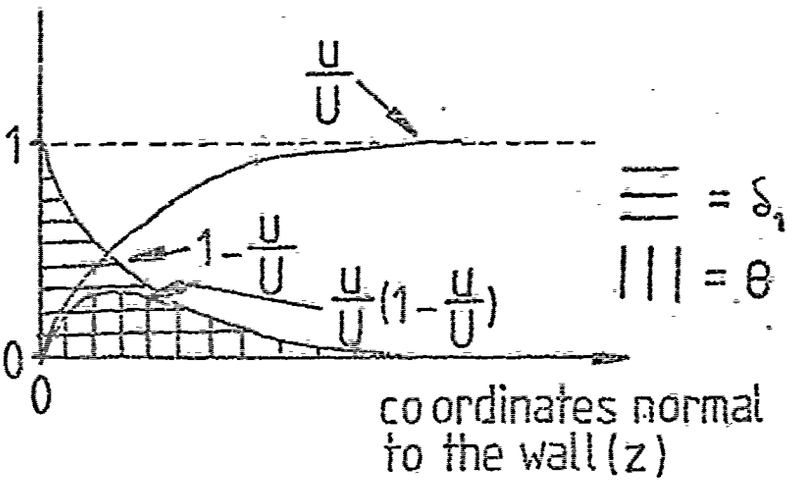

FIG A2-2 COMPARISON OF SPALDING'S INNER LAW WITH THE PIPE FLOW DATA OF LINDGREN (White 1974)

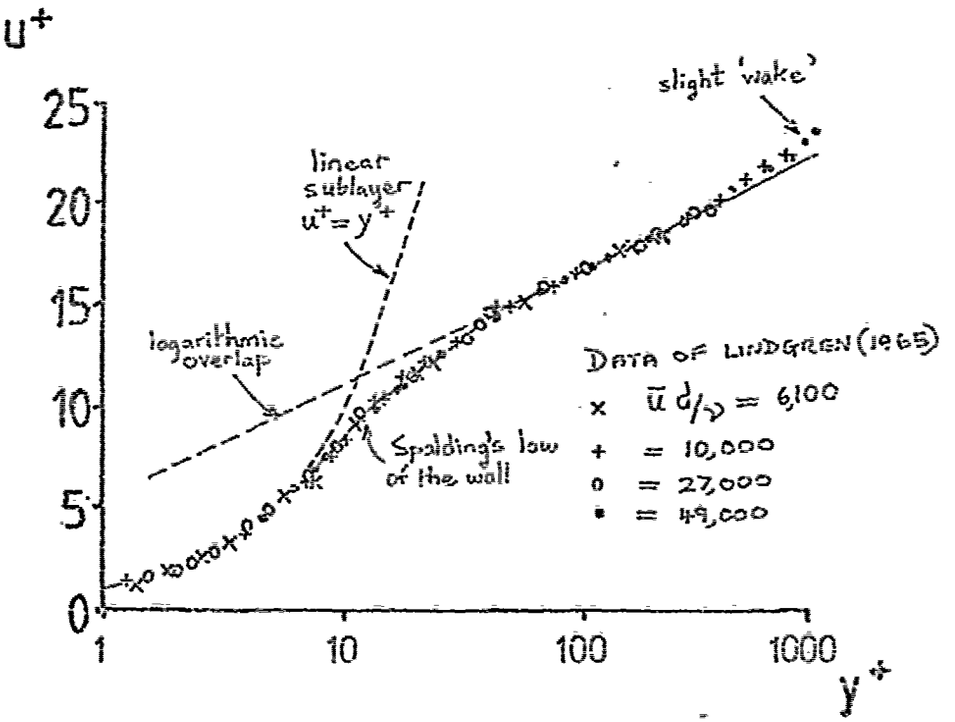

FIG A2-3 UNIVERSAL VELOCITY DISTRIBUTION FOR TURBULENT VELOCITY PROFILES NEAR SMOOTH WALLS (Clauser 1954)

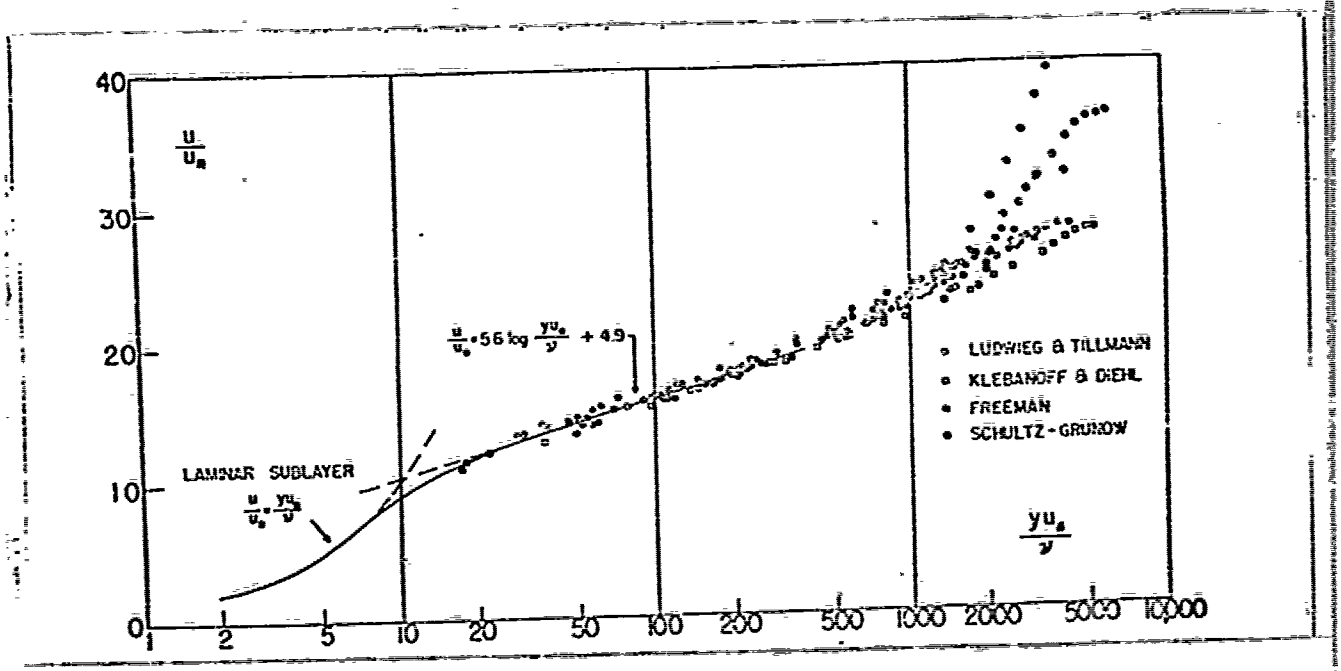

FIG A2-4 UNIVERSAL PLOT OF TURBULENT VELOCITY PROFILES FOR A KNOWN PRESSURE DISTRIBUTION (Clauser 1954)

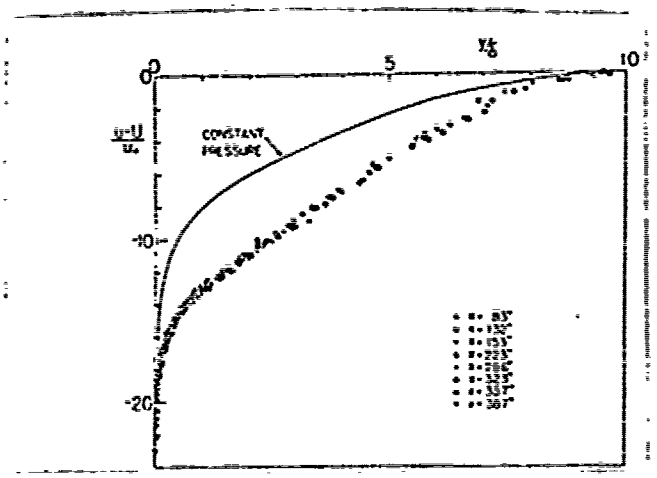

FIG A2-5 UNIVERSAL PLOT OF EQUILIBRIUM TURBULENT VELOCITY PROFILES (Clauser 1954)

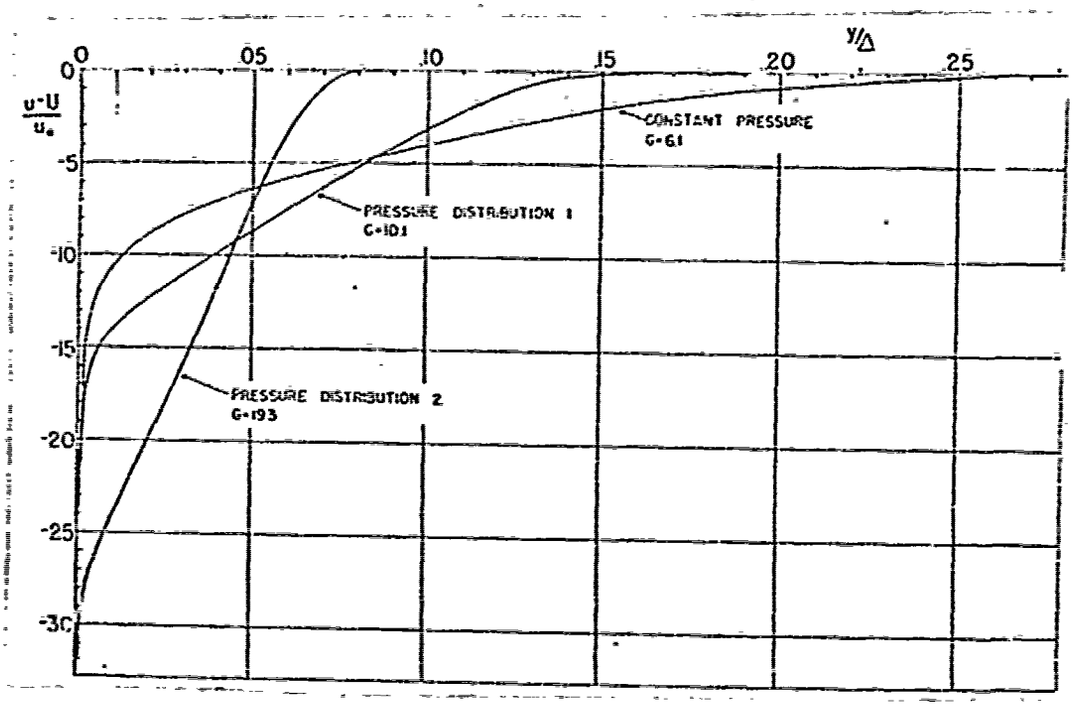

FIG A2-6 THE LAW OF THE WAKE (Coles 1956)

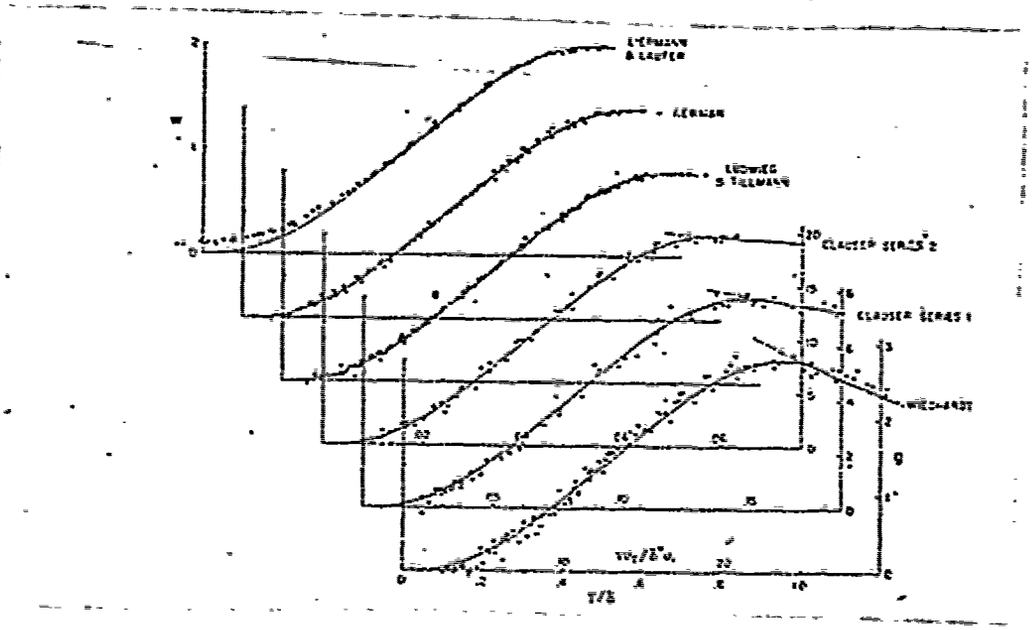

FIG A2-7 EMPIRICAL CORRELATION OF THE LAW-OF-THE-WAKE PARAMETER Π WITH CLAUSER'S EQUILIBRIUM PARAMETER β (White 1974)

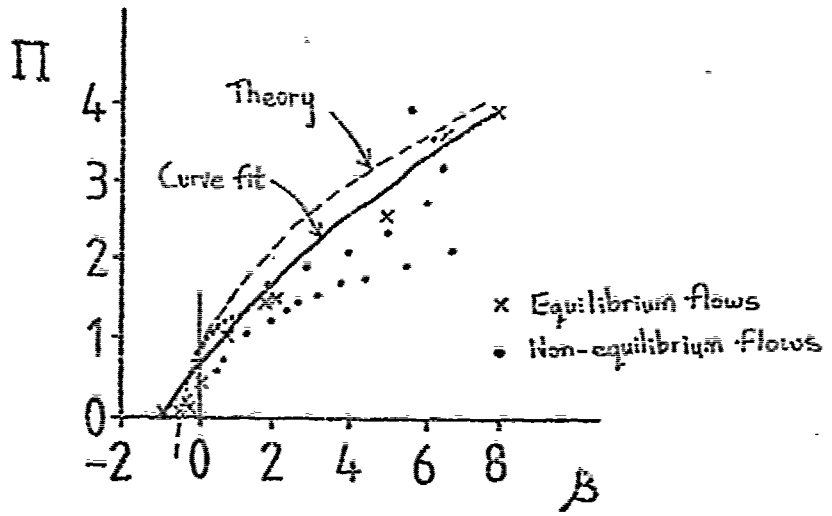

FIG A2-8 CONTROL VOLUME FOR MOMENTUM ANALYSIS

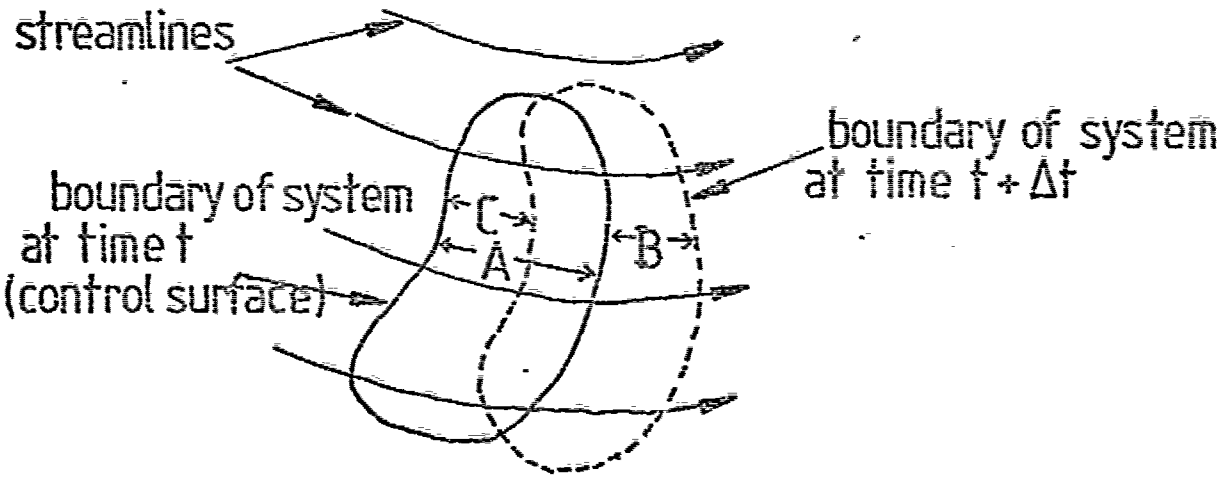

APPENDIX 3: STYLUS MEASUREMENT OF THE MICROGEOMETRY OF A COATED SURFACE

Stylus Measurement Of the Microgeometry of a Coated Surface

M.J. King and T.R. Thomas
Teesside Polytechnic*

The feasibility of using a stylus instrument for looking at a section through a coated surface is discussed. Experimental measurements of the deformation of paint by a stylus are presented, and it is shown that deformation has no significant effect on roughness measurements. Changes in the statistical microgeometry of a profile after successive coats of paint are examined by relocation profilometry. Most of the changes are found to occur after the first coat, the surface becomes smoother, its slopes become gentler, and its peaks more rounded. However, the shortest surface wavelengths are found to be relatively unaffected by painting.

INTRODUCTION

It is of some interest, both practical and theoretical, in the coating industry to establish the relationship between the microgeometry of the coated component and that of its coating. Such a measurement would show, for example, the extent to which the coating conformed to its substrate, which in turn might shed some light on the physical properties of the coating and on the mechanics of its adhesion.

For some time the measurement of the way in which a paint affects the surface finish of a material relied mainly on the use of taper-sectioning[1] and glossmeters.[2] In the first of those methods the specimen is sectioned at a very shallow angle, α, to the surface and the section is polished and examined microscopically. The result is a profile with its vertical scale exaggerated by a factor cot α, thus emphasizing the surface features. This method has the disadvantages of being destructive and time-consuming. The glossmeter, by measuring the reflecting properties of a surface, will give a relative determination of its average roughness but is incapable of measuring individual surface parameters.

The stylus instrument has for many years been used to record surface profiles of many types of engineering surfaces. In the stylus instrument, a pickup, driven by a gearbox, draws the stylus over the surface at a constant speed. The stylus is connected to a transducer which converts its vertical movement relative to some datum into an oscillating electrical signal which is electronically amplified to produce a trace on a chart recorder. This system has been modified to record the surface profile digitally on punched paper tape for subsequent computer analysis. The system has been described in detail elsewhere.[3]

The stylus instrument has previously been used by Hansen to measure profiles of painted surfaces.[4] Hansen used a Talysurf 4 instrument (Rank Taylor Hobson, Leicester) to measure a number of substrates and surface coatings. These measurements showed that identifiable differences in roughness could be detected with the stylus instrument for high gloss, semi-gloss, and flat coatings. It was also shown possible to detect the degree to which substrate irregularities are filled, and that substrate roughness can have a major influence on the appearance of the finished surface. Also vertical and horizontal distances could be measured directly from the chart recordings knowing the relevant magnifications. Thus, it was shown that the stylus instrument is a potentially applicable tool in the field of surface coatings.

In this paper Hansen's work is extended to show that the same stylus instrument will faithfully record the profile of even a soft coating. Some measurements of a painted surface made with a stylus instrument and their statistical analysis are described and discussed. All the coating measurements described were carried out on a shotblasted steel surface previously spray-coated with a two-pack reinforced edged-type primer paint (Metagard G250) and given subsequent brush-applied coats of a thixotropic anticorrosion marine paint (Silver Primocon®). Metagard 250 is for use with shotblasted surfaces. Its dry film thickness is about 20 μm. It contains 14% solids, weighs 0.95 kg/l and surface dries in three minutes. Silver Primocon has a recommended dry film thickness of 75-125 μm. It contains 39% solids, weighs 1.17 kg/l and surface dries in 6-8 hr. The microhardness of its dried film was measured by us as 50 VPN; hardness measurements on the primer were not feasible.

*Dept. of Mechanical Engineering, Middlesbrough, Cleveland TS1 3BA, United Kingdom

Primocon is a registered trademark of International Paint Co.

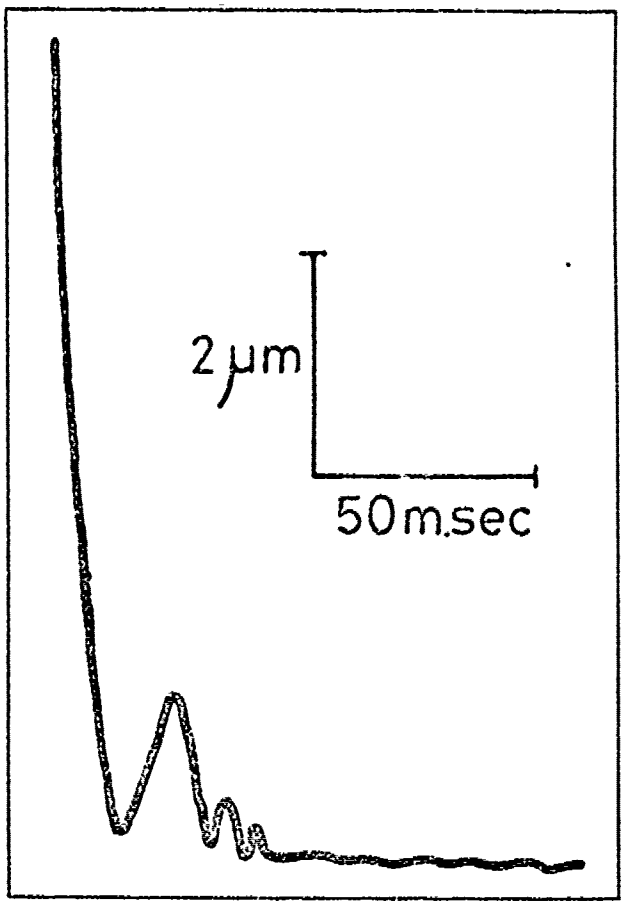

Figure 1—Oscillogram of the transducer output as the stylus falls towards and makes contact with the painted surface

SURFACE DAMAGE

Users of stylus instruments are sometimes concerned by the marks it occasionally leaves on the test surfaces, particularly if the material is soft, and the possibility that this damage can affect the accuracy of measurement. In this investigation, preliminary measurements were made to see if a stylus instrument could be used to measure a painted surface without the stylus ploughing through the surface geometry and thus misrepresenting the surface.

First a square of side equal to the traverse length of the stylus (8 mm) was scribed on a glass microscope slide painted three hours previously with a coat of the marine paint. A series of equally spaced traverses were taken within the scribed square parallel to one of its sides at intervals of time corresponding to paint drying times from three hours to eight hours. The paint was then allowed to dry for a total drying time of 24 hr. The film thickness was measured to be 13 μm.

Another series of parallel and evenly spaced traverses were then taken within the scribed squares and at right-angles to the initial traverses. Thus, the depth of ploughing of the stylus into the surface could be seen from the relative depth of the troughs on the chart recordings corresponding to the crossings of the initial traverses at various stages along their length and at different drying times. It was found from the chart recorder cross traces of the stylus that it does not produce any sign of surface damage after the paint has been allowed its manufacturer's specified drying time.

The possibility of the stylus deforming the painted surface elastically and thus misrepresenting the surface geometry was investigated further by pneumatically raising the stylus from the work surface and then letting it fall freely and observing the path of the stylus as it falls towards the surface, comes in contact, and any subsequent motion after initial contact. This was made possible with the connection of a storage oscilloscope to the amplified output of the stylus and by arranging the oscilloscope's triggering along with the storage facility to produce a photographic record of the reaction of the painted surface to the contact of the falling stylus.[3] From the results (*Figure* 1) there is no evidence of significant elastic deflection. It is concluded, on the basis of these preliminary experiments, that accurate measurement of the roughness of this particular coating material is feasible with a stylus instrument.

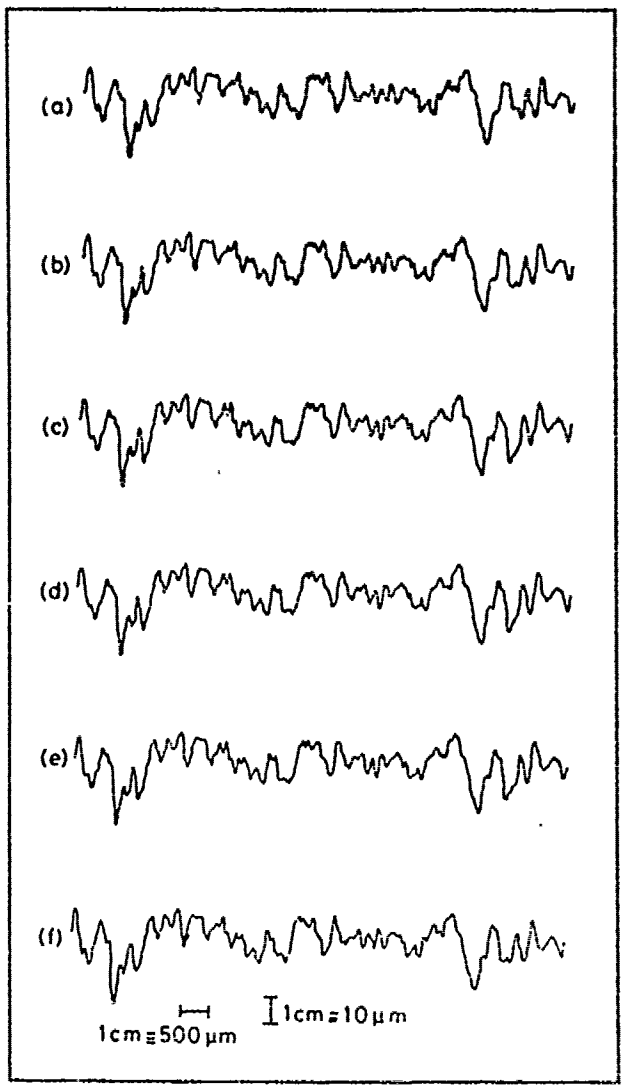

Figure 2—Profiles relocated at successive intervals of 24 hr

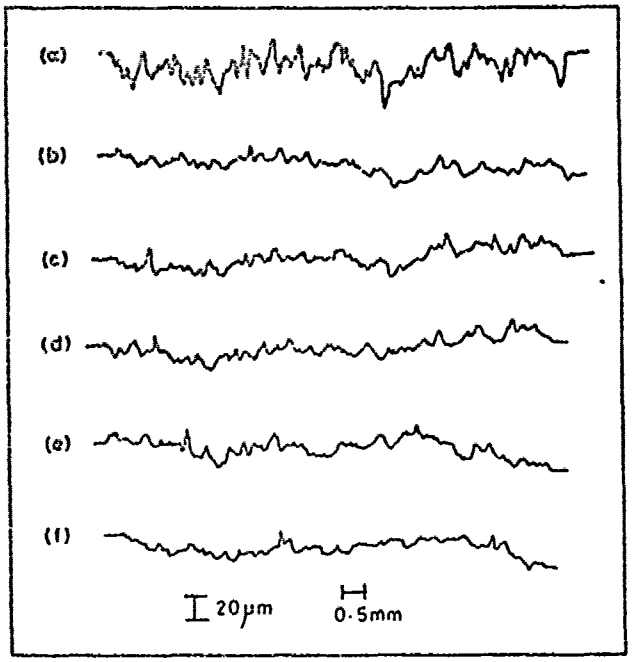

Figure 3—Relocated profiles of a shotblasted steel surface after coating with (a) primer, (b-f) successive top coats

RELOCATION

There are often situations, particularly in research, where it would be very useful to look at a particular section through a surface before and after an experiment, such as an investigation of wear, to see what changes have occurred to the surface geometry. It is clearly desirable that exactly the same section is traversed each time, otherwise the changes observed could be attributed to the displacement of the profile, and small but significant changes might not be observed at all. In general, however, the stylus, which is only 8 μm wide, will not retrace its path exactly unless constrained to do so. A jig for providing this constraint is termed a relocation table.[6]

The relocation table is bolted to the bed of the stylus instrument and the specimen stage is located kinematically and held in position at three points by three pneumatically operated pistons. The stage can be lowered and removed, an experiment of some kind performed on the specimen secured to the stage, and the stage with specimen replaced on the table. Relocation of the stylus then occurs to within the width of the original profile.[7] To preclude the possibility of lateral displacement it is necessary to raise the stylus both during the return stroke of the pickup and when the specimen stage is lowered and raised. The stylus is raised by directing two converging jets of compressed air, controlled by an electrically operated valve, onto the underside of the stylus arm.

The relocation table up to the present time had been used successfully over a maximum period of 24 hr only. Due to the drying time of the paint and the several coats required, it is necessary in the present investigation to rely on the relocation technique over a period of one week. This enhanced performance was achieved by

Table 1—Changes in the Microgeometry of a Shotblasted Steel Surface

Coating[a]	RMS Roughness (mm)	CLA Roughness (μm)	Mean Slope (degrees)	Mean Peak Curvature (μm)	Mean Valley Curvature (μm)
Primer only	10.4	8.4	9.3	12	−11
Primer +1 overcoat	7.0	5.9	6.4	20	−20
Primer +2 overcoats	6.2	5.0	5.8	19	−20

[a] Initial coat was a two-pack reinforced edged-type primer. Second coat was a thixotropic anti corrosive marine paint. The surface was then air-dried for 24 hr at 17°C and 60% R.H.

increasing in steps the air pressure to the three location pistons until the distance between the specimen stage and table as measured with slip gauges stops decreasing. The pressure required to fully relocate the stage plus specimen was thus established and was then used to check the relocation up to seven days.

In the second part of these measurements, chart traces were taken of traverses at 24 hr intervals over a period of seven days on a section of the primer-coated specimen surfaces. The specimen and stage were lowered after each traverse and removed from the relocation table as would be the case in the actual investigation. Prior to each traverse the stage with specimen was replaced and relocated with the previously determined relocation pressure; the resulting traces were compared and were found to show acceptable relocation of the specimen over the period of one week (*Figure* 2).

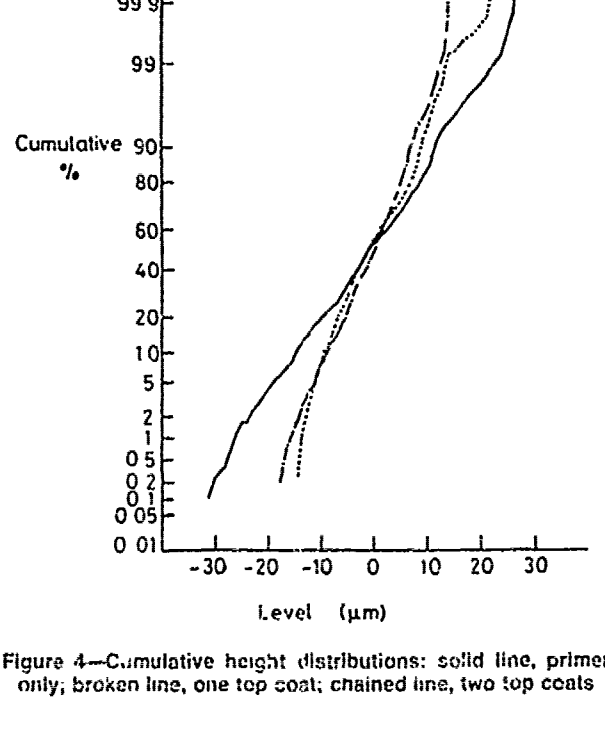

Figure 4—Cumulative height distributions: solid line, primer only; broken line, one top coat; chained line, two top coats

COATING MEASUREMENTS

A piece of ½ in. thick steel plate approximately 7 in. square was securely bolted to the top of the relocation specimen stage. The relocation housing was itself bolted to the bed of the stylus instrument. The initial specimen working surface was coated with a layer of primer paint to prevent corrosion. The surface was positioned so that traverses 8 mm in length could be taken approximately in the middle of the plate.

The raised stylus was brought to the start of its traverse, lowered, and the chart recorder was started. The traversing mechanism was put into gear and a traverse was taken. At the end of the traverse the gearbox was put into neutral, the stylus raised, and the arm was returned to its starting position. The specimen stage plus plate could now be lowered, removed from the rig, and then part of the working surface given an evenly brush-applied coat of marine paint.

After allowing the paint to dry for 24 hr, the specimen stage was replaced and relocated on the relocation table. The stylus was lowered and a traverse taken. This procedure was repeated to produce chart recordings of profiles of the initial primered surface and of the subsequently applied five coats of the marine paint. Any change in the surface profile produced by painting could then be seen by aligning the traces by their predominant surface features (*Figure* 3). The output from the stylus transducer on passing through the instrument's amplifier circuits represents the measured surface profile but with its horizontal and vertical scales distorted in relation to the actual surface. Thus, when looking at the traces it must be remembered that the vertical magnification is exaggerated relative to the horizontal by a factor of ×50.

The whole process of taking traverses and painting was repeated on another part of the working surface and this time the stylus transducer output was digitized and recorded on paper tape for computer processing. For this the sampling rate of the system had to be substantially increased to sample at a sufficiently large number of points on the profile for a statistical analysis to be made possible. The data logging system in use[3] was already in its maximum sampling mode and to achieve this desired greater sampling rate the sampling per unit length was increased by decreasing the stylus speed of traverse. To do this the gearbox was switched to neutral and a special gearbox connected to the stylus arm drive mechanism. Thus the ×20 horizontal magnification setting on the stylus instrument for the chart recorder traces was increased to ×1000 to produce the increased number of samples required for computer analysis. The vertical magnification was unaltered.

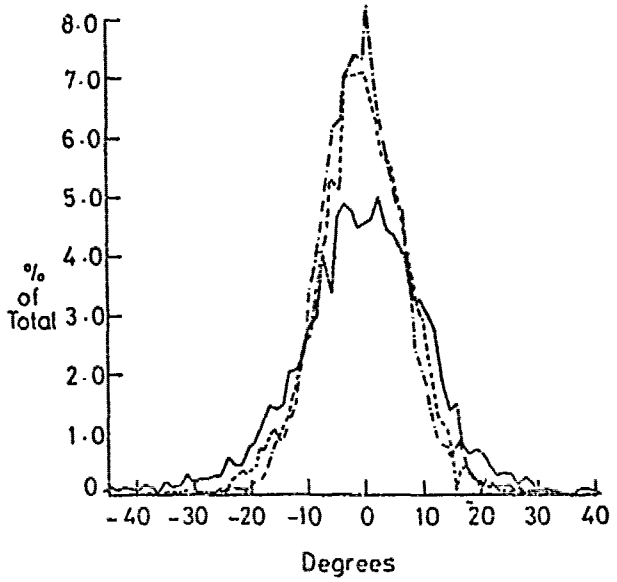

Figure 5—Slope distributions: legend as for Figure 4

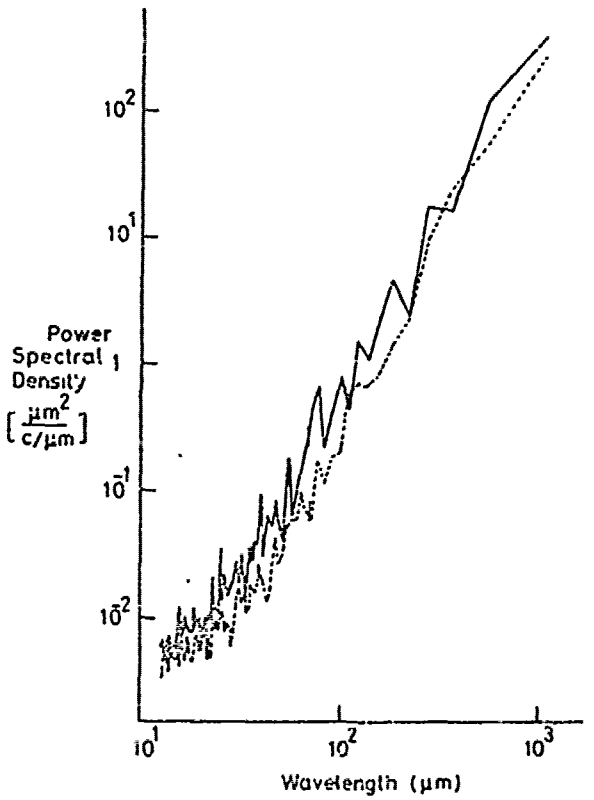

Figure 6—Power spectrum: legend as for Figure 4

From inspection of *Figure* 3 it appeared that few significant changes took place in the profile after the second applied coat. On the strength of these observations it was decided to take the repeat traverses, using the data logging system, on only two applied overcoats. This was thought adequate, in the time available, for a statistical analysis of the painted surface.

First, a general-purpose program written in Fortran IV for an ICL 1905E computer was used to analyze the profile data. This program computes root-mean-square roughness, center-line average roughness, peak and valley distributions, mean line crossings, peak and valley curvatures and their distributions, and profile slopes and curvatures and their distributions.[3] Height readings are input as voltages positive and negative with respect to some arbitrary reference. They are first

reinterpreted as heights and a mean line fitted, thus correcting for any slight mechanical misalignment in the measuring instrument. Second, a program, again written in Fortran IV, was used to compute the power spectral density functions of the data.

RESULTS AND DISCUSSION

A visual inspection of the profile chart recorder traces (*Figure* 3) gives a general indication of the surface changes. The traces show that on the application of the initial coat of paint the roughness of the surface is substantially decreased whereas on further applications of paint the surface roughness does not seem to change any further. This is confirmed by the computed results collected in *Table* 1.

One useful way of examining surface changes is to plot the cumulative height distributions on a normal probability scale (*Figure* 4). This is a scale so distorted that a Gaussian height distribution appears as a straight line, whose slope is inversely proportional to the roughness. The height distribution of the primered surface is quite closely Gaussian except for its topmost fraction, which is considerably smoother. This is a characteristic "transitional" topography and suggests that the original surface peaks had been removed by some finishing process. The same surface after one overcoat had been applied is very much smoother but less closely Gaussian. The effect of a further coat is confined to the top 1% of the height distribution. The roughness of the top 0.1% of the surface remains the same throughout as shown by the local slopes of the three curves. A possible explanation is that the paint flows off the highest peaks and leaves them as untouched "islands" of the original surface.

The distribution of slopes also changes (*Figure* 5). Not far from Gaussian for the primered surface, it becomes markedly more leptokurtic for the two coated surfaces, i.e., the fraction of smaller slopes is higher than a Gaussian distribution would predict. This no doubt reflects the inability of the paint to subtend a very steep angle as it dries. The absolute mean slope in fact decreased by 38% after the second coat, while the mean peak radius of curvature increased by 58% (*Table* 1). Numerical values of peak and valley radii of curvature are about the same, possibly a consequence of the limiting effect of surface tension.

When the power spectra of the surfaces are compared (*Figure* 6) it appears that the process of painting has reduced the height of surface irregularities whose horizontal dimensions range from about 20 μm to about 200 μm. It is interesting to speculate on the mechanism responsible for the lower limit. One possible limiting factor is the particle size of the aluminum filler. It was not possible to obtain a distribution of particle sizes from the manufacturer but the information is available that 0.7% of filler particles will not pass a 44 μm sieve, suggesting that a substantial fraction may be as large as 20 μm.

The inference is that due to the presence of a filler it will be impossible to obtain a painted surface smoother than a certain limiting roughness corresponding to wavelengths of less than about 20 μm, no matter how smooth the substrate. To test this a glass microscope slide of negligible roughness was painted; the roughness of the painted surface was measured as 2.0 μm CLA. The discrepancy between vertical and horizontal dimensions suggests that the larger flakes of filler, if lying flat, are about 10 times as long as they are thick.

The roughness of painted surfaces can be regarded as the sum of three components: one due to the composition of the paint, one due to the method of its application, and one due to the irregularities of the original substrate. The second of these components was effectively absent in the present investigation; no evidence of anisotropy was found in the surface measurements, and were any application effect present it is unlikely that *Figure* 3 would present its actual striking similarity between successive coats. The final microgeometry is clearly influenced heavily by the original substrate roughness. The composition of the paint must also play a part, however, otherwise it is difficult to see why power was not removed evenly across the whole spectrum of surface wavelengths.

CONCLUSIONS

It is important to know how painting changes roughness. This has been measured qualitatively in the past. With a stylus instrument, however, quantitative measurements are possible. Interesting results have already been obtained with a stylus instrument on a painted surface. But does the stylus damage the paint and so give false readings?

Our measurements were made on a shotblasted steel surface sprayed with primer and then brush-coated with successive layers of marine paint. To examine stylus damage, glass was painted and the surface was scratched with the stylus at intervals as it dried. Scratches made after the recommended drying time were imperceptible. The stylus was then dropped onto the surface to look for elastic deflection of the paint, but none could be found.

To ensure that the same section was examined before and after drying, the testpiece was mounted on a relocation table, which made sure that the testpiece was replaced in exactly the same position under the stylus. The table was modified so that it would work for a week and the testpiece, measured daily, was relocated perfectly.

Profiles 8 mm long were measured in the middle of the primer-coated testpiece. The testpiece was removed for each overcoat, replaced, and measured again. This was done for five overcoats, allowing the paint to dry for 24 hr before each measurement. The experiment was repeated and this time the profiles were recorded digitally. As no changes were observed visually in the first experiment after the second overcoat, the repeat was carried out for two overcoats only. The results were analyzed by computer.

The first overcoat made the surface about two-thirds as rough, but the second overcoat made it only 11% smoother. The roughness of the top 0.1% of the surface

did not change, suggesting that paint may not cover the highest peaks. Slopes and peak radii decreased by 48% and 58%, respectively, and there were fewer high slopes, probably due to the rheology of the paint. Wavelengths of between 20 μm and 200 μm were reduced in height, but the surface was just as rough below 20 μm, a dimension corresponding to the size of the larger particles of filler. This suggests that a smooth surface could actually be made rougher by painting, an effect which we confirmed by experiment.

ACKNOWLEDGMENTS

We are grateful to the British Ship Research Association, Wallsend, for supplying the marine paint, and to Smith's Dock Co. Ltd., Middlesbrough, for supplying the specimen surface. This work was supported by the Science Research Council.

References

(1) Nelson, H.R., "Taper Sectioning as a Means of Describing the Surface Contour of Metals," Proc. Conf. on Friction and Surface Finish, pp 217-237, 2nd Edition, M.I.T. Press, Cambridge, Mass., 1969.
(2) Westberg, J., "Development of Objective Methods for Judging the Quality of Ground and Polished Surfaces in Production," *Proc. Instn. of Mech. Engrs. 182*, Part 3K, 260 (1967/68).
(3) Thomas, T.R., "Recent Advances in the Measurement and Analysis of Surface Microgeometry," *Wear, 33*, 205 (1975).
(4) Hansen, C.M., "Surface Roughness Profiles and Coating Performance," JOURNAL OF PAINT TECHNOLOGY, *44*, No. 570, 61 (1972).
(5) Sayles, R.S., Unsworth, A., Anderson, J., Thomas, T.R., and Hanslock, I., "Measurement of the Surface Microgeometry of Articular Cartilage," *J. Biomech.*, (in press).
(6) Williamson, J.B.P. and Hunt, R.T., "Relocation Profilometry" *J Phys. E: Sci. Instrum., 1*, 749 (1968).
(7) Thomas, T.R., "Computer Simulation of Wear," *Wear, 22*, 83 (1972).
(8) Williamson, J.B.P., Pullen, J., and Hunt, R.T., "The Shape of Solid Surfaces," Ling, F.F., ed., in "Surface Mechanics," A.S.M.E., New York, 1969, 24-35.

APPENDIX

DATA LOGGING SYSTEM AND DATA ANALYSIS

The data logging system (*Figure* 7) consists of a demodulator, digital voltmeter (DVM), punch encoder, and paper-tape punch. The demodulator filters the 3K Hz carrier waveform from the signal on its way to the DVM. The DVM is an analogue-to-digital converter (ADC) which for each sampling sequence integrates the signal over a length of time (equivalent to horizontal distance) which is finite but small compared with the constant sampling interval.

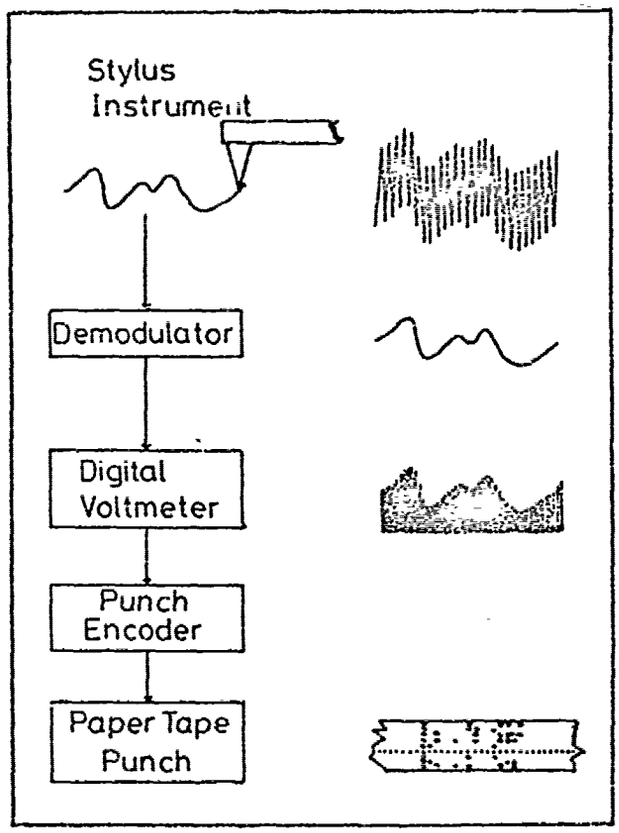

Figure 7—Block diagram of surface measurement and data logging system

The voltage readings are then output as a string of digital pulses to the punch encoder, the DVM output being displayed on a digital display. The punch encoder converts the pulses into a form which will be accepted by the paper-tape punch. The punch records the height readings as a sequence of six-character words comprising four digits, a polarity sign, and an end-of-word character. Four digits gives a height resolution to 1 part in 9999 which is theoretically more than adequate.[3]

The system is very slow, sampling at a maximum rate of three readings/sec, equivalent to 1.85 μm in horizontal distance. The length of stylus traverse was 8 mm.

APPENDIX 4: DETAILS OF THE COMPUTER PROGRAMS USED IN THE FLOW ANALYSIS

Two main computer programs are used to analyse the constant temperature anemometer flow data. Prior to the analysis a small program is used to compute the mean value of the sampled bridge voltages for each measuring point on a velocity profile. These mean voltage values are then plotted against the distance z from the work surface. The value of voltage equivalent to the free stream velocity and the approximate value of boundary layer thickness can then be determined by visual inspection of the plots. These values along with the mean bridge voltag data and the hot-film calibration are then used in the subsequent flow analysis.

Program MOOPPA computes the momentum integral parameters from each set of data making up a boundary layer velocity distribution at distance x from the flow channel inlet. The local coefficients of frictional resistance are then manually computed for each set of velocity profiles.

Program MOOPPB computes values of $C_{f(2)}$ and $C_{f(3)}$ for each measured velocity distribution.

```
$JOB ON
LIST(LP)
PROGRAM(FORT)
COMPACT DATA
COMPRESS INTEGER AND LOGICAL
INPUT 1=TR0
INPUT 3=CR0
OUTPUT 2=LP0
END
MASTER DATANAL
DIMENSION YII(50),U(50),V(50)
DIMENSION X(50),VOLT(50)
READ(3,2)BLT,REFVOLT,FRICTVEL,GNU
READ(1,1)REFVEL,GRAD,NUM,L1
  2 FORMAT(4F8.0)
  1 FORMAT(2F0.0,2I0)
    DO 16 I=1,L1
 16 READ(1,4)X(I),VOLT(I)
  4 FORMAT(2F0.0)
C
C       USE CTA CALIBRATION TO COMPUTE
C       SHEAR LAYER VELOCITY DISTRIBUTION
C       FROM SAMPLED CTA BRIDGE VOLTAGES
C
    YINTCPT=REFVOLT-(GRAD*REFVEL)
    WRITE(2,888)
888 FORMAT(//)
    WRITE(2,78)
 78 FORMAT(1H ,8X,27HVALUE OF Y-INTERCEPT(VOLTS))
    WRITE(2,888)
    WRITE(2,90)YINTCPT
 90 FORMAT(1H ,F15.6)
    WRITE(2,888)
    DO 77 I=1,L1
 77 IF(REFVOLT.EQ.VOLT(I))N=I
    WRITE(2,888)
    WRITE(2,555)
555 FORMAT(1H ,8X,47HVALUE OF BOUND. LAYER THICKN.(CM.) AND REFVOLT
    WRITE(2,888)
    WRITE(2,99)BLT,REFVOLT
    WRITE(2,888)
    WRITE(2,79)
 79 FORMAT(1H ,8X,38HVALUES OF Z(CM.) AND VELOCITY(CM/SEC.))
    WRITE(2,888)
    DO 11 I=1,L1
    YII(I)=X(I)
    U(I)=(VOLT(I)-YINTCPT)/GRAD
    IF(U(I).LT.0.0)U(I)=0.01
    WRITE(2,99)YII(I),U(I)
 11 CONTINUE
    WRITE(2,888)
    UIF=REFVEL
    WRITE(2,666)
666 FORMAT(1H ,8X,29HFREE-STREAM VELOCITY(CM/SEC.))
    WRITE(2,888)
    WRITE(2,100)UIF
100 FORMAT(1H ,F15.6)
 99 FORMAT(1H ,2F15.6)
    PI=3.141592E
C
C       CALCULATE:(1)MOMENTUM INTEGRAL PARAMETERS
C
    CALL MOMPARAMS(N,UIF,U,YII,NUM)
    STOP
    END
    SUBROUTINE MOMPARAMS(N,UIF,U,YII,NUM)
    DIMENSION X(50),Y(50),W(50),Z(50),YII(50),U(50)
    DIMENSION 0(50),DISPLTHICK(50),AMOMTHICK(50)
```

```
      DIMENSION DISPLTHICK(50),AMOMTHICK(50)
      DO 12 I=1,N
      W(I)=U(I)/UIF
      X(I)=1-(U(I)/UIF)
   12 Y(I)=(U(I)/UIF)*(1-(U(I)/UIF))
      WRITE(2,7)
      WRITE(2,7)
      WRITE(2,21)
   21 FORMAT(1H ,8X,28HDIST. FROM LEADING EDGE(CM.))
      WRITE(2,7)
      WRITE(2,23)NUM
   23 FORMAT(1H ,8X,I4)
      WRITE(2,7)
      WRITE(2,9)
    9 FORMAT(1H ,11X,3HYII,4X,8HVELOCITY,2X,
     114HNORM. VELOCITY,3X,18H(1-NORM. VELOCITY),
     23X,32HNORM. VELOCITY(1-NORM. VELOCITY))
      WRITE(2,7)
      DO 22 I=1,N
   22 WRITE(2,6)YII(I),U(I),W(I),X(I),Y(I)
    6 FORMAT(1H ,F15.4,F11.4,3X,F8.4,4X,F16.4,10X,F16.4)
      Z(1)=.5*(X(1)+X(2))*(YII(2)-YII(1))
      DISPLTHICK(1)=Z(1)
      DO 3 I=2,N-1
      Z(I)=.5*(X(I)+X(I+1))*(YII(I+1)-YII(I))
    3 DISPLTHICK(I)=DISPLTHICK(I-1)+Z(I)
      WRITE(2,7)
    7 FORMAT(//)
      WRITE(2,15)
   15 FORMAT(1H ,8X,31HVALUE OF DISPLACEMENT THICKNESS)
      WRITE(2,7)
      WRITE(2,8)DISPLTHICK(N-1)
    8 FORMAT(1H ,F15.6)
      Q(1)=.5*(Y(1)+Y(2))*(YII(2)-YII(1))
      AMOMTHICK(1)=Q(1)
      DO 5 I=2,N-1
      Q(I)=.5*(Y(I)+Y(I+1))*(YII(I+1)-YII(I))
    5 AMOMTHICK(I)=AMOMTHICK(I-1)+Q(I)
      WRITE(2,7)
      WRITE(2,17)
   17 FORMAT(1H ,8X,18HMOMENTUM THICKNESS)
      WRITE(2,7)
      WRITE(2,13)AMOMTHICK(N-1)
   13 FORMAT(1H ,F15.6)
      H=DISPLTHICK(N-1)/AMOMTHICK(N-1)
      WRITE(2,7)
      WRITE(2,18)
   18 FORMAT(1H ,8X,44HSHAPE FACTOR(DISPL. THICKN./MOMENT. THICKN.))
      WRITE(2,7)
      WRITE(2,14)H
      WRITE(2,7)
   14 FORMAT(1H ,F15.4)
      RETURN
      END
      FINISH
$***
<R
```

```
      LIST(LP)
      PROGRAM(FORT)
      COMPACT DATA
      COMPRESS INTEGER AND LOGICAL
      INPUT 1=TR0
      INPUT 3=CR0
      OUTPUT 2=LP0
      TRACE 2
      END
      MASTER DATANAL
      DIMENSION YII(50),U(50),V(50)
      DIMENSION X(50),VOLT(50)
      READ(3,2)BLT,REFVOLT,FRICTVEL,GNU
      READ(1,1)REFVEL,GRAD,NUM,L1
    2 FORMAT(4F0.0)
    1 FORMAT(2F0.0,2I0)
      DO 16 I=1,L1
   16 READ(1,4)X(I),VOLT(I)
    4 FORMAT(2F0.0)
C
C       USE CTA CALIBRATION TO COMPUTE
C       SHEAR LAYER VELOCITY DISTRIBUTION
C       FROM SAMPLED CTA BRIDGE VOLTAGES
C
      YINTCPT=REFVOLT-(GRAD*REFVEL)
  888 FORMAT(//)
      RN=(FLOAT(NUM)*REFVEL)/(GNU*10000.0)
      WRITE(2,90)
   90 FORMAT(1H ,24HVALUE OF REYNOLDS NUMBER)
      WRITE(2,888)
      WRITE(2,79)RN
   79 FORMAT(1H ,F15.2)
      DO 77 I=1,L1
   77 IF(REFVOLT.EQ.VOLT(I))N=I
      WRITE(2,888)
      DO 11 I=1,L1
      YII(I)=X(I)
      U(I)=(VOLT(I)-YINTCPT)/GRAD
      IF(U(I).LT.0.0)U(I)=0.01
   11 CONTINUE
      WRITE(2,888)
      UIF =REFVEL
      WRITE(2,666)
  666 FORMAT(1H ,8X,29HFREE-STREAM VELOCITY(CM/SEC.))
      WRITE(2,889)
      WRITE(2,100)UIF
  100 FORMAT(1H ,F15.6)
      PI=3.1415926
C
C       CALCULATE:
C       CF USING LOG-LAW
C       CF USING WAKE-LAW
      BLT=BLT/100.
      UIF=UIF/100.
      DO 5 I=1,L1
      YII(I)=YII(I)/100.
    5 U(I)=U(I)/100.
      CALL LOGLAW(UIF,L1,NUM,YII,GNU,U,PI,FRICTVEL)
      CALL WAKELAW(UIF,L1,NUM,YII,GNU,U,PI,FRICTVEL,BLT)
      STOP
      END
      SUBROUTINE LOGLAW(UIF,N,NUM,YII,GNU,U,PI,FRICTVEL)
C     LOG-PLOT METHOD FOR ASSESSING CF.....
C     NUM IS STATION NUMBER
C     UIF IS FREE-STREAM VELOCITY(M/S)
C     N IS NO. OF DATA POINTS.....
```

```
C     YII IS DISTANCE FROM WALL(MM)
C     UN IS VELOCITY NORMALISED BY UIF.............
C     GNU IS KINEMATIC VISCOSITY (M2/S)
C     U IS VELOCITY (M/S)
C     YUTON IS Y+
C     RESID  IS COLES RESIDUAL ...CONSTANTS ARE 2.5 AND 5.5.....
C     UOUT IS U+ ....................
      DIMENSION YII(50),U(50),YUTON(50),UOUT(50)
      DIMENSION  UN(50),RESID(50),UTAU(50),Z(50)
      DO 6 I=1,N
      FRICTVEL=0.001
      GO TO 101
  102 FRICTVEL=FRICTVEL+0.0001
  101 CONTINUE
      UTAU(I)=FRICTVEL
      UN(I)=U(I)/UIF
    4 CONTINUE
      YUTON(I)=UTAU(I)*YII(I)/GNU
      B=YUTON(I)
      UOUT(I)=U(I)/UTAU(I)
      Z(I)=(U(I)-UTAU(I)*(2.5*ALOG(B)+5.5))/(UOUT(I))
      UTAU(I)=UTAU(I)+Z(I)
       D=ABS(Z(I))
      IF(UTAU(I).LE.0.0.AND.D.GE.0.00001)GO TO 102
      IF(D.LT.0.00001) GO TO 11
      GO TO 4
   11 CONTINUE
      YUTON(I)=UTAU(I)*YII(I)/GNU
      UOUT(I)=U(I)/UTAU(I)
      RESID(I)=UOUT(I)-2.5*ALOG(B)-5.5
    6 CONTINUE
       L=0
      SUM=0.0
      DO 7 I=1,N
      B=YUTON(I)
      IF (B.LT.35)  GO TO 7
      IF (B.GT.350) GO TO 7
      L=L+1
      SUM=SUM+UTAU(I)
    7 CONTINUE
      WRITE (2,18) NUM
   18 FORMAT(1H ,8X,8HSTATION ,I5)
      WRITE(2,36)
   36 FORMAT (1H ,9X,2HY+,14X,2HU+,15X,5HRESID///)
      IF(L.EQ.0) GOTO41
      DO 8 I=1,N
      UTAU(I)=SUM/L
      UOUT(I)=U(I)/UTAU(I)
      YUTON(I)=UTAU(I)*YII(I)/GNU
      B=YUTON(I)
      RESID(I)=UOUT(I)-2.5*ALOG(B)-5.5
      WRITE(2,9) YUTON(I),UOUT(I),RESID(I)
    9 FORMAT(1H ,3F16.9)
    8 CONTINUE
      UTAU1=SUM/L
      CF=(SUM/L*1.0/UIF)**2*2
      WRITE(2,71)
   71 FORMAT(1H ,8X,27HVALUE OF UTAU1 USING LOGLAW)
      WRITE(2,72)UTAU1
   72 FORMAT(1H ,F16.9)
      WRITE(2,55)
   55 FORMAT(1H ,8X,24HVALUE OF CF USING LOGLAW)
      WRITE(2,19)CF
   19 FORMAT(1H ,F15.9)
   41 CONTINUE
      RETURN
      END
      SUBROUTINE WAKELAW(UIF,N,NUM,YII,GNU,U,PI,FRICTVEL,SLT)
```

```
C      NUM IS STATION NUMBER
C      UIF IS FREE-STREAM VELOCITY(M/S)
C      N IS NO. OF DATA POINTS.....
C      UTAU IS WALL FRICTION VELOCITY.....
C      YII IS DISTANCE FROM WALL(MM)
C      UN IS VELOCITY NORMALISED BY UIF.............
C      GNU IS KINEMATIC VISCOSITY (M2/S)
C      U IS VELOCITY (M/S)
C      YUTON IS Y+
C      RESID  IS COLES RESIDUAL ...CONSTANTS ARE 2.5 AND 5.5.....
C      UOUT IS U+ ..........................
       DIMENSION YII(50),U(50),YUTON(50),UOUT(50)
       DIMENSION  UN(50),RESID(50),UTAU(50),Z(50)
       DO 6 I=1,N
       FRICTVEL=0.001
       GO TO 101
  102  FRICTVEL=FRICTVEL+0.0001
  101  CONTINUE
       UTAU(I)=FRICTVEL
       UN(I)=U(I)/UIF
    4  CONTINUE
       YUTON(I)=UTAU(I)*YII(I)/GNU
       B=YUTON(I)
       UOUT(I)=U(I)/UTAU(I)
       F=SIN((PI*YII(I))/(2.*BLT))*SIN((PI*YII(I))/(2.*BLT))
       Z(I)=(U(I)-UTAU(I)*(2.5*ALOG(B)+5.5+2.5*F))/(UOUT(I))
       UTAU(I)=UTAU(I)+Z(I)
        D=ABS(Z(I))
       IF(UTAU(I).LE.0.0.AND.D.GE.0.00001)GO TO 102
       IF(D.LT.0.00001) GO TO 11
       GO TO 4
   11  CONTINUE
       YUTON(I)=UTAU(I)*YII(I)/GNU
       UOUT(I)=U(I)/UTAU(I)
       RESID(I)=UOUT(I)-(2.5*ALOG(B))-5.5-2.5*(F)
    6  CONTINUE
        L=0
       SUM=0.0
       DO 7 I=1,N
       B=YUTON(I)
       IF (B.LT.50)  GO TO 7
       L=L+1
       SUM=SUM+UTAU(I)
    7  CONTINUE
       WRITE (2,18) NUM
   18  FORMAT(1H ,8X,33HSTATION(DIST. FROM LEADING EDGE) ,I5)
       WRITE(2,36)
   36  FORMAT (1H ,9X,2HY+,14X,2HU+,15X,5HRESID///)
       IF(L.EQ.0) GOTO41
       DO 8 I=1,N
       UTAU(I)=SUM/L
       UOUT(I)=U(I)/UTAU(I)
       YUTON(I)=UTAU(I)*YII(I)/GNU
       B=YUTON(I)
       F=SIN((PI*YII(I))/(2.*BLT))*SIN((PI*YII(I))/(2.*BLT))
       RESID(I)=UOUT(I)-(2.5*ALOG(B))-5.5-2.5*(F)
       WRITE(2,9) YUTON(I),UOT(I),RESID(I)
    9  FORMAT(1H ,3F16.9)
    8  CONTINUE
       UTAU1=SUM/L
       CF=(SUM/L*1.0/UIF)**2*2
       WRITE(2,71)
   71  FORMAT(1H ,8X,28HVALUE OF UTAU1 USING WAKELAW)
       WRITE(2,72)UTAU1
   72  FORMAT(1H ,F16.9)
       WRITE(2,55)
   55  FORMAT(1H ,8X,25HVALUE OF CF USING WAKELAW)
       WRITE(2,19)CF
```

```
   55 FORMAT(1H ,8X,25HVALUE OF CF USING MAKELAW)
      WRITE(2,19)CF
   19 FORMAT(1H ,F15.9)
   41 CONTINUE
      RETURN
      END
      FINISH
****

*R
```

REFERENCES

ALLAN, J F and CUTLAND, R S

The effect of roughness on ship resistance, 1956.

ARCHARD, J F

Proc. R. Soc. A243, 190-205, 1957.

BETTERMAN, D

Int. J. of Heat and Mass Transfer, 9, 153- , 1966.

CANHAM, H J S

Notes on the recording, analysis and interpretation of Wall-Roughness Gauge records.

BSRA Technical Memorandum No. 79, 1956.

CANHAM, H J S

Determining the average roughness of a ship's hull.

BSRA Technical Memorandum No. 143, 1961.

CHAPLIN, P D

The analysis of hull surface roughness records.

BSRA Report NS103, 1965.

CLARKE, G M and THOMAS, T R

Roughness measurement with a Laser Scanning Analyser.

Proc. Int. Conf. on Metrology and Properties of Engng. Surfaces, Leicester, April 1979.

REFERENCES (continued)

CLAUSER, F H

Turbulent boundary layers in adverse pressure gradients.

J. of Aeronautical Sciences, 21, 91-108, 1954.

CLAUSER, F H

The turbulent boundary layer.

Advances in Appl. Mechs. 4, 1-51, 1956.

COLES, D

The problem of the turbulent boundary layer.

Zeitschrift Fur Angewandte Mathematik und Physik, 5, 181-203, 1954.

COLES, D

The law of the wake in the turbulent boundary layer.

J. Fluid Mech. 1, 191-226, 1956.

COLES, D and HURST, E A

Proc. Comput. Turbul. Boundary layers, Vol. II, Department of Mech. Engng., Stanford Univ., Stanford, California, 1968.

CONN, J F C et al.

BSRA resistance experiments on the Lucy Ashton. Part II - The ship-model correlation for the naked hull conditions.

Trans. Instn. Nav. Architects, 95, 350-436, '953.

DANIEL, H G

A study of abrasive blasted surfaces and their effect on paint thickness.

Trans. RINA, April 1969.

DEER, D H

Corrosion in Marine Environment.

International Sourcebook 1: Ship painting and corrosion, Wiley, 1977.

DRIFTMYER, R T and HORANOFF, E V

Two-component force balance for measuring skin friction and side force.

ICIASF, 161-168, 1975.

DVORAK, F A

Calculation of turbulent boundary layers on rough surfaces in pressure gradients.

AIAA J. 7, pt. 9, 1752-1759, 1969.

EINSTEIN, H A and BANKS, R B

Fluid resistance of composite roughness.

Trans. Am. Geophys. Union, 31, n4, 603-610, 1950.

FRANCIS

GEORGE, A F

A comparative study of surface replicas.

Proc. Int. Conf. Metrology and Properties of Engng. Surfaces,

Leicester, 1979.

GORTLER, H

Further development of a boundary layer profile for a given pressure distribution.

J. Roy. Aero. Soc. 45, 35-50, 1941.

GRANVILLE, P S

The viscous resistance of surface vessels and the skin friction of flat plates.

Trans. SNAME, 64, 209-240, 1956.

GRANVILLE, P S

The torque and turbulent boundary layer of rotating discs with smooth and rough surfaces, and in drag-reducing polymer solutions.

J. of Ship Res. 17, n4, 181-195, 1973.

GRANVILLE, P S

Similarity-law characterisation methods for arbitary hydrodynamic roughness.

Report No. 78-SPD-815-01, David W Taylor Naval Ship Res. and Dev. Centre, February 1978.

GRASS, A J

Structural features of turbulent flow over smooth and rough boundaries.

J. Fluid Mech. 50, pt. 2, 233-255, 1971.

GREENWOOD, J A and WILLIAMSON, J B P

Contact of nominally flat surfaces.

Proc. Roy. Soc. A295, 300-319, 1966.

HAMA, F R

Boundary layer characteristics for smooth and rough surfaces.

Trans. SNAME 62, 333-358, 1954.

HUDSON, J C et al.

The surface preparation of ship plate (outer bottom plating) for painting.

Trans. Instn. Nav. Archit. Lond. 185-206, 1959.

HUGHES, G

Frictional resistance of smooth plane surfaces in turbulent flow - new data and a survey of existing data.

Trans. Instn. Nav. Archit. Lond. 94, 287-322, 1952.

ITTC, 1978.

KARLSSON, R I

The effect of irregular surface roughness on the frictional resistance of ships.

Int. Symp. on Ship Resistance, SSPA, Goteborg, 1978.

KARMAN, VON

Turbulence and skin friction.

J. of the Aeronaut. Sciences, 1, 1-20, 1934.

KEMPF, G

On the effect of roughness on the resistance of ships.

Trans. Instn. Nav. Archit. 79, 109-120, 1937.

KEMPF, G

New results obtained in measuring frictional resistance.

Trans. Instn. Nav. Archit. Lond. 71, 104- , 1929.

KING, L V

On the convection of heat from small cylinders in a stream of fluid.

Phil. Trans. A214, 373- , 1914.

KING, M J and THOMAS, T R

Stylus measurement of the microgeometry of a coated surface.

J. of Coatings Tech. 50, n643, 56-61, 1978.

LACKENBY, H

Re-analysis of William Froude's experiments on Surface Friction and their extension in the light of recent development.

Trans. Instn. Nav. Archit. Lond. 79, 120- , 1937.

LACKENBY, H

Resistance of ships, with special reference to skin friction and hull surface condition.

Proc. Instn. Engrs. 176, 981-1014, 1962.

LEWKOWICZ, A K and MUSKER, A J

The surface roughness and turbulent wall friction on ship hulls: interaction in the viscous sub-layer.

Int. Symp. on Ship Viscous Resistance, SSPA, Goteborg, 1978.

REFERENCES (continued)

LONGUET-HIGGINS, M S

Statistical properties of an isotropic random surface.

Phil. Trans. Royal Soc. A250, 157-174, 1957.

LONGUET-HIGGINS, M S

The statistical geometry of random surfaces.

Proc. of the 13th Symp. on Appl. Maths, Am. Maths. Soc. 105-143, 1962.

LUDWIEG, H and TILLMANN, W

Investigations of the wall-shearing stress in turbulent boundary layers.

NACA TM 1285, 1950.

MANNING, P T

The influence of surface roughness on the gas flow through cracks.

Proc. Int. Conf. on Metrology and Properties of Engng. Surfaces,

Leicester, 1979.

MERONEY, R N and BRADSHAW, P

Turbulent boundary layer growth over a longitudinally curved surface.

AIAA Journal, 13, n11, 1974.

MILLIKAN, C B

A critical discussion of turbulent flows in channels and circular tubes.

1938

MONZAVI, M T

A resistance law for extreme natural roughness in pressure pipes based on statistical methods.

Technischer Bericht Nr. 8, August 1972.

MORRIS, N H

A new concept of flow in rough conduits.

J. Am. Soc. Civil Engrs. 80, pt. 390, 1954.

MUSKER, A J et al.

Investigation of the effect of surface roughness of a ship on the wall friction using a pipe flow technique.

Dept. Mech. Engng., University of Liverpool Report, SRC contract B/RG/6751.0

MUSKER, A J and LEWKOWICZ, A K

The effect of ship hull roughness on the development of turbulent boundary layers.

Int. Symp. on Ship Viscous Resistance, SSPA, Goteborg, 1978.

NAYAK, P R

Random process model of rough surfaces.

Trans. ASME Ser. F. J. Lubr. Tech. 93, n3, 398-407, 1971.

NIKURADSE. J

Stromungsgesetze in rauchen Rohren.

Forsch. Arb. Ing. Wes No. 361, 1933.

PEKLENIK, J

New developments in surface characterisation and measurements by means of random process analysis.

J. Conf. on Properties & Metrology of Surfaces, Oxford. Proc. I. Mech. E, 182, pt. 3K, 108-126, 1967/68.

PERRY, A E and JOUBERT, P N

Rough-wall boundary layers in adverse pressure gradients.

J. Fluid Mech. 17, pt. 2, 193-211, 1963.

POSEY, C J

Measurement of surface roughness.

Mech. Engng. 68, 305-306 and 338, 1946.

POWELL, R W

Flow in a channel of definite roughness.

Trans. Am. Soc. of Civil Engrs. 111, 531-547, 1946.

PRANDTL, L

Turbulent flow.

NACA Technical Mem. No. 435, Proc. Intn. Congr. for Appl. Mech., Zurich, September 1926.

PRESTON, J H

The determination of turbulent skin friction by means of pitot tubes.

J. Roy. Aero. Soc. 58, 109-121, 1954.

REDA, D C

Compressible turbulent skin friction on rough and rough/wavy walls in adiabatic flow.

Nav. Ordn. Lab., White Oak, Maryland, AD-777 385, NOLTR 74-34, 1974.

RICE, S O

Mathematical analysis of random noise.

Bell System Tech. J. 23, 282- , 1944.

RICE, S O

Mathematical analysis of random noise.

Bell System Tech. J. 24, 46- , 1945.

SAYLES, R S and THOMAS T R

Surface topography as a non-stationary random process.

Nature, 271, 431-434, 1977.

SCHLICHTING, H

Boundary layer theory.

Pergamon Press, Lond. 1968.

SCHOENHERR, K E

Resistance of flat surfaces moving through a fluid.

Trans. Soc. Nav. Archit. (NY) 40, 279-313, 1932.

SCHOFIELD, W H and PERRY, A E

The turbulent boundary layer as a wall confined wake.

Dept. of Supply, Australian Defc. Sci. Service Aero. Res. Labs. Mech. Engng. Report 134, February 1972.

SCHUBAUER, G B and KLEBANOFF, P S

Investigation of separation of the turbulent boundary layer.

NACA TN 2133, 1950.

SIMPSON, R L

A general correlation of rougnness density effects on the turbulent boundary layer.

AIAA J. 11, 242- , 1973.

SINGH, K and LUMLEY, J L

Effect of roughness on the velocity profile of a laminar boundary layer.

Appl. Sci. Res. 24, 168-186, 1971.

SMITH, D W and WALKER, J H

Skin-friction measurements in incompressible flow.

Nat. Aeronautics and Space Admin. Techn. Report R-26, 1957.

SMITH, A M O and CLUTTER, D W

AIAA J. 1, 2062- , 1963.

REFERENCES (continued)

SPALDING, D B

A single formula for the 'law of the wall'.

Trans. ASME, J. of Appl. Mechs., September 1961.

TELFER, E V

Economic speed trends.

Trans. SNAME, 59, 1951.

TELFER, E V

On taking the rough with the smooth.

Paper No. 1338, March 1969.

THOMAS, T R

Computer simulation of wear.

Wear, 22, 83- , 1972.

THOMAS, T R

Recent advances in the measurement and analysis of surface microgeometry.

Wear, 33, 205-233, 1975.

THOMAS, T R and KING, M J

Surface topography in engineering: a state of the art review and bibliography.

Brit. Hydromech. Res. Assn, Cranfield, 1977.

THOMAS, T R and KING, M J

Discussion on D J Whitehouse, Surfaces - A link between manufacture and function.

Proc. Instn. Mech. Engrs. 192, 179-188, 1978.

THOMAS, T R and SAYLES, R S

Some problems in the tribology of rough surfaces.

Tribology Intn. June 1978.

TODD, F H

Skin friction resistance and the effects of surface roughness.

Trans. Soc. Nav. Archit. (NY), 59, 315-374, 1951.

TOWNSIN, R L

Turbulence detection - results from the use of an unobstructive technique during ship model testing.

Trans. RINA, 102, 192-201, 1960.

TOWNSIN, R L

The economic importance of bottom maintenance.

Marine Week, January 21, 1977.

TOWNSIN, R L

The speed loss budget.

Lecture at WEGMT Graduate School, September 1978.

TOWNSIN, R L

Bottom condition and speed loss.

Lecture at WEGMT Graduate School, September 1978.

TOWNSIN, R L et al.

Penalties and palliatives for poor performance.

Proc. 4th Intn. Congr. on Marine Corrosion and Fouling.

WESTBERG, J.

Development of objective methods for judging the quality of ground and polished surfaces in production.

Proc. Inst. of Mech. Engrs. 182, pt. 3K, 260-273, 1967/68.

WHITE, F M

Viscous fluid flow.

McGraw-Hill, 1974

WHITEHOUSE, D J

The properties of random surfaces of significance in their contact.

PhD thesis, University of Leicester, 1971.

WHITEHOUSE, D J and ARCHARD, J F

The properties of random surfaces of significance in their contact.

Proc. Roy. Soc. Lond. 316A, 97-121, 1970.

WILLIAMSON, J B P and HUNT, R T

Relocation profilometry.

J. Phys. E1, 749- , 1968.

WILLS, J A B

The correction of hot-wire readings for proximity to a solid boundary.

YEH, and CUMMINS

1967

YOUNG, A D

The drag effects of roughness at high sub-critical speeds.